Investigation of Europium β-Diketonate Complexes as Spectral Converters for Solar Cells

Ahmad Abdulkarim Alsaleh

THE UNIVERSITY of EDINBURGH

Thesis submitted for the degree of

Doctor of Philosophy

The University of Edinburgh
School of Chemistry

2021

I would like to dedicate my dissertation to my loved ones, who mean everything to me. The love of my parents, four sisters, and wife, and their devotion to my pursuit of knowledge, knows no bounds. I love you all, and nothing else really matters.

This dissertation is also dedicated to my beloved country, which invested in my education and provided me with so many opportunities. I only hope that I can give back as much as I have been given.

Finally, I dedicate this dissertation to the memory of one of the chemistry greats, Ahmed Zewail (1946–2016), whose autobiography inspired me to become a chemist. Indeed, it all started there, proving that a book can change a life.

Abstract

Photovoltaic technologies for solar energy conversion are promising routes to renewable energy generation. A major difficulty in improving photovoltaic energy conversion efficiency lies in the spectral mismatch between the energy distribution of photons in the incident solar spectrum and the bandgap of semiconductor materials. Luminescent downshifting (LDS) layers and luminescent solar concentrators (LSCs) offer a passive approach to utilise the short-wavelength portion of the solar spectrum by absorbing short-wavelength photons and re-emitting at longer wavelengths, where the external quantum efficiency of the photovoltaic device is high. β-Diketonate-based europium(III) complexes are promising candidates for use as spectral converters due to their high quantum yields, extended absorption window, large Stokes shift between the absorption and emission spectra and narrow emission bands in the red region.

Two Eu(III) complexes have been synthesised, and their photophysical properties investigated: $Eu(tta)_3DPEPO$ and $Eu(hfac)_3DPEPO$, where tta is 2-Thenoyltrifluoroacetone, hfac is hexafluoroacetylacetone, and DPEPO is bis[2-(diphenylphosphino)phenyl]ether oxide. The photophysical properties of the complexes were examined in the solution phase and in polymethylmethacrylate (PMMA) films. Both complexes exhibited favourable photophysical properties with total quantum yields in the range of 0.75 to 0.85.

Co-doping europium complexes with light-harvesting organic chromophores were considered as a practical approach to cut the cost of the metal used and to extend the harvesting window in the UV region. The use of Förster resonance energy transfer to enhance ultraviolet excitation of the Eu(III) complexes in PMMA films co-doped with organic molecules was investigated. The absorption spectra of the chosen donors, DPEPO, indole, biphenyl, and p-terphenyl, complement those of the complexes, making them useful in harvesting high-energy photons in the 250–320 nm region. Examination of the excitation spectra of the europium complexes in the presence and absence of the donors showed that, in each case, an enhancement in UV excitation of the Eu(III) complex was observed, except for $Eu(hfac)_3DPEPO$ co-doped with indole.

The energy transfer efficiencies of the different donors were determined. DPEPO had the highest energy transfer efficiency for each complex, 33% and 38% for $Eu(tta)_3DPEPO$ and $Eu(hfac)_3DPEPO$, respectively. Preliminary solar testing experiments of $Eu(tta)_3DPEPO$ and $Eu(tta)_3DPEPO$ co-doped with DPEPO were conducted to evaluate their practical performance as spectral converters on c-Si solar cells. Results showed an improvement in the short-circuit current density and the external quantum yield of the device.

The role of an optically active host material in LDS layers and LSCs applications was considered in terms of their photophysical properties. The photoactive nature of Poly(N-vinylcarbazole) (PVK) and its unique photophysical properties were discussed. The use of PVK as an active host for Eu(hfac)$_3$DPEPO and Eu(tta)$_3$DPEPO was investigated. It was determined that energy transfer to the complexes occurs from the carbazole monomer excited state, not from the emitting excimer species. Thus, in PVK doped with the europium complexes, each complex acts as a trap for the migrating monomer excitons.

Energy transfer from PVK to Eu(hfac)$_3$DPEPO was found to occur with an efficiency of ~15% and appeared to be independent of complex concentration over the range of 2.5 to 16 wt%. However, absorption by the PVK matrix competes with direct excitation of the complex, resulting in an overall depletion in excitation intensity rather than the desired enhancement. It was predicted that if the energy transfer efficiency could be increased to 50%, there would be a substantial enhancement of the excitation intensity over the majority of the wavelength range. In contrast, for Eu(tta)$_3$DPEPO, the use of PVK as a matrix was found to give a beneficial enhancement in excitation intensity. The energy transfer efficiency from PVK to the complex was found to be ~20%, similar to that found for energy transfer in Eu(hfac)$_3$DPEPO. The effect of varying the PVK matrix concentration on energy transfer to Eu(tta)$_3$DPEPO was investigated. The effect of adding co-dopant organic chromophores to Eu(tta)$_3$DPEPO in the PVK matrix was also investigated. A multistep energy transfer process can be proposed to explain the enhancement in the excitation intensity by DPEPO and biphenyl.

In summary, the thesis reports the synthesis and photophysical characterisations of two europium complexes in the solution phase and PMMA for spectral converters applications. Co-doping the europium complexes with organic chromophores was investigated, and energy transfer process efficiencies were determined and analysed. The most efficient system was coupled to a c-Si solar cell for solar testing and evaluation. The role of an optically active polymer in transferring energy to the europium complexes and to the Eu(tta)$_3$DPEPO co-doped with organic molecules was discussed, and energy transfer processes were proposed and analysed.

Lay Summary

The sun shines on the earth every day, transmitting a tremendous amount of energy in the form of electromagnetic radiation (light) and providing more energy in a couple of hours than the world consumes in one year. Hence, tapping into this dense source of renewable energy has been an ongoing goal for humankind since early civilisations. Solar cells (photovoltaic devices) have been developed to harness the sun's power by converting sunlight to electricity. The process of efficiently converting sunlight to electricity is a major area of research for the scientific community.

Sunlight consists of minute packets of energy referred to as photons; these photons vary in energy. Some are high-energy (in the ultraviolet region of the spectrum), while others are lower-energy photons (in the visible region). One of the significant obstacles that stand in the way of the efficient conversion of light to electricity is solar cells' insensitivity to certain types of photons in sunlight, particularly high-energy photons. As a result, these photons are not well absorbed in solar cells, leading to decreased conversion efficiency.

Spectral convertors are interesting approaches that are being developed to tackle this problem. The working principle of spectral converters is to convert the incoming high-energy photons to lower-energy photons before they reach the solar cell, allowing the solar cell to absorb them; therefore, enhancing the overall efficiency process of converting sunlight to electricity. The work in this thesis focuses on luminescent down-shifting (LDS) layers and luminescent solar concentrators (LSCs) as spectral converters. LDS layers and LSCs absorb the high-energy photons of the ultraviolet region in the solar spectrum, then re-emit them at a lower energy level, where the efficiency of the solar cell is higher.

LDS layers and LSCs consist of luminescent molecules that can absorb and re-emit photons at more favourable energy levels. A polymer can act as a passive host to those luminescent molecules. Rare earth complexes, particularly europium complexes, are great candidates to serve as luminescent molecules due to their brightness, extended absorption window of high-energy photons, and intense emission in the red region. In addition, polymers (large molecules) are widely used as a host material to provide a suitable environment for these luminescent species.

The majority of the experimental work carried out in this thesis was conducted by fluorescence spectroscopy. Spectroscopy is an essential tool that chemists frequently use to obtain information about atoms and molecules by studying how they interact with light. When a molecule absorbs light, it acquires energy, which allows it to exist in an excited state—a higher energy level.

Upon reaching the excited state, atoms and molecules tend to discard the excess energy by emitting light before returning to the ground state—the lower energy level they existed in before acquiring the extra energy. The fluorescence of a molecule can tell us useful information; its colour reveals the energy of the excited state, its brightness indicates its intensity, and the lifetime—the time taken for the excited molecule to 'relax' back to the ground state—gives us additional details about the molecule and its environment. This information can be used to assess and optimise the lanthanide complexes to make them better spectral converters.

The europium ion has an intense red emission; its emission matches well the wavelength range where solar cells highly absorb. However, the europium ion cannot absorb light on its own; therefore, organic molecules are attached to it, to form a europium complex. The organic molecules harvest the high-energy photons and transfer the energy to the europium ion, and finally, energy in the form of bright red emission will be released to be absorbed by the solar cell.

In this thesis, two europium complexes have been synthesised and investigated. The complexes were examined in the solution phase and the solid phase. The investigation of the complexes involved measurements of brightness, of colour/energy of the absorbed and emitted light, and of the time it takes the excited molecule to relax and emit light. As a result, both complexes exhibited great efficiency regarding absorption and emission of light, making them suitable candidates for LSCs and LDS layers applications.

However, europium is an expensive metal. Therefore, part of this work was dedicated to investigating the possibility of decreasing the amount of metal used and adding inexpensive organic molecules to harvest more light and transfer the energy to the europium. Thus, we can collect more light and cut costs by decreasing the amount of metal used. Furthermore, this thesis's investigation examined the energy transfer process from four organic molecules to the europium complexes. Based on these results, we tested the best energy donor combined with a europium complex in a traditional silicon solar cell; preliminary results showed significant enhancement in the solar cell's efficiency.

Spectral converters usually consist of luminescent species and a passive host material that can provide a suitable environment for the luminescent species to absorb and emit light, but the last part of this work followed an interesting approach by turning the passive host into an active one. A different type of energy transfer process from an optically active polymer to europium complexes, and europium complexes co-doped with organic molecules, was observed. The nature of the energy transfer was investigated and analysed.

It was found that an optically active host can play the same role as co-doping europium complexes with organic molecules, thereby cutting costs and assisting in harvesting the high-energy photons in the ultraviolet region. Therefore, an overlooked source of energy can be harvested and utilised.

Overall, the work in this thesis has provided insights into the effectiveness of europium complexes in absorbing and emitting light and into the process of transferring energy from different donors to the complexes and how that affects the overall efficiency of solar cells. And finally, the process of how an optically active host material can transfer energy was elucidated.

Declaration

This declaration is to certify that the work contained within has been composed by myself and is entirely my own work, except where otherwise stated and indicated with a reference.

No part of the work contained within has been submitted for any other degree or professional qualification.

Signed:

Date:

Acknowledgements

'Troubles overcome are good to tell.'

—Yiddish Proverb

Indeed, overcoming troubles can make for the most incredible stories. Without the support I have received these past couple of years, overcoming the obstacles I faced would have been much harder to do. Without this support, the journey to my destination would not have been possible.

First and foremost, I would like to thank my supervisor, Professor Anita C. Jones. Anita has been very supportive of me and my project; I wish that I could underline the word 'supportive' several times to show how much her unwavering support has meant to me as I have faced hard times both personally and professionally. I am lucky to have experienced what it is like to have a great supervisor. Furthermore, one of the many pleasures of working with Anita was being introduced to the ever-exciting world of molecular photophysics, a world I came to love and appreciate every time I learned more about it. Through our meetings over the years, my skills improved in thinking about and solving problems as I learned and relearned various aspects of physical chemistry. Thank you so much for your support, Anita; it has been an absolute privilege to work under your supervision.

Second, I would like to thank my co-supervisor, Professor Neil Robertson. I greatly enjoyed learning about solar cells and how there are no walls between inorganic, organic, and physical chemistry when it comes to seeing the big picture in chemistry. To be able to work on an exciting subject like solar cells and then have the opportunity to make my own devices was a joy. Thank you, Neil, for giving me this opportunity.

My appreciation extends to people I worked with on a daily basis. Starting with the Jones Group, I would like to thank Dr. Rachel Fisher for welcoming me when I first joined the program and offering her support. I would like to thank Dr. Kyle Paterson and Dr. Alif Sussardi who helped me with the 3D printing of the setups used in this work. Finally, thank you to the current Jones Group: Sergio Bermudez, Alix Bailie, and Lara Casha; I thank you for your friendship and being the best group one could ask for.

In the Robertson Group, I would like to thank Dr. Michal Maciejczyk and Dr. Helen Benjamin for their help in synthesis and their guidance in the synthetic lab. I would like to thank fellow PhD students Ellie, German, Artit, Victoria, and Bingyu for their friendship.

Special thanks to Ying Yuan from the Robertson Group for dedicating her time to help me with solar testing and for her patience in showing me how to measure the performance of photovoltaic devices. I would also like to thank Dr. Guillaume Zoppi from Northumbria University for his help with the external quantum efficiency measurements.

Teaching science has always been my passion. One of the most fulfilling aspects of my PhD journey was teaching physical chemistry at the School of Chemistry. I would like to thank Professor Michael Seery, the former Director of Teaching at the School of Chemistry, for sharing his time and talent to make me a better teacher.

I also had a great time participating in public outreach activities such as the Edinburgh Science Festival and Spectroscopy in a Suitcase. Thanks to Neil, I also had the pleasure of heading the Solar Spark Initiative outreach to educate and engage people in solar energy. Solar Spark allowed me to see different parts of the United Kingdom that I would not have seen on my own. I made memorable trips to small Scottish towns such as Cowdenbeath and Crieff, and it was delightful to see the joy in the eyes of both the children and their parents during these trips.

One of the perks of doing physical chemistry at the School of Chemistry is being a member of the physical chemistry section—one of the most active sections in the school. The physical chemistry section was more than generous with organising exciting seminars, Christmas dinners, and even planned outdoor trips to Firbush. These trips created a wonderful environment to exchange ideas, talk science, and make friendships. I would like to thank Professor Philip Camp, the former head of the physical chemistry section, and Dr. Andrew J. Alexander, the current head of the physical chemistry section, along with all the members of the physical chemistry section for creating such a friendly environment and making the pursuit for my PhD fun.

I also would like to thank the entire technical and administrative staff at the School of Chemistry, particularly Ms. Gillian Law and Mr. Logan Mackay, for their support.

I am incredibly thankful that I have been given so many opportunities to grow personally and professionally. I take pride in my professional association with my supervisors and the School of Chemistry at Edinburgh University.

I would also like to thank my home university, King Saud University, and my beloved country, Saudi Arabia, for awarding me this scholarship to pursue my PhD studies. Without your financial support, this journey would not have been possible. I am grateful that I belong to a country that invests so much in the education of its citizens, ensuring that we get the best possible education. In return, I hope to give back to my country as much as I have been given.

The last acknowledgement will go to the most important people in my life. My family stuck with me through thick and thin. There are no words that can encapsulate the sheer magnitude of what my family has done for me through the years; it would be silly to describe the constant support that I have been fortunate to receive from them throughout my life. My thanks go to my father, Abdulkarim, and my mother, Haifa, who gave me a life. I would also like to thank my four sisters, who are better than I in every aspect, yet they never fail to treat me like I am the special one; Arwa, Asma, Mashael, and Maha; I am lucky to have you in my life. Finally, I want to thank my wife, Nourah, who means the world to me. Nothing is as enjoyable and assuring as going through life knowing that you are with me. Thank you all for being in my life.

List of Abbreviations and Symbols

Å	Angstrom
η	Sensitisation Efficiency
η_{D-A}	Energy Transfer Efficiency from a Donor Molecule to an Acceptor Molecule
ε	Molar Absorption Coefficient
τ	Lifetime
τ_{rad}	Radiative Lifetime
τ_{Ln}	Luminescence (observed) Lifetime
$\emptyset_{Ln}$	Intrinsic Quantum Yield of a Lanthanide Ion
$\emptyset_{tot}$	Total Quantum Yield
AM	Air-Mass Coefficient
a-Si	Amorphous Silicon
CdTe	Cadmium Telluride
CIGS	Copper Indium Gallium Selenide
c-Si	Crystalline Silicon
DPEPO	Bis[2-(diphenylphosphino)phenyl] ether oxide
DSSC	Dye-Sensitized Solar Cell
ED	Electric Dipole
EQE	External Quantum Efficiency
ET	Energy Transfer
FF	Fill Factor
FRET	Förster Resonance Energy Transfer
GaAs	Gallium Arsenide
HFAC	Hexafluoroacetylacetone
IC	Internal Conversion
IR	Infrared
IPCE	Incident Photon-to-Current Conversion
J_{sc}	Short-Circuit Current Density
Ln	Lanthanide
LDS	Luminescent Down-Shifting
LSC	Luminescent Solar Concentrators
mc-Si	Multi Crystalline Silicon
MD	Magnetic Dipole
n	Refractive Index
PC	Polycarbonate
PCE	Power Conversion Efficiency
PLQY	Photoluminescent Quantum Yield
PMMA	Poly(methyl Methacrylate)
PV	Photovoltaic
PVK	Poly(N-vinylcarbazole)
QDs	Quantum Dots
R_0	Förster Distance
TDM	Transition Dipole Moment
TIR	Total Internal Reflection
TTA	2-Thenoyltrifluoroacetone
UV	Ultraviolet
V_{oc}	Open-Circuit Voltage
Vis	Visible

Contents

List of Tables

Chapter 1

Chapter 4

Chapter 5

Chapter 6

List of Figures

Chapter 1

Chapter 2

Chapter 3

Chapter 4

Chapter 5

Chapter 6

Appendix

CHAPTER 1: Introduction

"The Stone Age came to an end, not for lack of stones, and the Oil Age will end, but not for lack of oil."

Ahmed Zaki Yamani - Saudi Oil Minister (1962-1986)

CHAPTER **1**

Introduction

This chapter aims to provide an overview of the use of lanthanides complexes as spectral converters for solar cells applications. I will briefly discuss the importance of solar energy and the recent developments in solar technologies. Then, I will emphasise the role of spectral converters in enhancing solar cells' efficiency and how lanthanides complexes can be used in such applications.

1.1 "Numbers, Not Adjectives"[1] – The Challenge of Energy Demand

The late Sir David Mackay, famous for writing an essential reference on sustainable energy, entitled "Sustainable Energy – without the hot air",[1] noted that there is a heated debate in the scientific community and amongst policymakers about the future of energy in our planet and the effect of climate change on our livelihood. The end of fossil fuels' reign would not be associated with the last drop of oil but when the supply cannot meet the demand. Knowing that we are approaching this point in the future, what is our plan to handle the energy demands? What about nuclear energy or renewable energy – how much do they cost economically and socially, and what are the risks? The debate, in essence, is about numbers, but, as the author noted, in such arguments, people tend to use adjectives such as 'huge', 'big', or 'expensive' when referring to energy policies. Using such adjectives is not sufficient to reach the right conclusions; we need numbers.[1]

The motivation behind any research or policy on sustainable energy stems from humankind's ever-increasing demand for a finite source of energy, leading to political, military, social, and economic conflicts.[2] According to the International Energy Outlook 2020 (IEO2020) report, the global consumption of energy will increase by 50% by 2050 with a 0.7% growth in global population per year.[3] The majority of the energy demand comes from nations outside the organisation for economic cooperation and development (OECD). It is projected to increase by 71% from 2012 to 2040, compared to only 18% from OCED nations.[4] More than 50% of the estimated increase in energy consumption worldwide from 2012 to 2040 will take place in Asia, where China and India are the fastest-growing economies.[5] In 2018, energy consumption witnessed an increase of 1.3%; this increase was primarily due to China followed by India and Indonesia.[6]

The production of electricity is a good indicator of the energy demand; the world production of electricity has increased each year continuously since 1974 with an exception when the world financial crisis hit the world in 2008–2009.[7] In the United Kingdom, the total energy consumption only decreased by 1.4 million tonnes of oil equivalent (mtoe), equivalent to 1%, to 142.0 mtoe in 2018–2919.[8]

Since the industrial revolution, the global energy systems have grown consistently with few exceptions during wars or economic recessions; in the last 50 years, we have witnessed a significant increase. This increase is expected to continue for the next several decades.[9] The international energy outlook presents the U.S. Energy Information Administration's (EIA) assessment of the outlook for global energy. In their report (IEO-2020), they project that fossil fuels will remain the primary source of energy, but by 2050 renewables will be the most-used energy source and will be the preferred fuel source for power generation (Figure 1.1).

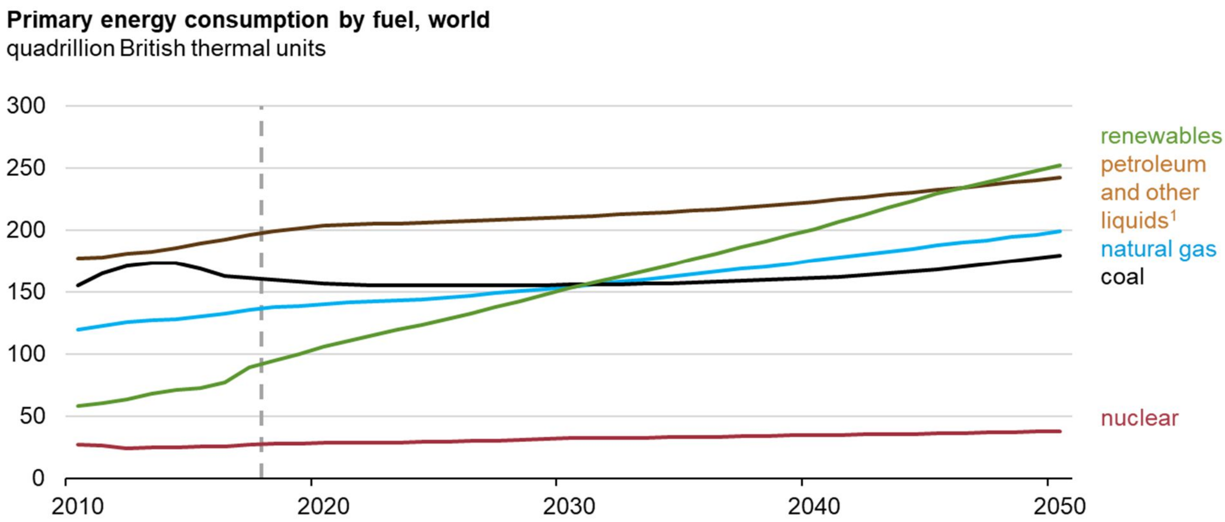

Figure 1.1 Total world energy consumption by energy source, from 2010 to 2050, in quadrillion British thermal units (Btu). Reproduced from.[10]

When dealing with the subject of energy consumption, policymakers, scientists and activists are asking three main questions: (i) how much of an energy resource do we have, and is it sustainable; (ii) how does the consumption of these resources affect the environment; (iii) what the nature of national security threats that might arise by importing energy such as oil from unstable countries or volatile regions is.[1] The current answers to all of these questions will raise a red flag. According to British Petroleum's statistical review of world energy (2020), 84% of the world's primary energy came from fossil fuels in 2019. Oil consumption has increased to a new record mainly due to the economic growth from China,[11] leading to a rise in the emission of carbon dioxide (CO_2).[12, 13]

Fossil fuels provide the wrong answer to the three questions of concern. First, fossil fuels are a finite source of energy. Although there are different speculations about how much oil is left to consume, we are sure that there will be a day when we will have to face oil depletion. Hence it is considered an unsustainable source of energy. Second, fossil fuels contribute to the problem of climate change by producing greenhouse gasses, most notably CO_2. The second half of the 20th century has witnessed an alarming phenomenon in the rise of concentration of CO_2 in the atmosphere converging on 400 parts per million (ppm), which is very close to the tipping point, at 450 ppm, where it could cause irreversible changes on climate.[12] To protect the ice sheets from irreversible loss, the concentration of CO_2 has to fall under 350 ppm.[12, 13] Reducing the dependence on fossil fuels is a crucial factor in achieving this goal. Thirdly, one of the greatest lessons of recent history was the economic vulnerability of countries to energy crises such as the 1973 and 1980s crises; as a result, securing oil supplies in volatile regions became a matter of national security.[14] On the other hand, and in contrast to fossil and nuclear fuels, the resources of renewable energy are accessible geographically to almost every country, an ideal solution to countries with limited resources of oil, and a game-changer in policymaking and geopolitics.[14]

Renewable energy may provide the right answer to all the concerns mentioned above. Indeed, many countries have already started to prepare for the energy transition to sustainable energy. In the UK, the government is expected to announce a ban on fossil fuel vehicles by 2030.[15] The state of California in the United States made a similar decision; the governor signed a bold executive order to ban fossil fuel vehicles by 2035.[16] One of the most exciting developments came from China, which accounts for 75% of the growth in the world's consumption of energy;[11] the Chinese government vowed to reach carbon neutrality by 2060.[16] Even petrostates could benefit from investing in renewable energy: Saudi Arabia, which is one of largest producers and exporters of oil, announced in 2017 its ambitious plan to prioritise the renewable energy sector in the country, part of a more extensive campaign (Vision 2030) to diversify its economy and to become less dependent on oil by 2030.[17] The Saudi minister of energy H.R.H Prince Abdulaziz Bin Salman said the country is aiming to be a pioneer in renewable energy technolgies.[18]

Out of the gloomy days of the coronavirus pandemic (COVID-19), renewable energy was the only energy source ever to grow in 2020 (shown in Figure 1.2).[19, 20] The rate of the demand for global energy declined by 6%, which is exceptional as it has only happened three times over the last century: during Spanish flu in the 1920s, the Great Depression in the 1930s and World War II in the mid-1940s.[19] And for the first time in 134 years, the United States consumed more renewable energy than coal.[21]

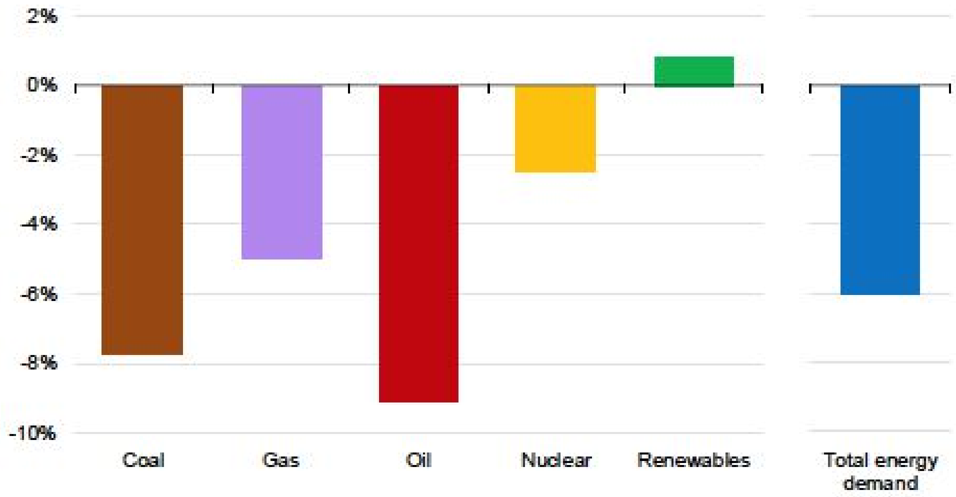

Figure 1.2 Projected change in primary energy demand by fuel in 2020 relative to 2019. Reproduced from [22].

Among the different renewable energy sources, solar energy is the most significant source and has the highest expectations. Every day an average of 90,000 terawatts of solar energy reaches the earth's surface.[23] The current global demand for energy is averaging from 15 to 17 terawatts, and compared with the energy capacity of other renewables sources, such as wind (870 terawatts), biomass (90 terawatts), and wave (7 terawatts), clearly solar energy has the most potential to meet global energy demand.[23] Thus, one of the primary drivers in science and engineering in terms of energy harvesting is the quest to harness the sun's energy as efficiently as possible.[24]

The International Renewable Energy Agency (IREA) confirmed that the global generation capacity of solar energy at the end of 2019 was up to 586 gigawatts, resulting in a 20% increase in generation capacity.[25] As of 2019, over 2% of the global electricity production came from solar energy; in Italy solar is responsible for generating more than 8% of the country's electricity.[26] Italy, Germany, and Spain hosted the biggest solar power plants in 2010,[27], and by 2017 China had become the host of one of the largest floating solar power plants, in the city of Huainan, with a capacity of 40 megawatts.[28] In India, the prime minister cited solar technology as the best solution to India's energy problems, and that his government would work to install 100 gigawatts by 2022, which would provide 10% of India's electricity.[29] Even Chevron, one of the top oil companies in the world, decided that it could use solar panels in its oil fields to cut the expense of its operations.[30]

1.2 Solar Energy

The electromagnetic spectrum coming from the sun is composed of photons of varying wavelengths, as shown in Figure 1.3. The solar radiation that reaches the top of the atmosphere consists of the following: ~8% of the photons are of the ultraviolet (UV) region, ~40% of the visible region, and ~52% of the infrared (IR) region.[27] The atmosphere plays a role in shaping the incoming solar spectrum; due to the attenuation of the electromagnetic flux, it changes during the day, and it varies based on the location and throughout different seasons of the year.[27, 31]

The energy current density that reaches the outer boundary of the atmosphere has an approximate value that varies from 1353 Wm^{-2} [32] to 1368 Wm^{-2}.[27] This value can be defined as the solar constant, which represents the "total radiant energy received vertically from the sun, per unit area per unit of time, just outside the Earth's atmosphere and assuming the planet is at its average distance from the sun".[27]

For this reason, scientists have agreed on a fixed definition of the solar spectrum. Air-mass (AM) is a scale indicating the path-length of extraterrestrial solar radiation passing the earth's atmosphere; it quantifies the losses in sunlight power as it passes the atmosphere.[33] The AM scale can serve as the definitive standard (source of illumination) to measure the performance of different solar cells; thus, other AM standards are used for various s applications. Air-mass zero (AM0) is a standard that describes the solar radiation outside the earth's atmosphere, and it is used to measure the performance of solar panels on orbiting satellites in space.[27]AM1.5 is a more convenient standard that corresponds to a solar zenith angle of 48.2 °C, representing mid-latitudes. This is the most-used standard for terrestrial applications– characterising the performance of solar cells. There has been a recent modification to update this standard to enhance its accuracy, resulting in AM1.5G, the "G" means global, which covers both direct and diffuse radiation.[27] The latter standard is usually referred to as "one Sun," a quantity that has an integrated power flux of 1000 Wm^{-2}.[34]

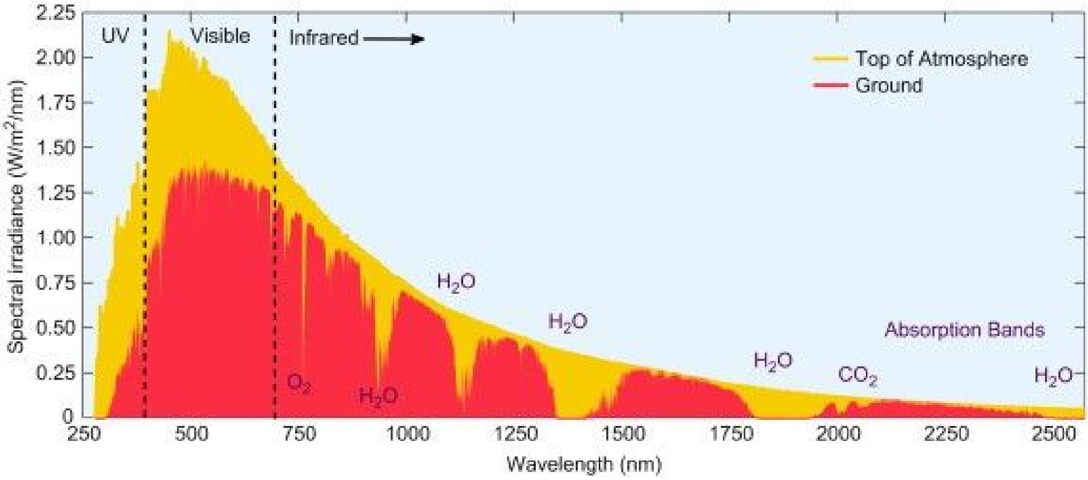

Figure 1.3 The Solar radiation spectrum, without atmospheric absorption (yellow region) and the spectrum at sea level (red area). Reproduced from [35].

1.2.1 Technological Developments – Harnessing the Sun's Energy

The sun, a 4.5 billion-year-old star, beams down a tremendous amount of energy every day. The sun radiates enough energy to the earth's surface in ~90 minutes to cover the world's energy consumption in one year.[23] Thus, the sun's energy is highly underutilised. For solar technologies, the goal is to harness solar power efficiently, which would achieve a smooth transition from fossil fuels. The technology for converting solar energy into electricity has vastly improved in the last four decades. Silicon solar panels used to cost thousands of dollars per watt, but by the mid-1970s, the cost had fallen to $100[23]. Since then, the cost of conventional solar panels has continued to dramatically decline from around $100 in 1976 to $0.23 per watt in 2019, a 99.3% decrease, as shown in Figure 1.4.[36]. The International Energy Agency declared solar technology as the cheapest source of electricity.[37] Despite many challenges, the growth of the solar industry and market seems unstoppable; from the mid-1990s to 2016, the global annual production of solar panels grew at a consistent pace of 40%.[29]

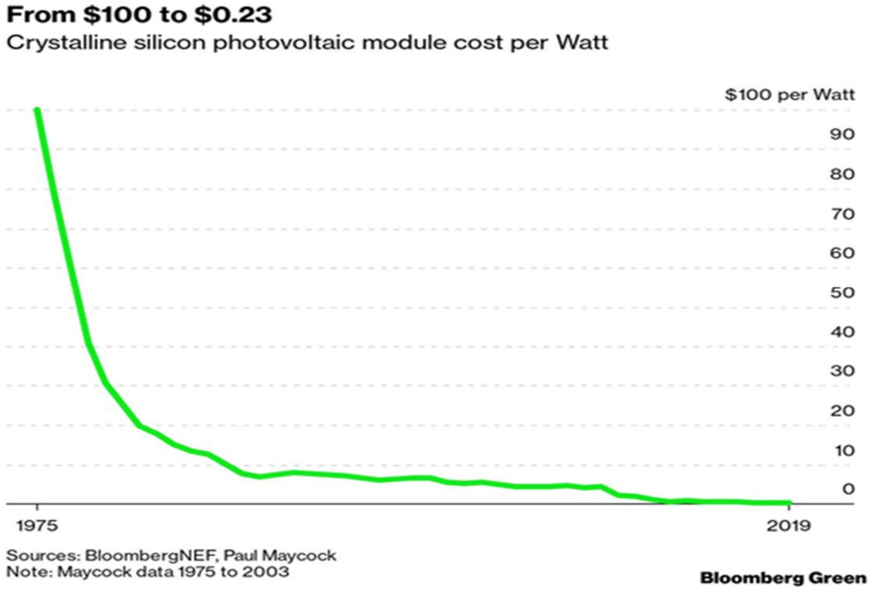

Figure 1.4 shows an illustration of the decreasing price per watt of the silicon solar panel over the last four decades. Reproduced from [36].

The electromagnetic radiation of the sun can be utilised in two ways: direct and indirect methods. The direct method of harnessing the sunlight can be either a passive or an active transformation.[27] A passive transformation occurs in buildings through the collection of sunlight for thermal and illuminative purposes. An active transformation approach involves storing and converting sunlight. This can take place in three different ways: thermal transformation, photochemical transformation or photovoltaic transformation.[27] We will focus on the photovoltaic conversion, as it is within the scope of this thesis

Humankind's quest to harness the sun's energy goes back over three thousand years when the Chinese invented "yangsui", or "burning mirrors" to concentrate sunlight and spark a fire.[29] Then came the Hero of Alexandria who made another advance by converting solar energy into mechanical work in the 1st century BC.[29]

However, it was not until the 19th century that the photovoltaic effect was first discovered.[27] In 1839, the French physicist Edmond Becquerel discovered the photovoltaic phenomenon. Upon illumination, a current and voltage were observed as silver chloride was immersed in an electrolyte solution and connected to a metal counter electrode.[27, 38] He also noticed that blue or ultraviolet light correlated with the best results, an inexplicable phenomenon at the time.[29]

In 1905, Albert Einstein published a paper that explained this phenomenon; he postulated that electromagnetic radiation is composed of photons varying in energy and that electrons in a metal or semiconductor can be emitted (or ejected) from orbiting around the nucleus when exposed to photons of specific energy. As a result, emitted electrons move freely, and more of the photons lead to a flow of free electrons, forming an electric current.[29, 39]

It took about a half-century for the basic solar technology to materialise. In 1941 the first silicon cell was produced with an efficiency of less than 1%.[40] The second half of the 20th century has witnessed the rise of the photovoltaic industry when Bell laboratories produced silicon solar cells with an efficiency of 4% in 1954, then improved it to 11% and consequently produced a 14% solar cell in 1960.[27] Photovoltaics were used for the first time in Vanguard 1, the first satellite that carried silicon solar panels in 1958, producing power of 0.5 watts for over six years.[23]

From the 1960s onwards, there has been an enormous improvement in terms of efficiency and the different types of semiconductor materials introduced to the photovoltaic industry. The types of semiconductors include crystalline silicon (c-Si), multi crystalline silicon (mc-Si), amorphous silicon (a-Si), cadmium telluride (CdTe), copper indium gallium selenide (CIGS), dye-sensitised (DSSC), gallium arsenide (GaAs), organic (OPV) and perovskite solar cells.

Silicon has many advantages: it is abundant, rigid, and non-toxic, but one of the main disadvantages is the manufacturing process, which is complex and uses a lot of energy.[41] In 2007, crystalline silicon solar cells occupied 90% of the photovoltaic market, leaving only 10% to thin-film solar cells, such as a-Si, CdTe, and GaAs.[27, 42] Thin-film photovoltaics such as CdTe and CIGS can be used as a better alternative to crystalline silicon solar cells, as they offer good absorption of sunlight, low-cost production, and good efficiencies.[29] In 2011, mainly due to technological advances, thin films started to take a small share from the c-Si market to make 20% of the total photovoltaic market.[27] Table 1.1 highlights the latest developments in photovoltaic devices in terms of their efficiencies.[43]

Table 1.1 The confirmed efficiencies of single-junction terrestrial cells and submodules under the global AM1.5 spectrum (1000 W/m^2) at 25℃. Reproduced from [44].

Classification	Efficiency (%)
Si (crystalline cell)	26.7 ± 0.5
GaAs (thin film cell)	29.1 ± 0.6
CIGS (cell)	23.35 ± 0.5
CdTe (cell)	21.0 ± 0.4
Si (amorphous cell)	10.2 ± 0.3
Perovskite (cell)	21.6 ± 0.6
Dye sensitised (cell)	11.9 ± 0.4
Organic (cell)	15.2 ± 0.2

1.3 Stating the Problem: Spectral Mismatch in Solar Cells

Solar cells are only sensitive to certain parts of the solar spectrum. The efficiency of the photovoltaic device in converting photons into electricity is mainly related to the bandgap, a semiconductor property that can be defined as "the amount of energy that an electron needs to break free from its host atom and contribute to the cell's electric output".[29] Photons carrying energy below the bandgap of the semiconductor material will be wasted, and those with energy above the bandgap will be used inefficiently.[45, 46] Photons carrying energy below the bandgap will pass through the cell without being absorbed and thus are considered "transparency losses".[45] Another type of optical loss occurs in the case of high energy photons (typically in the UV region) – photons carrying energy greater than the bandgap – as they will provide only the bandgap's energy to the electron, and the rest of the photon's energy will be wasted as a result of thermalisation through collision with the lattice.[45, 46] Both types of spectral losses, thermalisation of high energy photons (greater than the bandgap) and non-absorption of photons below the bandgap, result in losses of approximately 50% of the incident solar spectrum in silicon-based solar cells.[46, 47] One approach to address this spectral mismatch, hence enhancing the efficiency, is to find a way to utilise the high energy photons in the blue and UV region that are not fully absorbed.

1.4 Proposing a Solution: Spectral Converters – Manipulating the Photons' Frequency

There are two main approaches to utilise high-energy photons. The first approach is an active one: it has to improve and optimise the electronic properties of a solar cell by implementing multi-junction or interfering with the device's design through low doping levels and narrow junctions.[45, 48] The second approach could be described as a passive approach. It involves manipulating the frequency of high energy photons of the incident solar spectrum and converting it to match the highest spectral response of the target solar cell.[45, 49]

Solar cells vary in their spectral response to the solar spectrum in general. Therefore, external quantum efficiency (EQE) measurements are used to measure the wavelength-dependent photovoltaic response of a solar cell to the entire solar range.[50] Figure 1.5 shows the EQE of CdTe, c-Si, GaAs and mc-Si in response to the solar spectrum; it is clear that the performance of the aforementioned cells increases dramatically in the visible and near-infrared regions (λ> 550 nm), which makes a strong case for the importance of spectral converters.[45, 51] There are two innovative types of spectral converters: (i) luminescent solar concentrators (LSCs) and (ii) luminescent down-shifting layers (LDS).

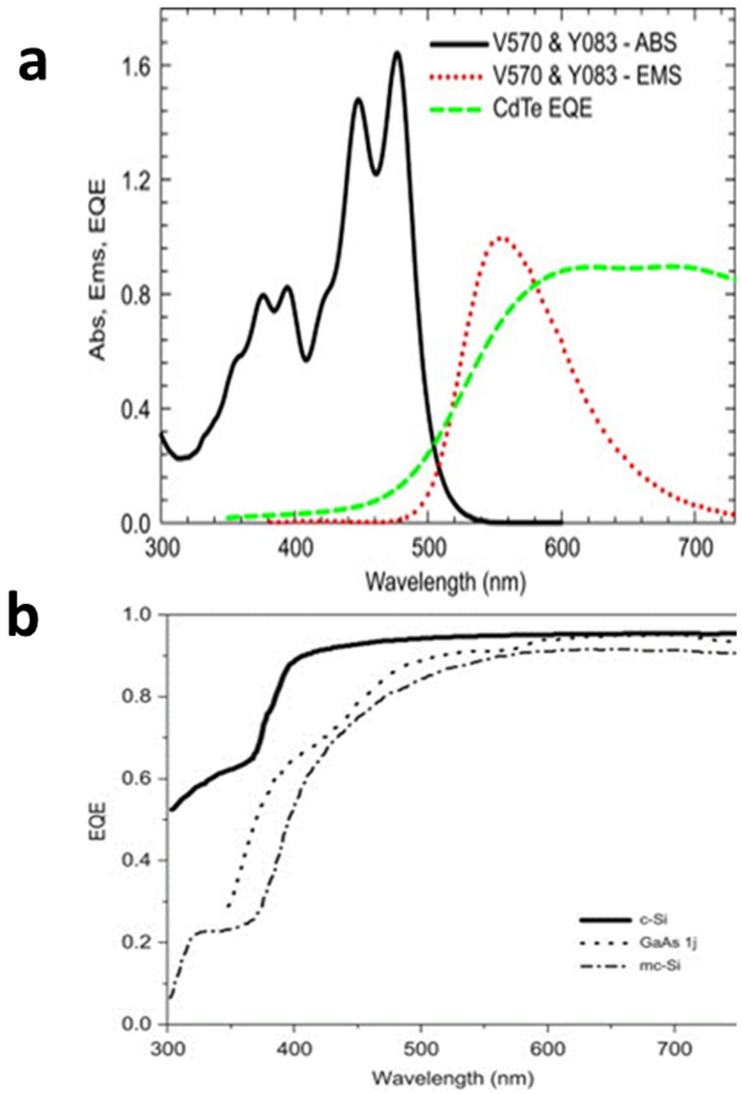

Figure 1.5 (a) The external quantum efficiency curve of CdTe solar cell in the green dashed line. Normalised absorption (Abs, black line) and emission (Ems, red dashed line) spectrum of a mixed dye down-shifting layer containing V570 and Y083 dyes is also shown, reproduced from[51] (b) External quantum efficiency curve of c-Si single junction (solid black line), GaAs (dotted line), and mc-Si solar cell (dashed line). Reproduced from [45].

1.4.1 Luminescent Solar Concentrators (LSCs)

In 1976 Weber and Lambe published a paper entitled "Luminescent greenhouse collector for solar radiation," which introduced the idea of luminescent solar concentrators (LSCs) to cut the cost of expensive solar panels by using large-area collectors – to collect sunlight – with minimal need for solar cells.[52] Throughout the 1970s and 1980s, Zewail and co-workers and other research groups continued to explore this concept and provided detailed theoretical treatments of some of the photophysical concepts involved in such a system, such as the nature of energy transfer and the role of dyes and matrices in LSCs.[52-57] At the time, two main challenges were facing silicon solar panels: first, they were considered an expensive technology; the second was the challenge of aesthetics. Integrating crystalline silicon solar cells into urban architecture (buildings) has proved to be difficult; they are unattractive, heavy and limited in their colour and design.[58-60] LSCs were invented to tackle these concerns: they can be inexpensive to produce; are adaptable to a wide variety of buildings with different colours and shapes; are transparent; and can be placed on windows and doors for interior design purposes, which would minimise the need for large sizes of photovoltaic (PV) devices to produce electricity.[59-61] Thus, LSCs can make significant contributions to facilitate the realisation of sustainable architectures, such as net-zero energy buildings.[62]

The working principles of LSCs are shown in Figure 1.6. LSCs are composed of thin transparent plastic or glass waveguides impregnated with luminescent molecules. The fluorescent molecules absorb the short wavelength portion of the incident solar radiation and then re-emit at a longer wavelength. The re-emitted photons are trapped in the waveguide by total internal reflection (TIR) to become more concentrated along the edges. The PV device is coupled at the edges to convert the concentrated light into electricity.[60, 61] Thus, the short-wavelength photons are utilised and converted to longer wavelengths which are better absorbed by the PV device. LCSs can suffer from several loss mechanisms, for example, by a reflection of the incident light on the front surface, incomplete absorption of incident light by the dye, or re-absorption of fluorescence by the luminescent molecules.[63, 64]

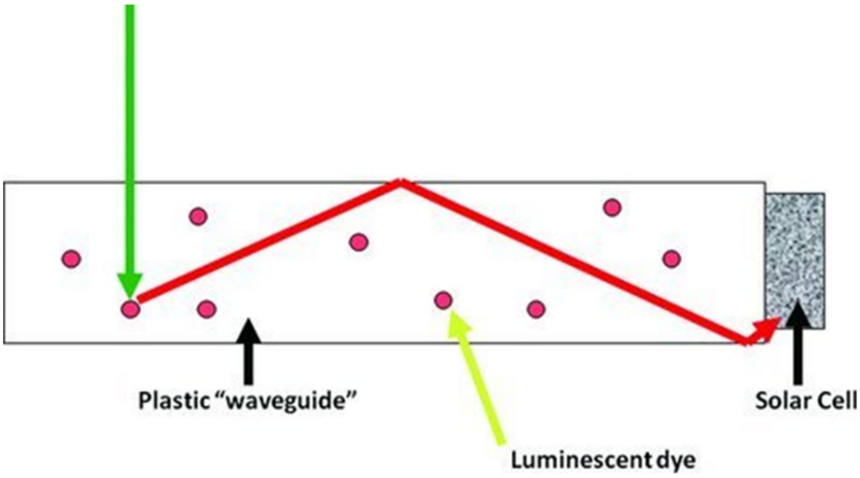

Figure 1.6 Incident short wavelength portion of the sunlight (green arrow) penetrates the waveguide and is absorbed by the luminescent molecules. Next, the light is re-emitted at a longer wavelength (red arrow) and confined by total internal reflection. Finally, the light reaches the edges of the waveguide, where the photovoltaic device exists to convert the light into electricity. Reproduced from [60].

There are several considerations for making an efficient LSC; one is that they must be able to keep the re-emitted photons 'trapped' in the waveguide, which is a function of the refractive index of the waveguide. Nevertheless, an efficient LSC involves more than photon trapping; the optical efficiency can describe it, η_{opt}, which is given by Equation 1-1[60]

$$\eta_{\mathrm{opt}} = (1-R)\, P_{\mathrm{TIR}} \cdot \eta_{\mathrm{abs}} \cdot \eta_{\mathrm{PLQY}} \cdot \eta_{\mathrm{Stokes}} \cdot \eta_{\mathrm{host}} \cdot \eta_{\mathrm{TIR}} \cdot \eta_{\mathrm{self}} \qquad \textbf{Equation 1-1}$$

where R is the reflection of the incident solar radiation from the waveguide surface; P_{TIR} is the total internal reflection efficiency; η_{abs} is the fraction of light absorbed by the dye(s); η_{PLQY} is the photoluminescent quantum yield of the chosen dye(s), which gives the emission probability of the re-emitted photons; η_{Stokes} is an indicator of the energy lost due to Stokes shift – the energy difference between the absorption and emission peaks, correlated with fluorescence; η_{host} is the transport efficiency of the confined photons through the waveguide, related to the collector's design, η_{TIR} is the efficiency related to the waveguide's geometry – absorption within the waveguide and reflection at the surfaces; and η_{self} is the transport efficiency of the re-emitted photons.[56, 60] It's worth noting that the η terms mentioned above describe efficiency with values ranging between 0 and 1.

To make LSCs of high optical efficiency, all of the different efficiencies mentioned in Equation 1-1 should be addressed. LSCs consist of two main components: the waveguide (host material) and luminescent dye(s). Host materials should fulfil several requirements to be used in LSCs. Most host matrices are polymers, primarily polymethyl methacrylate (PMMA) and polycarbonate (PC).[60] Such polymers are widely used because they are easily prepared and possess good optical transmission of photons in the visible region. Polymers facilitate the total internal reflection of the re-emitted luminescence with a refractive index of 1.5–1.6, which would minimise any losses caused by the waveguide, the refractive indices of PMMA and PC are 1.49 and 1.59, respectively.[61, 65] Polymeric matrices have disadvantages; in some cases, they become an active component and absorb the incident photons, contributing to losses in the LSC, and they suffer from degradation and limited photostability upon prolonged exposure to ultraviolet radiation.[60, 66] Organic-inorganic hybrid matrices provide an exciting alternative to the conventional polymers: in addition to their suitable refractive index they also provide enhanced stability due to the inorganic component (glasses).[65, 67] Environment-friendly alternatives to conventional polymers are also considered, to serve as a host material for LSCs application.[68]

The luminescent dye deserves special consideration; it is, after all, the essential part of LSCs. It performs the primary purpose of spectral conversion, harvesting the short wavelength photons and converting them into longer wavelengths. Optical efficiency is critical for an excellent LSC output; therefore, several requirements ensure an excellent optical efficiency. The ideal luminescent dye should exhibit a wide absorption window, especially in the ultraviolet and visible region below 550 nm; it should have a high molar absorption coefficient and a large Stokes shift (minimal overlap between the absorption and emission bands) to minimise the losses due to reabsorption; it should have close to unity efficiency of fluorescence, η_{PLQY} (high quantum yield) the energy of the re-emitted photons ought to match the optimal spectral response of the coupled photovoltaic device; it should have good thermal and photostability; and it should be soluble in the host matrix.[60, 61, 69]

Since the invention of LSCs, organic dyes have been considered suitable candidates due to their good photostability, high quantum yields, and high absorption coefficients.[69] Rhodamine 6G, for example, was used in the early stages of this application.[52] Bipyridines,[70] perylenes,[71] also coumarins, naphthalimides,[60, 61], and Lumogen F dyes have been used in LCSs.[72] The dye that has been particularly examined in LSCs application is the perylene bisimide dye, known as Lumogen Red 305, as it has a high quantum yield (97%) in PMMA, is flexible, has good photostability, and has red emission where silicon solar cells have the highest response.[69, 73-75] However, there are limits to organic dyes, primarily that they have small Stokes shifts, leading to losses due to re-absorption, and aggregation-caused quenching of fluorescence.[69]

Inorganic quantum dots (QDs) were also proposed as an alternative to organic emitters for LSCs application.[76] Their advantages stem from the tunability of its absorption and emission spectra by a combination of material design, high quantum yield, and good stability.[77] For example, CdS quantum dots have exhibited high quantum yield (>95%) with large Stokes shift,[76] but they do have toxicity issues as a result of the metals used in conventional QDs, such as Cd or Pb.[78, 79] Other challenges might come from the difficulties in physically incorporating QDs within the waveguides.[73]

1.4.2 Luminescent Down-Shifting Layers

Luminescent down-shifting layers were first developed in the late 1970s as a result of the research on LCSs.[45, 52, 56] Hovel and co-workers were the first to apply a planar luminescent sheet on the top of a solar panel.[45, 48] Instead of concentrating the emitted photons to the attached PV devices at the edges, the LDS layer shifts and converts the high energy portion of the incident light before it reaches the top of the PV device, as shown in Figure 1.7.[45, 47] As a result of the down-shifting, the emitted photons will be well-matched with the PV device's spectral response, thus enhancing the EQE as more electron-hole pairs are produced.[45, 47] The benefit of LDS layers is not limited exclusively to enhancing solar cells' efficiency, but it can also serve as a protective layer against the harmful photons of the ultraviolet region, leading to PV devices with an extended lifetime and stability.[80, 81] The same requirements for the luminescent dyes and the host matrices in LSCs can be applied to LDS layers.

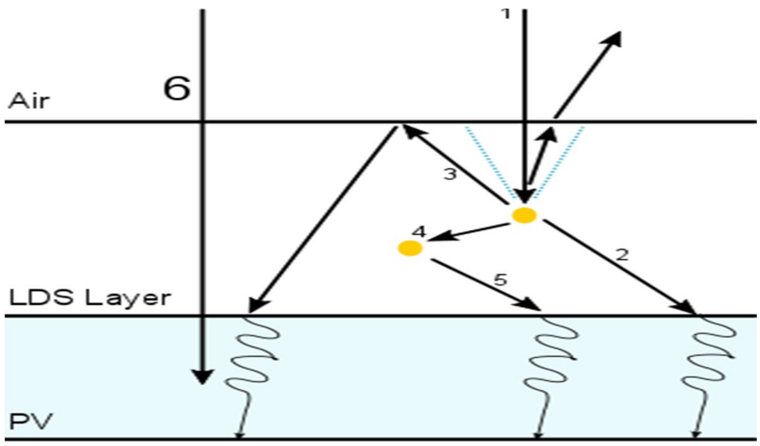

Figure 1.7 shows the working principle of the LDS layer on the top of a PV device. A luminescent dye (in yellow) absorbs a portion of incident light (1). It will re-emit its longer wavelengths either directly (2) or it reaches the PV device following total internal reflection (3), or it can be reabsorbed by the neighbouring molecules (4) and re-emitted again (5). The portion of the light that is out of absorption bands of the luminescent dye will be transmitted directly to the PV device (6). Reflection on the surface of the LDS layer and other losses has been neglected. Adapted and modified from [45].

1.5 Using Lanthanides Complexes in Luminescent Solar Concentrators and Luminescent Down-Shifting Applications

The first practical application of lanthanides (Ln) goes back to 1891 when Carl Auer added 1% of CeO_2 to ThO_2 to obtain the incandescent gas mantle commonly known as Auer's lamp.[82, 83] Since then, lanthanides, due to their unique luminescence properties, have become a fixture in high-end products and technologies, such as smartphones, electronics, lasers, light generation and conversion, electric wind turbines and molecular biology.[49, 82, 84] Lanthanides even became a matter of national security when the U.S. government declared some of the lanthanide elements as critical materials, and they became part of the trade war between the U.S. and China.[84]

The main interest in lanthanides stems from their exceptional spectroscopic properties.[49] Due to their electronic configuration, the 4f orbitals in the trivalent lanthanide cations are occupied with electrons, generating a wealth of electronic levels.[85] One of the interesting facts about 4f orbitals in Ln^{III} is that they are shielded by 54 electrons (core electrons), notably the filled $5s^2$ and $5p^6$ subshells, which are lower in energy.[85] This fact explains the similarities in the lanthanide cations' chemical properties and accounts for their unique optical properties.[85, 86] The effects of shielding the 4f orbitals extend to the interaction with the surrounding ligands; when Ln^{III} is inserted into the chemical environment, it causes a weak crystal-field splitting, of the order of 100 cm^{-1}, which can be treated as a perturbation, limiting the metal ions from forming covalent bonding. The absence of crystal-field effects is behind the characteristic narrow and sharp bands in absorption and emission spectra of Ln^{III}.[87-89]

The unique optical properties of lanthanides make them excellent candidates for LSC and LDS layers applications. They have narrow emission bands that can be tuned depending on the metal ion: red emission in the case Eu^{III} and green in Tb^{III}. They have long-lived excited states on the scale of micro to milliseconds and, in contrast to organic dyes, a large Stokes shift is easily obtained: in some of the Eu^{III} complexes the pseudo-Stokes shift is >300 nm, minimising the reabsorption losses in LSC and LDS.[47, 49, 69 90]

According to Laporte's parity selection rule, states of the same parity cannot be connected to the electric dipole in electromagnetic radiation; as a result, the f-f transitions are forbidden.[82] Thus, lanthanides have very low molar absorption coefficients (ε) in the range 1–10 M^{-1} cm^{-1}, leading to inefficient direct excitation. This obstacle makes them unattractive as spectral converters, in terms of their harvesting abilities, even if they exhibit an excellent quantum yield, close to one in the case of the red phosphors Y_2O_3:Eu.[82]

1.5.1 Sensitisation of Lanthanide Emission – The 'Antenna' Effect

The problem of low molar absorption coefficients in lanthanides can be overcome by attaching an organic chromophore to the lanthanide ion. The organic chromophore acts as an 'antenna' to harvest the solar radiation, then transfers the energy from the excited states of the organic molecule to the metal ion, which eventually results in emission.[91] Figure 1.8 depicts a simplified scheme of the processes involved in sensitising the emission in a europium complex. The energy migration path starts with ligand-centered absorption, resulting in an excited singlet state (S_1^*), followed by intersystem crossing ($S_1^* \rightarrow T^*$, k_{ISC}) to the long-lived first excited triplet state of the ligand, from which an intermolecular energy transfer is undergone ($T^* \rightarrow Eu^{III}$, k_{ET}), to the emissive states in Eu^{III}, then the light conversion process will be completed by a europium-centred emission.[82, 91]

Since the light-harvesting occurs mainly through an organic chromophore, the ligands must be designed and tailored for this purpose. The ligands should be highly absorbing, with large molar absorption coefficients, and facilitate efficient energy transfer to the metal ion, with minimal losses, and suppress and minimise non-radiative relaxation processes of the excited lanthanide ion.[82]

The overall quantum yield of lanthanide luminescence ($\emptyset_{tot}$) is the ratio of the number of photons emitted by the metal ion to the number of photons absorbed by the ligand. Therefore, the ligand sensitisation, efficient energy transfer, and the intrinsic quantum yield of the lanthanide ion ($\emptyset_{Ln}$) must be addressed. For this reason, aromatic or hetero-aromatic ligands (highly π-conjugated systems) accompanied with high absorption coefficients and high quantum yield values are preferred. Another consideration is the energy of the first excited triplet state in the ligand, as it must be moderately above the excited state of the lanthanide ion for an efficient energy transfer and to prevent reversible transfer processes from taking place.[61, 91]

Another important consideration when it comes to ligand design is the issue of non-radiative deactivation caused by vibrational excitation of the ligands; this problem becomes more critical in the case of ions emitting in the red region, such as Eu^{III}, in which the energy gap between the excited and ground states is comparable in magnitude to the vibrational energy of high-frequency modes of bonds such as O-H, C-H, N-H, etc.[82] This can be solved by replacing hydrogen with heavier atoms through deuteration or fluorination.[61, 82]

Rare-earth ions and complexes have been investigated since the late 1970s for photovoltaic applications. Neodymium (Nd) and holmium (Ho) were among the first candidates to be considered as luminescent dyes in LSCs application.[57, 76] Neodymium, terbium, and samarium complexes are still being investigated for different solar energy conversion applications.[49, 76, 92-96] Due to their bright red emission, europium (Eu^{3+}) complexes have been used heavily in LSC and LDS devices; the red emission around 614 nm is well-matched with high spectral response in c-Si,[97] CdTe, CIGS[98, 99] and DSSC[100] solar cells. In addition to its practical use to enhance solar cell efficiency, the characteristic emission of europium which consists of a pure magnetic dipole transition can be used to calculate different photophysical parameters,[101], which will be discussed in the following chapter. A review of the literature on europium complexes will be presented in the Introduction to Chapter 4.

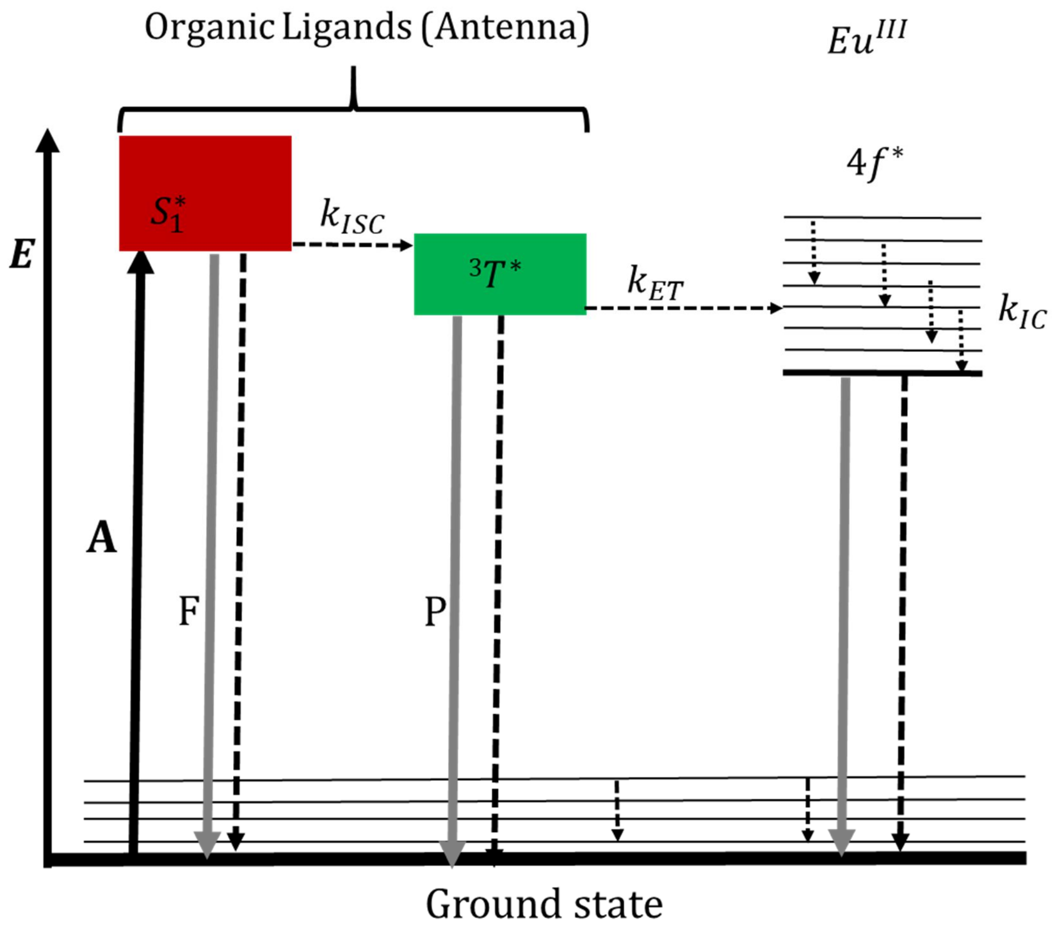

Figure1.8 depicts a simplified scheme of photophysical processes involved and the main migration path in sensitising the emission of the europium complex. Absorption (bold black arrow), non-radiative decay processes (dashed and dotted black arrows), emission (solid grey arrows). S_1^* = first singlet excited state (red box), T^* = first triplet excited state (green box), A = absorption, F = fluorescence, P = phosphorescence, k_{IC} = rate of internal conversion, k_{ISC} = rate of intersystem crossing, and k_{ET} = rate of energy transfer. Secondary migration mechanisms and back transfer processes have been omitted for clarity. Adapted and modified from [91].

1.6 Chapters Outline

Chapter 2 provides the fundamental theoretical background relevant to absorption and emission spectroscopies and energy transfer in a donor-acceptor system. It will include a brief description of the underpinning concepts for the experimental work undertaken through this thesis and the relevant equations and calculation methods used in the thesis. Chapter 3 offers a description of the practical techniques used throughout the thesis and the details for the synthesis procedures of DPEPO, $Eu(hfac)_3DPEPO$ and $Eu(tta)_3DPEPO$.

The introduction of Chapter 4 provides an overview of the use of europium β-diketonate complexes in LSCs and LDS layers, in addition to reporting the photophysical properties of $Eu(hfac)_3DPEPO$ and $Eu(tta)_3DPEPO$ both in the solution phase and when encapsulated in PMMA polymer. The photophysical investigation included quantum yield and lifetime measurements. The role that ligands (DPEPO, hfac, and tta) play in transferring energy to the europium centre will be discussed.

Chapter 5 investigates the possibility of cutting the cost of the lanthanide metal used by adding inexpensive co-dopants that can assist in light-harvesting and transferring the energy to europium complexes. The use of Förster resonance energy transfer to enhance the ultraviolet excitation of the $Eu(hfac)_3DPEPO$ and $Eu(tta)_3DPEPO$ in PMMA films co-doped with organic molecules was investigated. The commercial availability and the absorption spectra of the chosen donors, DPEPO, indole, biphenyl, and p-terphenyl, complement those of complexes that would make them helpful in harvesting high energy photons in the 250–320 nm region. The energy transfer efficiencies of the different donors were determined. Preliminary experiments of $Eu(tta)_3DPEPO$ co-doped with DPEPO on c-Si solar cells were carried out to evaluate their practical performance as spectral converters. The solar testing measurements included measuring the current density and the external quantum yield of the examined devices.

The introduction of Chapter 6 provides an overview on the role of host materials in LDS layers and LSCs, then discusses the photoactive nature of Poly(N-vinylcarbazole) (PVK) and its unique photophysical properties, such as strong absorption in the UV region, fluorescence emission and the nature of energy transfer in the PVK matrix. The use of PVK as an active host for $Eu(hfac)_3DPEPO$ and $Eu(tta)_3DPEPO$ was investigated. The energy transfer from the PVK host to europium complexes was examined, calculated, and analysed. The effect of adding co-dopant to $Eu(tta)_3DPEPO$ in the PVK matrix was assessed.

The final chapter in this thesis, Chapter 7, summarises the most important findings, presents the overall conclusions, and suggests future directions to pursue further work based upon the results shown in this thesis.

1.7 References

1. MacKay, D. J. C., *Sustainable Energy: Without the Hot Air*. UIT Cambridge, 2009.
2. Breyer, C.; Bogdanov, D.; Gulagi, A.; Aghahosseini, A.; Barbosa, L. S.; Koskinen, O.; Barasa, M.; Caldera, U.; Afanasyeva, S.; Child, M., On the role of solar photovoltaics in global energy transition scenarios. *Progress in Photovoltaics: Research and Applications* **2017,** *25* (8), 727-745.
3. World Energy Outlook 2020. IEA (2020), World Energy Outlook 2020, IEA, Paris https://www.iea.org/reports/world-energy-outlook-2020. (last accessed 20th October 2021)
4. International Energy Outlook with projection to 2040 (2016) International Energy Outlook 2016 (eia.gov) (last accessed 20th October 2021)
5. International Energy Outlook (2016) https://www.eia.gov/ outlooks/ieo/pdf /0484(2016) .pdf (last accessed 20th October 2021)
6. BP Statistical Review of World Energy 2020 (69th edition), *BP* p.l.c, London (last accessed 20th October 2021) https://www.bp.com/content/dam/bp/business-sites/en/global /corporate /pdfs/energy-economics/statistical-review/bp-stats-review-2020-full-report.pdf
7. IEA (2021), World Energy Balances: Overview, IEA, Paris. https://www.iea.org/ reports /world -energy-balances-overview (last accessed 10th August 2021).
8. Energy Consumption in the UK *Department for Business, Energy and Industrial Strategy* **2020**. 22th October 2020 https://www.gov.uk/government/statistics/energy-consumption-in-the-uk-2020 (last accessed 10th August 2021).
9. Global Energy Outlook 2020:Energy Transition or Energy Addition? *Resources for the Future*. May 20th , 2020. https://www.rff.org/publications/reports/global-energy-outlook-2020/ (last accessed 10th August 2021).
10. U.S. Energy Information Administration's International Energy Outlook 2020 (IEO2020) https://www.eia.gov/outlooks/ieo/pdf/ieo2020.pdf (accessed 10th August 2021).
11. Rapier, R. Fossil Fuels Still Supply 84 Percent Of World Energy — And Other Eye Openers From BP's Annual Review. https://www.forbes.com/sites/rrapier/2020/06/20/bp-review-new-highs-in-global-energy-consumption-and-carbon-emissions-in-2019/?sh=2e7efb4366a1 (accessed 10th August 2021).
12. Irvine, S. J. C.; Candelise, C., Chapter 1 Introduction and Techno-economic Background. In *Materials Challenges: Inorganic Photovoltaic Solar Energy*, The Royal Society of Chemistry: 2015; pp 1-26.

13. Hansen, J.; Satoa, M.; Kharechaa, P.; Beerlingc, D.; Bernerd, R.; Masson-delmottee, V.; Paganid, M.; Raymof, M.; Royerg, D. L.; Zachosh, J. C., Target Atmospheric CO_2: Where Should Humanity Aim?" The Open Atmospheric Science Journal, **2008,** *2*, *217-231*.
14. Overland, I., The geopolitics of renewable energy: Debunking four emerging myths. *Energy Research & Social Science* **2019,** *49*, 36-40.
15. Ambrose, J., UK plans to bring forward ban on fossil fuel vehicles to 2030. *The Guardian* [Online] Sep 21st **2020**. https://www.theguardian.com/environment/2020/sep/21/uk-plans-to-bring-forward-ban-on-fossil-fuel-vehicles-to-2030 (last accessed 20th October 2021)
16. Bordoff, J., Everything You Think About the Geopolitics of Climate Change Is Wrong. *Foreign Affairs* [Online] Oct 5th **2020**. https://foreignpolicy.com/2020/10/05/climate-geopolitics-petrostates-russia-china/ (last accessed 20th October 2021)
17. Vision 2030. https://www.vision2030.gov.sa/thekingdom/explore/energy/ (accessed 10th August 2021).
18. FII: KSA aims to 'be another Germany' within the renewable energy sector FII: KSA aims to 'be another Germany' within the renewable energy sector

https://www.arabnews.com/node/1801291/business-economy (accessed 10th August 2021).
19. IEA (2020), Global Energy Review 2020, IEA, Paris https://www.iea.org/reports/global-energy-review-2020 (last accessed 20th October 2021)
20. IEA (2020), World Energy Outlook 2020, IEA, Paris https://www.iea.org/reports/world-energy-outlook-2020 (last accessed 10th August 2021).
21. U.S. Consumed More Renewables Than Coal for First Time in 134 Years. *WSJ* **May 28, 2020** https://www.wsj.com/articles/u-s-consumed-more-renewables-than-coal-for-first-time-in-134-years-11590691919 (last accessed 10th August 2021).
22. IEA, Projected change in primary energy demand by fuel in 2020 relative to 2019, IEA, Paris https://www.iea.org/data-and-statistics/charts/projected-change-in-primary-energy-demand-by-fuel-in-2020-relative-to-2019 (accessed 14th January 2021).
23. Goodall, C., *The switch: How solar, storage and new tech means cheap power for all*. Profile Books: 2016.
24. Andrews, D. L. (Editor), *Energy harvesting materials. (University of East Anglia, UK)* World Scientific: 2005.
25. The International Renewable Energy Agency (IREA)- Renewable Capacity Highlights https://www.irena.org//media/Files/IRENA/Agency/Publication/2020/Mar/IRENA_RE_Capacity_Highlights_2020.pdf (last accessed 16th October 2021).

26. Hannah Ritchie and Max Roser (2020) - "Energy". Published online at OurWorldInData.org. Retrieved from: 'https://ourworldindata.org/energy' [Online] (last accessed 20th October 2021)

27. Balzani, V.; Armaroli, N., *Energy for a sustainable world: from the oil age to a sun-powered future*. John Wiley & Sons: 2011.

28. China just switched on the world's largest floating solar power plant. https://www.smithsonianmag.com/smart-news/china-launches-largest-floating-solar-farm-180963587/ (last accessed 10th June 2020).

29. Sivaram, V., *Taming the Sun: innovations to harness solar energy and power the planet*. MIT Press: 2018.

30. Chevron Is Installing Solar Panels — To Produce Oil More Cheaply. https://www.bloomberg.com/news/articles/2020-07-22/chevron-is-installing-solar-panels-to-produce-oil-more-cheaply (last accessed 10th August 2020)

31. http://www.pveducation.org/pvcdrom/appendices/standard-solar-spectra (accessed 5th June 2017).

32. Würfel, P.; Würfel, U., *Physics of solar cells: from basic principles to advanced concepts*. John Wiley & Sons: Weinheim, 2016.

33. http://www.pveducation.org/pvcdrom/2-properties-sunlight/air-mass. (last accessed 20th October 2021)

34. http://www.pveducation.org/pvcdrom/appendices/standard-solar-spectra (last accessed 6th June 2017).

35. Section 10 - Solar. In *Handbook of Energy*, Cleveland, C. J.; Morris, C., Eds. Elsevier: Amsterdam, 2013; pp 405-450.

36. Bullard, N., The Energy Revolution That Started in 1954 Is Reaching Its Crescendo. *Bloomberg* 24 April 2020. https://www.bloomberg.com/news/articles/2020-04-23/the-energy-revolution-that-started-in-1954-is-reaching-its-crescendo (last accessed 10th August 2020)

37. Solar is now 'cheapest electricity in history', confirms IEA. *CarbonBrief* **13 October 2020**. https://www.carbonbrief.org/solar-is-now-cheapest-electricity-in-history-confirms-iea (last accessed 10th August 2020)

38. Becquerel, E., On electric effects under the influence of solar radiation. *Compt. Rend.* **1839,** *9*, 561.

39. Einstein, A., Concerning an heuristic point of view toward the emission and transformation of light. *American Journal of Physics* **1965,** *33* (5), 367.

40. Green, M. A., The path to 25% silicon solar cell efficiency: History of silicon cell evolution. *Progress in Photovoltaics: Research and Applications* **2009,** *17* (3), 183-189.

41. Green, M. A., Commercial progress and challenges for photovoltaics. *Nature Energy* **2016,** *1* (1), 15015.
42. http://solarcellcentral.com/markets_page.html#tf_mkt_share (last accessed 10th August 2020).
43. Green, M. A.; Dunlop, E. D.; Hohl-Ebinger, J.; Yoshita, M.; Kopidakis, N.; Hao, X., Solar cell efficiency tables (version 56). *Progress in Photovoltaics: Research and Applications* **2020,** *28* (7), 629-638.
44. Green, M.; Dunlop, E.; Hohl-Ebinger, J.; Yoshita, M.; Kopidakis, N.; Hao, X., Solar cell efficiency tables (version 57). *Progress in Photovoltaics: Research and Applications* **2021,** *29* (1), 3-15.
45. Klampaftis, E.; Ross, D.; McIntosh, K. R.; Richards, B. S., Enhancing the performance of solar cells via luminescent down-shifting of the incident spectrum: A review. *Solar Energy Materials and Solar Cells* **2009,** *93* (8), 1182-1194.
46. Connolly, J. P.; Mencaraglia, D., Chapter 7 III-V Solar Cells. In *Materials Challenges: Inorganic Photovoltaic Solar Energy*, The Royal Society of Chemistry: 2015; pp 209-246.
47. Huang, X.; Han, S.; Huang, W.; Liu, X., Enhancing solar cell efficiency: the search for luminescent materials as spectral converters. *Chemical Society Reviews* **2013,** *42* (1), 173-201.
48. Hovel, H. J.; Hodgson, R. T.; Woodall, J. M., The effect of fluorescent wavelength shifting on solar cell spectral response. *Solar Energy Materials* **1979,** *2* (1), 19-29.
49. Bünzli, J.-C. G.; Chauvin, A.-S., Chapter 261 - Lanthanides in Solar Energy Conversion. In *Handbook on the Physics and Chemistry of Rare Earths*, Jean-Claude, G. B.; Vitalij, K. P., Eds. Elsevier: 2014; Vol. Volume 44, pp 169-281.
50. Hierrezuelo-Cardet, P.; Palechor-Ocampo, A. F.; Caram, J.; Ventosinos, F.; Pérez-del-Rey, D.; Bolink, H. J.; Schmidt, J. A., External quantum efficiency measurements used to study the stability of differently deposited perovskite solar cells. *Journal of Applied Physics* **2020,** *127* (23), 235501.
51. Danos, L.; Parel, T.; Markvart, T.; Barrioz, V.; Brooks, W. S. M.; Irvine, S. J. C., Increased efficiencies on CdTe solar cells via luminescence down-shifting with excitation energy transfer between dyes. *Solar Energy Materials and Solar Cells* **2012,** *98*, 486-490.
52. Weber, W. H.; Lambe, J., Luminescent greenhouse collector for solar radiation. *Appl. Opt.* **1976,** *15* (10), 2299-2300.
53. Swartz, B.; Cole, T.; Zewail, A., Photon trapping and energy transfer in multiple-dye plastic matrices: an efficient solar-energy concentrator. *Optics Letters* **1977,** *1* (2), 73-75.
54. Batchelder, J. S.; Zewail, A. H.; Cole, T., Luminescent solar concentrators. 1: Theory of operation and techniques for performance evaluation. *Appl. Opt.* **1979,** *18* (18), 3090-3110.
55. Batchelder, J. S.; Zewail, A. H.; Cole, T., Luminescent solar concentrators. 2: Experimental and theoretical analysis of their possible efficiencies. *Appl. Opt.* **1981,** *20* (21), 3733-3754.

56. Goetzberger, A.; Greube, W., Solar energy conversion with fluorescent collectors. *Applied physics* **1977,** *14* (2), 123-139.
57. Levitt, J. A.; Weber, W. H., Materials for luminescent greenhouse solar collectors. *Appl. Opt.* **1977,** *16* (10), 2684-2689.
58. Chemisana, D., Building Integrated Concentrating Photovoltaics: A review. *Renewable and Sustainable Energy Reviews* **2011,** *15* (1), 603-611.
59. Wiegman, J. W. E.; van der Kolk, E., Building integrated thin film luminescent solar concentrators: Detailed efficiency characterization and light transport modelling. *Solar Energy Materials and Solar Cells* **2012,** *103*, 41-47.
60. Debije, M. G.; Verbunt, P. P. C., Thirty Years of Luminescent Solar Concentrator Research: Solar Energy for the Built Environment. *Advanced Energy Materials* **2012,** *2* (1), 12-35.
61. Congiu, M. Synthesis and Characterisation of Luminescent Lanthanide Dyes for Solar Energy Conversion. PhD Thesis, the University of Edinburgh, Edinburgh, 2013.
62. Meinardi, F.; Bruni, F.; Brovelli, S., Luminescent solar concentrators for building-integrated photovoltaics. *Nature Reviews Materials* **2017,** *2* (12), 17072.
63. Rowan, B. C.; Wilson, L. R.; Richards, B. S., Advanced Material Concepts for Luminescent Solar Concentrators. *IEEE Journal of Selected Topics in Quantum Electronics* **2008,** *14* (5), 1312-1322.
64. James L. Banal, K. P. G. a. W. W. H. W., Aggregate-induced emission chromophores for luminescent solar concentrators. *SPIE*. https://spie.org/news/6383-aggregate-induced-emission-chromophores-for-luminescent-solar-concentrators?SSO=1 (last accessed 10th August 2020)
65. Griffini, G., Host Matrix Materials for Luminescent Solar Concentrators: Recent Achievements and Forthcoming Challenges. *Frontiers in Materials* **2019,** *6* (29).
66. Pintossi, D.; Colombo, A.; Levi, M.; Dragonetti, C.; Turri, S.; Griffini, G., UV-curable fluoropolymers crosslinked with functional fluorescent dyes: the way to multifunctional thin-film luminescent solar concentrators. *Journal of Materials Chemistry A* **2017,** *5* (19), 9067-9075.
67. Reisfeld, R.; Levchenko, V.; Saraidarov, T., Interaction of luminescent dyes with noble metal nanoparticles in organic–inorganic glasses for future luminescent materials. *Polymers for Advanced Technologies* **2011,** *22* (1), 60-64.
68. Fattori, V.; Melucci, M.; Ferrante, L.; Zambianchi, M.; Manet, I.; Oberhauser, W.; Giambastiani, G.; Frediani, M.; Giachi, G.; Camaioni, N., Poly (lactic acid) as a transparent matrix for luminescent solar concentrators: a renewable material for a renewable energy technology. *Energy & Environmental Science* **2011,** *4* (8), 2849-2853.

69. McKenna, B.; Evans, R. C., Towards Efficient Spectral Converters through Materials Design for Luminescent Solar Devices. *Advanced Materials* **2017,** *29* (28), 1606491.
70. Vollmer, F.; Rettig, W., Fluorescence loss mechanism due to large-amplitude motions in derivatives of 2,2′-bipyridyl exhibiting excited-state intramolecular proton transfer and perspectives of luminescence solar concentrators. *Journal of Photochemistry and Photobiology A: Chemistry* **1996,** *95* (2), 143-155.
71. Reisfeld, R.; Eyal, M.; Chernyak, V.; Zusman, R., Luminescent solar concentrators based on thin films of polymethylmethacrylate on a polymethylmethacrylate support. *Solar Energy Materials* **1988,** *17* (6), 439-455.
72. Wilson, L. R.; Richards, B. S., Measurement method for photoluminescent quantum yields of fluorescent organic dyes in polymethyl methacrylate for luminescent solar concentrators. *Appl. Opt.* **2009,** *48* (2), 212-220.
73. Kaniyoor, A.; McKenna, B.; Comby, S.; Evans, R. C., Design and Response of High-Efficiency, Planar, Doped Luminescent Solar Concentrators Using Organic–Inorganic Di-Ureasil Waveguides. *Advanced Optical Materials* **2016,** *4* (3), 444-456.
74. Carbone, I. A.; Frawley, K. R.; McCann, M. K., Flexible, Front-Facing Luminescent Solar Concentrators Fabricated from Lumogen F Red 305 and Polydimethylsiloxane. *International Journal of Photoenergy* **2019,** *2019*, 8680931.
75. Zhang, B.; Zhao, P.; Wilson, L. J.; Subbiah, J.; Yang, H.; Mulvaney, P.; Jones, D. J.; Ghiggino, K. P.; Wong, W. W. H., High-Performance Large-Area Luminescence Solar Concentrator Incorporating a Donor–Emitter Fluorophore System. *ACS Energy Letters* **2019,** *4* (8), 1839-1844.
76. Roncali, J., Luminescent Solar Collectors: Quo Vadis? *Advanced Energy Materials* **2020,** *10* (36), 2001907.
77. Zhou, Y.; Benetti, D.; Fan, Z.; Zhao, H.; Ma, D.; Govorov, A. O.; Vomiero, A.; Rosei, F., Near Infrared, Highly Efficient Luminescent Solar Concentrators. *Advanced Energy Materials* **2016,** *6* (11), 1501913-n/a.
78. Purcell-Milton, F.; Gun'ko, Y. K., Quantum dots for Luminescent Solar Concentrators. *Journal of Materials Chemistry* **2012,** *22* (33), 16687-16697.
79. Liu, X.; Luo, B.; Liu, J.; Jing, D.; Benetti, D.; Rosei, F., Eco-friendly quantum dots for liquid luminescent solar concentrators. *Journal of Materials Chemistry A* **2020,** *8* (4), 1787-1798.
80. Fernandes, R. V.; Urbano, A.; Duarte, J. L.; Bristow, N.; Kettle, J.; Laureto, E., Tuning the optical properties of luminescent down shifting layers based on organic dyes to increase the efficiency and lifetime of P3HT: PCBM photovoltaic devices. *Journal of Luminescence* **2018,** *203*, 165-171.

81. Yang, D.; Liang, H.; Liu, Y.; Hou, M.; Kan, L.; Yang, Y.; Zang, Z., A large-area luminescent downshifting layer containing an Eu3+ complex for crystalline silicon solar cells. *Dalton Transactions* **2020,** *49* (15), 4725-4731.
82. Bünzli, J.-C. G., On the design of highly luminescent lanthanide complexes. *Coordination Chemistry Reviews* **2015,** *293–294*, 19-47.
83. SELLA, A., Auer's lamp. *Chemistry World*.[On line] Sep 23rd, 2015 https://www. chemistryworld.com/opinion/auers-lamp/8967.article (last accessed 20th October 2021)
84. Hsu, J., Don't Panic about Rare Earth Elements. *Scientific American*. [On line] May 31st, 2019 https://www.scientificamerican.com/article/dont-panic-about-rare-earth-elements/(last accessed 20th October 2021)
85. Werts, M. H. V., Making sense of Lanthanide Luminescence. *Science Progress* **2005,** *88* (2), 101-131.
86. Bunzli, J.-C. G.; Eliseeva, S. V., Intriguing aspects of lanthanide luminescence. *Chemical Science* **2013,** *4* (5), 1939-1949.
87. Electronic and Magnetic Properties of the Lanthanides. In *Lanthanide and Actinide Chemistry*, 2006; pp 61-87.
88. Eliseeva, J.-C. G. B. a. S. V., Basics of Lanthanide Photophysics. In *Lanthanide Luminescence*, Hänninen, P., Härmä, Harri, Ed. springer 2011.
89. Moore, E. G.; Samuel, A. P. S.; Raymond, K. N., From Antenna to Assay: Lessons Learned in Lanthanide Luminescence. *Accounts of Chemical Research* **2009,** *42* (4), 542-552.
90. Moudam, O.; Rowan, B. C.; Alamiry, M.; Richardson, P.; Richards, B. S.; Jones, A. C.; Robertson, N., Europium complexes with high total photoluminescence quantum yields in solution and in PMMA. *Chemical Communications* **2009,** (43), 6649-6651.
91. Bünzli, J.-C. G.; Eliseeva, S. V., Basics of lanthanide photophysics. In *Lanthanide Luminescence*, änninen, P., Härmä, Harri Ed. Springer: 2011; pp 1-45.
92. Moore, E. G.; Benaglia, M.; Bergamini, G.; Ceroni, P., Synthesis, Stability and Sensitised Lanthanide Luminescence of Heterobimetallic d/f Terpyridine Complexes. *European Journal of Inorganic Chemistry* **2015,** *2015* (3), 414-420.
93. Paul-Roth, C. O.; Lehn, J.-M.; Guilhem, J.; Pascard, C., Synthesis, Characterization, and Structural Properties of Luminescent Lanthanide Complexes. *Helvetica Chimica Acta* **1995,** *78* (8), 1895-1903.
94. de Boer, D. K.; Broer, D. J.; Debije, M. G.; Keur, W.; Meijerink, A.; Ronda, C. R.; Verbunt, P. P., Progress in phosphors and filters for luminescent solar concentrators. *Optics express* **2012,** *20* (103), A395-A405.

95. Andreiadis, E. S.; Gauthier, N.; Imbert, D.; Demadrille, R.; Pécaut, J.; Mazzanti, M., Lanthanide Complexes Based on β-Diketonates and a Tetradentate Chromophore Highly Luminescent as Powders and in Polymers. *Inorganic Chemistry* **2013,** *52* (24), 14382-14390.
96. van der Ende, B. M.; Aarts, L.; Meijerink, A., Lanthanide ions as spectral converters for solar cells. *Physical Chemistry Chemical Physics* **2009,** *11* (47), 11081-11095.
97. Fix, T.; Nonat, A.; Imbert, D.; Di Pietro, S.; Mazzanti, M.; Slaoui, A.; Charbonnière, L. J., Enhancement of silicon solar cells by downshifting with Eu and Tb coordination complexes. *Progress in Photovoltaics: Research and Applications* **2016,** *24* (9), 1251-1260.
98. Gavriluta, A.; Fix, T.; Nonat, A.; Paire, M.; Slaoui, A.; Charbonnière, L. J.; Guillemoles, J.-F., Enhancement of Copper Indium Gallium Selenide Solar Cells Using Europium Complex as Photon Downshifter. *Advanced Optical Materials* **2016,** *4* (11), 1846-1853.
99. Gavriluta, A.; Fix, T.; Nonat, A.; Slaoui, A.; Guillemoles, J.-F.; Charbonnière, L. J., Tuning the chemical properties of europium complexes as downshifting agents for copper indium gallium selenide solar cells. *Journal of Materials Chemistry A* **2017,** *5* (27), 14031-14040.
100. Zhang, L.; Wang, X.; Sun, X., Improvement of dye-sensitized solar cell performances through introducing europium dye with multiple excitation: dual enhancement in light absorption. *New Journal of Chemistry* **2019,** *43* (33), 13249-13255.
101. Binnemans, K., Interpretation of europium(III) spectra. *Coordination Chemistry Reviews* **2015,** *295*, 1-45.

CHAPTER 2: Theory

"Still and all," added Pencroff, "there's so much knowledge in the world. What a fat book could be made, Mr. Cyrus, out of everything we know!"

"And an even fatter one out of everything we don't" answered Cyrus Smith.

Jules Verne – The Mysterious Island

Theory

This chapter summarises some of the essential principles that are considered central to conducting experimental techniques and for analysing and understanding the results presented throughout this thesis. We begin by discussing the basic concepts related to electronic spectroscopy, followed by background information associated with the unique photophysics of lanthanides and energy transfer in a donor–acceptor system. Further details regarding specific spectroscopic measurements and calculations will be outlined in the appropriate experimental section of each chapter. The contents of this chapter are primarily based on the following resources: P. Atkins, de Paula, and J. Keeler[1], G.Bünzli[2], A. Gilbert and J. Baggott[3], J. Lakowicz[4], and D. Andrews[5].

2.1 Electronic Spectroscopy

Spectroscopy is associated with examining information obtained from the interaction of light with atoms and molecules. The ability of an atom or a molecule to absorb and emit light depends on its electronic and nuclear composition. The principles of quantum mechanics, through the solution of Schrödinger's Equation, constitute that each atom and molecule have discrete levels of energy, which provides them with the capacity to deduce and determine information from the interaction of matter with light.[1,3] Electronic spectroscopy, which is the focus of this thesis, deals with the transitions between the electronic energy states in molecules.

2.1.1 Absorption and Electronic Excitation

An excited-state species is created when a molecule, M, absorbs electromagnetic radiation. Equation 2.1 illustrates this process as follows:

$$M + hv \rightarrow M^{*}$$ **Equation 2-1**

where h is Planck's constant and v is the frequency of incident radiation.

The radiation absorbed by the molecule promotes an electron from its ground state (i) to the excited state (f), as shown in Figure 2.1. Transitions to higher electronic levels in a molecule are associated with changes in vibrational energy as well, leading to the formation of electronic excited states and vibrational excited states. Absorption of radiation can only occur in the case of coupling between the oscillating electric field of the incident radiation with the more mobile electrons in a molecule.

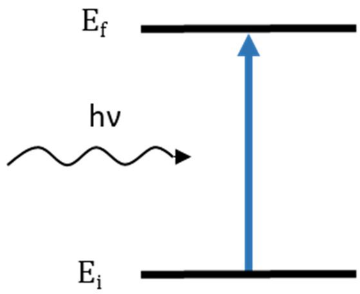

Figure 2.1 Absorption of radiation with energy, E, resulting in the excitation of a molecule from the ground state (E_i) to the excited state (E_f). The energy difference between the two energy levels is $E_f - E_i = E = h\nu$ (where h = Planck's constant and ν = frequency of the incident radiation).

Molecules, in general, follow the Born–Oppenheimer principle, which is based on the fact that nuclei have much more mass and correspond to much slower motion than electrons. This principle allows the separation of a molecular wavefunction Φ_M into two parts—nuclear and electronic.

$$\Phi_M(q, Q) \approx \psi^{elec}(q)\, \boldsymbol{\psi}^{nuc}(Q) \qquad \textbf{Equation 2-2}$$

where q and Q are labels that indicate the electron coordinates and nuclear coordinates, respectively.

Based on the molecular wavefunction in Equation 2-2, molecular energies can be expressed as the sum of three terms:

$$E = E_{elec} + E_{vib} + E_{rot} \qquad \textbf{Equation 2-3}$$

where E_{elec} is electronic energy, E_{vib} is vibrational energy, and E_{rot} is rotational energy.

In the context of lanthanides, the process of absorption only occurs through operators related to the nature of the electromagnetic radiation: the electric dipole (ED), the even-parity magnetic dipole (MD), and electric quadrupole (EQ).

A further consequence of the Born–Oppenheimer approximation establishes the basis of the Franck–Condon principle (FC), which assumes that nuclei of a molecule are fixed during electronic transitions; therefore, the transition can be represented as a vertical line when we draw the potential energy diagram, as illustrated in Figure 2.2.

The probability of electronic-vibrational (vibronic) transitions, and consequently the spectra profiles, are dictated by the Franck–Condon principle. The extent of overlap between vibrational wavefunctions in the ground and excited states determines the probability of transition. A significant overlap leads to higher absorption. In Figure 2.2, the 4-0 transition is depicted to be the most probable.

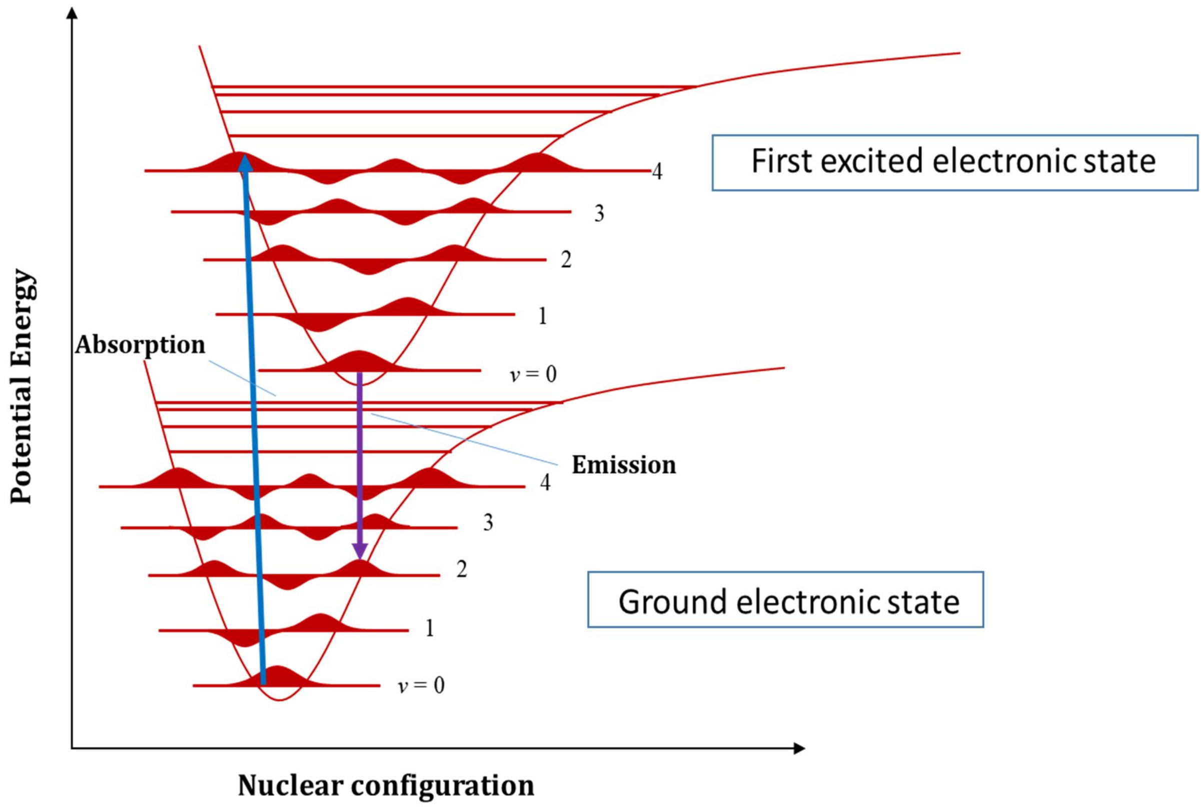

Figure 2.2 Schematic potential energy diagram, showing the electronic transitions (absorption and fluorescence) denoted by vertical arrows between the ground and excited states. The horizontal displacement (shift in nuclear configuration) of the excited electronic state potential in addition to the overlap between the ground and excited-state vibrational densities determines the difference between the maximum absorption and fluorescence energies.

Electromagnetic radiation includes perpendicular electric and magnetic fields oscillating in time. The coupling of the oscillating electric field, in particular, with the mobile electrons in a molecule leads to absorption.

To describe the size and magnitude of this interaction, and later, to establish the formulae that describe the absorption measurements, it is best to start with a formula that describes the relationship between the intensity I of light (power/unit) and the strength of electric field E:

$$I = \frac{1}{2}\, c\varepsilon_0 E^2$$ **Equation 2-4**

where c is the speed of light and ε_0 is the vacuum permittivity.

For a photon to be absorbed by a molecule, the existence of a transitional dipole moment allows the molecule to be promoted to the excited state. The dominant mechanism of coupling between the electric field and the mobile electrons requires a dipolar interaction with the electric field of light. The following equation describes this interaction

$$H_{int} = -\hat{\mu}.E$$ **Equation 2-5**

where H_{int} is the interaction operator and $\hat{\mu}$ is the ED quantum operator.

The transition dipole moment (TDM) is a transient dipole moment that exists during the process of transitioning from one state to another. To achieve a transition from the initial state with a wavefunction ψ_i to a final state with wavefunction, ψ_f, the following integral gives the value of TDM:

$$\mu_{fi} = \int \psi_f^* \cdot \hat{\mu} \cdot \psi_i dq$$ **Equation 2-6**

where ψ_f^* is the wavefunction of the final (excited) state, ψ_i is the wavefunction of the initial ground state, and dq includes the relevant spatial coordinates such as nuclear position (bond length) and the positions of all the electrons involved.[5]

TDM indicates if the transition is allowed and demonstrates the strength of an electronic transition. If the value of TDM is zero, then the probability of the transition is zero; thus, the transition is forbidden. If the TDM value is anything but zero, then the transition is allowed. It should be noted that taking the square of the TDM value determines the probability of an electronic transition to occur.

The energy of the electromagnetic radiation in the UV to the visible region, which is within the scope of this thesis, corresponds to the transitions between electronic energy levels leading to electronic excitation. Thus, the absorption measurements are carried out using UV-Vis spectrometry.

2.1.1.1 Absorption Measurement

The underlying theoretical framework of measuring the absorption of a photon by a single molecule can be traced to Fermi's golden rule, which is a well-known formula in theoretical physics. The following equation describes the rate, Γ, of photon absorption by a molecule from the initial state$|i\rangle$ to a set of final states $|f\rangle$:

$$\Gamma_{i\to f} = \frac{2\pi}{\hbar}\ |\langle f|H_{int}|i\rangle|^2\ \ \rho, \qquad \textbf{Equation 2-7}$$

where ħ is the reduced Plank constant ($h/2\pi$), and ρ is the density of states.

From the above Equations (2-5),(2-6), and (2-7), it is clear that a relationship exists between the intensity of light passing and the square of TDM and the square of the electric field. It is also evident from Equation (2-8) that the loss of intensity rate upon travelling through an absorbing medium is proportional to the concentration of absorbing species, C. Therefore, we can get the differential form of the Beer-Lambert law:

$$-\frac{dI}{dz} = \alpha IC \qquad \textbf{Equation 2-8}$$

where $\frac{dI}{dz}$ is the rate of change of intensity along propagation z, α is the absorption coefficient, a value related to the density of the states and the square of transition moment, and I is the instantaneous intensity.

Solving this differential equation will result in an exponential decay function - the integral form of the Beer-Lambert law (Equation 2-9). The intensity of an absorption transition can be experimentally determined, as shown in Equations (2-9 and 2-10).

$$I = I_0 e^{-\alpha Cl} \qquad \textbf{Equation 2-9}$$

where l is the path length.

The product of αCl can be given by the symbol A, the absorbance of the sample, and it is related to the transmittance $T = I/I_0$. Expressing the above equation in logarithmic form makes it more accessible in terms of calculations.

$$A = log_{10}\left(\frac{I_0}{I}\right) = \boldsymbol{\varepsilon c l} \qquad \textbf{Equation 2-10}$$

where $\varepsilon = \alpha/2.303$ and is referred to as the molar absorption coefficient.

The molar absorption coefficient is an intrinsic molecular property that can be experimentally obtained. The molar absorption coefficient is the degree to which a molecule absorbs light at a specific wavelength and can be related to the TDM. Consequently, a connection between experimental electronic spectroscopy and quantum mechanics can be established.

2.2 Excited-state Decay Processes

Following the absorption of electromagnetic radiation, the excited-state population decays back to the ground state. Two types of decay processes exist; radiative decay transitions and non-radiative decay transitions. Radiative decay transitions (or luminescence) involve the emission of light (e.g., fluorescence or phosphorescence). Non-radiative decay transitions do not involve light emission but involve the loss of energy as heat.

The differences between fluorescence and phosphorescence depend on whether the transitions are allowed or forbidden. The possibility of a transition to be allowed is governed by the spin multiplicity, which states that spin must be conserved in the course of an electronic transition. The spin multiplicity is given by 2S+1, where S is the total spin quantum number. In the case of a singlet state, a molecule with all spin paired electrons possesses S = 0, and the spin multiplicity has a value of 1; hence, the word 'singlet' is used.

However, a molecule with two unpaired electrons possesses S = 1. Consequently, the spin multiplicity has a value of 3; thus, the state is called the triplet state. Transition is allowed if the electron is in the excited state in which the spin of the excited-state electron is paired (antiparallel) to the electron in the ground state. However, if the spin of the excited electron becomes parallel to the electron in the ground state, this transition is forbidden.

The intramolecular photophysical processes leading to the decay of the excited state are illustrated in the following Jablonski diagram (Figure 2.3).

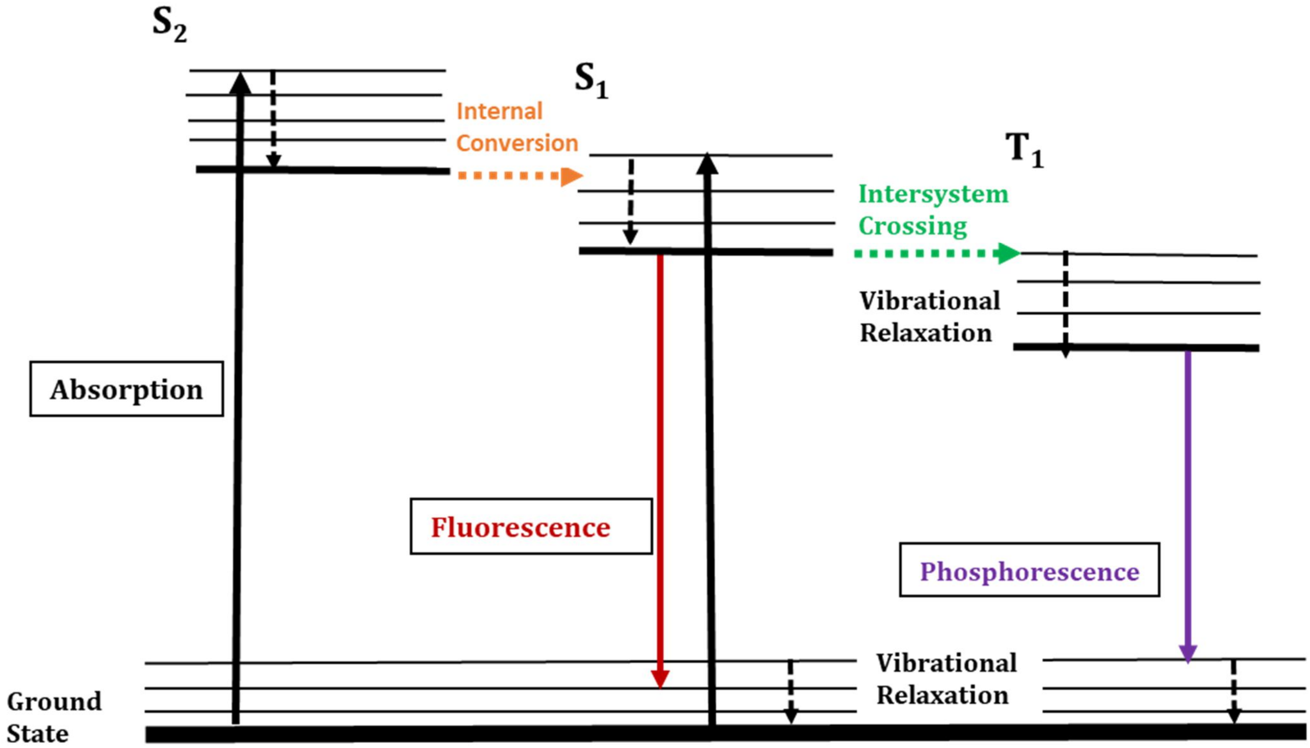

Figure 2.3 A simplified Jablonski diagram illustrates radiative (vertical lines) and non-radiative (horizontal lines) processes in the excited states. The transitions shown are absorption (solid black line), fluorescence (solid red line), phosphorescence (solid purple line), vibrational relaxation (dashed black lines), internal conversion (dotted orange line), and intersystem crossing (dotted green line).

2.2.1 Fluorescence and Phosphorescence

In the Jablonski diagram, S_1 and S_2 represent the first and second excited singlet electronic states, respectively; T_1 is the lowest energy excited triplet state. In the case of fluorescence, an electron in the first excited state S_1 relaxes via vibrational relaxation (dotted vertical lines). When excitation occurs to higher excited levels, i.e. the second excitation singlet level, an electron in the second excited state S_2 relaxes via vibrational relaxation (dotted vertical lines) then undergo internal conversion (dotted orange line) to S_1. Following this step, the excited molecule returns to the electronic ground state, thus emitting a photon (fluorescence). Intersystem crossing (ISC) (dotted green line) from the first singlet excited state is the process whereby (T_1) becomes populated.

It is worth mentioning, in molecules, the rate constant of internal conversion (IC) and vibrational relaxation is much greater than the rate of emission from (S_1 or T_1) to the ground singlet state. This is described best by Kasha's rule (attributed to Michael Kasha), which states that the energy of emission does not depend on which electronically excited state is initially excited and that emission always occurs from the lowest electronic excited level of a given spin multiplicity.[6]

Although emission occurs solely from the lowest excited state, emission spectra cover a wide range of wavelengths because of transitions to multiple vibrational energy levels in the ground state. In addition, IC and vibrational relaxation to the lowest excited state also leads to an energy difference between the absorbed and emitted photons. Thus, the emitted photon has lower energy. The difference in wavenumber or wavelength between the absorption peak and the emission peak is referred to as the Stokes shift.

Since fluorescence occurs from the emitting state of the same multiplicity, which is in the ground state, the transition is spin-allowed. Thus, the fluorescence is an intense transition and occurs at fast rates; typically, it occurs in the picosecond (10^{-12} s) to microsecond (10^{-6} s) timescales.

In contrast, phosphorescence is the radiative transition that occurs when the excited electron decays back from an excited state that is different from that of the ground state in terms of spin multiplicity, such as the transition from the first excited triplet state (T_1) to the ground singlet state (S_0). Consequently, phosphorescence occurs at longer wavelengths. Because this is a spin-forbidden transition, phosphorescence cannot be observed. In the presence of a heavy atom, phosphorescence as transition becomes partially allowed; however, the transition itself is not as intense as fluorescence. Compared with the fast transitions observed in fluorescence, phosphorescence occurs less rapidly; typical timescales range from the millisecond (10^{-3} s) to second.

2.2.2 Non-Radiative Decay

Intramolecular non-radiative decay occurs by vibrational relaxation, IC, and intersystem crossing (shown as dotted lines in Figure 2-3). IC involves the conversion between states of the same multiplicity; on the other hand, intersystem crossing involves conversion between states of different multiplicity. Non-radiative decay also occurs because of intermolecular interactions, described by the general term fluorescence quenching. Various types of intrmolecular interactions, such as electronic energy transfer from a donor to an acceptor, can cause quenching.

2.3 Quantum Yield and Lifetime

The luminescence lifetime is defined by the decay kinetics of the excited state. The overall rate of decay of a populated excited state can be described by considering radiative processes and non-radiative processes (IC, ISC, quenching, etc.). A population of excited-state molecules, [M*], decays according to the following equation:

$$-\frac{d[M^*]}{dt} = (k_r + k_{nr})[M^*] \qquad \textbf{Equation 2-11}$$

where k_R and k_{NR} are the radiative and non-radiative rate constants of the decay transitions, respectively.

If we define k as the sum of the rate constants for radiative and non-radiative decay processes ($k = k_r + k_{nr}$), and integrate Equation 2-11, we get an expression for the concentration of the excited-state population as a function of time

$$[M^*](t) = [M^*]_0 e^{-(\mathrm{k}t)} \qquad \textbf{Equation 2-12}$$

where $[M^*]_0$ is the concentration of M^* at t = 0.

The property observed during fluorescence experiments is the fluorescence intensity, I, which is related to the excited-state population:

$$I(t) = I_0 e^{\frac{-t}{\tau}} \qquad \textbf{Equation 2-13}$$

where I_0 is the intensity of fluorescence at t = 0 (= $k_R[M^*]_0$), and τ = $(1/k)$ is the lifetime of the excited-state population, known as the fluorescence lifetime. Equation 2-13 relates observable intensity to the fluorescence lifetime and determines the lifetime experimentally.

From emission spectroscopy, we can measure the parameter that quantifies the efficiency of the luminescence process, which is the total quantum yield (ϕ_{tot}), as defined in Equation 2-14:

$$\phi_{tot} = \frac{number\ of\ emitted\ photons}{number\ of\ absorbed\ photons} \qquad \textbf{Equation 2-14}$$

Quantum yields can also be expressed in terms of the rate constants for the radiative and non-radiative decay processes, as shown in Equation 2-15:

$$\phi_{tot} = \frac{k_r}{k_r + k_{nr}} \qquad \textbf{Equation 2-15}$$

2.3.1. Quantum Yield of Lanthanide Complexes

The photophysics of lanthanide complexes is unique because of the forbidden nature of f–f transitions. The excitation is indirect (organic ligands act as an antenna), and energy is transferred through ISC then undergo intramolecular energy transfer into the 4f levels of the lanthanide ion. Thus, the quantum yield calculation is not straightforward. The definition of the total quantum yield would become the ratio of the number of photons emitted by the metal to the number of photons absorbed by the ligand/matrix, which is the quantum yield of the Ln-centered emission upon ligand excitation, as shown in Equation 2-16:

$$\phi_{tot} = \eta\phi_{Ln}$$ **Equation 2-16**

where η, commonly referred to as sensitisation efficiency, is the efficiency of energy transfer from the ligand's excited state to the accepting Eu^{3+} ion, and ϕ_{Ln} is the quantity describing the intrinsic quantum yield of a lanthanide ion. From the equation, the value of energy transfer efficiency can be obtained if both values of total and intrinsic quantum yield are known. In the rare case of having ϕ_{Ln} that is equal to unity and 100% energy transfer efficiency, we would get an overall quantum yield of 1.

The word 'intrinsic' is used to emphasise that this is the quantum yield of the luminescence originated from the metal centre when the lanthanide ion is directly excited. It indicates the scale of the processes of non-radiative deactivation in the inner coordination sphere and outer coordination sphere of the lanthanide ion. Notably, the words 'intrinsic' and 'internal' are used interchangeably in the literature.[7]

The intrinsic quantum yield of emission of the lanthanide ion can be expressed in terms of the radiative or 'natural' lifetime τ_{rad} and the luminescence lifetime τ_{obs} or in rate constants of the de-excitation of the excited states, as shown in Equation 2-17.

$$\phi_{Ln} = \frac{\tau_{obs}}{\tau_{rad}} = \frac{k_r}{k_r + k_{nr}}$$ **Equation 2-17**

where the luminescence lifetime $\tau_{obs} = \frac{1}{k_{obs}}$ is the observed luminescence decay , which can be obtained experimentally. The luminescence rate constant k_{obs} is the sum of the radiative rate constant and the non-radiative rate constant. τ_{rad} describes the lifetime when all non-radiative deactivation processes are absent. Therefore, when the non-radiative deactivation processes are absent, the radiative lifetime equal that of the luminescence lifetime ($\tau_{rad} = \tau_{obs}$) and the value of the intrinsic quantum yield would be one; however, this scenario only occurs in very few cases.

Therefore, to determine the intrinsic quantum yield, we ought to obtain the radiative lifetime in addition to the luminescence lifetime. Calculating the radiative lifetime is a significant task; it usually requires obtaining Einstein's coefficients for spontaneous emission, which can be extracted from the Judd–Ofelt parameters.[8] However, in the particular case of europium, the radiative lifetime can be determined by applying a simplified equation that contains variables obtained from the emission spectrum.[8, 9]

According to Laporte's parity selection rule, electronic transitions of the same parity are forbidden. Therefore, f–f transitions are not allowed by the ED mechanism. However, f–f transitions are allowed by the MD mechanism and the induced or 'forced' ED mechanism.[9] MD transitions have weak intensities, and they are largely independent of the lanthanide ion's chemical surroundings. However, in contrast to MD transitions, some of the induced ED transitions are extremely sensitive to the changes in the chemical surroundings of the Eu(III) ion; one of the transitions ($^5D_0 \rightarrow {}^7F_2$) is referred to as the 'hypersensitive' transition.

In the case of the Eu^{3+} ion, the radiative lifetime can be directly calculated from the emission spectrum using the values extracted from the observed pure MD transition ($^5D_0 \rightarrow {}^7F_1$), and the total Eu^{3+} emission spectrum as, shown in Equation 2-18: [9]

$$\frac{1}{\tau_{rad}} = A_{MD,0} \cdot n^3 \left(\frac{I_{tot}}{I_{MD}}\right) \qquad \textbf{Equation 2-18}$$

where $A_{MD,0}$ is the spontaneous emission probability for MD transition *in vacuo* and is equal to 14.65 s^{-1}. I_{tot} refers to the integration of the total area of the emission spectrum from the ($^5D_0$) level to the ^7F_J manifold, and I_{MD} refers to the integrated area of emission intensity of the pure MD transition ($^5D_0 \rightarrow {}^7F_2$). n is the refractive index of the medium (the solvent or the polymer).

Notably, the radiative lifetime is not a fixed value and depends on the refractive index and the environment surrounding the lanthanide ion.[8]

2.3.2 Measuring the Total Quantum Yield

Measurements of the total luminescence quantum yield are conceptually straightforward but can be challenging to implement experimentally. In the present work, the fact that the samples are polymeric thin films will make these measurements more difficult to conduct.

There are two main methods to measure the total quantum yield. The first is the absolute method, which depends on using an integrating sphere, which is considered a state-of-the-art accessory but is not widely used.[10]

The other method is the relative (or comparative) method, in which the sample is compared to a reference (standard) with a known quantum yield. The comparative method was used to obtain all the data related to the quantum yields in this work. The relative quantum yield was calculated according to the following equation[11, 12]:

$$\phi_S = \phi_{ref} \cdot \frac{I_S}{I_{ref}} \frac{A_{ref}}{A_S} \frac{n_S^2}{n_{ref}^2} \qquad \textbf{Equation 2-19}$$

where ϕ_{S} and ϕ_{ref} are the quantum yield of the sample and the known quantum yield of a reference, respectively. I_{S} is the integrated emission spectrum of the sample, I_{ref} is the integrated emission spectrum of the reference, A_{S} is the absorbance at the excitation wavelength of the sample, A_{ref} is the absorbance at the excitation wavelength of the reference, n_S and n_{ref} are the refractive indices of the sample and reference, respectively.

The comparative method requires careful consideration of many factors to obtain accurate measurements, as shown in Equation 2-19. These factors include choosing an appropriate reference with a known quantum yield and measuring the emission from the sample and the reference under the same experimental conditions.

2.4 Energy Transfer in Donor–Acceptor Systems

The work presented in this thesis is concerned with two types of energy transfer: i) intramolecular energy transfer from the organic ligands to the emitting levels of the Eu^{3+} ion and ii) energy transfer from an external donor to the europium complexes. This section focuses on the latter.

The use of Förster resonance energy transfer to enhance ultraviolet excitation of the Eu(III) complexes in PMMA films co-doped with organic molecules was investigated in Chapter 5.

Besides the straightforward radiative energy transfer, which is a 'trivial'[13] energy transfer, in which energy transfer occurs by the acceptor's reabsorption of the emission originated from the donor, there are two primary energy transfer mechanisms, of which energy can be transferred between the acceptor and the donor systems: Dexter and Förster. Both are non-radiative processes.

A short-range electron exchange mechanism (Dexter)[14], which heavily depends on the distance, requires the orbitals of the donor and acceptor to overlap; thus, the distance between the donor and the acceptor should be less than 10 Å. In the Dexter mechanism, an exchange of electrons occurs between the excited donor and the acceptor. It is distance-dependent since the rate constant of the energy transfer exponentially decreases as the distance between the donor and acceptor increases.[13]

However, Förster resonance energy transfer (FRET) occurs over much larger distances between the donor and acceptor. [15] It is a long-range Coulombic interaction between an excited donor, say (D^*), and an acceptor (A); typical distances are in the range of 10–100 Å, which is a well-suited mechanism in the context of the system consisting of polymeric films of lanthanide complexes co-doped with organic molecules. The mechanism involves electrostatic interaction of similar energy transitions dipoles in (D^*) and (A); therefore, it is a Coulombic energy transfer mechanism. The following equation can illustrate it:

$$D^* + A \rightarrow D + A^* \qquad \textbf{Equation 2-20}$$

where the asterisk denotes an electronic excited state. Theoretically, it can be based on the donor as an oscillating dipole exchange energy with an acceptor (an oscillating dipole with comparable resonance energy).

The rate constant of energy transfer, k_{ET}, for a single donor and acceptor separated by distance, r, depends on multiple factors such as the distance between D and A, the donor lifetime τ_0 in the absence of the acceptor:[13]

$$k_{ET} = \left(\frac{1}{\tau_0}\right)\left(\frac{R_0}{r}\right)^6 \qquad \textbf{Equation 2-21}$$

where R_0 (Förster distance) is the critical distance for energy transfer between the donor and acceptor at which the rate of fluorescence (radiative decay) from the donor is equal to the competing energy transfer to the acceptor. R_0 is expressed by the following Equation:[4]

$$R_0 = 9.78 \times 10^3 (\kappa^2 . \emptyset_D . n^{-4} . J(\lambda))^{1/6} \quad (\text{in Å}) \qquad \textbf{Equation 2-22}$$

where $\emptyset_D$ is the quantum yield of donor emission determined in the absence of acceptor. κ^2 is the term that describes the orientations of the transitions of dipoles of the acceptor and the donor. n is the refractive index of the medium (solvent/polymer). $J(\lambda)$ is the spectral overlap integral of the emission spectrum of the donor and the absorption spectrum of the acceptor.

According to Swartz et al.[16], who investigated the energy transfer in multiple-dye planer luminescent solar concentrators, Förster theory can also give the critical concentration of the acceptor $C_0(A)$, as illustrated in the following equation:

$$C_0(A) = 8.35 \times 10^{-3} {N_0}^{-1} {R_0}^{-3}$$ **Equation 2-23**

where N_0 is the Avogadro's number.

An efficient Förster energy transfer mechanism can manifest itself in reducing the fluorescence intensity of the donor, decreasing the donor's lifetime, and enhancing the fluorescence intensity of the acceptor.

In summary, the rate of energy transfer in the Förster mechanism depends on the high value of the donor quantum yield, the well-matched relative orientation of the donor and acceptor dipole moments, and the optimum distance between the donor and acceptor. Furthermore, the spectral overlap between the emission of the donor and the absorption of the acceptor is fundamental to having an efficient resonance energy transfer mechanism.

2.4.1 Calculating the Energy Transfer in the Donor–Acceptor System

To experimentally determine the energy transfer efficiency for a system consisting of a donor–acceptor system, where we have one or more excitation energy donors, we must consider the direct excitation of the acceptor (organic ligands in the europium complex) in the absence of donor(s) and excitation of the donor(s) followed by transfer of energy to the acceptor. The equations (below) that describe the energy transfer efficiency in this work were based on the work of Da-Guang Xu and T.M. Nordlund.[17]

$A_a(\lambda_{ex}),\ A_d(\lambda_{ex}), and\ A_{tot}(\lambda_{ex})$ are the absorbance of the acceptor in the absence of the donor, the absorbance of the donor alone, and total absorbance (acceptor + donor), respectively. If the acceptor in the absence of donor is directly excited at a wavelength λ_a (at 340 nm, in the case of Eu(tta)$_3$DPEPO), the measured fluorescence intensity would be

$$F_a(\lambda_a) = \Delta\, I_a(\lambda_a)\emptyset_0$$ **Equation 2-24**

where $\Delta I_a(\lambda_a)$ is the number of photons per second absorbed by the acceptor, and $\emptyset_0$ is the normal fluorescence quantum yield that was obtained under suitable sample conditions.

When the donor is exclusively excited (e.g., at 250-275 nm in the case of the donors used in this work), which transfers energy to the acceptor with average efficiency $\eta_{D-A}(\lambda_d)$, the measured intensity of fluorescence would be

$$F_d(\lambda_d) = \Delta I_d(\lambda_d)\, \eta_{D-A}(\lambda_d)\, \emptyset_0 \qquad \textbf{Equation 2-25}$$

When the acceptor and the donor are both excited at a specific wavelength (λ_{ex}), the measured intensity of fluorescence would be

$$F_{tot}(\lambda_{ex}) = \left(\frac{A_a\,(\lambda_{ex})}{A_{tot}\,(\lambda_{ex})} + \frac{A_d\,(\lambda_{ex})}{A_{tot}\,(\lambda_{ex})}\,\eta_{D-A}(\lambda_{ex})\right) \Delta I(\lambda_{ex})\emptyset_0 \qquad \textbf{Equation 2-26}$$

where $\Delta I(\lambda_{ex})$ is the total number of photons absorbed per second. Notably, $\Delta I_a = (\frac{A_a}{A_{tot}})\Delta I$ and $\Delta I_d = (\frac{A_d}{A_{tot}})\Delta I$. Since

$$F_a(\lambda_{ex}) = \frac{A_a\,(\lambda_{ex})}{A_{tot}\,(\lambda_{ex})} \Delta I(\lambda_{ex})\emptyset_0 \qquad \textbf{Equation 2-27}$$

Then,

$$\Delta I(\lambda_{ex})\emptyset_0 = F_a(\lambda_{ex}) \frac{A_{tot}\,(\lambda_{ex})}{A_a\,(\lambda_{ex})} \qquad \textbf{Equation 2-28}$$

By rearranging the term $\Delta I(\lambda_{ex})\emptyset_0$ in Equation 2-27 with Equation 2-28, we get

$$F_{tot}(\lambda_{ex}) = \left(\frac{A_a\,(\lambda_{ex})}{A_{tot}\,(\lambda_{ex})} + \frac{A_d\,(\lambda_{ex})}{A_{tot}\,(\lambda_{ex})}\,\eta_{D-A}(\lambda_{ex})\right) F_a(\lambda_{ex}) \frac{A_{tot}\,(\lambda_{ex})}{A_a\,(\lambda_{ex})} \qquad \textbf{Equation 2-29}$$

The equation can be rearranged to obtain $\eta_{D-A}(\lambda_{ex})$

$$\eta_{D-A}(\lambda_{ex}) = \left\{\left(\frac{F_{tot}\,(\lambda_{ex})}{F_a\,(\lambda_{ex})} . \frac{A_a\,(\lambda_{ex})}{A_{tot}\,(\lambda_{ex})}\right) - \frac{A_a\,(\lambda_{ex})}{A_{tot}\,(\lambda_{ex})}\right\} \frac{A_{tot}\,(\lambda_{ex})}{A_d\,(\lambda_{ex})} \qquad \textbf{Equation 2-30}$$

$$\eta_{D-A}(\lambda_{ex}) = \frac{F_{tot}\,(\lambda_{ex})}{F_a\,(\lambda_{ex})} \frac{A_a\,(\lambda_{ex})}{A_d\,(\lambda_{ex})} - \frac{A_a\,(\lambda_{ex})}{A_d\,(\lambda_{ex})} \qquad \textbf{Equation 2-31}$$

Then, we can arrive at the equation used in this work to calculate the average energy transfer efficiency from the donors to the europium complexes.

$$\eta_{D-A} = \frac{A_a\,(\lambda_{ex})}{A_d\,(\lambda_{ex})}\left(\frac{F_{tot}\,(\lambda_{ex})}{F_a\,(\lambda_{ex})} - 1\right) \qquad \textbf{Equation 2-32}$$

This equation deals with the case in which there is unavoidable absorption by the acceptor at the wavelength used to excite the donor.

2.5 References

1. Atkins, P.; de Paula, J.; Keeler, J., *Atkins' Physical Chemistry 11e*. Oxford University Press UK: 2018.
2. Bünzli, J.-C. G.; Eliseeva, S. V., Basics of Lanthanide Photophysics. In *Lanthanide Luminescence: Photophysical, Analytical and Biological Aspects*, Hänninen, P.; Härmä, H., Eds. Springer Berlin Heidelberg: Berlin, Heidelberg, 2011; pp 1-45.
3. Gilbert, A.; Baggott, J. E., *Essentials of molecular photochemistry*. *Wiley-VCH, Weinheim, 1991.*
4. Lakowicz, J. R., *Principles of fluorescence spectroscopy*. Springer science & business media: 2010.
5. Andrews, D. L., *Molecular photophysics and spectroscopy*. Morgan & Claypool Publishers: 2014.
6. Kasha, M., Characterization of electronic transitions in complex molecules. *Discussions of the Faraday Society* **1950,** *9* (0), 14-19.
7. Wong, K.-L.; Bünzli, J.-C. G.; Tanner, P. A., Quantum yield and brightness. *Journal of Luminescence* **2020,** *224*, 117256.
8. Aebischer, A.; Gumy, F.; Bünzli, J.-C. G., Intrinsic quantum yields and radiative lifetimes of lanthanide tris(dipicolinates). *Physical Chemistry Chemical Physics* **2009,** *11* (9), 1346-1353.
9. Werts, M. H.; Jukes, R. T.; Verhoeven, J. W., The emission spectrum and the radiative lifetime of Eu 3+ in luminescent lanthanide complexes. *Physical Chemistry Chemical Physics* **2002,** *4* (9), 1542-1548.
10. Levitus, M., Tutorial: measurement of fluorescence spectra and determination of relative fluorescence quantum yields of transparent samples. *Methods and applications in fluorescence* **2020,** *8* (3), 033001.
11. Würth, C.; Grabolle, M.; Pauli, J.; Spieles, M.; Resch-Genger, U., Comparison of Methods and Achievable Uncertainties for the Relative and Absolute Measurement of Photoluminescence Quantum Yields. *Analytical Chemistry* **2011,** *83* (9), 3431-3439.
12. FluoroMax-3 & FluoroMax-P with FluorEssence - Operation and Maintenance. Horiba-Jobin-and Yavon Inc. New Jersey.
13. Bushby, L. M. Photochemistry and photophysics of lanthanide complexes. PhD Thesis, Durham University, 2001.
14. Dexter, D. L., A Theory of Sensitized Luminescence in Solids. *The Journal of Chemical Physics* **1953,** *21* (5), 836-850.
15. Főrster, T., 10th Spiers Memorial Lecture. Transfer mechanisms of electronic excitation. *Discussions of the Faraday Society* **1959,** *27* (0), 7-17.
16. Swartz, B. A.; Cole, T.; Zewail, A. H., Photon trapping and energy transfer in multiple-dye plastic matrices: an efficient solar-energy concentrator. *Opt. Lett.* **1977,** *1* (2), 73-75.

17. Xu, D.-G.; Nordlund, T. M., Sequence dependence of energy transfer in DNA oligonucleotides. *Biophysical Journal* **2000,** *78* (2), 1042-1058.

CHAPTER 3: Experimental

"Every science must devise its own instruments. The tool required for philosophy is language. Thus, philosophy redesigns language in the same way that, in a physical science, pre-existing appliances are redesigned."

Alfred N. Whitehead – Process and Reality

CHAPTER **3**

Experimental

This chapter will describe the main experimental techniques used throughout this thesis, such as absorption spectroscopy, steady-state fluorescence spectroscopy, and luminescence lifetime. The synthesis of the ligand DPEPO, $Eu(tta)_3DPEPO$, and $Eu(hfac)_3DPEPO$ is reported as well. Further details regarding the experimental discussion will be included in the following chapters.

3.1 Instrumentation

3.1.1 UV-Vis Absorption Measurements

A Varian Cary 300 UV-Vis spectrometer was used to obtain the UV-visible absorption spectra of the solution-phase samples. The spectrometer was operated in double-beam mode, and the samples were contained in 10 mm-path-length fused silica cuvettes (Starna Scientific Ltd). All solution-phase measurements were conducted at room temperature. The absorption spectra of the thin films deposited on 25 mm x 25 mm x 1mm quartz slides (Agar Scientific Ltd) were measured using a Jasco V-670 spectrophotometer with SpectraManager™ software in single-beam mode at room temperature. In the solution-phase and solid-phase measurements of the europium complexes and organic ligands, a baseline was taken by subtracting the absorption spectra of the solvent or the polymer, respectively.

3.1.2 Steady-State Fluorescence

A FluoroMax 3P spectrofluorometer (Horiba Jobin Yvon) was used for the steady-state measurements. FluorEssence™ software v.3.5. was used to control the spectrofluorometer. The solution-phase measurements were conducted at room temperature, with solutions contained in a 10 mm-path-length fused silica cuvette (Starna Scientific Ltd).

Figure 3.1 shows a schematic representation of the FluoroMax spectrometer. The excitation source in FluoroMax 3P is an ozone-free Xenon arc lamp. The fluorometer is equipped with modified Czerny-Turner monochromators in the excitation and emission positions. Both monochromators have a groove density of 1200 grooves/mm; the grating disperses light from 200–900 nm. Also, each monochromator has a slit width that can be adjusted to control the bandpass as well as the intensity of the light. In this work, the excitation and emission slit width was kept to 3 nm to avoid saturation of the detector in the solution-phase measurements.

The excitation slit width was increased to 15 nm for the solid-state measurements, and the emission slit width was kept at 3 nm. Upon excitation, a beam splitter directed ~8% of the excitation light to the reference photodiode. The reference photodiode monitors the output of the Xenon lamp, correcting the wavelength dependence of the lamp intensity.[1, 2] The ratio of the fluorescence signal to the lamp reference signal is used. The spectra presented throughout this thesis have been corrected accordingly. In addition, to cut off undesirable second emissions from the monochromators, an optical filter was used.

The excitation light is directed toward a monochromator for solution-phase measurement, and the selected wavelength is focused through the sample solution. The emission from a sample is collected at a 90-degrees angle to the excitation source. Photon emitted passes through an emission monochromator, and the dispersed emission is monitored by a photomultiplier detector operating in photon counting mode.

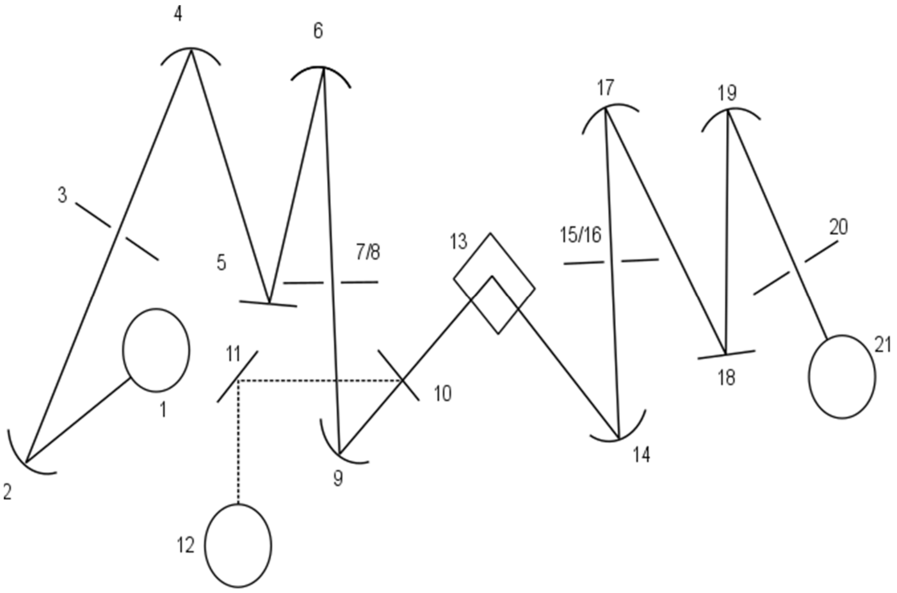

1. Ozone-free xenon lamp
2. Collection mirror (excitation)
3. Entrance slit (excitation)
4. Collection mirror (excitation)
5. Grating
6. Focusing mirror (excitation)

7/8. Excitation slit/shutter
9. Collection mirror (excitation)
10. Beam splitter
11. Deflection mirror (reference)
12. Photodiode reference detector
13. Sample position

14. Sample collection mirror
15/16. Emission shutter/slit
17. Collection mirror (emission)
18.Grating
19. Focusing mirror
20. Exit slit
21. Photomultiplier tube

Figure 3.1 Schematic representation of the FluoroMax spectrometer (reproduced from [3])

For the solid-state measurements, thin films consisting of europium complexes in polymeric matrices were spin-coated on quartz slides. They were characterized using a different approach than the solution-phase measurements. Two optical fibres (HORIBA RSU246-1-SQ) attached to the FluoroMax 3P were used to convey light to and from the FluoroMax spectrometer. In order to measure the emission/excitation spectra and lifetimes, a sample mould was 3D-printed, with the sample mounted and inserted into a fixed slot, as shown in Figure 3.2. The fibre optics can be attached at a fixed angle and kept at a certain distance from the studied sample; by using this sample mould, any change in the intensity of the excitation or the emission spectrum could only be attributed to a change in the sample itself and thus ensuring the precision and reproducibility of the measurements.

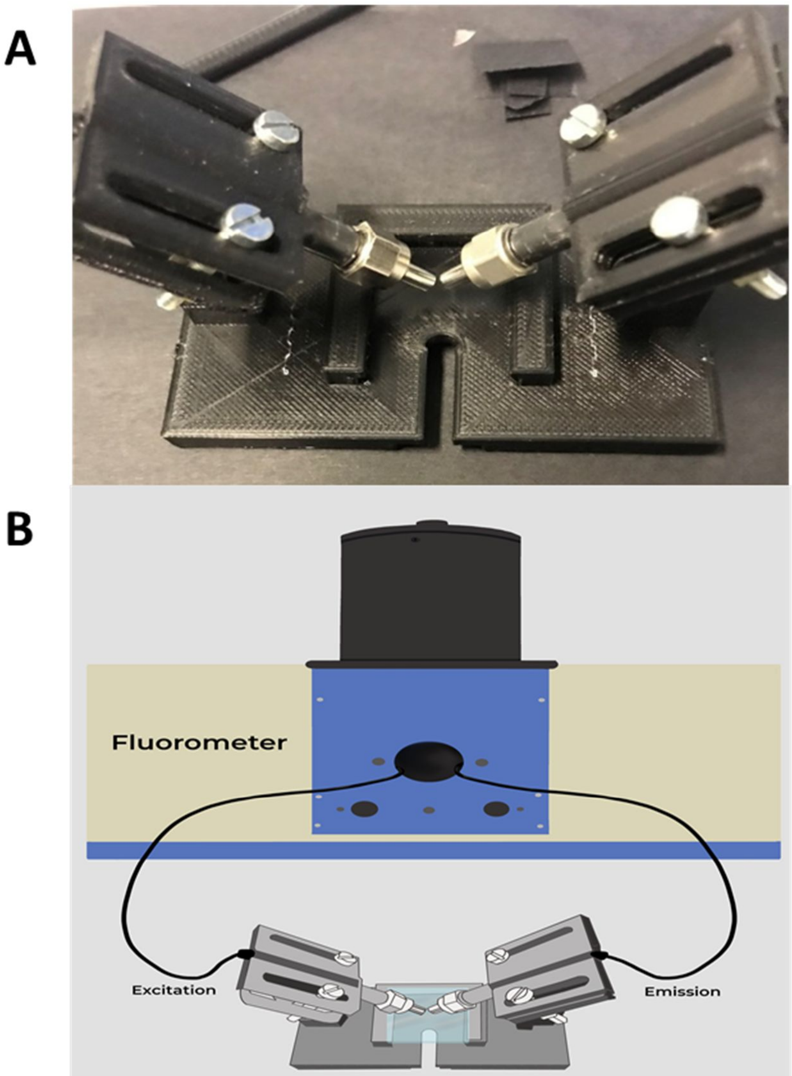

Figure 3.2 A) a photo of the sample mould obtained through 3D printing with optical fibres, B) a graphic representation of the sample mould with optical fibres attached to the FluoroMax 3P spectrometer used for solid-state measurements.

3.1.3 Luminescence Lifetime

The FluoroMax 3P spectrofluorometer has a second source of illumination, a pulsed Xenon lamp, used for phosphorescence measurement. The samples were excited with a pulse light, and an R928P photon-counting detector detected the phosphorescence. According to the manufacturer of the FluoroMax 3P spectrofluorometer: '*The flash lamp operates at up to 25 Hz. The control module triggers each lamp pulse. When the start of the light output is detected, a signal is sent to the control module for timing purposes[..] A typical sequence of data acquisition starts with a flash from the pulsed lamp, sensed by the control module as time t = 0. The light enters the excitation monochromator, where it is dispersed. Monochromatic light from the monochromator excites the sample. Luminescence emission from the sample then passes through the emission monochromator to the photomultiplier-tube detector. The control module includes a gate-and-delay generator, allowing the signal at the detector to be integrated only during a specific period after the flash (the Dealy After Flash) for a pre-determined length of time (the Sample Window)*.'[1]

Phosphorescence decay by delay feature was used via phosphorimeter operations to measure the europium lifetimes. A fixed window is set, and the delay between the flash and the opening of that widow is incrementally increased, thus building up the decay curve. There are several conditions for recording the lifetimes. The parameters and conditions used are as follows: a 3 ms sample window; a delay increment of 0.01 ms; an initial delay of 0.05 ms; and a maximum delay 5 ms. Concentrations and slit widths were adjusted to avoid saturation of the detector. The luminescence lifetime was obtained from the decay data and fitted via a single exponential function using an iterative non-linear least-squares algorithm with the 'Solver' function in Microsoft Excel. For the solid-state measurements, the same sample mould was used, as shown in Figure 3.2.

3.1.4. Measurement of Fluorescence Spectra, Lifetimes, and Total Quantum Yields

The fluorescence spectra, lifetimes, and total quantum yields were measured in air-equilibrated solutions (oxygen was not purged) for europium complexes and organic molecules in the solution phase. The absorption of the lanthanide complex and organic ligands were maintained below 0.1 to minimize the inner filter effect. The total quantum yields of Eu(hfac)$_3$DPEPO and Eu(tta)$_3$DPEPO were measured at an excitation wavelength of 300 and 340 nm, respectively. The quantum yields were determined using a comparative method, with quinine sulphate in 0.5 M H_2SO_4 (ϕ = 0.546)[4] as a reference.

For the solid-state measurements, the total quantum yield of $Eu(tta)_3DPEPO$ in PMMA was determined using $Eu(hfac)_3DPEPO$ in PMMA as a reference because it is well-known and was previously determined by Moudam et al.[6] The lifetime measurements were measured at a fixed wavelength for each complex.

3.2 Materials

3.2.1 Chemicals

Acetone, hexane, dichloromethane, H_2O, H_2SO_4, chloroform, and ethanol were HPLC grade with the exception of ethanol (Absolute) and 30% (w/w) H_2O_2, which were obtained from Fisher Chemicals. All solvents were used without further purifications. Europium(III) chloride hexahydrate (99.9%), potassium tert-butoxide, hexafluoroacetylacetone (98%), sodium hydroxide, quinine hemisulfate salt monohydrate (90%), 2-thenoyltrifluoroacetone (99%), and bis(2-(diphenylphosphino)phenyl) ether (98%) were sourced from Alfa Aesar.

3.2.2 Synthesis

All the solvents used in this study to synthesise the europium complexes and DPEPO were degassed (by purging N_2 for 1 hr). All reactions were performed in standard glassware under a nitrogen atmosphere. Mr. Stephen Boyer determined the elemental analyses at London Metropolitan University, North Campus, Holloway Road, London, N7 8DB. The mass spectra were obtained using Bruker ESI. In addition, ^1H measurements were performed at room temperature with Bruker ava 500 MHz spectrometer (2-channel instrument with a 5 mm DCH CryoProbe™ optimised for ^1H).

3.2.2.1 Synthesis of DPEPO

The synthesis of the ligand DPEPO is a one-step synthesis, as shown in Figure 3.3. Bis(2-(diphenylphosphino)phenyl) ether (2.69 g, 5 mmol) was dissolved in 10 ml of 1,4-dioxane at room temperature. Then, 1 ml of 30% H_2O_2 (10.5 mmol) was added dropwise with vigorous stirring, and the mixture was then stirred for 2 hr. Then, 10 ml of water was added to stop the reaction. The mixture was extracted with 3 × 30 ml of dichloromethane. The oil phase was washed with 2 × 30 ml water to remove the 1,4-dioxane. The organic layer was dried with $MgSO_4$. The solvent was removed in a vacuum, and a white powder (soluble in CH_3Cl) was obtained. This method followed the synthesis protocol described by Xu et al. [5]. ($C_{36}H_{28}O_3P_2$, Mwt = 570,55 g.mol^{-1}) ESI MS: m/z = 571.15.

^{1}H NMR (500 MHz, Chloroform-*d*) δ 7.75 – 7.59 (m, 1H), 7.54 – 7.22 (m, 1H), 7.13 (dddd, *J* = 8.2, 7.3, 1.9, 0.9 Hz, 0H), 7.06 (tdd, *J* = 7.6, 1.8, 1.1 Hz, 0H), 6.03 (dd, *J* = 5.0, 1.0 Hz, 0H).

3.2.2.2 Synthesis of Eu(hfac)$_3$DPEPO

The complex Eu(hfac)$_3$DPEPO was synthesised in two steps, as shown in Figure 3.3. First, Eu(hfac)$_3$(H_2O)$_2$ was synthesised as follows: 3 mmol of potassium tert-butoxide was added to a solution of 3mmol hexafluoroacetylacetone in water (20 ml). The mixture was stirred until the dissolution of the reagents; then 1 mmol of europium (III) chloride hexahydrate was added to afford a white precipitate. The mixture was stirred under N_2 at 60°C for one hour and then at room temperature for three hours. The white precipitate was filtered, washed with cold water (100 ml) and hexane (5 ml), and dried under a vacuum for 12 h, as described by Moudam et al. [6]

Then, the white precipitate was used to synthesise Eu(hfac)$_3$DPEPO following the protocol described by Moudam et al.[6] Following this, 0.175 mmol of Eu(hfac)$_3$(H_2O)$_2$ was added to (0.175 mmol) of DPEPO dissolved in a 30 ml solution of water: ethanol (15:15), resulting in a white precipitate. The mixture was stirred at 60°C for one hour under N_2 and then for three hours at room temperature. The white precipitate was filtered off, washed with cold water (100 ml) and hexane (5 ml), and left under a vacuum for 12 hours. Elemental analysis: Calculated ($C_{51}H_{31}EuF_{18}O_9P_2$) (1343.67 g mol^{-1}): %C 45.59; %H 2.33. Found: %C: 45.62; %H, 2.23

3.2.2.3 Synthesis of Eu(tta)$_3$DPEPO

Eu(tta)$_3$DPEPO was synthesised via one-pot synthesis, as shown in Figure 3.3. This was carried out with a slight modification to the procedure reported by Gavriluta et al.[7] A solution of 2-thenoyltrifluoroacetone (2.4 mmol) was added to (0.8 mmol) of DPEPO in 20 ml of ethanol, and an aqueous NaOH solution (2.4 ml, 1 Molar, 2.4 mmol) was added dropwise. The mixture was heated at 70–75 °C for 5 min, and then a solution of europium (III) chloride hexahydrate (0.8 mmol dissolved in 6 ml of water) was added dropwise, as described by Gavriluta et al.[7]. A white precipitate was formed upon the addition of the $EuCl_3.6H_2O$ solution. The hot suspension was agitated and cooled to an ambient temperature and stirred for 24 hours. It was then filtered off and washed with ethanol (50%) (2 x 3 ml) followed by hexane and dried in a vacuum. Elemental analysis: Calculated ($C_{60}H_{40}EuF_9O_9P_2S_3$) (1386.05 g.mol^{-1}): %C 51.99; %H, 2.91. Found: %C: 52.09; %H: 2.91.

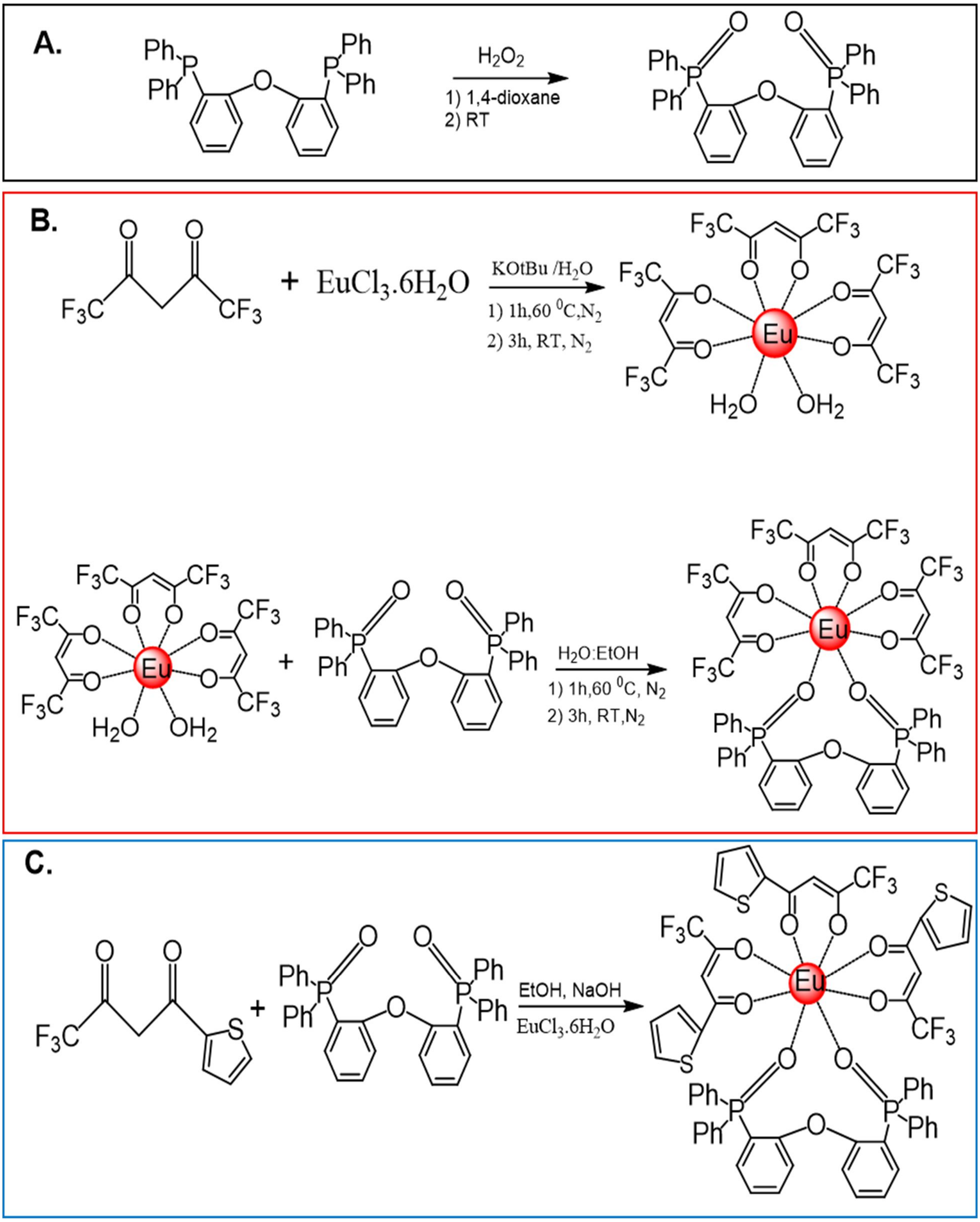

Figure 3.3 Synthesis route and chemical structures of A) DPEPO, B) Eu(hfac)$_3$DPEPO, and C) Eu(tta)$_3$DPEPO.

3.3 References

1. FluoroMax-3 & FluoroMax-P with FluorEssence -Operation and Maintenance. Horiba-Jobin and Yavon Inc.: New Jersey.

2. Wu, X. Use of 2-Aminopurine Fluorescence as a probe of DNA and computational studies of a new class of base analogues. University of Edinburgh, 2012.

3. Neely, R. K. Photophysical properties of 2-aminopurine and its application as a probe of DNA-protein interactions. PhD, 2005.

4. Ortiz, S. C.; Ospino, E. M.; Cabanzo, R. In Spectroscopy characterization and quantum yield determination of quantum dots, Journal of Physics: Conference Series, IOP Publishing: 2016; p 012097.

5. Xu, H.; Wang, L.-H.; Zhu, X.-H.; Yin, K.; Zhong, G.-Y.; Hou, X.-Y.; Huang, W., Application of Chelate Phosphine Oxide Ligand in EuIII Complex with Mezzo Triplet Energy Level, Highly Efficient Photoluminescent, and Electroluminescent Performances. The Journal of Physical Chemistry B 2006, 110 (7), 3023-3029.

6. Moudam, O.; Rowan, B. C.; Alamiry, M.; Richardson, P.; Richards, B. S.; Jones, A. C.; Robertson, N., Europium complexes with high total photoluminescence quantum yields in solution and in PMMA. Chemical Communications 2009, (43), 6649-6651.

7. Gavriluta, A.; Fix, T.; Nonat, A.; Slaoui, A.; Guillemoles, J.-F.; Charbonnière, L. J., Tuning the chemical properties of europium complexes as downshifting agents for copper indium gallium selenide solar cells. Journal of Materials Chemistry A 2017, 5 (27), 14031-14040.

CHAPTER 4: Luminescent Europium Complexes for Solar Cell Applications

"My title is from Keats, who believed that Newton had destroyed all the poetry of the rainbow by reducing it to the prismatic colours[…] Newton's unweaving of the rainbow led on to spectroscopy, which has proved the key to much of what we know today about the cosmos. And the heart of any poet worthy of the title Romantic could not fail to leap up if he beheld the universe of Einstein, Hubble, and Hawking."

Richard Dawkins – In the Preface of his book 'Unweaving the Rainbow'.

CHAPTER **4**

Luminescent Europium Complexes for Solar Cell Applications

4.1 Introduction

In Chapter 1, luminescent solar concentrators (LSCs) and luminescent down-shifting (LDS) layers were proposed to address the spectral mismatch in the photovoltaic devices by acting as spectral converters to manage the photon frequency and consequently enhancing the efficiency of conversion in solar cells. Lanthanide (III) complexes, europium, in particular, were considered as suitable candidates for solar energy applications due to their unique photophysical properties and intense red emission, which coincides with the highest spectral response of several solar cells such as organic dye-sensitized, silicon (Si) or copper indium gallium selenide (CIGS).[1-4]

Because f-f transitions are parity forbidden, lanthanide ions suffer from low absorption coefficients ($\varepsilon < 10\ M^{-1}cm^{-1}$); to overcome this limitation, organic chromophores can be introduced to act as 'antennae'. The rare-earth ions act as strong Lewis acids; as a result, ionic bonding is more dominant than covalent bonding. Therefore, they form bonds with ligands with donor atoms such as phosphate, nitrate sulfate, and carboxylate.[5-7] In the context of europium complexes used in solar energy applications, 1,3-diketones, commonly referred to as β-diketonates, have been the most frequently used ligands and have been thoroughly investigated over the past four decades.[6-11]

In the appropriate pH range, β-diketonate ligands can be easily deprotonated at the α-carbon atom, making tris β-diketonate. Furthermore, this mono-negative bidentate ligand readily coordinates with the Ln (III) ions to form stable and electrically neutral lanthanide complexes.[6] Since organic chromophores play a crucial role in harvesting the incoming electromagnetic radiation and transferring the excitation energy from the ligand to the europium ion, the design and synthesis of such ligands ought to be carefully considered.

The efficiency of β-diketonate ligands as sensitizers (often referred to as antennae) stems from several properties. Firstly, their adjustable light-harvesting window (285-360 nm) can be tuned based on different atoms or functional groups within the β-diketonate ligands and have relatively high molar absorption coefficients. Secondly, their intense π-π^* transitions facilitate efficient ligand to metal energy transfer. Thirdly, they are easily synthesised. These are the primary reasons for choosing β-diketonate ligand-based complexes for solar cell applications.[6, 12]

2,4-pentanedione (referred to as Hacac) is the simplest aliphatic form of a β-diketonate ligand; it was first described by Claisen more than a century ago.[13, 14] Since then, numerous derivatives of β-diketonate ligands have been synthesised for a wide variety of applications, such as improving the power of extraction, bioluminescent probes, and light-emitting diodes.[15, 16] Fluorinated β-diketonate ligands, as exemplified in Figure 4.1, have received particular attention for their luminescence properties.[6, 17, 18]

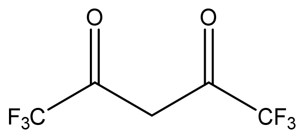

Hexafluoroacetylacetone

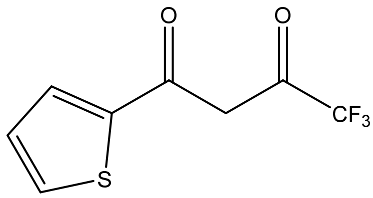

2-thenoyltrifluoroacetone

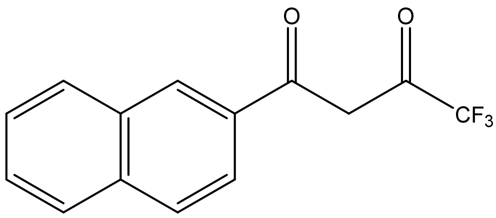

2-naphthoyltrifluoroacetone

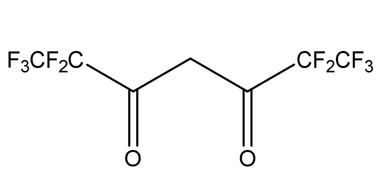

1,1,1,2,2,6,6,7,7,7-decafluoro-3,5-heptanedione

Figure 4.1 Examples of fluorinated β-diketonate ligands

Careful consideration of the choice and design of ligands attached to the lanthanide ion is essential to obtain highly luminescent lanthanide complexes. To efficiently convert absorbed light into emitted photons, which is referred to as the overall photoluminescence quantum yield (ϕ_{tot}), the surrounding ligands of the lanthanide ion must exhibit a wide absorption window in the UV/blue region with a large absorption coefficient, efficiently transfer the energy to the metal ion, and minimise the nonradiative deactivation caused by the presence of high-frequency vibrations.[19, 20]

Fluorinated β-diketonate ligands satisfy the conditions mentioned above, as high-frequency oscillators that causes radiationless transitions, such as C-H, O-H, and N-H, etc., can be fluorinated or deuterated to increase the luminescence lifetime of lanthanide complexes in solution, as shown by Hasegawa et al., and Yanagida et al., [21, 22] and to reduce the vibrational quenching. [20, 23-25] The coordination number of β-diketonate europium complexes can vary from six to ten, with eight being the most frequently studied. Since the bonding is mainly electrostatic, the structures of such complexes do not follow a particular pattern and heavily depend on steric factors.[6]

Most of the synthesised complexes naturally coordinate with solvent molecules, such as H_2O, CH_3CH_2OH, or CH_3OH, containing high energy oscillators, and it was proposed to replace the solvent molecules with bulkier ligands that have low-frequency oscillators, such as P=O, to suppress the radiationless quenching and add more rigidity to the complex.[6, 26-29]

There is another consideration when it comes to choosing the suitable ligands in europium complexes. An efficient energy transfer from the ligand 'antenna' to the europium ion requires careful positioning of the ligand's singlet and triplet states; they must be sufficiently higher in energy than the europium levels to prevent back energy transfer processes. Experimental data and theoretical calculations have demonstrated that the energy of the first excited triplet state of the ligand plays a crucial role to facilitate efficient intramolecular energy transfer from the ligand to the emitting levels in the metal ion and prevent back energy transfer; ideally, the energy level of the first excited triplet state of the ligand ought to be 2500–3000 cm^{-1} higher than the main luminescent state in the Eu^{3+} ion, which lies 16,286 cm^{-1} above the ground state. [6, 30, 31]

Acknowledging the factors mentioned above, researchers in the last three decades have been working on the synthesis of highly luminescent europium complexes. For example, the quantum yield of the complex $Eu(tta)_3(H_2O)_2$ where tta=2-thenoyltrifluoroacetone was just 23%, but when the solvent molecules were replaced with monodentate dibenzyl sulfoxide (DBSO) to form $Eu(tta)_3(DBSO)_2$ the total quantum yield increased dramatically to 85%.[32] Indeed, experimental data show the effect of optimising the ligand on obtaining higher quantum yields and long lifetimes of the europium ion.[33] Chen Wei et al. reported highly emissive europium complexes upon the introduction of diphenylphosphoryl (DPPO), where the total quantum yield (ϕ_{tot}) increased up to 92% in PMMA.[34] Cuan et al. showed the highest reported optical efficiency for Eu(III) complexes, where the quantum yield went up to 96% when embedded in organic–organic hybrid materials.[35] Eu(III) ternary β-diketonate with exceptionally high quantum yield are no longer rare. [36-39]

The presence of neutral ancillary ligands in europium β-diketonate complexes plays a significant role in completing the coordination sphere, absorbing energy, and transferring the absorbed energy to the β-diketonate ligands or europium ion.[40, 41] Bis(2-(diphenylphosphino)phenyl) ether oxide (DPEPO) as a bidentate ancillary ligand was first introduced by Xu et al. as a better alternative to the ordinary phosphine oxide ligands.[42] It turns out that using DPEPO to replace solvent molecules not only gives more rigidity to the complex but it provides an impressive enhancement to the overall photophysical properties; in one study, adding DPEPO led to an increase in total quantum yield from 2% to 30%, sensitization efficiency from 8% to 45%, and an increase in the observed lifetime from 250 μs to 1060 μs.[43]

This chapter reports the photophysical studies of two Eu(III) complexes: $Eu(hfac)_3DPEPO$ and $Eu(tta)_3DPEPO$, where hfac is hexafluoroacetylacetone, and tta is 2-thenoyltrifluoroacetone. $Eu(hfac)_3DPEPO$ was first reported by Moudam et al.[44] and has a high quantum yield in PMMA. $Eu(tta)_3DPEPO$, as reported by Xu et al.[42] has an absorption window covering the UV/blue region and a high quantum yield in PMMA[3], which makes it useful in light conversion applications. In the case of $Eu(tta)_3DPEPO$, the photophysical properties listed in Chapter 4 such as the total quantum yield, intrinsic quantum yield, radiative lifetime, luminescence lifetime, and sensitisation efficiency are reported for the first time in a single study.

In the current project, it was necessary to synthesise these complexes and establish their photophysical properties prior to using them in the energy transfer studies presented in Chapters 5 and 6. We will highlight the role of the ligand in the energy transfer process and report relevant photophysical properties, such as the luminescence lifetime, radiative lifetime, intrinsic quantum yield, and total quantum yield, in solution and PMMA.

4.2 Experimental

4.2.1 Chemicals

Dichloromethane and chloroform were HPLC grade obtained from Fisher Chemicals and were used without further purifications. Poly(methyl methacrylate) (PMMA, average MW 120,000) was sourced from Sigma-Aldrich. Eu(tta)$_3$DPEPO, and Eu(hfac)$_3$DPEPO, and DPEPO were synthesised as described in Chapter 3.

4.2.2 Polymeric Film Preparation

A solution of 3(w/w%) of PMMA polymer and an appropriate amount of Eu(β-Dik)$_3$DPEPO were dissolved in chloroform and were heated at 55 °C and stirred for 2 hr. Eu(hfac)$_3$DPEPO in PMMA was prepared at different concentrations (w/w)% : 5, 8, 12, and 14. Eu(tta)$_3$DPEPO in PMMA was prepared at different concentrations (w/w)% 1.2, 2.1, 3.2, and 4.1. The total concentration of the polymer in the solution was kept fixed to ensure the undoped polymer and doped polymer had the same thickness. A suitable volume of the solution (100 μL) was spin-coated using a pipette on quartz slides (25 mm x 25 mm x 1 mm) for each measurement. Dynamic spin coating (the substrate is already spinning) was used for 60s at 500 rotation per minute (r.p.m) to ensure the formation of thin homogenous luminescent films after the spin-coated films were left for 24 hr at room temperature to allow for complete evaporation of the solvent.

4.3 Results and Discussion

Figure 4.2 shows the chemical structures of the synthesised Eu(tta)$_3$DPEPO, Eu(hfac)$_3$DPEPO and the ligand DPEPO.

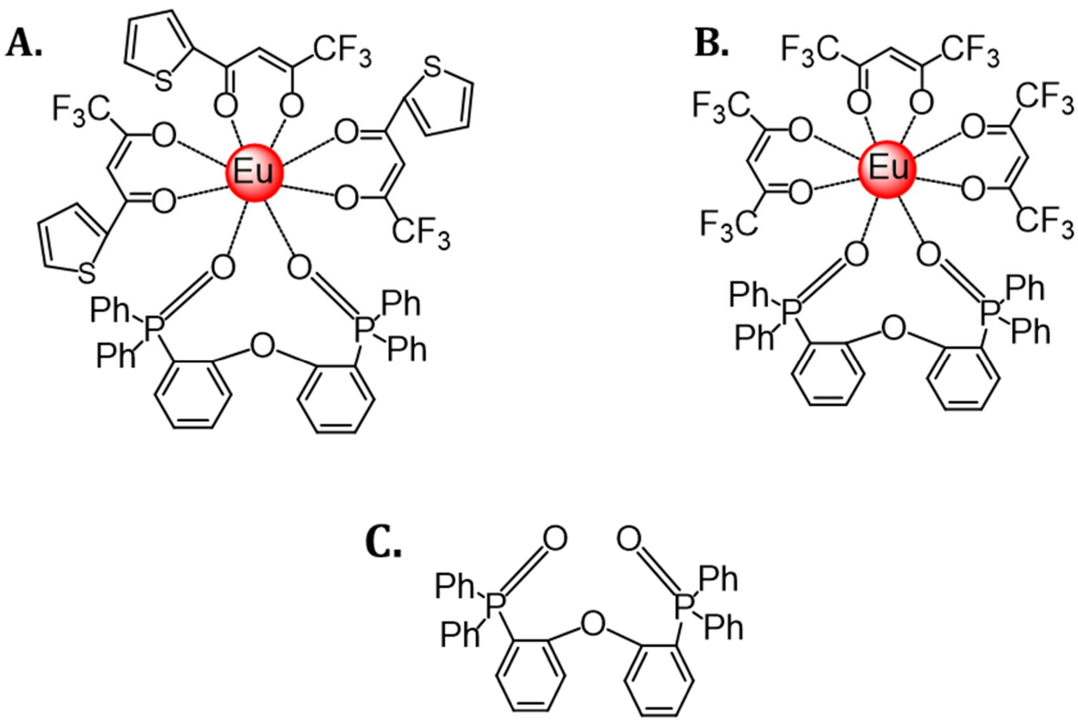

Figure 4.2 Molecular structure of A) Eu(tta)$_3$DPEPO, B) Eu(hfac)$_3$DPEPO, and C) DPEPO.

4.3.1 Solution-phase UV/Vis Absorption Spectra

The UV/Vis absorption spectra of the complexes in DCM solution are shown in Figure 4.3, and those of the free ligands are shown in Figure 4.4. The UV/Vis absorption measurements for free ligands in DCM have been reported in previous work.[42, 45, 46] The absorption spectrum of Eu(hfac)$_3$DPEPO shows an absorption onset at 28,736 cm^{-1} (349 nm), and λ_{max} at 33,898 cm^{-1} (295 nm, ε = 28,306 M^{-1} cm^{-1}). Figure 4.4 demonstrates the contribution of the hfac ligand, which shows an absorption onset at 28,736 cm^{-1} (349 nm), λ_{max} at 33,333 cm^{-1} (300 nm). The DPEPO ligand, which has an absorption onset around 33,000 cm^{-1}(303 nm) and λ_{max} at 34,722 cm^{-1} (288 nm, ε = 8,863 M^{-1} cm^{-1})[41]. The complexation of hfac and DPEPO with europium has a small blue shift effect on λ_{max} position with a 5 nm difference between the complex and hfac, which can be attributed to the overlap with the absorption of DPEPO, which strongly absorbs in the range 285 –290 nm. The contribution of DPEPO to the complex spectrum can be seen in the overall broadening of the peak and the absorption in the region 250–270 nm since hfac has no absorption in this region.

For Eu(tta)$_3$DPEPO, the absorption spectrum shows an absorption onset at 25,380 cm^{-1} (394 nm) and λ_{max} at 29411 cm^{-1} (340 nm, ε = 46,770 M^{-1} cm^{-1}) as shown in Figure 4.3. Since DPEPO has λ_{max} at 288 nm, the main peak at 340 nm can be assigned to the ligand tta, but, as shown in Figure 4.4, the free tta has λ_{max} at 30,769 cm^{-1} (325 nm). Upon the complexation with the metal centre, the tta peak at 325 nm (π-π* transition) undergoes a redshift from 325 nm to 340 nm. This can be attributed to the complexation of the enol tautomer, which can lead to a bathochromic effect, a common characteristic for β-diketonate metal complexes in general.[3, 47, 48] The contribution of the DPEPO can be seen in the region 250-295 nm since tta has small absorption in this particular region. It is worth noting that the absorption spectrum of the complex reported by Xu et al.[42] was cut off at 300 nm and thus did not show the contribution of the short wavelength band.

Congiu et al. studied the Gd(hfac)$_3$DPEPO complex in DCM to gain insights into the nature of excited states of hfac and DPEPO, as gadolinium's first excited state has high energy, therefore cannot be excited by energy transfer from the ligands.[49] The comparison of the absorption spectrum of the free ligand DPEPO, Gd(hfac)$_3$(H$_2$O)$_2$ and Gd(hfac)$_3$DPEPO indicates an enhancement in the overall absorption of the ligands compared with the free ligands and the presence of a synergistic effect between DPEPO and hfac in the complex.[49] Eu(tta)$_3$DPEPO exhibits a similar synergistic effect between the ligands DPEPO and tta.[42]

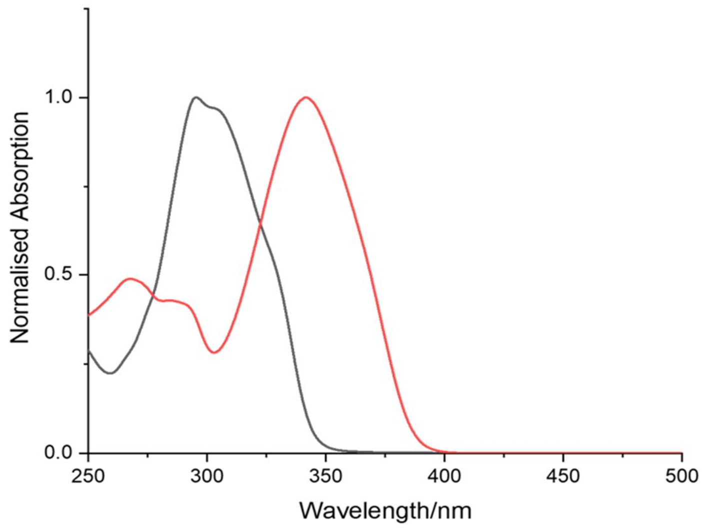

Figure 4.3. Normalised UV/Vis absorption spectra of Eu(hfac)$_3$DPEPO (black line) and Eu(tta)$_3$DPEPO (red line) in DCM at room temperature.

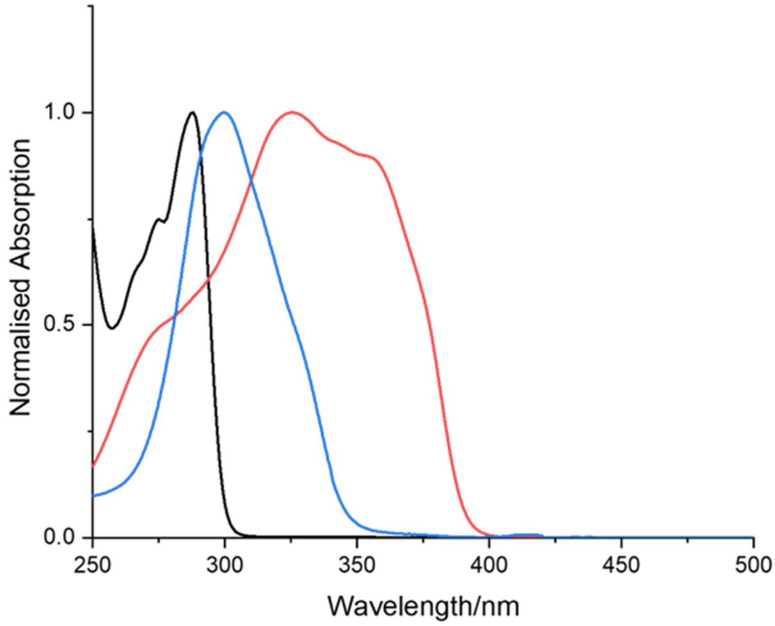

Figure 4.4. Normalised UV/Vis absorption spectra of the free constituent ligands; DPEPO (black line), hfac (blue line), and tta (red line) in DCM at room temperature.

4.3.2 Solution-phase Photoluminescence

As shown in Figure 4.5, both complexes exhibit characteristic intense red emission with sharp narrow bands in the range 575-710 nm, which can be attributed to the europium-centred transitions $^5D_0 \rightarrow {}^7F_J$ (J = 0–4). The four main emission bands are $^5D_0 \rightarrow {}^7F_0$ transition (570-585 nm), $^5D_0 \rightarrow {}^7F_1$ transition (585-600 nm), $^5D_0 \rightarrow {}^7F_2$ transition (610-615 nm), $^5D_0 \rightarrow {}^7F_3$ transition (640-660 nm), and $^5D_0 \rightarrow {}^7F_4$ transition (680-710 nm). The $^5D_0 \rightarrow {}^7F_2$ transition is very intense, shown in (Figure 4.5) compared to the other transitions. Its peak is referred to as the hypersensitive peak since it is highly sensitive to the changes in the europium ion environment. The emission spectra also show the absence of ligand-centred fluorescence in both complexes, indicating efficient intersystem crossing, a pre-requisite for efficient energy transfer from the ligand's triplet state to the Eu^{3+} ion.

The excitation spectrum of each complex (Figure 4.5) corresponds closely to its absorption spectrum (Figure 4.3). The excitation spectra show that, in both complexes, the energy transfer (sensitization) efficiency does not depend on which of the two ligands (DPEPO/hfac, DPEPO/tta) is initially excited. Following initial excitation, there may be inter-ligand energy transfer in the singlet or triplet manifolds. Figure 4.5 also shows a large pseudo-Stokes shift (> 30,000 cm^{-1})

between both complexes' absorption and emission maxima. From the absorption spectra, it is evident that the S_1 state of DPEPO is higher in energy than the S_1 state of hfac or tta. The energy level diagram, obtained from the phosphorescence spectra of gadolinium complexes, depict the triplet state of the constituting ligands it can be seen that the T_1 state of DPEPO lies above the T_1 states of the other two ligands, as shown in Figure 4.6.[42, 46]

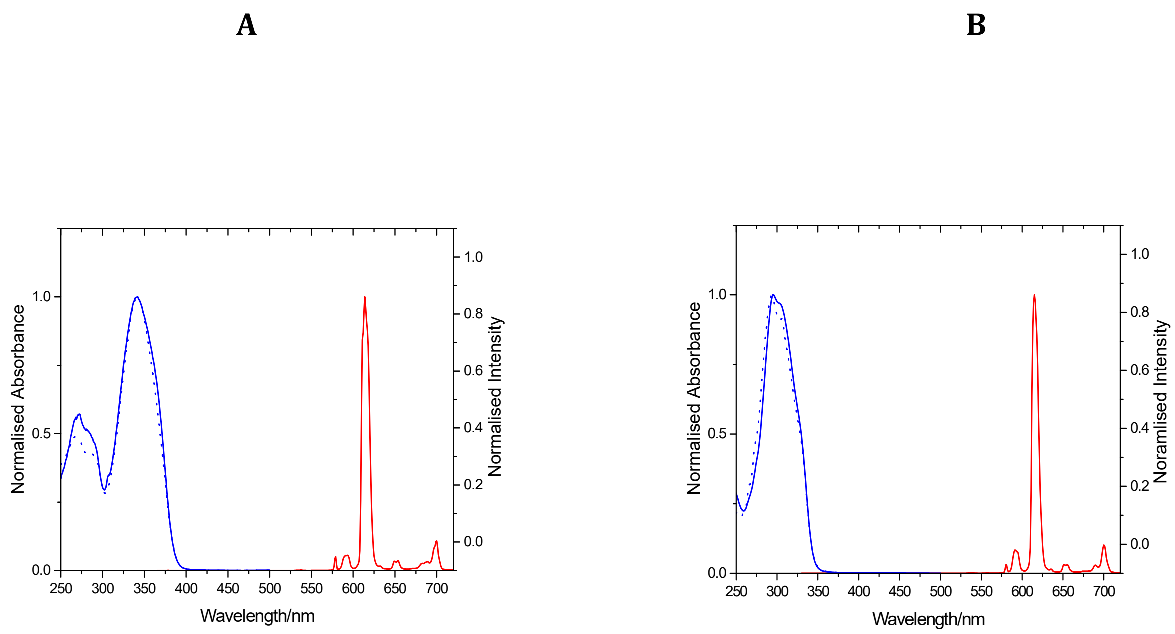

Figure 4.5. (A) the emission spectrum (red), excited at 340 nm, the excitation spectrum, detected at 614 nm (blue), and the absorption spectrum (dotted blue) of Eu(tta)$_3$DPEPO, (B) the emission spectrum (red), excited at 294 nm, the excitation spectrum, detected at 614 nm (blue), and the absorption spectrum (dotted blue) of Eu(hfac)$_3$DPEPO in DCM at room temperature. Spectra are normalised to the maximum intensity in each case.

An understanding of the intramolecular energy transfer pathways from the ligands to the metal centre can be gained from examining the energy of the first excited triplet state of each ligand in relation to the emissive state of the Eu^{3+} ion at 614 nm (at 16,286 cm^{-1}). Each ligand's first excited triplet state must be at least 2500 cm^{-1} higher than the emissive state Eu^{3+}.

According to Sager et al.[45] and Congiu et al.[49] the lowest energy level of the first excited triplet state for tta, hfac, and DPEPO were found to be at 20,400 cm^{-1}, 22,300, and 27,600 cm^{-1}, respectively (shown in Figure 4.6). Xu et al.[42] concluded in the case of $Eu(tta)_3DPEPO$ the main energy transfer to Eu^{3+} occur from tta since its first triplet excited state is lower than that of DPEPO. The work of Congiu et al.[49] suggested a similar energy transfer pathway from hfac to Eu^{3+} in the case of $Eu(hfac)_3DPEPO$.

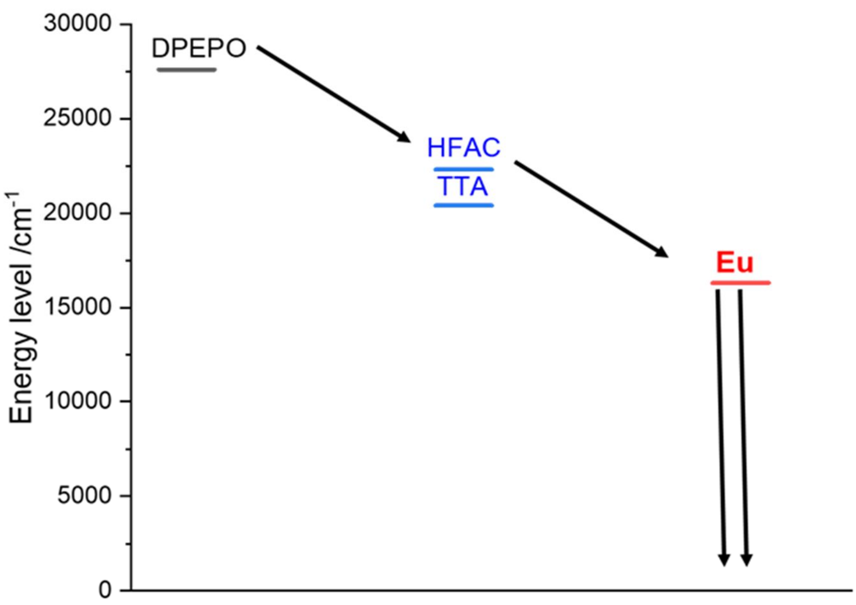

Figure 4.6 Energy level diagram for the first excited triplet state of the constituting ligands in relation to the emissive state of Eu^{3+}, indicating the photosensitization process.

The total quantum yield (ϕ_{tot}) of each complex was determined relative to quinine sulfate by plotting luminescence integrated intensity versus absorbance (Equation 2-19), as shown in Figure 4.7. The values obtained were 0.79 and 0.65 for $Eu(hfac)_3DPEPO$ and $Eu(tta)_3DPEPO$, respectively. The luminescence decays of the complexes are shown in Figure 4.8 and Figure 4.9. These were fitted to single-exponential functions, indicating the presence of a single emitting species, giving luminescence lifetimes of 0.86 ms and 0.70 ms for $Eu(hfac)_3DPEPO$ and $Eu(tta)_3DPEPO$, respectively.

A B

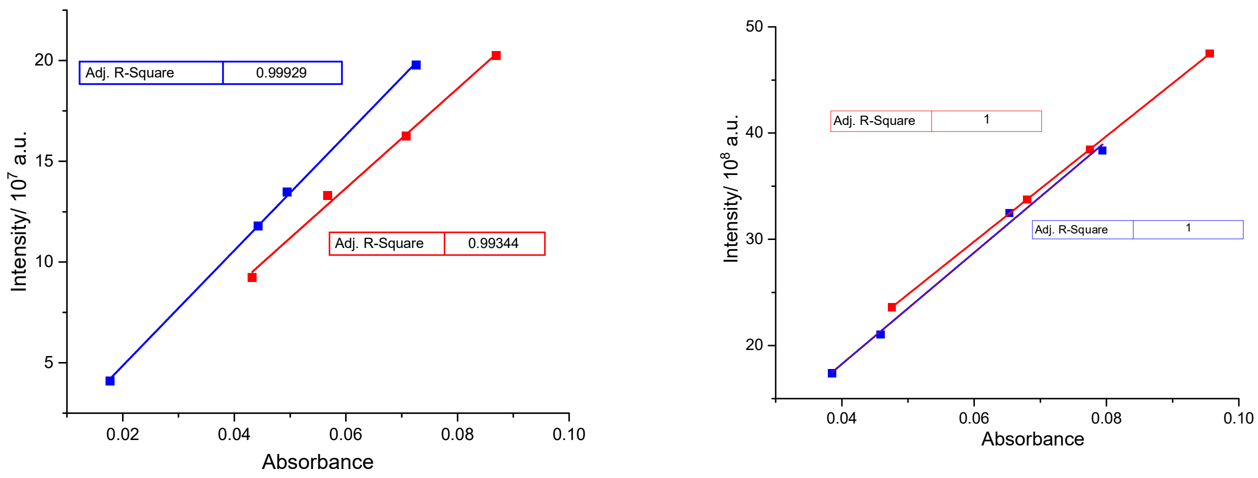

Figure 4.7 Plot of integrated luminescence intensity versus absorbance for A) Eu(hfac)$_3$DPEPO (blue) with quinine sulfate (red), and B) Eu(tta)$_3$DPEPO (blue) with quinine sulfate (red) at room temperature.

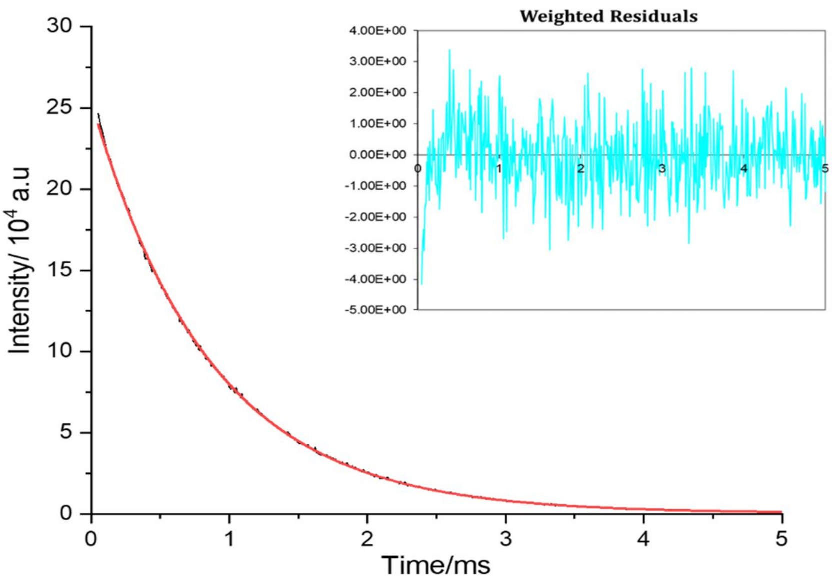

Figure 4.8 Decay data(black), fitted single exponential function (red), and weighted residuals of Eu(hfac)$_3$DPEPO excited at 294 nm and monitored at 614 nm in DCM.

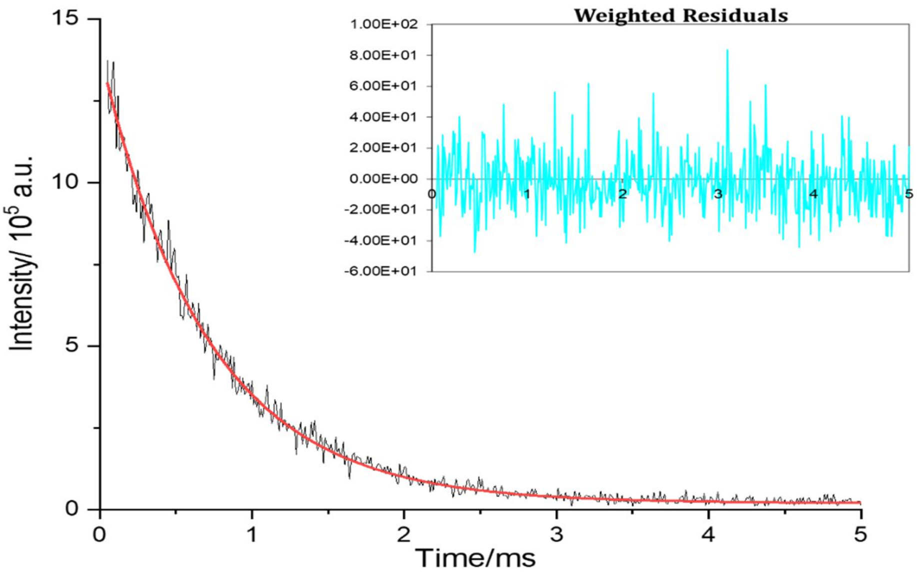

Figure 4.9 Decay data (black), fitted single exponential function (red) and weighted residuals of [Eu(tta)$_3$DPEPO] excited at 340 nm and monitored at 614 nm in DCM.

Table 4.1 reports the luminescence and radiative lifetimes, the intrinsic and total quantum yields, and sensitization (energy transfer) efficiencies of both complexes. It can be seen that both complexes display very high sensitization efficiencies. Values presented in Table 4.1 are an average of three measurements in DCM. Errors have been calculated by obtaining the standard deviation.

Table 4.1 Photophysical properties of Eu(hfac)$_3$DPEPO and Eu(tta)$_3$DPEPO in DCM. The estimated error in the reported values is ±10%

	Eu(hfac)$_3$DPEPO	**Eu(tta)$_3$DPEPO**
τ_{Ln} /ms	0.86	0.70
ϕ_{Ln}	0.78	0.71
τ_R /ms	1.10	0.99
η_{sens}	1.0	0.91
ϕ_{tot}	0.79	0.65

The values in Table 4.1 for $Eu(hfac)_3DPEPO$ are in good agreement with literature values reported by Moudam et al.[44] with estimated error values of ±10%. The literature values of the photophysical properties are: 0.86, 0.78, 1.11, 0.97, and 0.76 for $\tau_{Ln}, \phi_{Ln}, \tau_R, \eta_{sens}$ and ϕ_{tot} respectively. In the case of $Eu(tta)_3DPEPO$, among the five photophysical properties summarised in Table 4.1, the total quantum yield was the only value reported by Xu et al.[42] The ϕ_{tot} value was (0.55), which can be considered in good agreement with estimated error values of ±10%. The rest of the photophysical properties: $\tau_{Ln}, \tau_R, \phi_{Ln}$ and η_{sens} are reported for the first time in a single study.

The total quantum yield (ϕ_{tot}), defined in Chapter 2, is of particular importance in terms of light-converting technologies such as light concentration and down-shifting. Since ϕ_{tot} is the product of η_{sens} and ϕ_{Ln}, an examination of both properties is required to explain the high ϕ_{tot} values. For the complex $Eu(hfac)_3DPEPO$, comparison to the corresponding values of the DPEPO-free hydrated compound $Eu(hfac)_3(H_2O)_2$[44] shows that the introduction of DPEPO to the complex enhances ϕ_{Ln} value from 0.61 to 0.78, and increases the sensitisation efficiency to unity; consequently, the total quantum yield increases from 0.32 to 0.79.

The effect of DPEPO extends to $Eu(tta)_3DPEPO$. The corresponding value of ϕ_{tot} of $Eu(tta)_3(H_2O)_2$ is only 0.23.[32] Even when Filipescu et al.[32] replaced the water molecules with the 1,10-phenanthroline (phen) ligand, it only enhanced the ϕ_{tot} to 0.36 in dimethylformamide solution.

Xu et al. [42] found that the rigid and compact structure of DPEPO led to more than twice the enhancement in ϕ_{tot} in comparison with the monodentate triphenylphosphine oxide (TPPO) ligand; they reported that the $Eu(tta)_3(TPPO)_2$ complex had a ϕ_{tot} of just 0.26. The combination of a sensitization efficiency of 0.91 and ϕ_{Ln} of 0.71 is a testament to the significant role DPEPO plays in minimising the non-radiative deactivation processes of metal centred luminescence and in promoting efficient energy transfer from the excited triplet state to the metal centre over non-radiative decay transitions in the triplet state.

4.3.3 UV/Vis Absorption Spectra in PMMA

As shown in Figure 4.10, the UV/Vis absorption spectrum of each complex in PMMA is in agreement with that in the solution phase (Figure 4.3), indicating that the complexes remain intact when embedded in the polymer matrix, and there is a negligible contribution from the PMMA to the absorption spectrum in this wavelength range. As shown in Figure 4.11, pure PMMA shows a negligible absorption at wavelengths longer than 250 nm compared to the absorption of the complex embedded in PMMA of the same concentration. The absorption spectrum of $Eu(hfac)_3DPEPO$ shows an absorption onset at 28,736 cm^{-1} (349 nm) and λ_{max} at 300 nm.

For $Eu(tta)_3DPEPO$, the tta ligand contribution to the absorption spectrum can be seen in absorption onset at 394 nm and λ_{max} at 340 nm.

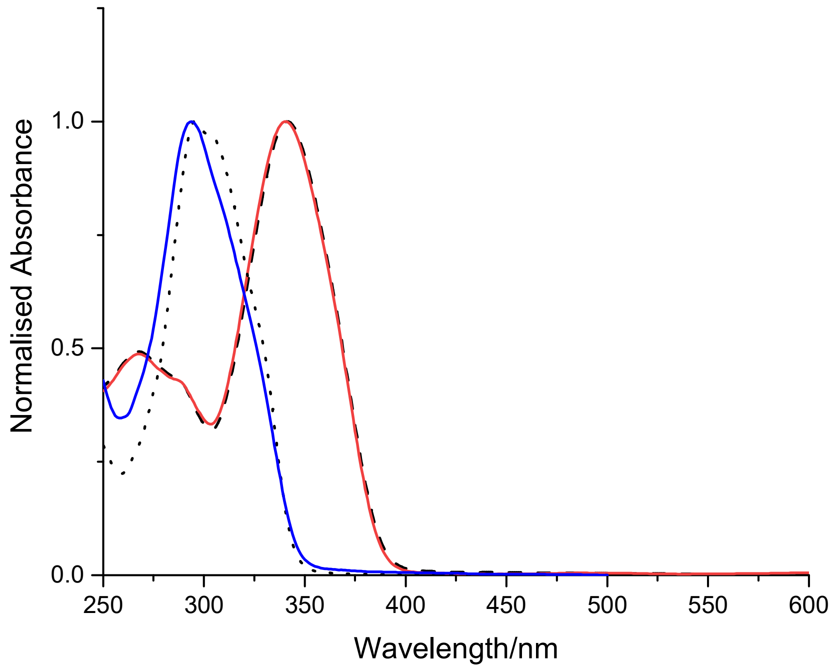

Figure 4.10. Normalised UV/Vis absorption spectra of $Eu(hfac)_3DPEPO$ (red line) and $Eu(tta)_3DPEPO$ (black line) in PMMA, compared with the absorption spectra of both complexes (dotted and dashed lines) in DCM.

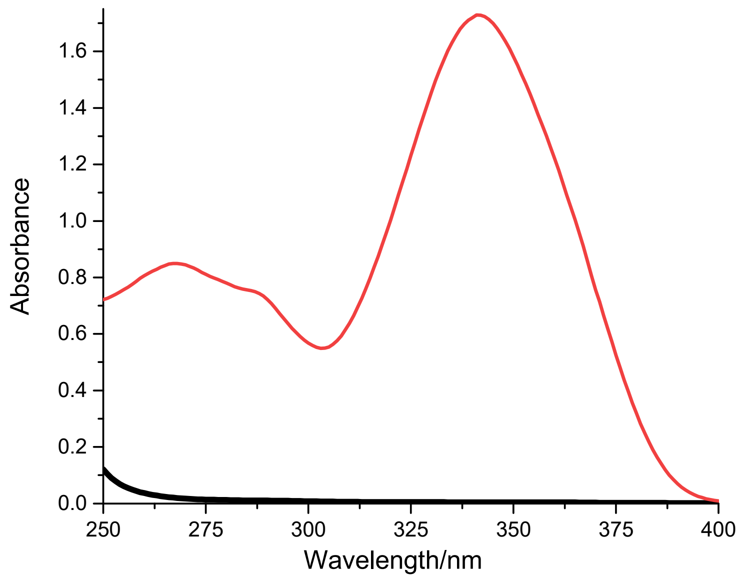

Figure 4.11. UV/Vis absorption spectra of 10 wt% Eu(tta)$_3$DPEPO in 3wt% PMMA (red line) and undoped PMMA (3wt %) (black line).

The absorption spectrum of each complex was measured as a function of concentration, as shown in Figures 4.12 and 4.13. Each complex exhibited a linear correlation between absorbance (measured at 340 nm for Eu(tta)$_3$DPEPO and 298 nm for Eu(hfac)$_3$DPEPO) and concentration, demonstrating the absence of aggregation or deformities in films over the concentration range.

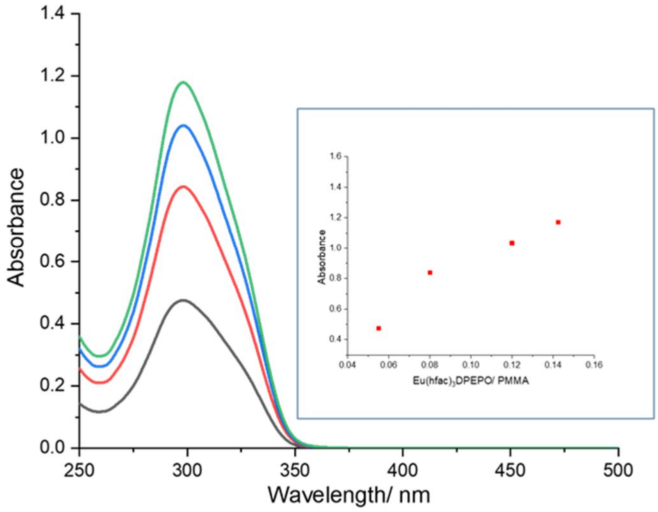

Figure 4.12 UV/Vis absorption spectra of Eu(hfac)$_3$DPEPO in PMMA at different concentrations (w/w)% : 5 (black), 8 (red), 12 (blue), and 14 (green). The inset shows a plot of absorbance versus concentration (w/w) % of the complex in PMMA.

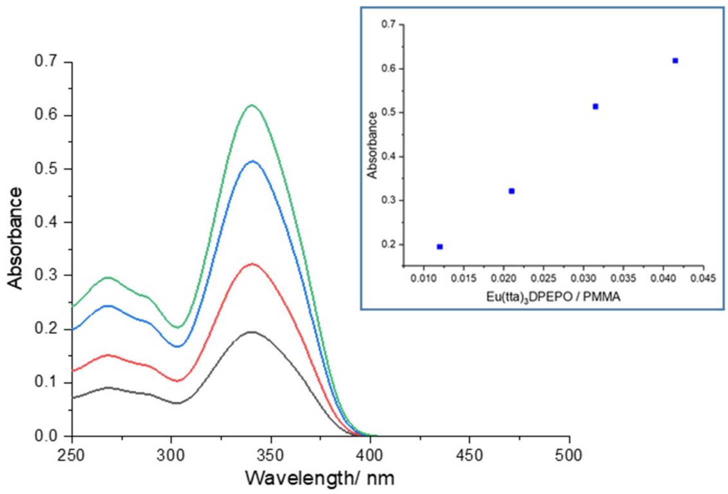

Figure 4.13 UV/Vis absorption spectra of Eu(tta)$_3$DPEPO in PMMA at different concentration (w/w)% : 1.2 (black), 2.1(red), 3.2(blue), and 4.1 (green). The inset shows a plot of absorbance versus concentration (w/w) % of the complex in PMMA.

4.3.4 Photoluminescence in PMMA

Photoluminescence studies were conducted in PMMA to examine the effect of the polymer matrix on the luminescence properties of the europium complexes. Figure 4.14 shows the excitation and emission spectrum of each complex in PMMA at room temperature. Upon excitation, at 300 nm for Eu(hfac)$_3$DPEPO and 340 nm Eu(tta)$_3$DPEPO, both complexes exhibited characteristic red emission with sharp narrow bands in the range 575–710 nm attributed to the europium-centred transitions $^5D_0 \rightarrow {}^7F_J$ (J = 0–4). The absence of emission from the ligands in the UV/blue region indicates an efficient intramolecular energy transfer to the metal ion in PMMA. However, in the case of Eu(tta)$_3$DPEPO, the emission spectrum shows a weak emission band at 425–500 nm. Since the energy transfer efficiency is not 100% in this complex (Table 4.2), this can be attributed to phosphorescence from DPEPO ligand, as reported by Xu et al.[42]

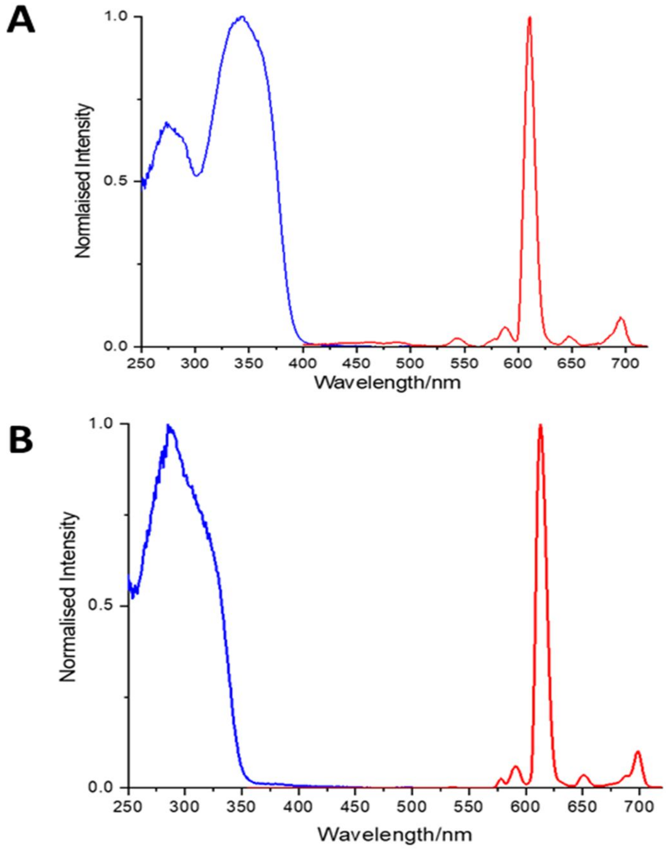

Figure 4.14 A) the emission spectrum (red), excited at 340 nm, and excitation spectrum, detected at 610 nm (blue) of Eu(tta)$_3$DPEPO in PMMA. B) the emission spectrum (red), excited at 300 nm, and excitation spectrum, detected at 610 nm (blue) of Eu(hfac)$_3$DPEPO in PMMA.

Although the excitation spectra of both complexes mimic the ones in DCM, there is a difference that, in the case of encapsulation in PMMA, the excitation peaks tend to be broader and red-shifted (less than 10 nm), which can be explained by the inner filter effect. However, it could also be due to the interaction of the ligands with the PMMA matrix, as PMMA can coordinate with the europium metal via oxygen donors.[1]

The total quantum yield of Eu(tta)$_3$DPEPO was measured to be 0.75, using Eu(hfac)$_3$DPEPO as a reference, based on the literature value of 0.85 reported by Moudam et al.[44], as shown in Figure 4.15.

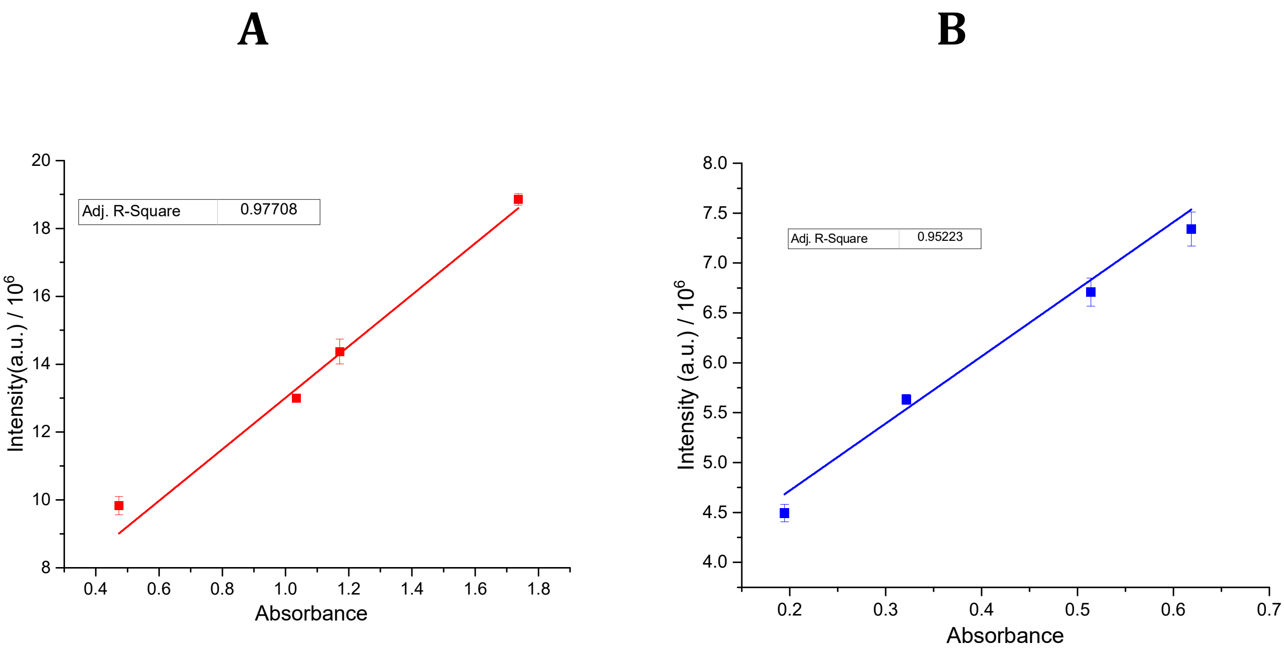

Figure 4.15 Plot of integrated luminescence intensity versus absorbance for A) Eu(hfac)$_3$DPEPO (red) excited at 300 nm and B) Eu(tta)$_3$DPEPO (blue) excited at 340 nm and Eu(hfac)$_3$DPEPO in PMMA.

Figure 4.16 shows the luminescence decay curve of Eu(tta)$_3$DPEPO in PMMA. As in DCM, the decay of each complex in PMMA was fitted to a single-exponential function, indicating the presence of a single emitting species in the polymer matrix.

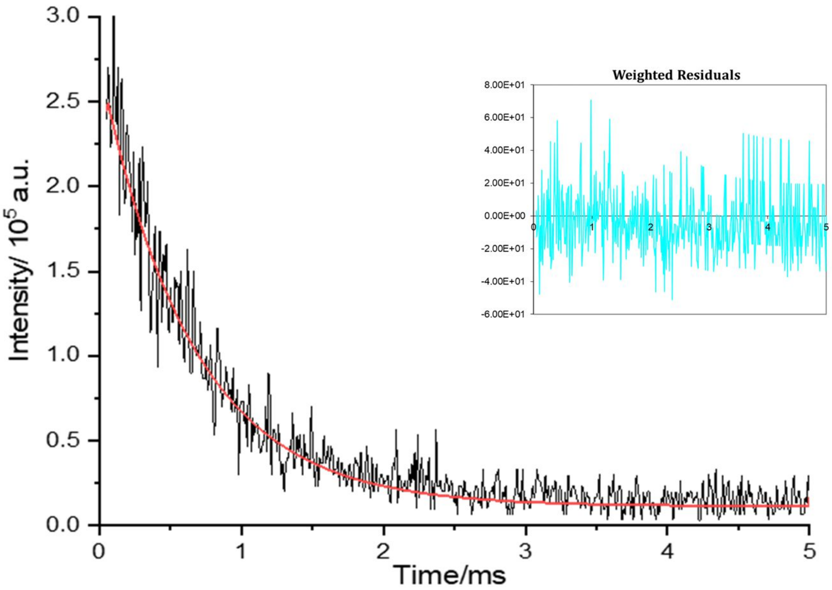

Figure 4.16 Decay data(black), fitted single exponential function (red), and weighted residuals of Eu(tta)$_3$DPEPO in PMMA, excited at 340 nm and monitored at 610 nm.

Moudam et al.[44] reported the photophysical properties of Eu(hfac)$_3$DPEPO in PMMA. Their work, summarised in Table 4.2, showed the significant role DPEPO plays in the PMMA matrix. The ϕ_{tot} value of Eu(hfac)$_3$(H$_2$O)$_2$ in PMMA was only 0.26, and the presence of DPEPO increased ϕ_{tot} to 0.85, indicating that the influence of DPEPO on the luminescence efficiency is more significant in PMMA than DCM. Values presented in Table 4.2 are an average of three measurements in PMMA.

Table 4.2 Photophysical properties of Eu(hfac)$_3$DPEPO and Eu(tta)$_3$DPEPO in PMMA.

	Eu(hfac)$_3$DPEPO (as reported by Moudam et al.) [44]	**Eu(tta)$_3$DPEPO**
τ_{Ln} /*ms*	0.77	0.64
ϕ_{Ln}	0.80	0.82
τ_R /*ms*	0.96	0.75
η_{sens}	1.0	0.91
ϕ_{tot}	0.85	0.75

For the complex $Eu(tta)_3DPEPO$ the ϕ_{tot} value increased from 0.65 in DCM to 0.75 in PMMA, which is in agreement with the value of 0.74 reported in the literature (determined by the absolute method).[3] The ϕ_{Ln} was enhanced from 0.71 to 0.82. The sensitization efficiency is unchanged in PMMA compared with DCM; therefore, the increase of ϕ_{tot} can be attributed to the enhancement of the ϕ_{Ln} value.

Table 4.3 lists the radiative, k_r, and non-radiative rate constants, k_{nr}, of $Eu(hfac)_3DPEPO$ and $Eu(tta)_3DPEPO$ in DCM and PMMA. These rate constants are calculated from the radiative and luminescence lifetimes, as described in Chapter 2. For $Eu(hfac)_3DPEPO$, the rate of non-radiative decay remains unchanged ongoing from DCM to PMMA, and the slight increase in ϕ_{Ln} in PMMA is due, therefore, to the slight increase in the radiative rate constant. It should be recalled that the value of k_r depends on the cube of the refractive index, *n* (Equation 2-18). In the case of PMMA and DCM, the ratio of n^3 is 1.14, and this accounts for the increase in the value of k_r in PMMA. In contrast, for $Eu(tta)_3DPEPO$, there is a substantial decrease in the rate of non-radiative decay ongoing from DCM to PMMA, indicating that for this complex, the PMMA matrix plays a significant role in suppressing quenching of the europium emission.

Table 4.3 Radiative and non-radiative rate constants of $Eu(hfac)_3DPEPO$ and $Eu(tta)_3DPEPO$ in DCM and PMMA.

	$Eu(hfac)_3DPEPO$	**$Eu(tta)_3DPEPO$**
	DCM	
k_r/s^{-1}	910	1010
k_{nr}/s^{-1}	250	420
	PMMA	
k_r/s^{-1}	1040	1330
k_{nr}/s^{-1}	250	230

The encapsulation $Eu(tta)_3DPEPO$ in PMMA makes a transparent film, but upon UV irradiation, its high quantum yield value is apparent visibly as intense red emission all over the PMMA, as shown in Figure 4.17. The intensity is exceptionally high at the edges due to the total internal reflection within the film, the effect that is exploited in luminescent solar concentrators.

Figure 4.17 PMMA film containing $Eu(tta)_3DPEPO$ (left) and upon UV irradiation (right).

4.4 Conclusion

In this chapter, we addressed the photophysical properties of $Eu(hfac)_3DPEPO$ and $Eu(tta)_3DPEPO$. The roles that the ligands play in energy transfer were elucidated; tta and hfac ligands have lower triplet states than DPEPO; thus, energy transfer from DPEPO to the metal ion occurs via these ligands. The DPEPO ligand plays a significant role in enhancing the luminescence properties by replacing the solvent molecules, leading to a reduction in radiationless deactivation pathways and hence to efficient energy transfer and enhancement in the total quantum yields of both complexes.

Encapsulation in PMMA enhances the total quantum yields of both complexes as a result of an increase in the intrinsic quantum yield of europium emission. This effect is more significant for $Eu(tta)_3DPEPO$, where there is a substantial decrease in the rate of non-radiative decay in PMMA compared with DCM. The absorption windows of the two complexes are complementary in covering different parts of the UV/Vis region to harvest the desired high energy photon from 250-390 nm. The total quantum yield values in PMMA of 0.85 and 0.75 for $Eu(hfac)_3DPEPO$ and $Eu(tta)_3DPEPO$, respectively, make these europium complexes efficient light harvesters in the UV/blue regions and therefore excellent candidates for LSD and LSC applications.

4.5 References

1. Gavriluta, A.; Fix, T.; Nonat, A.; Paire, M.; Slaoui, A.; Charbonnière, L. J.; Guillemoles, J.-F., Enhancement of Copper Indium Gallium Selenide Solar Cells Using Europium Complex as Photon Downshifter. *Advanced Optical Materials* **2016,** *4* (11), 1846-1853.
2. Fix, T.; Nonat, A.; Imbert, D.; Di Pietro, S.; Mazzanti, M.; Slaoui, A.; Charbonnière, L. J., Enhancement of silicon solar cells by down-shifting with Eu and Tb coordination complexes. *Progress in Photovoltaics: Research and Applications* **2016,** *24* (9), 1251-1260.
3. Gavriluta, A.; Fix, T.; Nonat, A.; Slaoui, A.; Guillemoles, J.-F.; Charbonnière, L. J., Tuning the chemical properties of europium complexes as down-shifting agents for copper indium gallium selenide solar cells. *Journal of Materials Chemistry A* **2017,** *5* (27), 14031-14040.
4. Griffini, G.; Bella, F.; Nisic, F.; Dragonetti, C.; Roberto, D.; Levi, M.; Bongiovanni, R.; Turri, S., Multifunctional Luminescent Down-Shifting Fluoropolymer Coatings: A Straightforward Strategy to Improve the UV-Light Harvesting Ability and Long-Term Outdoor Stability of Organic Dye-Sensitized Solar Cells. *Advanced Energy Materials* **2015,** *5* (3), 1401312-n/a.
5. Jones, C. J., *d-and f-Block Chemistry*. 2001.
6. Huang, C.-H., Rare earth coordination chemistry: fundamentals and applications. John Wiley & Sons: 2011.
7. Bünzli, J.-C. G., 2.6 Coordination chemistry. *Rare Earth Chemistry* **2020**, 185.
8. Vigato, P. A.; Peruzzo, V.; Tamburini, S., The evolution of β-diketone or β-diketophenol ligands and related complexes. *Coordination Chemistry Reviews* **2009,** *253* (7-8), 1099-1201.
9. Carlos, L. D.; Ferreira, R. A. S.; Bermudez, V. d. Z.; Ribeiro, S. J. L., Lanthanide-Containing Light-Emitting Organic–Inorganic Hybrids: A Bet on the Future. *Advanced Materials* **2009,** *21* (5), 509-534.
10. Wei, C.; Ma, L.; Wei, H.; Liu, Z.; Bian, Z.; Huang, C., Advances in luminescent lanthanide complexes and applications. *Science China Technological Sciences* **2018,** *61* (9), 1265-1285.
11. Bünzli, J.-C. G.; Moret, E.; Foiret, V.; Schenk, K. J.; Mingzhao, W.; Linpei, J., Structural and photophysical properties of europium (III) mixed complexes with β-diketonates and o-phenanthroline. *Journal of alloys and compounds* **1994,** *207*, 107-111.
12. Pawlowski, V.; Strasser, A.; Vogler, A., Synthesis, Electronic Spectra and Solvent-Induced Reversible Dissociation of Diphosphine(hexafluoroacetylacetonato)copper(I) Complexes. *Zeitschrift für Naturforschung B* **2003,** *58* (10), 950-954.
13. Claisen, L.; Ehrhardt, E. F., Ueber die Darstellung des Acetylacetons und seiner Homologen. *Berichte der deutschen chemischen Gesellschaft* **1889,** *22* (1), 1009-1019.
14. Aromí, G.; Gamez, P.; Reedijk, J., Poly beta-diketones: Prime ligands to generate supramolecular metalloclusters. *Coordination Chemistry Reviews* **2008,** *252* (8), 964-989.

15. Kumar, P.; Rao, A.; Ramakumar, K. L., Supercritical fluid extraction of thorium from tissue paper matrix employing β-diketones. *rca - Radiochimica Acta* **2009,** *97* (2), 105-112.
16. Santos, G.; Fonseca, F. J.; Andrade, A. M.; Deichmann, V.; Akcelrud, L.; Braga, S. S.; Coelho, A. C.; Gonçalves, I. S.; Peres, M.; Simões, W.; Monteiro, T.; Pereira, L., Organic light emitting diodes with europium (III) emissive layers based on β-diketonate complexes: The influence of the central ligand. *Journal of Non-Crystalline Solids* **2008,** *354* (19), 2897-2900.
17. Pointillart, F.; Maury, O.; Le Gal, Y.; Golhen, S.; Cador, O.; Ouahab, L., 4-(2-Tetrathiafulvalenyl-ethenyl)pyridine (TTF−CH═CH−Py) Radical Cation Salts Containing Poly(β-diketonate) Rare Earth Complexes: Synthesis, Crystal Structure, Photoluminescent and Magnetic Properties. *Inorganic Chemistry* **2009,** *48* (15), 7421-7429.
18. Mech, A.; Gajek, Z.; Karbowiak, M.; Rudowicz, C., Crystal-field energy level analysis for Nd3+ions at the low symmetry C1site in [Nd(hfa)4(H2O)](N(C2H5)4) single crystals. *Journal of Physics: Condensed Matter* **2008,** *20* (38), 385205.
19. Huang, X.; Han, S.; Huang, W.; Liu, X., Enhancing solar cell efficiency: the search for luminescent materials as spectral converters. *Chemical Society Reviews* **2013,** *42* (1), 173-201.
20. Bünzli, J.-C. G., On the design of highly luminescent lanthanide complexes. *Coordination Chemistry Reviews* **2015,** *293–294*, 19-47.
21. Hasegawa, Y.; Murakoshi, K.; Wada, Y.; Kim, J.-H.; Nakashima, N.; Yamanaka, T.; Yanagida, S., Characteristic emission of β-diketonato Nd3+ complexes dressed with perfluoroalkyl groups in DMSO-d6. *Chemical physics letters* **1996,** *260* (1-2), 173-177.
22. Yanagida, S.; Hasegawa, Y.; Murakoshi, K.; Wada, Y.; Nakashima, N.; Yamanaka, T., Strategies for enhancing photoluminescence of Nd3+ in liquid media. *Coordination chemistry reviews* **1998,** *171*, 461-480.
23. Bünzli, J.-C. G.; Eliseeva, S. V., Basics of lanthanide photophysics. In *Lanthanide Luminescence*, änninen, P., Härmä, Harri Ed. Springer: 2011; pp 1-45.
24. Bünzli, J.-C. G.; Chauvin, A.-S., Chapter 261 - Lanthanides in Solar Energy Conversion. In *Handbook on the Physics and Chemistry of Rare Earths*, Jean-Claude, G. B.; Vitalij, K. P., Eds. Elsevier: 2014; Vol. Volume 44, pp 169-281.
25. Bunzli, J.-C. G.; Eliseeva, S. V., Intriguing aspects of lanthanide luminescence. *Chemical Science* **2013,** *4* (5), 1939-1949.
26. Bauer, H.; Blanc, J.; Ross, D. L., Octacoordinate chelates of lanthanides. Two series of compounds. *Journal of the American Chemical Society* **1964,** *86* (23), 5125-5131.
27. Klink, S. I.; Hebbink, G. A.; Grave, L.; Oude Alink, P. G. B.; van Veggel, F. C. J. M.; Werts, M. H. V., Synergistic Complexation of Eu3+ by a Polydentate Ligand and a Bidentate Antenna to Obtain Ternary Complexes with High Luminescence Quantum Yields. *The Journal of Physical Chemistry A* **2002,** *106* (15), 3681-3689.

28. Pietraszkiewicz, M.; Kłonkowski, A.; Staniszewski, K.; Karpiuk, J.; Bianketti, S., Novel phosphinoxide-bearing ligands and their photoluminescent complexes: Spectroscopic studies. *Journal of Alloys and Compounds* **2004,** *380* (1), 241-247.
29. Xu, H.; Huang, W., Spectroscopic study of intramolecular energy transfer in a phosphine oxide Eu3+ complex: A stepwise process induced by intermediate energy levels. *Journal of Photochemistry and Photobiology A: Chemistry* **2011,** *217* (1), 213-218.
30. Steemers, F. J.; Verboom, W.; Reinhoudt, D. N.; van der Tol, E. B.; Verhoeven, J. W., New Sensitizer-Modified Calix[4]arenes Enabling Near-UV Excitation of Complexed Luminescent Lanthanide Ions. *Journal of the American Chemical Society* **1995,** *117* (37), 9408-9414.
31. Gupta, K.; Patra, A. K., A Luminescent pH-Responsive Ternary Europium(III) Complex of β-Diketonates and Terpyridine Derivatives as Sensitizing Antennae – Photophysical Aspects, Anion Sensing, and Biological Interactions. *European Journal of Inorganic Chemistry* **2018,** *2018* (18), 1882-1890.
32. Malta, O. L.; Brito, H. F.; Menezes, J. F. S.; Gonçalves e Silva, F. R.; de Mello Donegá, C.; Alves, S., Experimental and theoretical emission quantum yield in the compound Eu(thenoyltrifluoroacetonate)3.2(dibenzyl sulfoxide). *Chemical Physics Letters* **1998,** *282* (3), 233-238.
33. Stanley, J. M.; Zhu, X.; Yang, X.; Holliday, B. J., Europium Complexes of a Novel Ethylenedioxythiophene-Derivatized Bis(pyrazolyl)pyridine Ligand Exhibiting Efficient Lanthanide Sensitization. *Inorganic Chemistry* **2010,** *49* (5), 2035-2037.
34. Wei, C.; Sun, B.; Cai, Z.; Zhao, Z.; Tan, Y.; Yan, W.; Wei, H.; Liu, Z.; Bian, Z.; Huang, C., Quantum Yields over 80% Achieved in Luminescent Europium Complexes by Employing Diphenylphosphoryl Tridentate Ligands. *Inorganic Chemistry* **2018,** *57* (13), 7512-7515.
35. Cuan, J.; Yan, B., Luminescent lanthanide-polyoxometalates assembling zirconia–alumina–titania hybrid xerogels through task-specified ionic liquid linkage. *RSC Advances* **2014,** *4* (4), 1735-1743.
36. Kalyakina, A. S.; Utochnikova, V. V.; Zimmer, M.; Dietrich, F.; Kaczmarek, A. M.; Van Deun, R.; Vashchenko, A. A.; Goloveshkin, A. S.; Nieger, M.; Gerhards, M.; Schepers, U.; Bräse, S., Remarkable high efficiency of red emitters using Eu(iii) ternary complexes. *Chemical Communications* **2018,** *54* (41), 5221-5224.
37. McKenna, B.; Evans, R. C., Towards Efficient Spectral Converters through Materials Design for Luminescent Solar Devices. *Advanced Materials* **2017,** *29* (28), 1606491.
38. Raj, D. B. A.; Francis, B.; Reddy, M. L. P.; Butorac, R. R.; Lynch, V. M.; Cowley, A. H., Highly Luminescent Poly(Methyl Methacrylate)-Incorporated Europium Complex Supported by a Carbazole-Based Fluorinated β-Diketonate Ligand and a 4,5-Bis(diphenylphosphino)-9,9-dimethylxanthene Oxide Co-Ligand. *Inorganic Chemistry* **2010,** *49* (19), 9055-9063.

39. Correia, S. F. H.; de Zea Bermudez, V.; Ribeiro, S. J. L.; Andre, P. S.; Ferreira, R. A. S.; Carlos, L. D., Luminescent solar concentrators: challenges for lanthanide-based organic-inorganic hybrid materials. *Journal of Materials Chemistry A* **2014,** *2* (16), 5580-5596.
40. Shi, M.; Li, F.; Yi, T.; Zhang, D.; Hu, H.; Huang, C., Tuning the Triplet Energy Levels of Pyrazolone Ligands to Match the 5D0 Level of Europium(III). *Inorganic Chemistry* **2005,** *44* (24), 8929-8936.
41. Khan, M. S.; Ilmi, R.; Sun, W.; Dutra, J. D. L.; Oliveira, W. F.; Zhou, L.; Wong, W.-Y.; Raithby, P. R., Bright and efficient red emitting electroluminescent devices fabricated from ternary europium complexes. *Journal of Materials Chemistry C* **2020,** *8* (16), 5600-5612.
42. Xu, H.; Wang, L.-H.; Zhu, X.-H.; Yin, K.; Zhong, G.-Y.; Hou, X.-Y.; Huang, W., Application of Chelate Phosphine Oxide Ligand in EuIII Complex with Mezzo Triplet Energy Level, Highly Efficient Photoluminescent, and Electroluminescent Performances. *The Journal of Physical Chemistry B* **2006,** *110* (7), 3023-3029.
43. Biju, S.; Reddy, M. L. P.; Cowley, A. H.; Vasudevan, K. V., Molecular Ladders of Lanthanide-3-phenyl-4-benzoyl-5-isoxazolonate and Bis(2-(diphenylphosphino)phenyl) Ether Oxide Complexes: The Role of the Ancillary Ligand in the Sensitization of Eu3+ and Tb3+ Luminescence. *Crystal Growth & Design* **2009,** *9* (8), 3562-3569.
44. Moudam, O.; Rowan, B. C.; Alamiry, M.; Richardson, P.; Richards, B. S.; Jones, A. C.; Robertson, N., Europium complexes with high total photoluminescence quantum yields in solution and in PMMA. *Chemical Communications* **2009,** (43), 6649-6651.
45. Sager, W. F.; Filipescu, N.; Serafin, F. A., Substituent Effects on Intramolecular Energy Transfer. I. Absorption and Phosphorescence Spectra of Rare Earth β-Diketone Chelates. *The Journal of Physical Chemistry* **1965,** *69* (4), 1092-1100.
46. Congiu, M. Synthesis and Characterisation of

Luminescent Lanthanide Dyes for Solar Energy Conversion. The University of Edinburgh, Edinburgh, 2013.
47. Susumu, S.; Masanobu, W., Relations between Intramolecular Energy Transfer Efficiencies and Triplet State Energies in Rare Earth β-diketone Chelates. *Bulletin of the Chemical Society of Japan* **1970,** *43* (7), 1955-1962.
48. Xin, H.; Shi, M.; Gao, X. C.; Huang, Y. Y.; Gong, Z. L.; Nie, D. B.; Cao, H.; Bian, Z. Q.; Li, F. Y.; Huang, C. H., The Effect of Different Neutral Ligands on Photoluminescence and Electroluminescence Properties of Ternary Terbium Complexes. *The Journal of Physical Chemistry B* **2004,** *108* (30), 10796-10800.

49. Congiu, M.; Alamiry, M.; Moudam, O.; Ciorba, S.; Richardson, P. R.; Maron, L.; Jones, A. C.; Richards, B. S.; Robertson, N., Preparation and photophysical studies of [Ln(hfac)3DPEPO], Ln = Eu, Tb, Yb, Nd, Gd; interpretation of total photoluminescence quantum yields. *Dalton Transactions* **2013,** *42* (37), 13537-13545.

CHAPTER 5: Electronic Energy Transfer from Donors to Europium Complexes in PMMA

"... we find that two molecules – or atoms – of the same kind, say of hydrogen, have the same properties, though one has been compounded with carbon and buried in the earth as coal for untold ages, while the other has been 'occluded' in the iron of a meteorite, and after unknown wanderings in the heavens has at last fallen into the hands of some terrestrial chemist"

–James C. Maxwell

CHAPTER **5**

Electronic Energy Transfer from Donors to Europium Complexes in PMMA

5.1 Introduction

As reported in Chapter 4, $Eu(tta)_3DPEPO$ and $Eu(hfac)_3DPEPO$ were synthesised, and their photophysical properties were determined. Both complexes demonstrated favourable photophysical properties, with total quantum yield ($\emptyset_{tot}$) values of 0.75 and 0.85, respectively, in PMMA. Such values would make them excellent candidates for light conversion technologies such as luminescent down-shifting layers (LDS) and luminescent solar concentrators (LSCs).

In the context of solar technology and renewable energy technologies in general, rare earth metals are deemed critical materials. Indeed lanthanides ions are an essential component to many sophisticated technologies such as wind turbines (terbium, neodymium, samarium); batteries (lanthanum); fiber-optic technology (ytterbium); fluorescent lighting, liquid crystal displays, solar technologies and phosphors (europium).[1, 2]Although they were discovered in 1778, the demand for rare earths started in the 1960s, coinciding with their use in the aforementioned technologies, in addition to their use in the oil industry and computer systems. As a result of this demand, the production and consumption of rare earth metals started to increase dramatically, with the expectation for global demand to increase in the future.[3] This is undoubtedly the case for europium, which is considered among the 'heavy' lanthanides elements that are hard to find and expensive to mine and process compared to the rest of the lanthanides.[1,4]

The main problem with the supply of rare earth metals stems from the fact that they are not accessible: very few countries have accessible reserves of lanthanides. China is the largest exporter and has a monopoly over the mining and production of rare earths, holding 90% of the world market.[5] The restriction of the production and mining of rare earths to a few countries represents a security challenge over the unpredictability of the supply chain, making rare earths a matter of national security.[2] As a result, rare earth metals are expensive; for example, the price for europium reached 5870 US$/kg in 2011.[6] At the time of writing this thesis, the cost of $EuCl_3.6H_2O$ – the starting material for the synthesised complexes presented in this work – is £137 for 5 grams.[7]

For this reason, one of the goals of this work is to investigate whether it is possible to reduce the amount of the europium complexes used while maintaining many of the photophysical advantages of europium, such as intense narrow emission bands in the red region, long lifetimes, and favourable quantum yields. It may be possible to achieve this by incorporating a donor as a dopant in the PMMA film to enhance photosensitisation of the europium emission. In such a donor-acceptor fluorophore system, inexpensive and simple organic molecules could be used as donors, with Eu(III) complexes acting as acceptors. These aromatic molecules would assist in harvesting high energy photons in the UV region (250–300 nm), transferring their excitation energy (via Förster resonance energy transfer – FRET) to the Eu(III) complexes in PMMA. Thus, the co-doping of Eu(III) complexes with organic molecules in PMMA films could reduce the amount of metal used and improve the harvesting of high energy photons in the wavelength range that is not covered by the absorption windows of both complexes.

A donor-acceptor fluorophore system has been adopted before to tackle the problem of reabsorption losses, one of the main factors affecting the performance in LSCs and LDS that use organic dyes with small Stokes shifts.[8] For their quest to minimise the reabsorption losses in LSCs, Zhang et al. demonstrated that perylene diimide-based donor–emitter fluorophores helped to increase the total quantum yield and minimise the reabsorption losses in large-area LSCs. Although they did not quantify the energy transfer efficiencies, a highly efficient FRET process was observed, indicated by the decrease in the donor emission, and most of the overall emission (> 95%) originated from the acceptors; as a result, the overall quantum yield was enhanced to 97.6% .[8, 9] Fernandes et al. showed a mixture of organic dye and a europium complex could be used as an LDS layer on a photovoltaic device, but the presence of the organic dye with europium complex led to a decrease in the total quantum yield, and there was no indication of an energy transfer process, which may be attributed to the lack of the spectral overlap between the two components.[10] Danos et al. demonstrated the effect of an efficient excitation energy transfer between multiple dyes compared to one dye as an LDS layer in CdTe solar cells: the performance of an LDS layer (in PMMA) comprising two dyes led to an enhancement in the external quantum efficiency of the CdTe cell. An increase in the acceptor fluorescence intensity in the presence of the donor molecules indicated that the energy transfer process had occurred.[11] In the aforementioned studies, it is worth noting the energy transfer efficiencies were assessed in terms of the overall quantum yields or by measuring the external quantum efficiencies of the whole system, but specific quantitative calculations of the energy transfer process between donor and acceptor were not discussed.

The conventional use for Förster resonance energy transfer is associated with common organic dyes such as pyrene, coumarin, fluorescein, rhodamine and cyanine as donor-acceptor.[12] The scope of FRET can extend beyond organic dyes to include luminescent lanthanide complexes.[13-15] Selvin et al. demonstrated that FRET could be extended to pair a europium or terbium complex with an organic molecule in a donor-acceptor system.[16, 17] In these studies, both europium and terbium were used as donors, lifetime and quantum yields measurements showed consistency with FRET process, and specific energy transfer calculations were carried out; however, these studies were conducted in a solution phase and intended for biological applications.[16, 17]

As described in Chapter 2, it is critical for the process of energy transfer that the emission spectrum of the donor overlaps with the absorption spectrum of the acceptor.[18] In this study, four organic molecules were chosen to act as donors, DPEPO, biphenyl, indole, and p-terphenyl, with Eu(III) complexes acting as acceptors. Figure 5.1 shows the chemical structures of the donors used with $Eu(tta)_3DPEPO$ and $Eu(hfac)_3DPEPO$. These donors have several advantages: i) favourable absorption coefficients; ii) high absorption in the UV region, especially in 250–300 nm, which could complement the absorption profile in the Eu(III) complexes; iii) good spectral overlap of their emission with the acceptor's absorption; iv) inexpensive and commercially available in large quantities, except for DPEPO which was synthesised from an inexpensive starting material. The prices of donors used were inexpensive; for example, the price of indole is £20/kg and £23/ kg for biphenyl, compared to £137 for 5 grams of Eu(III).

This chapter reports the observation of energy transfer in PMMA films containing $Eu(tta)_3DPEPO$ and $Eu(hfac)_3DPEPO$ co-doped with DPEPO, biphenyl, indole and p-terphenyl in PMMA. Energy transfer efficiencies have been measured for each donor-acceptor system for a range of concentrations of donor and acceptor.

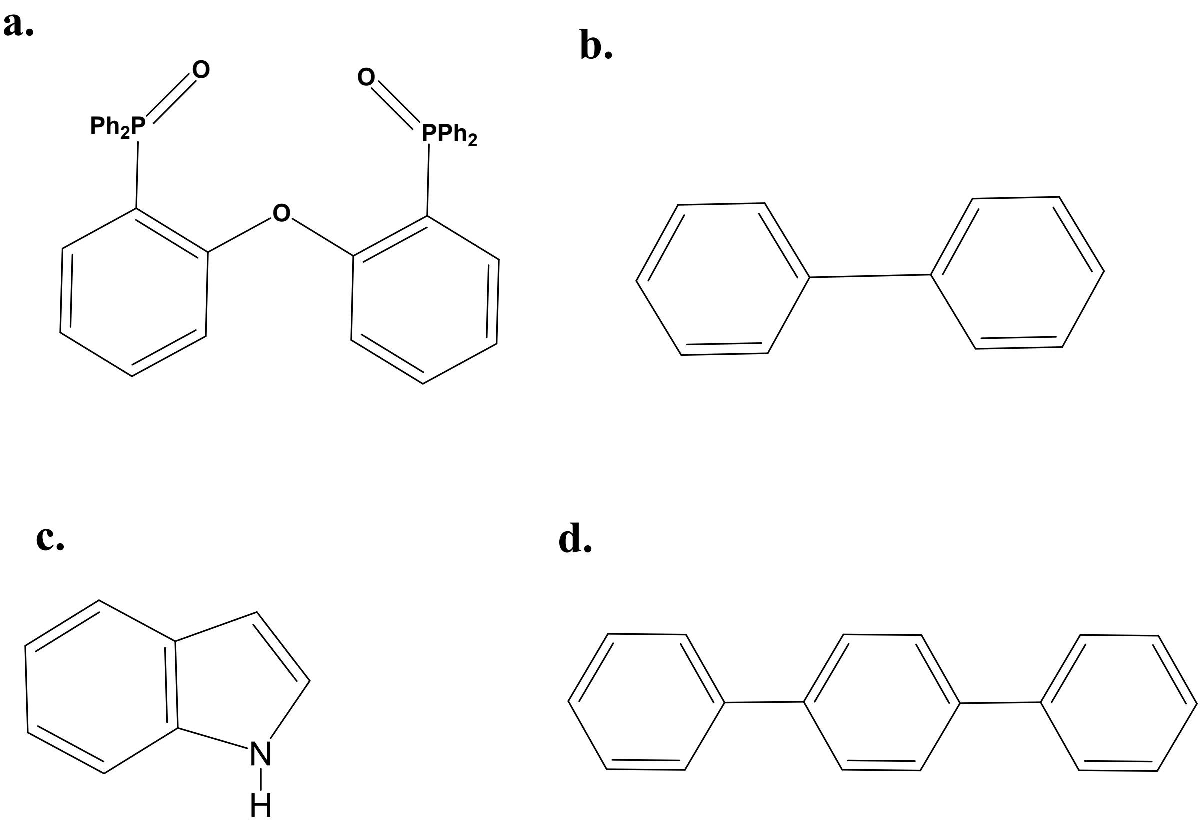

Figure 5.1 Chemical structures of the donors: (a) DPEPO, (b) biphenyl, (c) indole, (d) p-terphenyl.

5.2 Experimental

5.2.1 Chemicals

Dichloromethane and chloroform was HPLC grade obtained from Fisher Chemicals, was used without further purifications. Eu(tta)$_3$DPEPO, Eu(hfac)$_3$DPEPO and DPEPO were synthesised as described in Chapter 3. Biphenyl (99.5%), indole (≥99%), p-terphenyl (≥99.5%) and poly(methyl methacrylate) (PMMA, average MW 120, 000) were sourced from Sigma-Aldrich.

5.2.2 Polymeric Film Preparations

2.6 mM of Eu(tta)$_3$DPEPO, 6 and 9 mM of Eu(hfac)$_3$DPEPO in a solution of 3(w/w%) of PMMA were added with different concentrations of donors in 3 ml of chloroform and were heated at 55 °C and stirred for 5 hr. The total concentration of the polymer in the solution was kept fixed to ensure the blank polymer and doped polymer had the same thickness. For each measurement, a suitable volume of the solution (100 µL) was spin-coated using a pipette on quartz slides (25 mm x 25 mm x 1 mm). Dynamic spin coating (the substrate is already spinning) was used for 60 s at 500 rotation per minute (rpm) to ensure the formation of thin homogenous polymer films. After spin-coating, films were left for 24 hr at room temperature to allow for complete evaporation of the solvent.

5.2.3 Donor-Acceptor Energy Transfer Calculations

The energy transfer efficiencies $\eta_{D\text{-}A}$ of different co-doped europium complexes were determined based on Equation 5-1, as described in detail in Chapter 2. This deals with the case where there is unavoidable absorption by the acceptor at the wavelength used to excite the donor.

$$\eta_{D\text{-}A} = \frac{A_a\ (\lambda_{ex})}{A_d\ (\lambda_{ex})} \left(\frac{F_{tot}(\lambda_{ex})}{F_a(\lambda_{ex})} - 1\right) \qquad \textbf{Equation 5-1}$$

where A_a and A_d are the absorbance of the acceptor alone and the donor alone, respectively, at the excitation wavelength λ_{ex}, F_{tot} is the luminescence intensity of the acceptor in the presence of the donor (i.e. due to both energy transfer from the donor and direct excitation of the acceptor); and F_a is the luminescence intensity of the acceptor in the absence of the donor (i.e. due to direct excitation of the acceptor).

Two samples were measured for each energy transfer calculation, an acceptor only and a donor-acceptor combination. The UV/Vis absorbance and the photoluminescence measurements were conducted on both systems. The energy transfer efficiency was determined by measuring the excitation spectrum of the acceptor (Eu complex) in the presence and absence of the donor. The efficiency was calculated from the respective intensities at an excitation wavelength where the donor was dominant. The concentration of the acceptor was kept fixed as far as possible between the acceptor-only and donor-acceptor samples, but correction for inevitable, small differences was carried out by scaling the acceptor-only absorbance (or excitation intensity) to be equal to that of the D-A sample at a wavelength where only A absorbs. An example of a calculation is given below.

Consider the case of (2.6 mM) Eu(tta)$_3$DPEPO co-doped with (21 mM) DPEPO. The UV/Vis absorption spectra of Eu(tta)$_3$DPEPO (acceptor) alone (scaled) and that of Eu(tta)$_3$DPEPO co-doped with DPEPO are shown in Figure 5.2. The long-wavelength absorption band (340 nm) can be identified exclusively with the tta ligand in the complex. However, there is a slight complication in the scaling process for this complex because there is a shift in the tta band when the DPEPO donor is added.

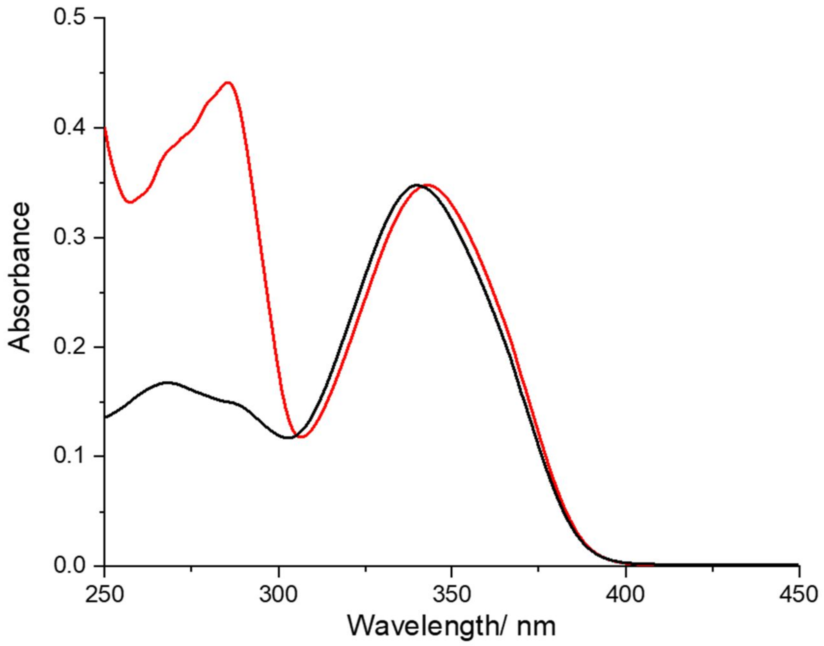

Figure 5.2 UV/Vis absorption spectra of 2.6 mM Eu(tta)$_3$DPEPO (black line) - scaled at the maximum intensity of the tta band- and the complex co-doped with DPEPO at 21 mM (red line) in PMMA.

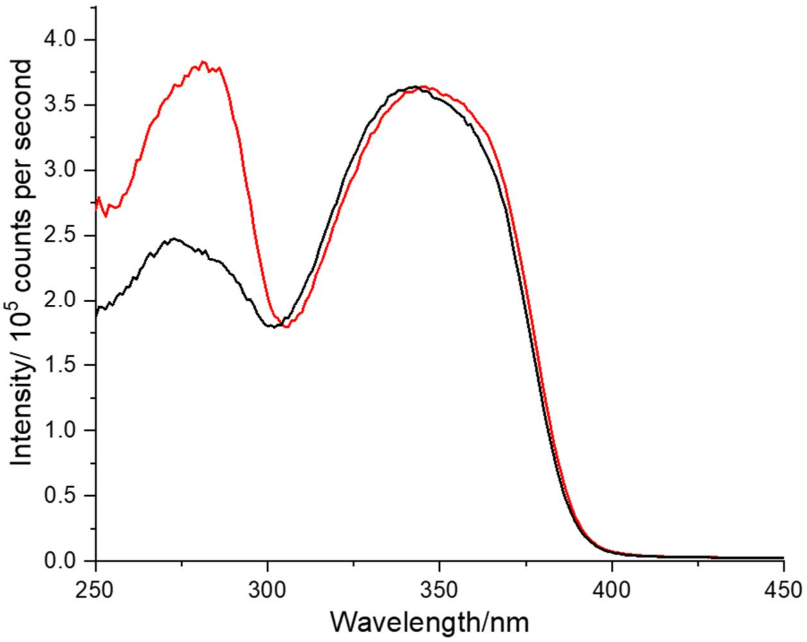

Figure 5.3 Excitation spectra, detected at 610 nm, of 2.6 mM Eu(tta)$_3$DPEPO (black line), and the complex co-doped with DPEPO at 21 mM (red line) in PMMA.

Therefore, the λ_{max} of the tta band, rather than a constant wavelength, was used for scaling the absorbance of the acceptor spectrum. The excitation spectra are shown in Figure 5.3. The excitation spectrum Eu(tta)$_3$DPEPO (acceptor) alone has been scaled in the same fashion as the absorption spectrum. The donor, DPEPO, absorbs strongly at 285 nm; therefore, energy transfer was measured at this excitation wavelength.

The value of A_a at 285 nm was determined from the complex-only absorption spectrum, and A_d was obtained by subtracting A_a from the absorbance of the co-doped complex (donor-acceptor system) at 285 nm. The ratio of F_{tot} to F_a is equal to the ratio of the excitation intensities (at 285 nm) of the co-doped complex and the complex only.

Thus, the energy transfer efficiency $\eta_{D\text{-}A}$ can be calculated using Equation 5-1:

$$\eta_{D\text{-}A} = \frac{0.15}{0.29}\left(\frac{3.76 \times 10^5}{2.30 \times 10^5}\text{-}1\right) = 0.33$$

Equation 5-1 can be used to calculate the quantum yield of the excitation due to the energy transfer from the donors. The quantum yield for excitation of the donor, ϕ_{FRET}, is the product of the energy transfer efficiency and the total quantum yield from direct excitation, ϕ_{total} (measured in Chapter 4). Therefore, Equation 5-1 is equivalent to the ratio of the ϕ_{FRET} for the FRET process (excitation of the donor) to the ϕ_{total} for direct excitation of the acceptor as shown in Equation 5-4, which results from the derivations in Equations 5-2 and 5-3:

$$\eta_{D\text{-}A} = \frac{A_a\ (\lambda_{ex})}{A_d\ (\lambda_{ex})}\left(\frac{F_{tot}(\lambda_{ex})}{F_a(\lambda_{ex})}\text{-}1\right) = \frac{A_a\ (\lambda_{ex})}{A_d\ (\lambda_{ex})}\left(\frac{F_{tot}(\lambda_{ex})\text{-}F_a(\lambda_{ex})}{F_a(\lambda_{ex})}\right) \qquad \textbf{Equation 5-2}$$

$$F_{FRET}(\lambda_{ex}) = F_{tot}(\lambda_{ex})\text{-}F_a(\lambda_{ex}) \qquad \textbf{Equation 5-3}$$

where $F_{FRET}(\lambda_{ex})$ is the intensity of (acceptor) fluorescence due to energy transfer from the donor.

$$\eta_{D\text{-}A} = \frac{A_a\ (\lambda_{ex})}{A_d\ (\lambda_{ex})}\left(\frac{F_{FRET}(\lambda_{ex})}{F_a(\lambda_{ex})}\right) = \left(\frac{F_{FRET}(\lambda_{ex})/A_d\ (\lambda_{ex})}{F_a(\lambda_{ex})/A_a\ (\lambda_{ex})}\right) = \frac{\phi_{FRET}}{\phi_{total}} \qquad \textbf{Equation 5-4}$$

5.2.4 Solar Cells Testing

The luminescent materials were added to 3(w/w%) PMMA dissolved in 2 ml chloroform and were spin-coated using a volume of 100 μL for 30 s at 400 rpm on c-Si PV wafers (20 mm x 20 mm) purchased from SUPERCELLS. Then the devices were kept in the oven at 40 °C for 3 hr.

For the current-voltage (J-V) curves measurements, a Sciencetech SLB-300A compact solar simulator class AAA was used to irradiate the solar cells with an AM 1.5G simulated sunlight at 100 mW cm^{-2}. An Autolab PGSTAT30 potentiostat was used to record the J-V curves. The active area was covered by a black mask with an aperture size of 0.50 cm^2. The J-V testing was performed at 25 °C with a forward and reverse scan rate at 100 mV s^{-1}.

For the incident photon-to-current conversion efficiency (IPCE) measurements, a Bentham Instruments system based on TM300 with a double grating monochromator and chopped light source (from IL1 quartz halogen) was used. Incident irradiance was monitored with a calibrated Si photodiode to obtain a spectral response and quantum efficiency. The IPCE measurements were conducted by Dr Guillaume Zoppi at Northumbria University.

5.2.4.1 Brief Background on Solar Cells Testing

Two types of measurements were conducted to assess the performance of the co-doped complex on the photovoltaic devices: the J-V curves and the incident photon-to-current conversion efficiency (IPCE).

5.2.4.1.1 J-V Curves

Power conversion efficiency (PCE) is a key parameter to assess the efficiency of a photovoltaic device, which is the ratio of the incident solar power to the output electrical power. PCE values and other key parameters can be calculated by conducting current-voltage (I-V) measurements, which consists of applying different voltages to a photovoltaic device while it is under illumination and measuring the output current at each step.[19] It is worth noting that current density (J) is usually used instead of current (I) in order to eliminate the dependence of the solar cell area. From J-V curves, several parameters can be obtained:

- The short-circuit current density (J_{sc}) is defined as the photo-generated current density when the voltage across the photovoltaic device is zero. This parameter depends on many factors, such as the power of the incident solar radiation and the optical properties of the device.
- The open-circuit voltage (V_{oc}) is the voltage at which zero current flows through an external circuit; it is the maximum voltage available from a photovoltaic device.
- Fill Factor (FF) is the ratio between the maximum power ($P_{max} = J_{mpp}\ V_{mpp}$) generated by a solar cell and the product of J_{sc} and V_{oc} as described in equation 5-5:[20]

$$FF = \frac{P_{max}}{J_{sc}\ V_{oc}} = \frac{J_{mpp}\ V_{mpp}}{J_{sc}\ V_{oc}} \qquad \textbf{Equation 5-5}$$

where the subscript “mpp” denotes the maximum power point of the PV device.

- Power conversion efficiency (PCE) describes the ratio of maximum electrical power out (P_{out}) to the solar power input (P_{in}) into the device (Equation 5-6):

$$\mathrm{PCE} = \frac{P_{out}}{P_{in}} = \frac{J_{sc}\, V_{oc}\, FF}{P_{in}} \qquad \textbf{Equation 5-6}$$

5.2.4.1.2 Incident Photon-to-Current Conversion Efficiency (IPCE)

The wavelength-dependent response of a photovoltaic device can be assessed by the incident photon-to-current conversion efficiency (IPCE), commonly referred to as the external quantum efficiency (EQE). The EQE is a dimensionless parameter defined as the ratio of the number of electrons in the outer circuit to the number of photons at each wavelength incident on the front surface of the cell.[21]

5.3 Results and Discussion

5.3.1 Solution-phase UV/Vis Absorption Spectra of the Donors

The UV absorption spectra of the donors, DPEPO, biphenyl, indole and p-terphenyl, in DCM solution are shown in Figure 5.4. The absorption spectrum of biphenyl shows an absorption onset at 34,722 cm^{-1} (288 nm) and λ_{max} at 40,160 cm^{-1} (249 nm, ε = 17,045 M^{-1} cm^{-1}). Indole shows an absorption onset at 33222 cm^{-1} (301 nm) and λ_{max} at 36,630cm^{-1} (273 nm, ε = 10,350 M^{-1} cm^{-1}). The absorption spectrum of p-terphenyl shows an onset at 31,055 cm^{-1} (322 nm) and λ_{max} at 35,842 cm^{-1} (279 nm, ε = 32,740 M^{-1} cm^{-1}). DPEPO has an absorption onset around 33,000 cm^{-1} (303 nm) and λ_{max} at 34,722 cm^{-1} (288 nm, ε = 8,863 M^{-1} cm^{-1} [22]). All donors, aromatic molecules, have intense absorption bands (π-π^* transitions) in the UV region, which make them excellent light harvesters.

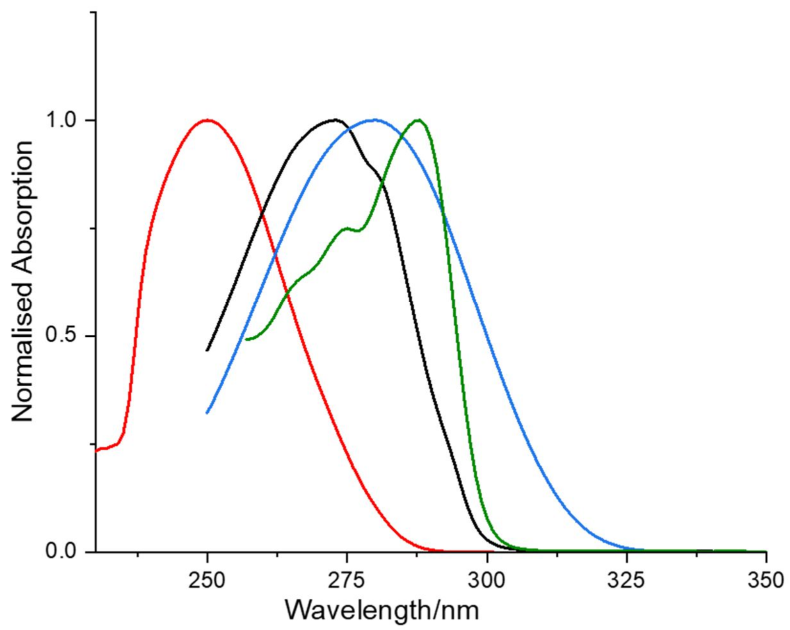

Figure 5.4 UV absorption spectra of biphenyl (red line), indole (black line), p-terphenyl (blue line) and DPEPO (green line) in DCM at room temperature.

5.3.2 UV/Vis Absorption Spectra of Donor-Acceptor Systems

Figures 5.5 to 5.12 show the absorption spectra of each donor embedded with complexes in PMMA, and of Eu(tta)$_3$DPEPO and Eu(hfac)$_3$DPEPO without the presence of the donor in PMMA. The absorption window of each donor complements the absorption spectra of complexes in the region 250–300 nm. The absorption spectra of donors in PMMA are in agreement with that in the solution phase (Figure 5.4), indicating that the donors remain intact when embedded in the polymer matrix. As discussed in Chapter 4, PMMA has a negligible absorption of photons at wavelengths above 250 nm (Figure 4.11).

The absorption spectrum of 2.6 mM Eu(tta)$_3$DPEPO co-doped with 18 mM biphenyl is shown in Figure 5.5. It can be seen that co-doping of biphenyl at 18 mM does not affect the absorption band at 340 nm, due to the tta ligand, where biphenyl does not absorb. The intense absorption by biphenyl at shorter wavelengths, peaking at 250 nm, is evident. The biphenyl absorption band overlaps the intrinsic absorption band of the complex that arises from the DPEPO ligand; in the case of Eu(hfac)$_3$DPEPO, the absorption of biphenyl does overlap with the absorption bands that arise from hfac and DPEPO (Figure 5.6). The same statement can be made about the absorption profiles for Eu(hfac)$_3$DPEPO co-doped with indole, DEPPO and p-terphenyl, as shown in Figures 5.8, 5.10 and 5.12.

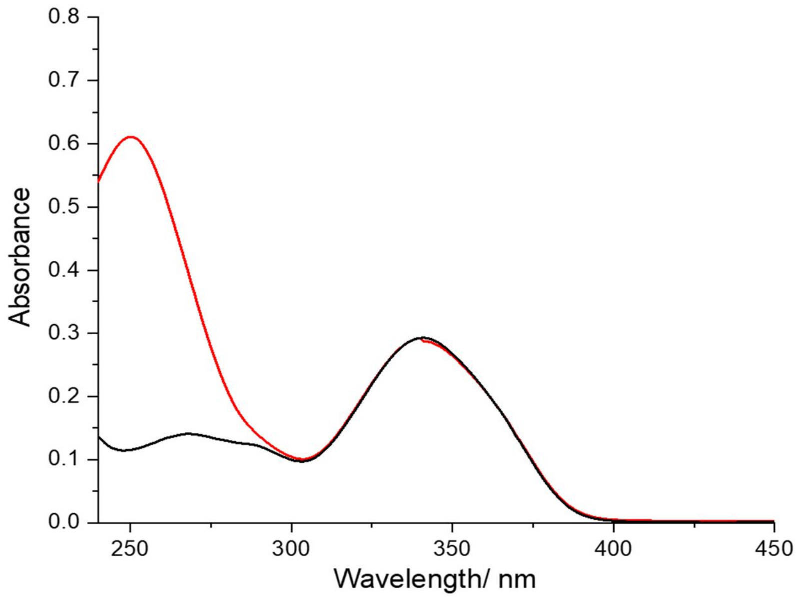

Figure 5.5 UV/Vis absorption spectra of 2.6 mM Eu(tta)$_3$DPEPO (black line), and the complex co-doped with biphenyl at 18 mM (red line) in PMMA.

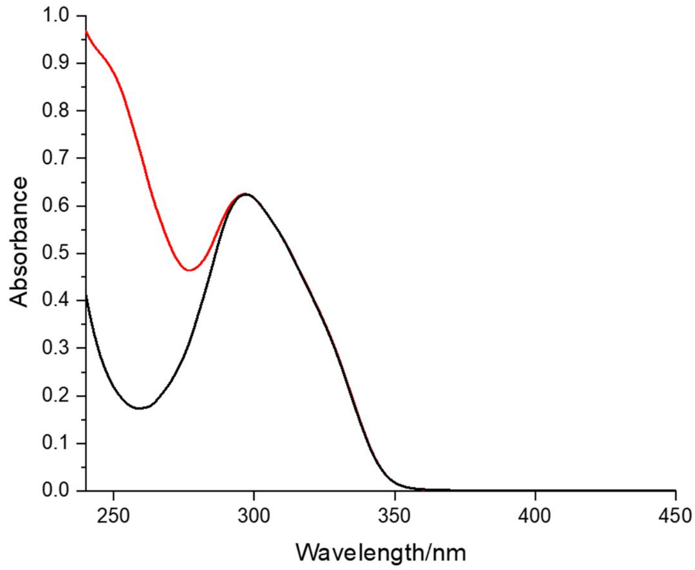

Figure 5.6 UV/Vis absorption spectra of 9 mM Eu(hfac)$_3$DPEPO (black line), and the complex co-doped with biphenyl at 18 mM (red line) in PMMA.

Figure 5.7 shows the absorption spectrum of 2.6 mM Eu(tta)$_3$DPEPO co-doped with 107.5 mM indole. The absorption band of indole with λ_{max} at 273 nm is clear.

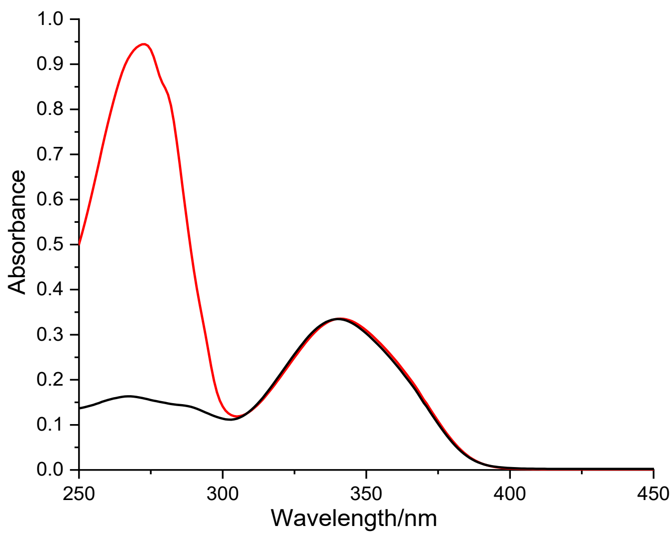

Figure 5.7 UV/Vis absorption spectra of 2.6 mM Eu(tta)$_3$DPEPO (black line), and the complex co-doped with indole at 107.5 mM (red line) in PMMA.

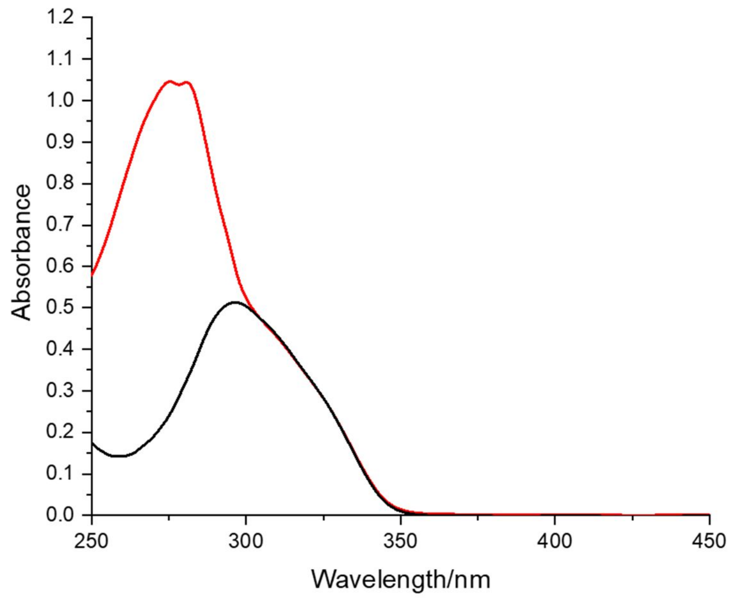

Figure 5.8 UV/Vis absorption spectra of 6 mM Eu(hfac)$_3$DPEPO (black line), and the complex co-doped with indole at 107.5 mM (red line) in PMMA.

As shown in Figure 5.9, co-doping with DPEPO causes a small shift in the absorption band of the complex due to the tta ligand, suggesting that the presence of the donor affects the local environment of the complex. The enhanced absorption due to the DPEPO donor is clear at wavelengths below 300 nm. In the case of Eu(hfac)$_3$DPEPO (Figure 5.10), the strong overlap between the absorption of hfac and DPEPO led to a slight blue shift in the absorption spectrum when co-doped with DPEPO, which strongly absorbs below 300 nm.

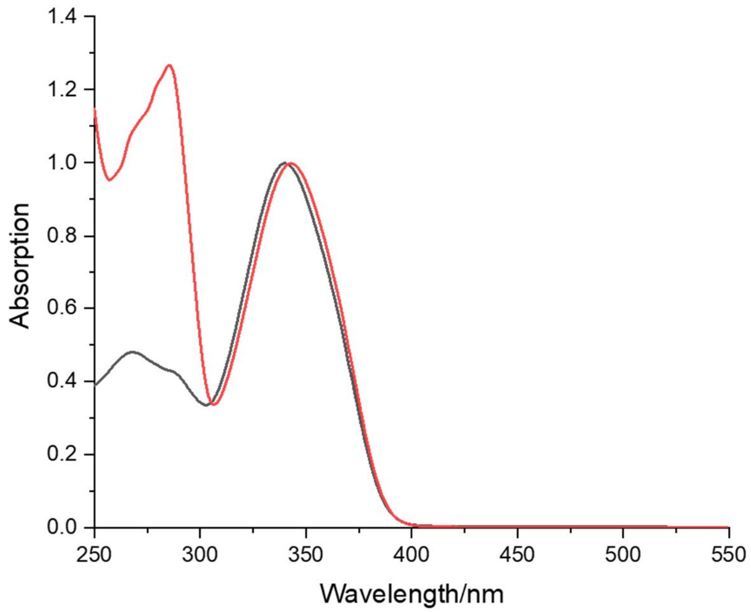

Figure 5.9 UV/Vis absorption spectra of 2.6 mM Eu(tta)$_3$DPEPO (black line), and the complex co-doped with DPEPO at 21 mM (red line) in PMMA.

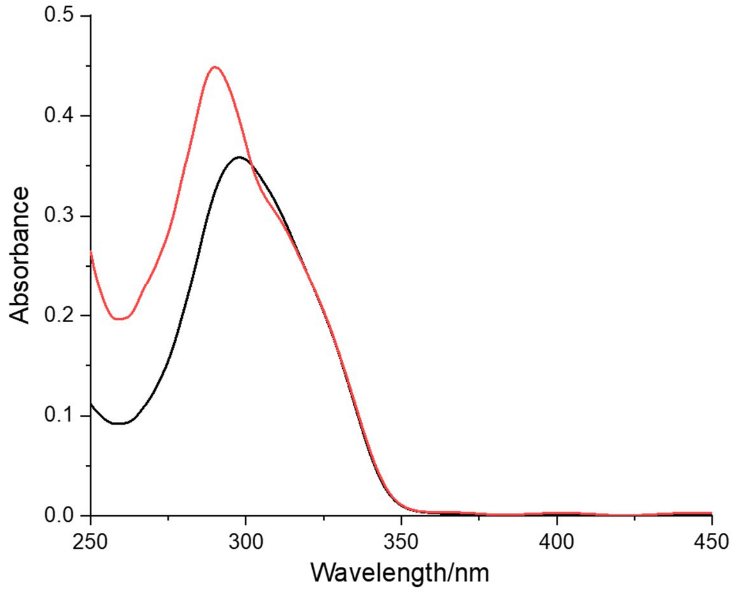

Figure 5.10 UV/Vis absorption spectra of 6 mM Eu(hfac)$_3$DPEPO (black line), and the complex co-doped with DPEPO at 20 mM (red line) in PMMA.

Figures 5.11 to 5.12 show the effect of co-doping the complex with 27 mM of p-terphenyl. In the case of p-terphenyl, the donor's absorption window extends from 250 to 325 nm. The absorption band of p-terphenyl with λ_{max} at 279 nm is prominent.

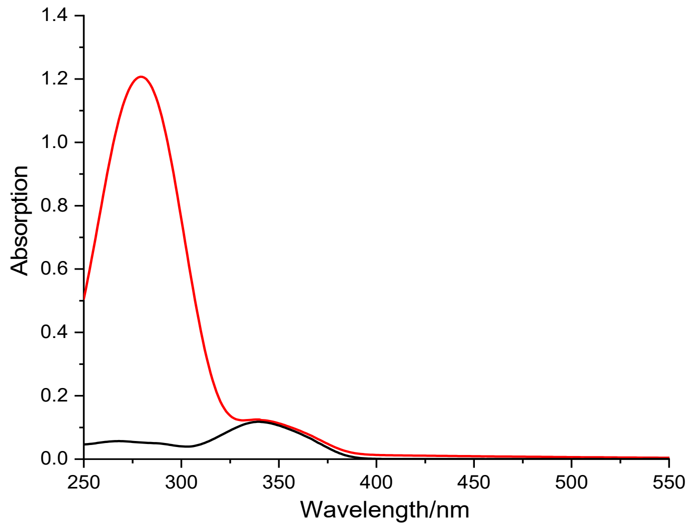

Figure 5.11 UV/Vis absorption spectra of 2.6 mM Eu(tta)$_3$DPEPO (black line), and the complex co-doped with p-terphenyl at 27 mM (red line) in PMMA.

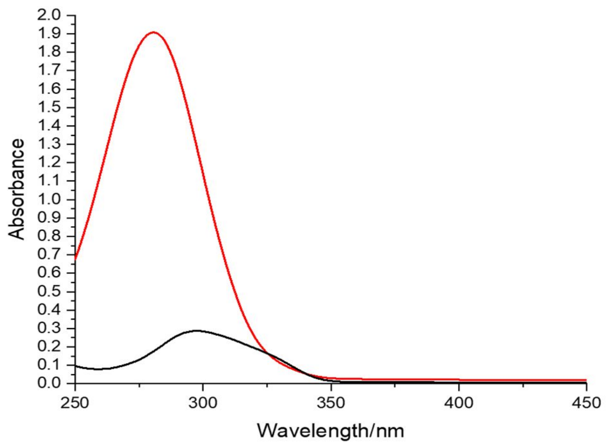

Figure 5.12 UV/Vis absorption spectra of 6 mM Eu(hfac)$_3$DPEPO (black line), and the complex co-doped with p-terphenyl at 27 mM (red line) in PMMA.

Overall, Figures 5.5–5.12 confirm that the absorption profile of each co-doped donor-acceptor system is in good agreement with the individual absorption spectra of the complex and the donor.

5.3.3 Photoluminescence of Donor-Acceptor Systems

Photoluminescence studies were conducted in PMMA at room temperature to investigate energy transfer from the donors to each of the europium complexes. Excitation spectra showing qualitative evidence of energy transfer will be presented first, followed by quantitation of energy transfer efficiencies.

5.3.3.1 Complexes Co-doped with Biphenyl

Figure 5.13(a) shows the emission spectra of $Eu(tta)_3DPEPO$ and that of $Eu(tta)_3DPEPO$ co-doped with 18 mM biphenyl, following direct excitation of the complex at 340 nm. In both cases, characteristic red emission is observed, with sharp narrow bands in the range 575–710 nm attributed to the europium-centred transitions $^5D_0 \rightarrow {}^7F_J$ (J = 0–4).[23] There was no observed difference in the relative intensities of the emission bands when co-doped with biphenyl, confirming that the local environment of the Eu(III) remained intact.

As shown in Figure 5.13(b), the excitation spectrum of the co-doped complex compared to that of the complex shows an apparent increase in intensity in the short wavelength part of the spectrum, where the donor, biphenyl, absorbs. This indicates the occurrence of energy transfer from biphenyl to the europium complex. However, the relative intensity of the excitation band due to biphenyl is significantly less than that of its absorption band (Figure 5.5), indicating that the efficiency of energy transfer is much less than one.

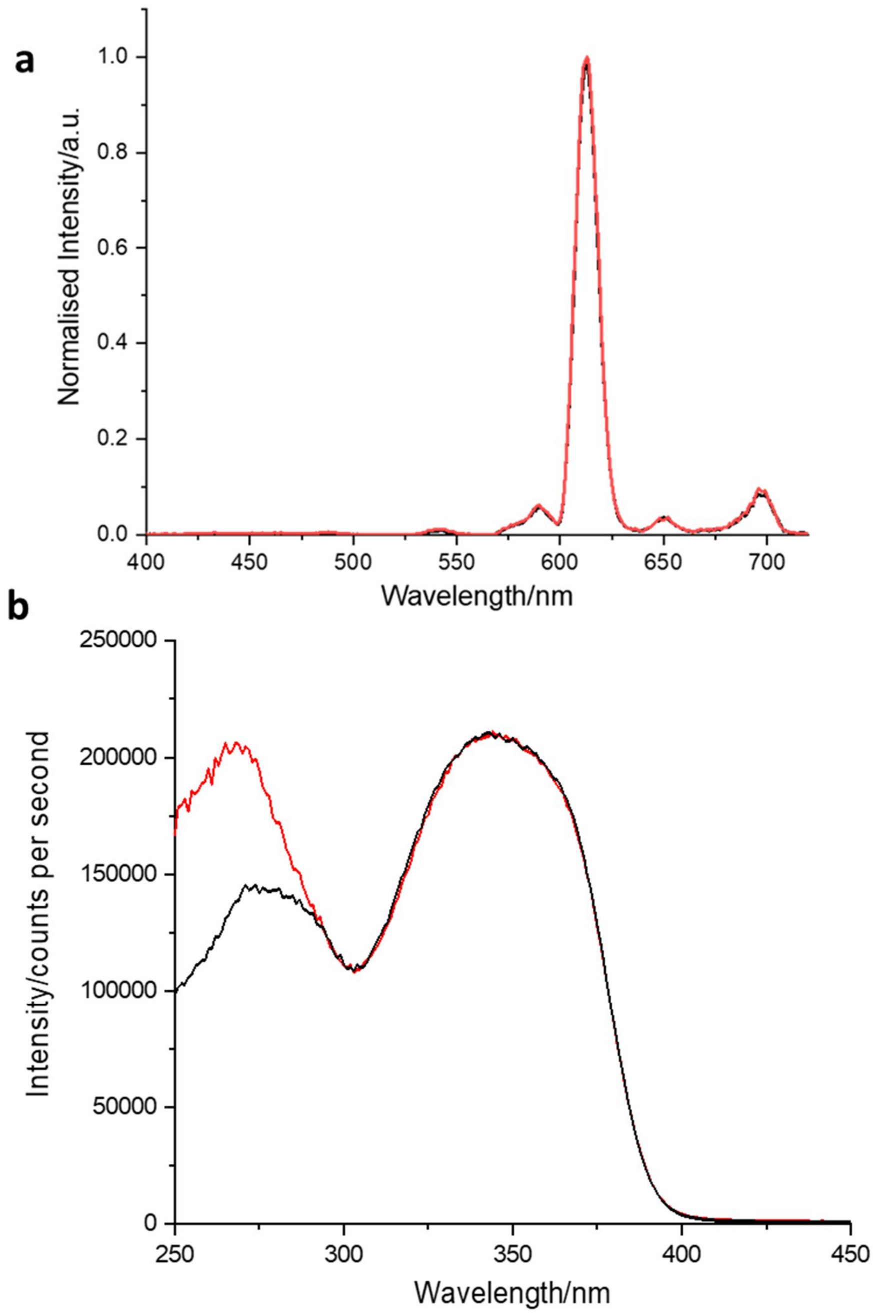

Figure 5.13 (a) The emission spectra (excited at 340 nm) of Eu(tta)$_3$DPEPO (black line), and Eu(tta)$_3$DPEPO co-doped with 18 mM biphenyl (red line) in PMMA. (b) The excitation spectra (detected at 610 nm) of Eu(tta)$_3$DPEPO (black line) and Eu(tta)$_3$DPEPO co-doped with 18 mM biphenyl (red line) in PMMA.

The emission spectra of Eu(hfac)$_3$DPEPO and Eu(hfac)$_3$DPEPO co-doped with 18 mM biphenyl (Figure 5.14(a)) in PMMA showed a similar effect observed in the Eu(tta)$_3$DPEPO co-doped with biphenyl. As shown in Figure 5.14(b), the excitation spectrum of the Eu(hfac)$_3$DPEPO complex co-doped with biphenyl shows evidence of energy transfer from biphenyl. However, the relatively low increase in excitation intensity at around 250 nm, compared with the increase in absorbance (Figure 5.6), suggests a low energy transfer efficiency.

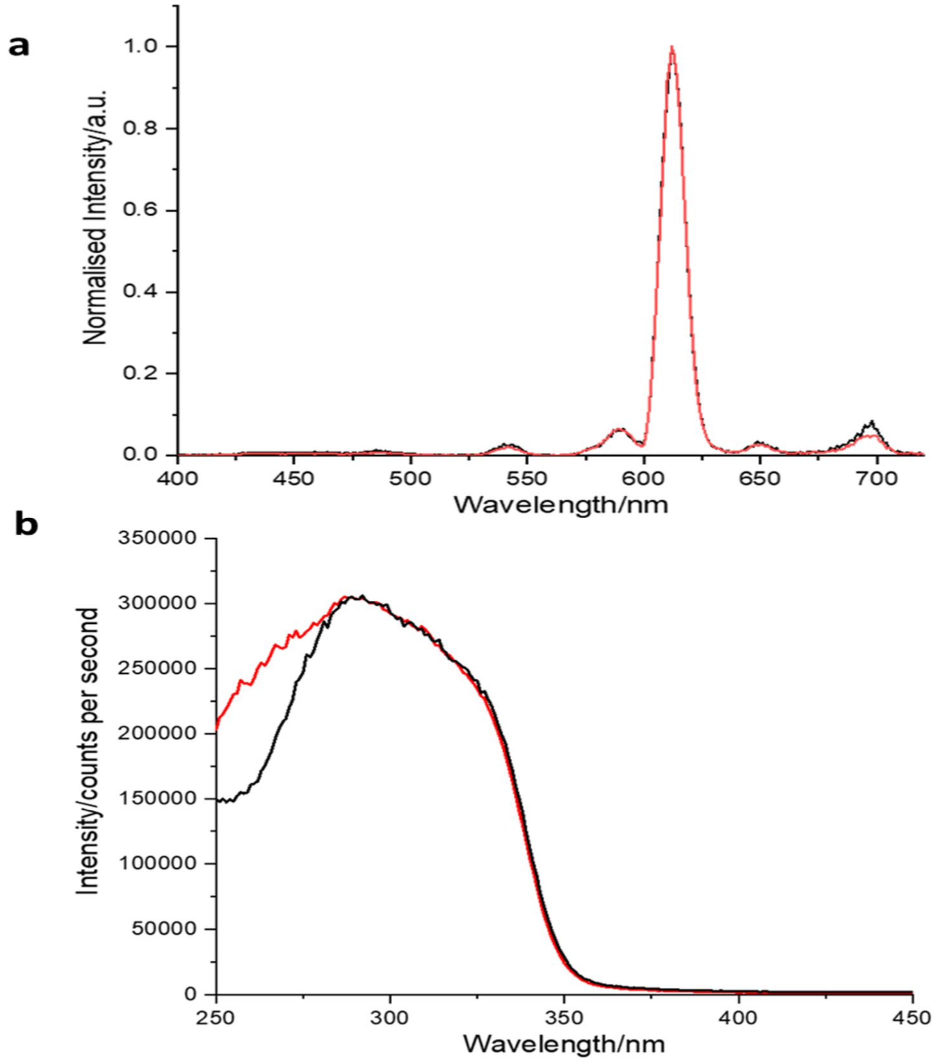

Figure 5.14 (a) The emission spectra (excited at 300 nm) of Eu(hfac)$_3$DPEPO (black line), and Eu(hfac)$_3$DPEPO co-doped with 18 mM biphenyl (red line) in PMMA. (b) The excitation spectra (detected at 610 nm) of Eu(hfac)$_3$DPEPO (black line) and Eu(hfac)$_3$DPEPO co-doped with 18 mM biphenyl (red line) in PMMA.

5.3.3.2 Complexes Co-doped with Indole

Figure 5.15(a) shows the emission spectra of Eu(tta)$_3$DPEPO and Eu(tta)$_3$DPEPO co-doped with 107.5 mM indole, following direct excitation of the complex; the emission spectrum of the co-doped complex shows the typical Eu(III) emission bands, indicating no distortion to the local environment. The excitation spectrum (Figure 5.15(b)) of the co-doped complex compared with that of the complex shows enhanced intensity in the donor absorption region (250–300 nm), but this is much less than the enhancement in absorption (Figure 5.7), indicating a low efficiency of energy transfer. Figure 5.16 shows the excitation spectra for Eu(hfac)$_3$DPEPO and Eu(hfac)$_3$DPEPO co-doped with 107.5 mM indole. The excitation spectrum of the co-doped complex compared with that of the complex demonstrated a negligible difference in the intensity in the donor absorption region (250–300 nm), which is much less compared with the enhancement in its absorption (Figure 5.8), indicating an inefficient energy transfer process.

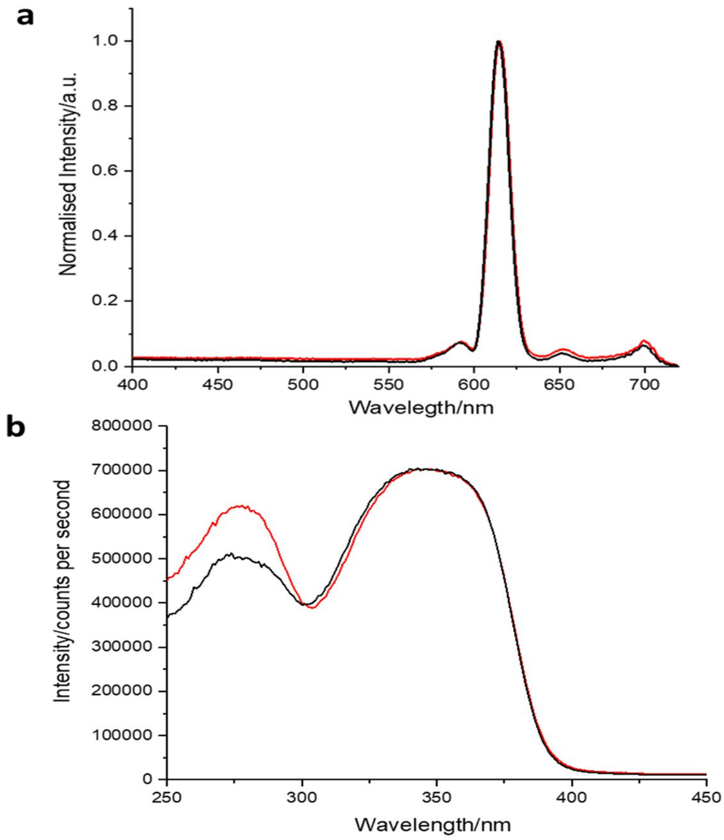

Figure 5.15 (a) The emission spectra (excited at 340 nm) of Eu(tta)$_3$DPEPO (black line) and Eu(tta)$_3$DPEPO co-doped with 107.5 mM Indole (red line) in PMMA. (b) The excitation spectra (detected at 610 nm) of Eu(tta)$_3$DPEPO (black line) and Eu(tta)$_3$DPEPO co-doped with 107.5 mM indole (red line) in PMMA.

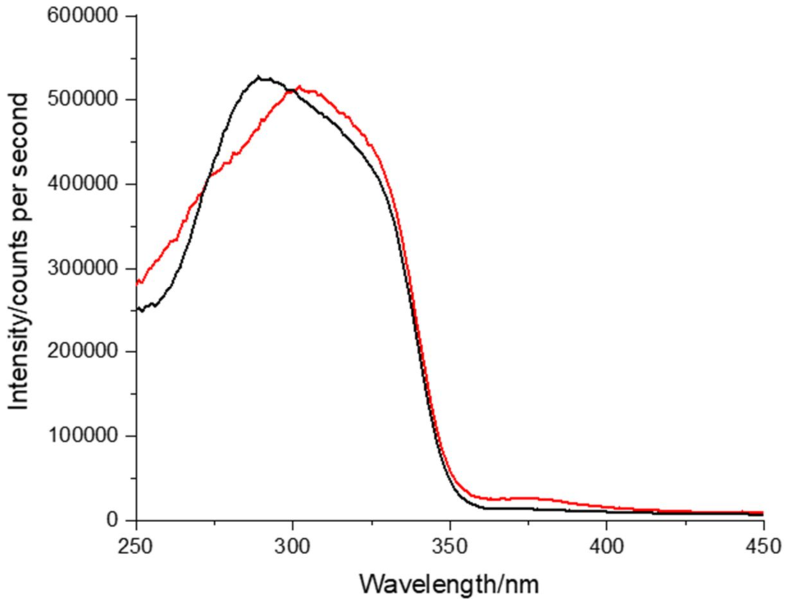

Figure 5.16 Excitation spectra (detected at 610 nm) of Eu(hfac)$_3$DPEPO (black line) and Eu(hfac)$_3$DPEPO co-doped with 107.5 mM indole (red line) in PMMA.

5.3.3.3 Complexes Co-doped with DPEPO

Figure 5.17(a) shows the emission spectra of Eu(tta)$_3$DPEPO and Eu(tta)$_3$DPEPO co-doped with 21 mM DPEPO following direct excitation of the complex. Co-doping with DEPEPO did not affect the emission profile compared to the complex. The excitation spectrum (Figure 5.17(b)) of the co-doped complex shows a significantly enhanced intensity in the region (250–300 nm) assigned to DPEPO, but this is somewhat less than the enhancement in absorption by the presence of the free DPEPO donor (Figure 5.9). A similar enhancement in excitation intensity is seen in the case of the Eu(hfac)$_3$DPEPO co-doped with DPEPO, as shown in Figure 5.18.

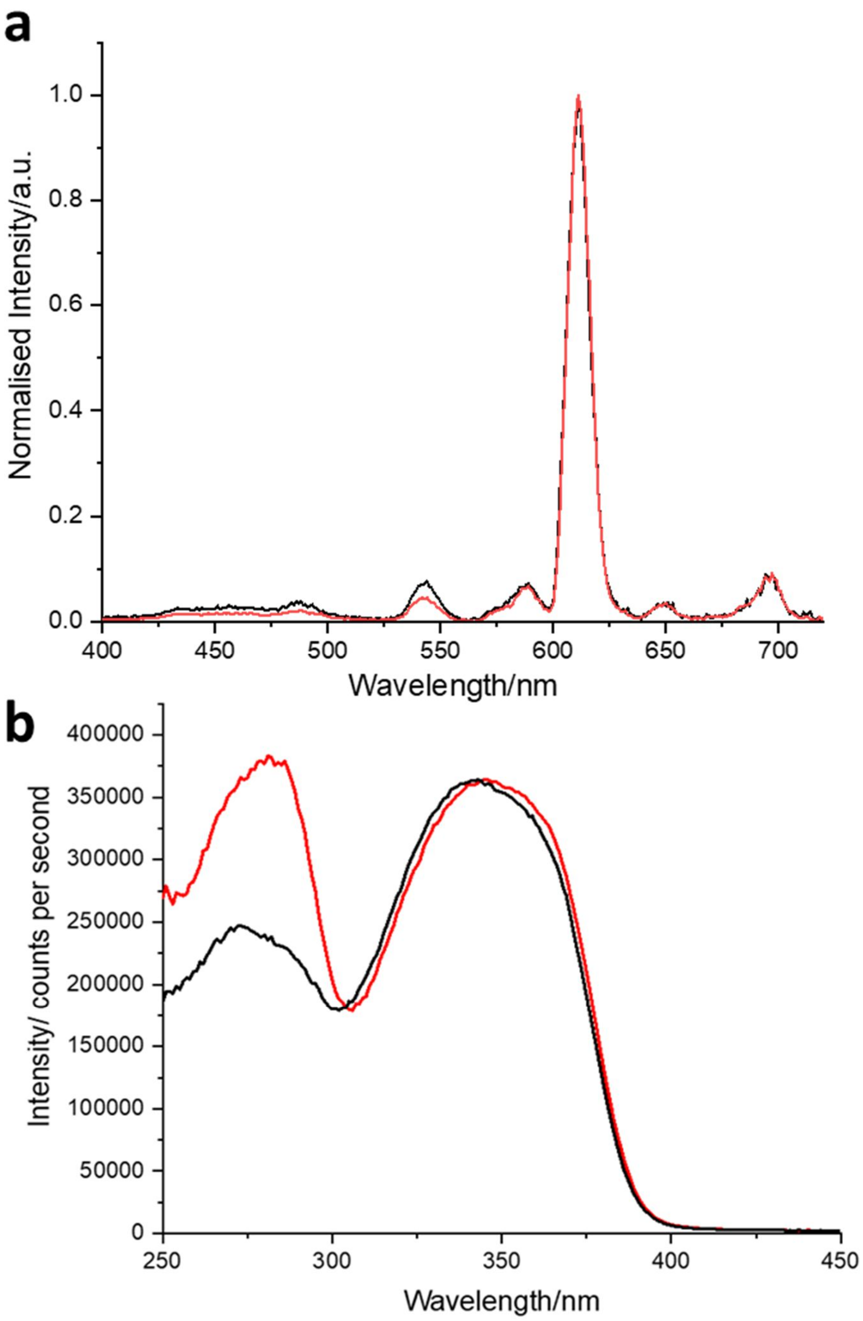

Figure 5.17 (a) The emission spectra (excited at 340 nm) of Eu(tta)$_3$DPEPO (black line) and Eu(tta)$_3$DPEPO co-doped with 21 mM DPEPO (red line) in PMMA. (b) The excitation spectra (detected at 610 nm) of Eu(tta)$_3$DPEPO (black line) and Eu(tta)$_3$DPEPO co-doped with 21 mM DPEPO (red line) in PMMA.

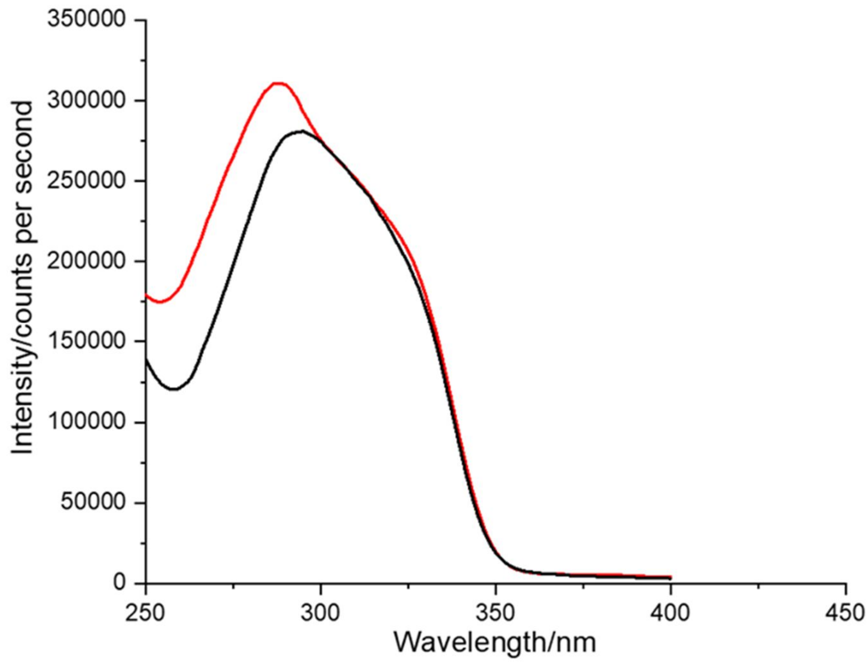

Figure 5.18 Excitation spectra (detected at 610 nm) of Eu(hfac)$_3$DPEPO (black line) and Eu(hfac)$_3$DPEPO co-doped with DPEPO (red line) in PMMA.

5.3.3.4 Complexes Co-doped with p-Terphenyl

The emission spectra of Eu(tta)$_3$DPEPO and Eu(tta)$_3$DPEPO co-doped with 27 mM p-terphenyl, following direct excitation of the complex, are shown in Figure 5.19(a). There was no observed difference in the relative intensities when co-doped with p-terphenyl, confirming that the local environment of the Eu(III) remains intact. The excitation spectrum of the co-doped complex (Figure 5.19(b)) shows a significant increase in intensity in the 250–300 nm region which can be assigned to the absorption of p-terphenyl. However, this is less than the increased absorbance due to the donor (Figure 5.11), indicating a low energy transfer efficiency.

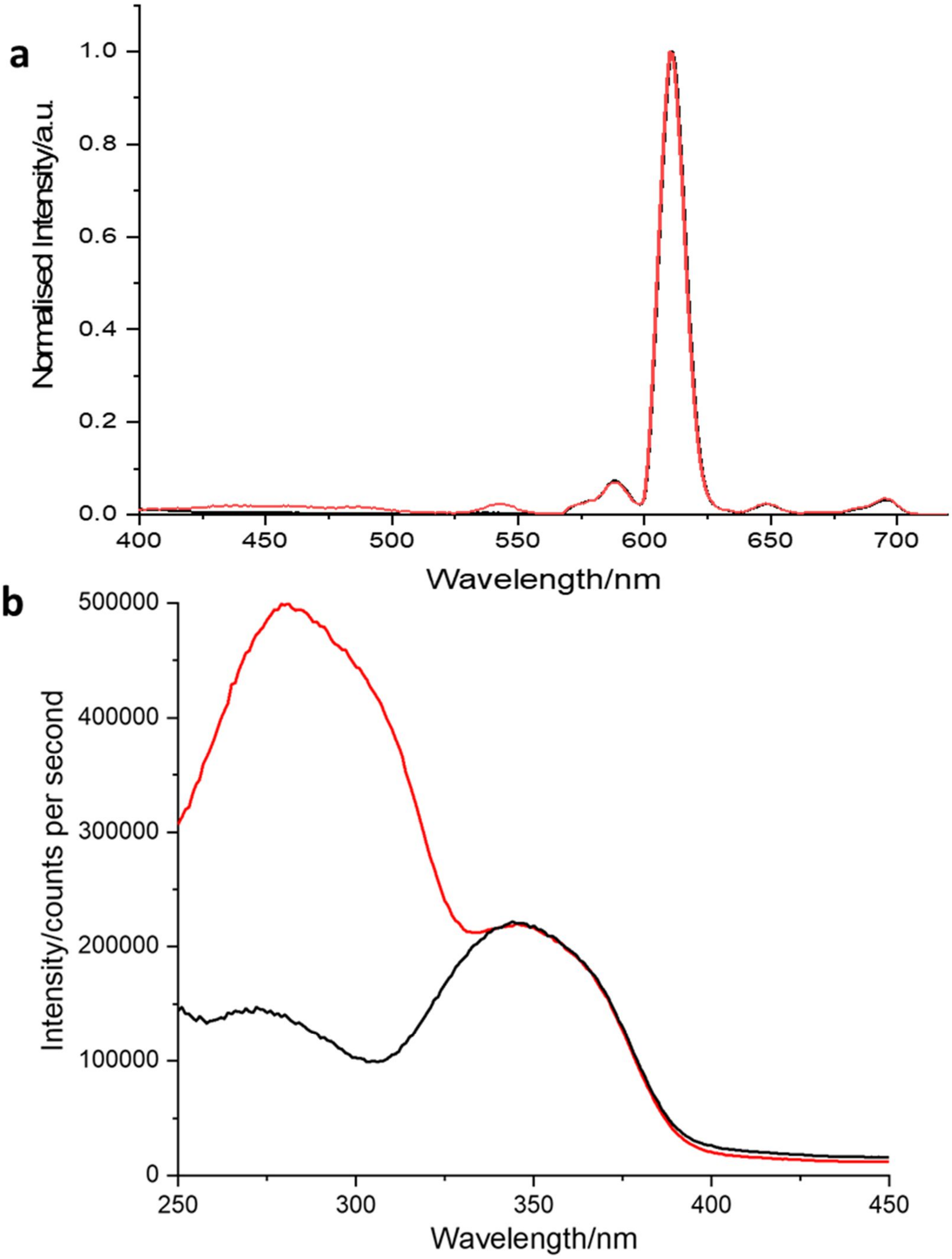

Figure 5.19 (a) The emission spectra (excited at 340 nm) of Eu(tta)$_3$DPEPO (black line) and Eu(tta)$_3$DPEPO co-doped with 27 mM p-terphenyl (red line) in PMMA. (b) The excitation spectra (detected at 610 nm) of Eu(tta)$_3$DPEPO (black line) and Eu(tta)$_3$DPEPO co-doped with 27 mM p-terphenyl (red line) in PMMA.

In the case of the $Eu(hfac)_3DPEPO$ co-doped, there is also an enhancement in the excitation spectrum intensity (Figure 5.20) which can be assigned to the absorption of the p-terphenyl. The excitation spectrum of the co-doped complex shows an increase in intensity in the 250–300 nm region which can be assigned to the presence of p-terphenyl. However, this is much less than the increased absorbance due to the donor (Figure 5.12), indicating a low energy transfer efficiency.

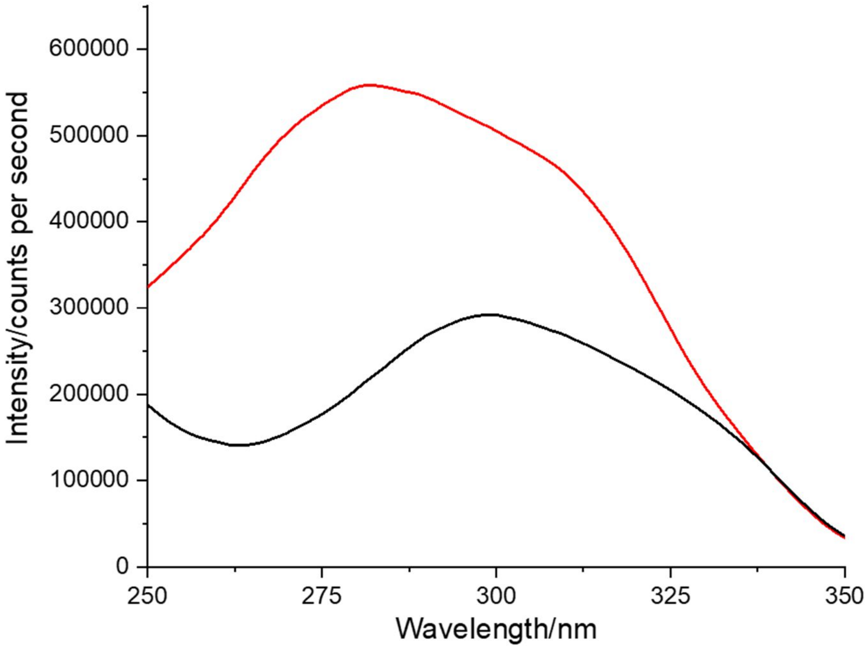

Figure 5.20 Excitation spectra (detected at 610 nm) of $Eu(hfac)_3DPEPO$ (black line) and $Eu(hfac)_3DPEPO$ co-doped with 27 mM p-terphenyl (red line) in PMMA.

5.3.4 Lifetimes of Donor-Acceptor Systems

The luminescence decays of the europium complexes co-doped with biphenyl, indole, DPEPO and p-terphenyl are summarised in Table 5.1. These were all fitted to single-exponential functions, indicating the presence of a single emitting species; therefore, the presence of the donors in the europium complexes did not distort the local environment of the Eu(III). Figures 5.21 and 5.22 show luminescence decays of Eu(tta)$_3$DPEPO co-doped with p-terphenyl and Eu(hfac)$_3$DPEPO co-doped with p-terphenyl, respectively. The rest of the luminescence decays can be found in the Appendix of this thesis.

As mentioned in Chapter 4, the luminescence lifetimes of Eu(hfac)$_3$DPEPO and Eu(tta)$_3$DPEPO in PMMA were 0.77 ms and 0.64 ms, respectively. The τ_{Ln} values of complexes co-doped with different donors along with the undoped complexes are listed in Table 5.1 show small variation from the un-doped complexes but fall within the margin of error. Values presented in Table 5.1 are an average of three measurements in PMMA.

Table 5.1 Luminescence lifetimes (τ_{Ln}) of Eu(hfac)$_3$DPEPO and Eu(tta)$_3$DPEPO co-doped with biphenyl, indole, DPEPO and p-terphenyl in PMMA.

	Eu(hfac)$_3$DPEPO τ_{Ln} ***/ms***	**Eu(tta)$_3$DPEPO** τ_{Ln} ***/ms***
Undoped	0.77	0.64
biphenyl	0.72	0.73
indole	0.77	0.65
DPEPO	0.68	0.64
p-terphenyl	0.75	0.59

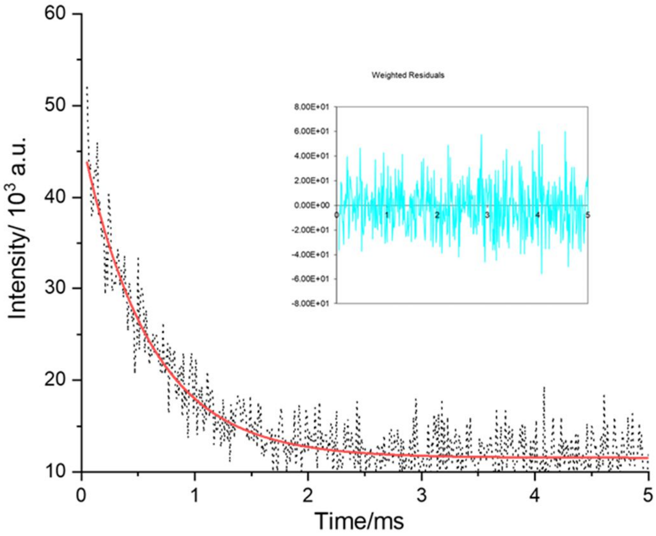

Figure 5.21 Decay data (dotted black), fitted single exponential function (red line) and weighted residuals of Eu(tta)$_3$DPEPO co-doped with p-terphenyl excited at 340 nm and monitored at 610 nm in PMMA.

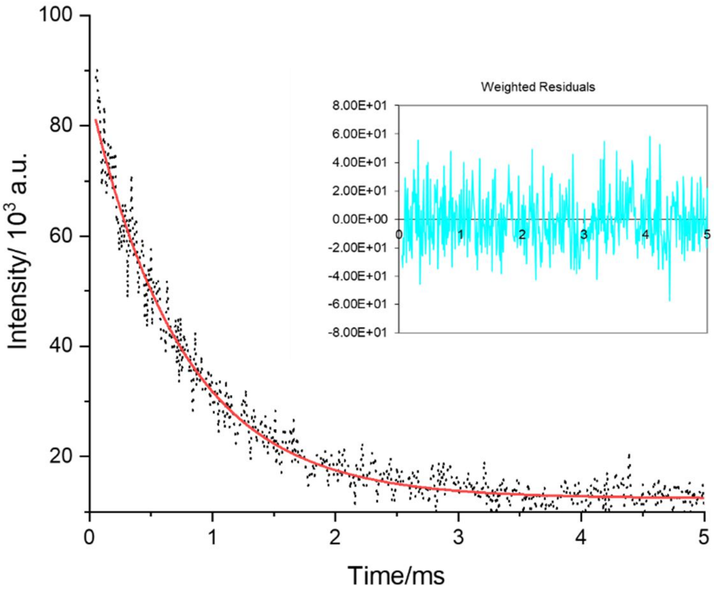

Figure 5.22 Decay data (dotted black), fitted single exponential function (red line) and weighted residuals of Eu(hfac)$_3$DPEPO co-doped with p-terphenyl excited at 300 nm and monitored at 610 nm in PMMA.

5.3.5 Energy Transfer Efficiencies

Table 5.2 lists the efficiency of energy transfer ($\eta_{D\text{-}A}$), enhancement factors and quantum yield of the energy transfer (ϕ_{FRET}) from the donors (DPEPO, biphenyl, indole and p-terphenyl) to Eu(hfac)$_3$DPEPO. In the case of Eu(hfac)$_3$DPEPO, the concentration of the acceptor was varied to ensure the best solubility with the donor in PMMA. In addition to $\eta_{D\text{-}A}$, an emission enhancement factor is given; this is defined as the ratio of the 610-nm emission intensity at λ_{ex} in the presence of the donor to that in the absence of the donor.

Table 5.2 The efficiency of energy transfer ($\eta_{D\text{-}A}$) at the excitation wavelength (λ_{ex}) enhancement factor, and quantum yield of the energy transfer (ϕ_{FRET}) from DPEPO, biphenyl, indole and p-terphenyl to Eu(hfac)$_3$DPEPO in PMMA.

Donor	Concentration of the Acceptor /mM	Concentration of the Donor /mM	$\eta_{D\text{-}A}$(λ_{ex}/nm)	Enhancement Factor	ϕ_{FRET}
DPEPO	6	20	0.38 (285 nm)	1.21	0.32
biphenyl	9	18	0.19 (268 nm)	1.31	0.16
indole	6	107.5	0.00 (273 nm)	1.00	0
p-terphenyl	6	27	0.17 (282 nm)	2.57	0.14

The highest energy transfer efficiency, 38%, to Eu(hfac)$_3$DPEPO was observed for DPEPO as a donor, followed by biphenyl with 19%, p-terphenyl with 17% and indole, which shows no measurable energy transfer to the acceptor. Good spectral overlap between the emission of the donor with the absorption of the acceptor is a prerequisite for energy transfer. As shown in Figure 5.23, the emission of DPEPO has excellent overlap with the absorption of the hfac ligands, which may explain the efficient energy transfer to the complex. In addition, DPEPO is readily soluble in the PMMA solution resulting in the formation of a homogeneously doped thin film.

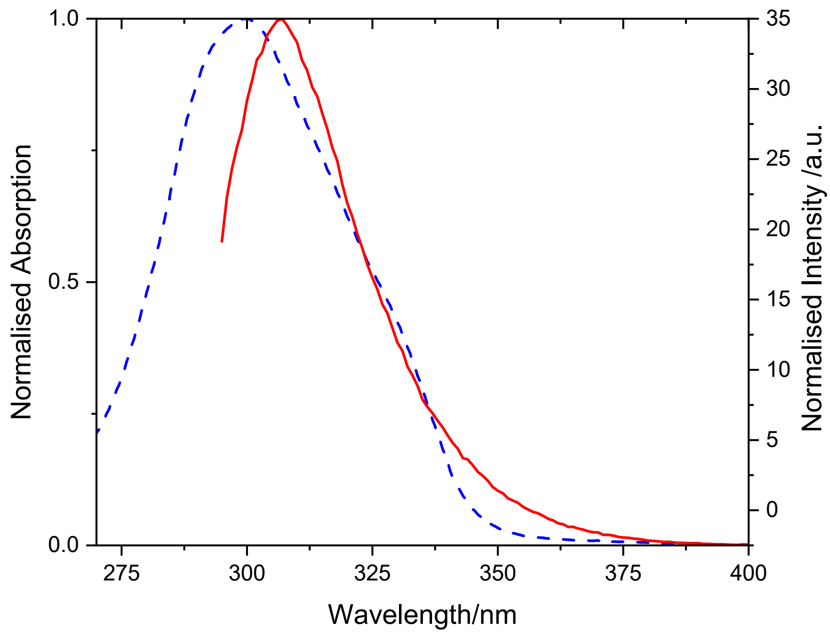

Figure 5.23 UV/Vis absorption spectrum of hfac (blue dashed line) and the emission spectrum (excited at 285 nm) of DPEPO (red line) in PMMA.

Next to DPEPO comes biphenyl with 19% energy transfer efficiency. Figure 5.24 shows the overlap between the emission of biphenyl with the absorption spectra of DPEPO and hfac ligands. Biphenyl's emission overlaps more with the hfac absorption than DPEPO, suggesting an energy transfer pathway from biphenyl to hfac. Indole demonstrates a similar overlap (Figure 5.25) with hfac and less with DPEPO but shows no significant energy transfer efficiency. For p-terphenyl, the overlap between its emission and the absorption of hfac and DPEPO is less than other donors (Figure 5.26); however, the energy transfer efficiency, 17%, is higher than indole and close to biphenyl. This can be explained by the high quantum yield value of p-terphenyl (0.94)[24] compared to (0.18) in biphenyl[25] and (0.39) in indole.[26] Donors with high quantum yield, such as p-terphenyl, can transfer energy even with minimal overlap with the acceptor because photons harvested by the donor have a higher probability of undergoing energy transfer rather than decaying by other non-radiative pathways. The absence of energy transfer efficiency measured for indole may be due to its high concentration, as discussed below. The quantum yield for the energy transfer (ϕ_{FRET}) is another way of expressing the efficiency of the energy transfer process. The highest ϕ_{FRET}, 32%, to $Eu(hfac)_3DPEPO$, was observed for DPEPO as a donor, followed by biphenyl with 16%, p-terphenyl with 14%, and indole which shows no energy transfer to the acceptor. For example, in the case of DPEPO the value of ϕ_{FRET} can be interpreted as 32% of the photons absorbed by the donor result in emission from $Eu(hfac)_3DPEPO$.

The enhancement factor shows how the presence of each donor contributed to the increase in the total luminescence excitation intensity. The highest enhancement was 257%, observed for p-terphenyl, followed by biphenyl with 31%, then DPEPO with 21% and indole showed no enhancement in the excitation intensity. As shown in the case of p-terphenyl, using a donor that gives a substantial increase in absorbance over that shown by the complex alone can give rise to a significant enhancement in the europium emission intensity, although the energy transfer efficiency is not high.

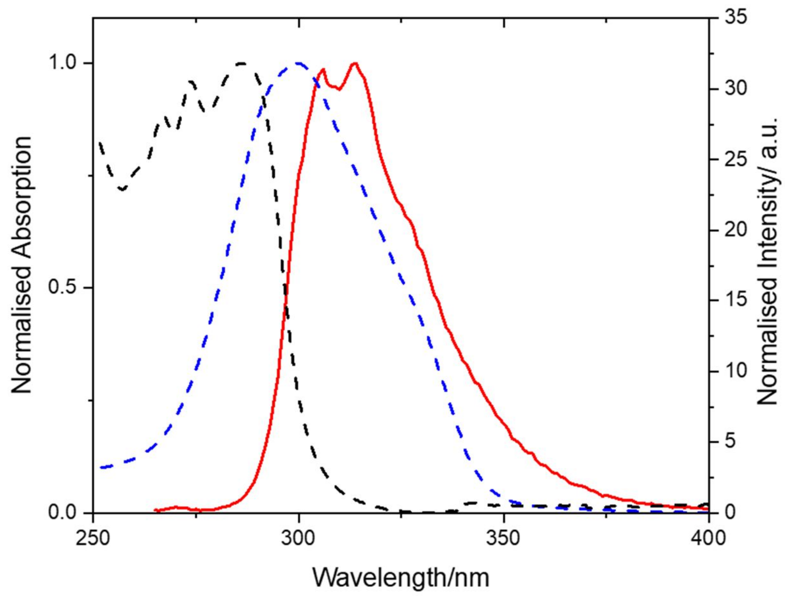

Figure 5.24 UV/Vis absorption spectra of DPEPO (black dashed line) and hfac (blue dashed line) and the emission spectrum (excited at 250 nm) of biphenyl (red line) in PMMA.

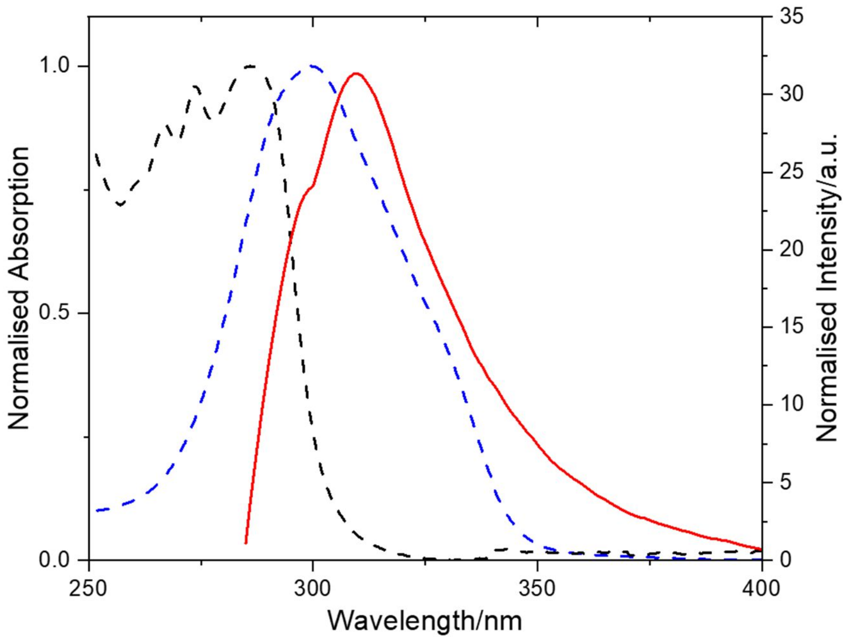

Figure 5.25 UV/Vis absorption spectra of DPEPO (black dashed line) and hfac (blue dashed line) and the emission spectrum (excited at 270 nm) of indole (red line) in PMMA.

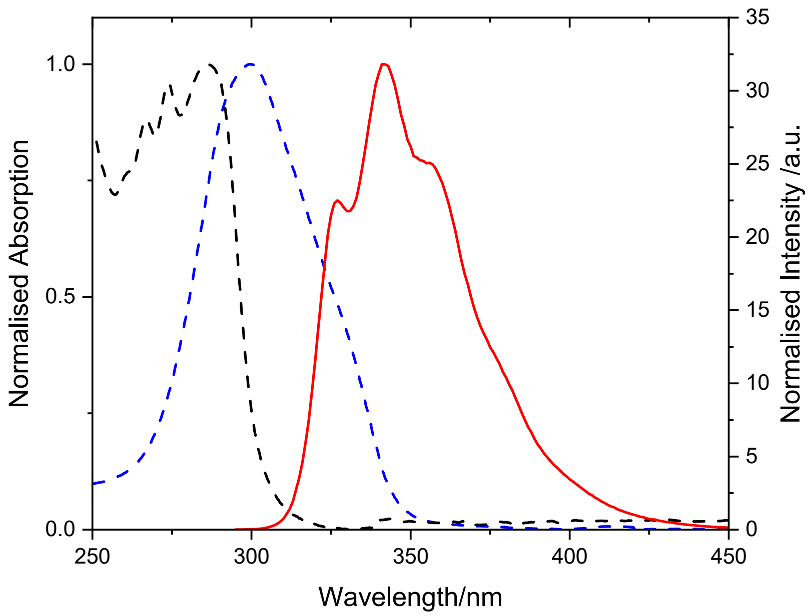

Figure 5.26 UV/Vis absorption spectra of DPEPO (black dashed line) and hfac (blue dashed line) and the emission spectrum (excited at 275 nm) of p-terphenyl (red line) in PMMA.

Table 5.3 lists the efficiency of energy transfer (η_{D-A}), enhancement factors and quantum yield of the energy transfer (ϕ_{FRET}) from the donors (DPEPO, biphenyl, indole and p-terphenyl) to $Eu(tta)_3DPEPO$. In the case of $Eu(tta)_3DPEPO$, the concentration of the acceptor was fixed at 2.6 mM for better solubility with different donors in PMMA.

The energy transfer efficiencies for the DPEPO donor were determined as a function of its concentration. DPEPO showed the highest energy transfer at 21 mM (33%). As the concentration of the donor increased, the η_{D-A} value almost halved to 17% at 64 Mm and 12% at 85 mM. This may be due to aggregation-caused quenching, which is a well-documented phenomenon that stems from the observation that at higher concentrations, phenyl rings in rigid organic chromophores may undergo intense π-π stacking interaction, leading to the formation of aggregates that often induce non-radiative deactivation pathways upon excitation.[27, 28] Figure 5.27 shows the overlap between the emission of DPEPO with the absorption spectrum of the $Eu(tta)_3DPEPO$ complex. The emission of DPEPO has a good overlap with the absorption of the tta, which may explain the efficient energy transfer to the acceptor that was discussed in Chapter 4. Although the concentration of the acceptor (2.6 mM) is significantly lower than that in $Eu(hfac)_3DPEPO$ (6 mM), the η_{D-A} value of DPEPO is above 30% in both complexes.

Table 5.3 The efficiency of energy transfer (η_{D-A}) at excitation wavelength (λ_{ex}) enhancement factor and quantum yield of the energy transfer (ϕ_{FRET}) from DPEPO, biphenyl, indole and p-terphenyl to $Eu(tta)_3DPEPO$ in PMMA. The concentration of $Eu(tta)_3DPEPO$ was 2.6 mM.

Donor	Concentration of the Donor /mM	η_{D-A} (λ_{ex}/nm)	Enhancement Factor	ϕ_{FRET}
DPEPO	21	0.33 (285 nm)	1.63	0.25
	64	0.17 (285 nm)	1.87	0.13
	85	0.12 (285 nm)	1.82	0.09
biphenyl	18	0.27 (268 nm)	1.50	0.20
	42	0.16 (273 nm)	1.35	0.12
	52	0.14 (273 nm)	1.36	0.11
	70	0.13 (273 nm)	1.41	0.1
	110	0.14 (273 nm)	1.61	0.11
	127.5	0.12 (273 nm)	1.56	0.09
indole	107.5	0.05 (278 nm)	1.24	0.04
p-terphenyl	70	0.31 (279 nm)	2.77	0.23
	27	0.14 (279 nm)	3.60	0.11

The enhancement factor highlights how the presence of each donor contributed to the increase in the total fluorescence excitation intensity in Eu(tta)$_3$DPEPO. The highest enhancement was 360%, observed for p-terphenyl (27 mM), then it decreased to 277% at 70 mM, followed by DPEPO with 63%, 87% and 82% at 21, 64, and 85 mM, respectively. Biphenyl showed the highest enhancement (61%) at 110 mM, and the lowest enhancement (35%) at 42 mM, and indole showed the least enhancement (24%), which was much improved than when it was doped with Eu(hfac)$_3$DPEPO (0%). In the case of p-terphenyl, an increase in the concentration does not necessarily lead to an increase to an enhancement in the fluorescence excitation energy, which may be due to the aggregation-induced quenching; for DPEPO and biphenyl, an increase in the concentrations slightly enhance the fluorescence excitation energy.

The quantum yield for the energy transfer (ϕ_{FRET}) is the highest, 25%, when Eu(tta)$_3$DPEPO is co-doped with DPEPO, followed by p-terphenyl (70 mM) at 23%, then biphenyl at 20% (18 mM) and indole, which shows only 4%.

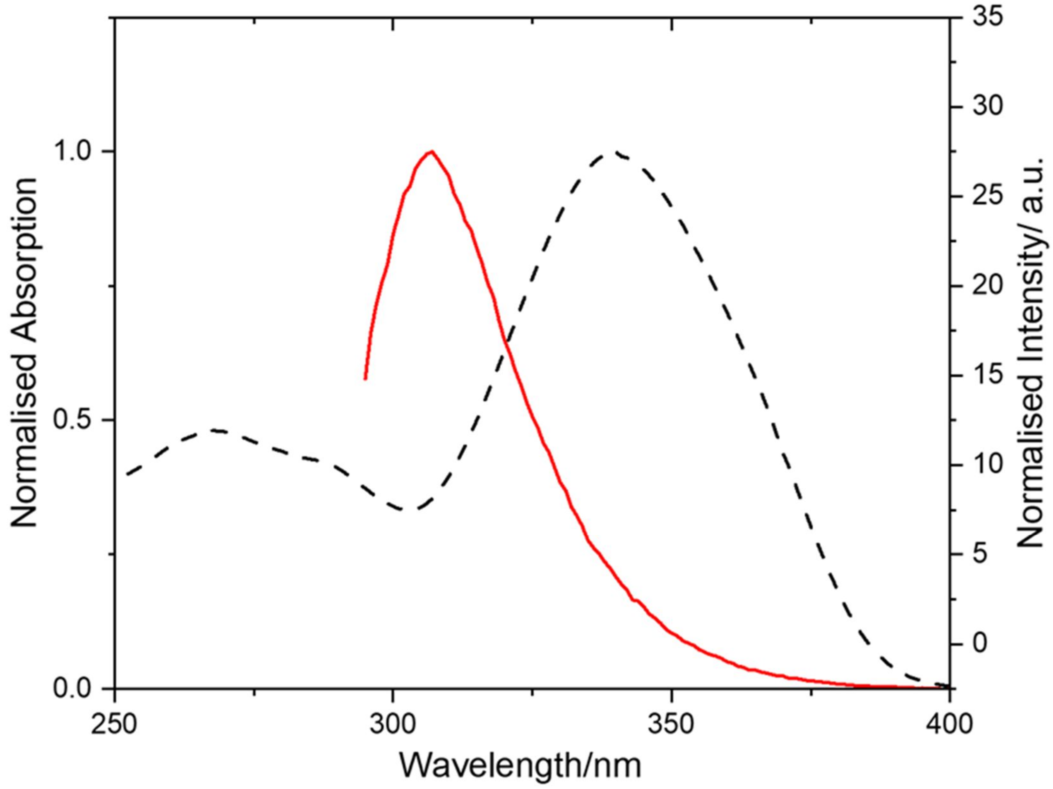

Figure 5.27 UV/Vis absorption spectrum of Eu(tta)$_3$DPEPO (black dashed line) and the emission spectrum (excited at 285 nm) of DPEPO (red line) in PMMA.

The energy transfer efficiencies of biphenyl were determined as a function of its concentration. Like DPEPO, biphenyl had the highest energy transfer (27%) at the lowest concentration, 18 mM, and decreased to 16% on increasing the concentration to 42 mM. At concentrations above 42 mM, the $\eta_{D\text{-}A}$ values plateaued, suggesting donor aggregation at concentrations above 20 mM. Biphenyl has a good spectral overlap with the complex, as shown in Figure 5.28. At the same concentration and compared to its performance with $Eu(hfac)_3DPEPO$ with $\eta_{D\text{-}A}$ of 19%, biphenyl works better with $Eu(tta)_3DPEPO$. The $\eta_{D\text{-}A}$ value of indole was determined with only one concentration, 107.5 mM, resulting in only 5% efficiency, although that indole has a good spectral overlap with the complex (Figure 5.29). In each complex, indole had a lower energy transfer compared to other donors, which may be due to the films at high concentrations resulting in aggregation. In addition, obtaining a homogeneous distribution of the films is difficult; this can be confirmed by inspection of the films as they are not entirely transparent. This suggests that indole at high concentrations is incompatible with europium complexes in PMMA solutions.

p-Terphenyl has an excellent spectral overlap between its emission and the absorption of the complex, as shown in Figure 5.30. The energy transfer efficiencies of p-terphenyl are 14% at 27 mM; in contrast to other donors, it increased to 31% at 70 mM. p-Terphenyl and DPEPO were the best donors in terms of efficiencies with $Eu(tta)_3DPEPO$. However, in contrast to DPEPO, it was not possible to study p-terphenyl at different concentrations due to its poor solubility.

p-Terphenyl's performance in $Eu(hfac)_3DPEPO$ suggests that even with minimal spectral overlap, a high quantum yield of the donor (0.94 in p-terphenyl)[24] can make a difference. However, the case of $Eu(tta)_3DPEPO$ highlights the role that excellent overlap and the high quantum yield play in enhancing the energy transfer efficiency. The poor solubility of p-terphenyl can be problematic if its behaviour at higher concentrations is to be studied. This can be overcome by changing the solvent and conditions used in this study.

It became evident that careful consideration should be taken when choosing a suitable donor. The criteria for choosing the best donor are delicate balancing of good spectral overlap, high quantum yield, and good solubility.

Zhang et al.[8] observed FRET processes in organic molecules for LSCs application with concentrations of the donor and the acceptor at 60 and 12 mM, respectively. Thus, observing FRET processes at low concentrations such as 2.6 mM for the acceptor $Eu(tta)_3DPEPO$) and 21 mM for the donor (DPEPO) can be useful in the context of spectral converters.

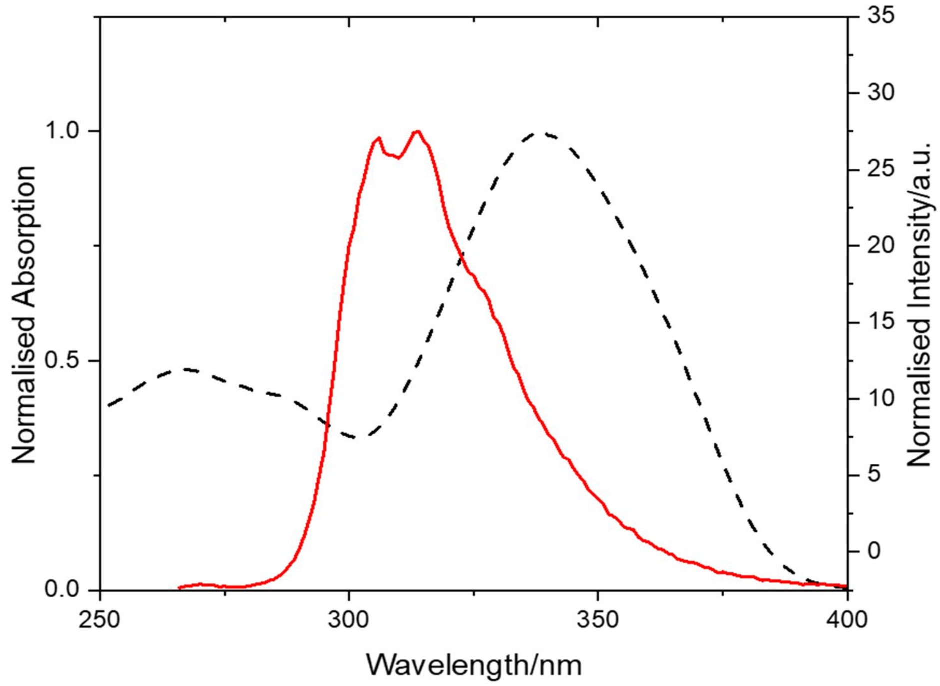

Figure 5.28 UV/Vis absorption spectrum of Eu(tta)$_3$DPEPO (black dashed line) and the emission spectrum (excited at 250 nm) of biphenyl (red line) in PMMA.

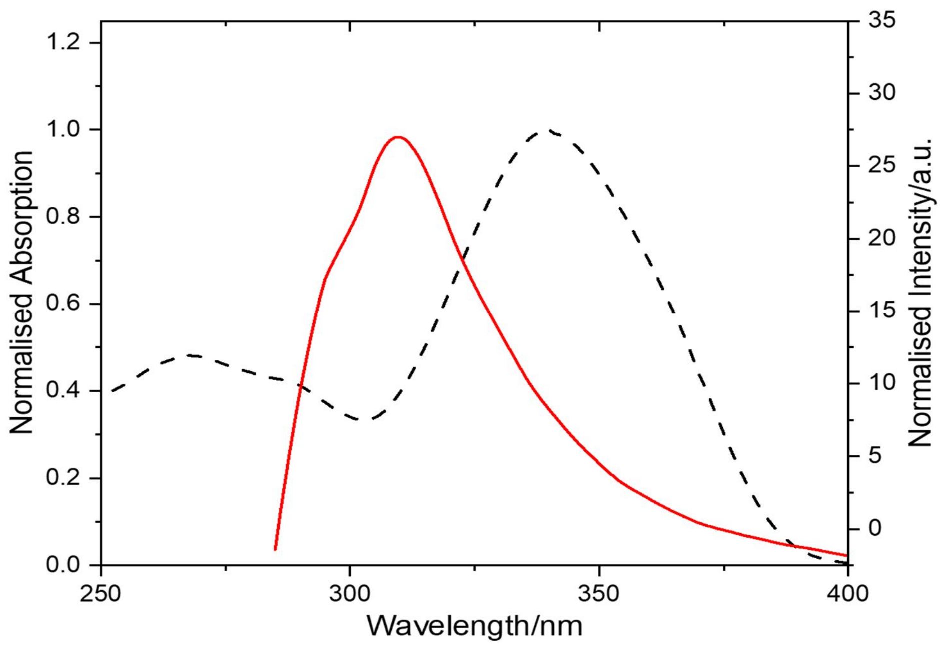

Figure 5.29 UV/Vis absorption spectrum of Eu(tta)$_3$DPEPO (black dashed line) and the emission spectrum (excited at 270 nm) of indole (red line) in PMMA.

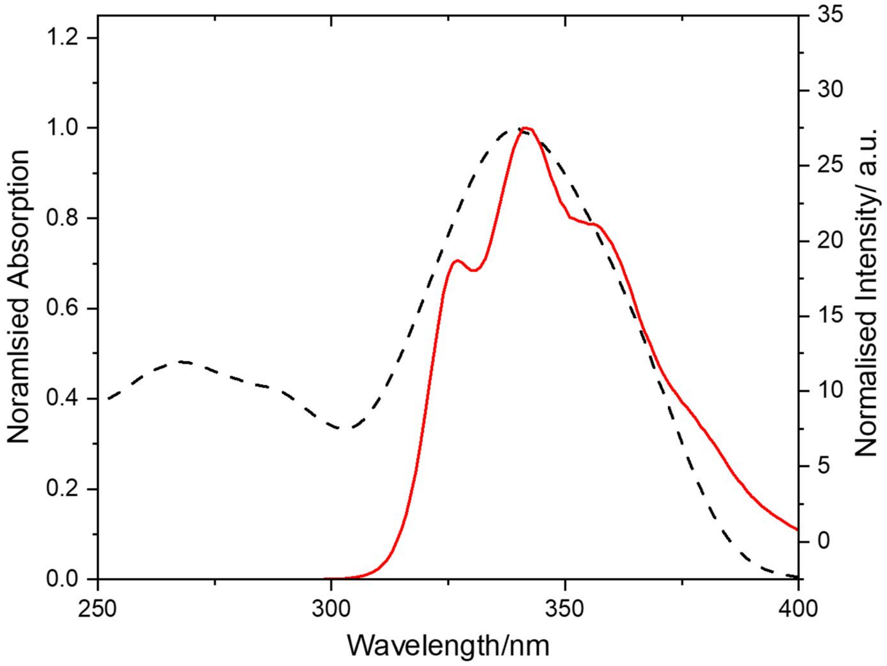

Figure 5.30 UV/Vis absorption spectrum of Eu(tta)$_3$DPEPO (black dashed line) and the emission spectrum (excited at 275 nm) of p-terphenyl (red line) in PMMA.

5.3.6 Solar Testing

Based on the energy transfer efficiencies described in the previous section, $Eu(tta)_3DPEPO$ co-doped with 21 mM DPEPO was chosen to be explored as a luminescent downshifter for c-Si solar cells. To evaluate the performance of the complex co-doped with DPEPO, the compound was embedded into the PMMA polymer matrix and then spin-coated on the photovoltaic device as described in section 5.2.4. Figure 5.31 shows the J-V curves of reference layer PMMA (black line), $Eu(tta)_3DPEPO$ (blue line), and the $Eu(tta)_3DPEPO$ co-doped with DPEPO (red line) on c-Si solar measured under standard solar illumination AM1.5G.

The J-V curves of the aforementioned devices show that co-doping with DPEPO resulted in the highest increase in the current density followed by the un-doped europium complex.

From the J-V curves, solar cell parameters can be calculated as detailed in section 5.2.4.1. Table 5.4 lists the short-circuit current (J_{sc}), open-circuit voltage (V_{oc}), fill factor (FF), and the power conversion efficiency (PCE) of PMMA, $Eu(tta)_3DPEPO$ and $Eu(tta)_3DPEPO$ co-doped with DPEPO encapsulated on a c-Si solar cell.

Table 5.4 The short-circuit current (J_{sc}), open-circuit voltage (V_{oc}), fill factor (FF) and the power conversion efficiency (PCE) of PMMA, $Eu(tta)_3DPEPO$ and $Eu(tta)_3DPEPO$ co-doped with DPEPO encapsulated on c-Si solar cell

Device	V_{oc} [V]	J_{sc} [mA/cm^2]	FF	PCE(%)
PMMA (reference layer)	0.44	33.70	0.46	6.84
$Eu(tta)_3DPEPO$	0.44	37.30	0.53	8.93
$Eu(tta)_3DPEPO$ co-doped with DPEPO	0.43	39.90	0.53	9.35

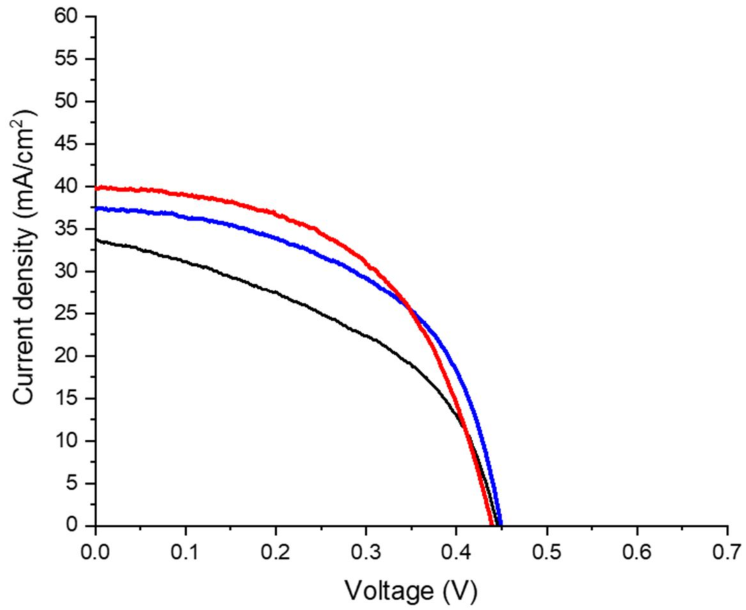

Figure 5.31 J-V curves of c-Si with PMMA (black line), un-doped Eu(tta)$_3$DPEPO (blue line) and Eu(tta)$_3$DPEPO co-doped with DPEPO (red line) under AM 1.5 illumination.

From Table 5.4, both the un-doped complex and the co-doped complex show an increase in the current density compared to PMMA on c-Si; this shows that the un-doped complex itself can act as an LDS layer to produce current up to 37.30 mA/cm^2 compared with PMMA (reference layer) at 33.70 mA/cm^2.

By generating more current density (39.90 mA/cm^2), co-doping the europium complex with DPEPO surpassed the un-doped complex. The open-circuit voltage remained unchanged. As the open-circuit voltage relates to the energy levels and charges recombination in the device, it is expected that such value remains unchanged when the light harvesting is increased or decreased.

The fill factors slightly increased to 0.53, compared to 0.46 in the reference layer, but remained unchanged (0.53) with the co-doped complex. The FF values relate to series resistance within the device; therefore, they ought to remain unchanged. The fact that there is a change might be due to the quality of the connections to the terminals of the devices. The aforementioned values make it hard to evaluate the real impact of the un-doped and the co-doped complexes on the performance of the solar cell. Power conversion efficiency (PCE), which depends on the fill factor, short-circuit current, and the open-circuit voltage, increased to 8.93% in the un-doped complex and 9.35% in the co-doped complex, compared to 6.84% in the reference layer.

This accounts for a 2.09% and 2.51% absolute enhancement in the power conversion efficiency for the un-doped complex and the co-doped complex, respectively. Measurements of incident photon-to-current conversion efficiency (IPCE), commonly referred to as external quantum efficiency (EQE), was conducted to investigate whether the enhancement in the efficiency can be assigned to the down-shifting contribution by the europium complex and the co-doping complex with DPEPO in converting the photons in the UV region. Figure 5.32 shows the external quantum efficiency spectra of the c-Si solar cell encapsulated with $Eu(tta)_3DPEPO$ (red line) and $Eu(tta)_3DPEPO$ co-doped with DPEPO (blue line) in PMMA. The EQE spectrum of the co-doped complex shows a significant increase (~20 %) in the UV region (300–390 nm) compared to the un-doped complex. The increase of the EQE in the UV region can be assigned to the role of DPEPO as a donor. The increase in generating more current density compared to the un-doped complex and in the EQE may be attributed to the role of DPEPO in harvesting the high energy photons in the UV region followed by undergoing an energy transfer via FRET to the complex as highlighted in the previous section. It is worth noting that the performance of the co-doped complex started to fall off on the longer wavelength portion of the spectrum, suggesting inconsistency in the film quality that might affect the longer wavelength region.

The short-circuit current (J_{sc}) can be calculated from the EQE spectrum in Figure 5.32. Calculations showed the photocurrent generated by the co-doped complex and the un-doped complex were 26.1 mA/cm^2 and 28.3 mA/cm^2, respectively. The un-doped complex surpassed the co-doped complex in the photocurrent generated (+2.26 mA/cm^2); this may be due to the performance of the co-doped complex over the longer wavelength portion of the EQE spectrum. One of the shortcomings of the EQE measurements is the absence of the control experiment (PMMA layer), which was not included due to technical difficulties. The other shortcoming of the EQE measurements is that the signal of the detector tends to be noisy or low at wavelengths below 350 nm due to the limited capability of the detector used and the fact that this particular portion of the AM1.5G spectrum is low in power.

The results obtained from the J-V curves, both the un-doped and the co-doped complexes, showed an enhancement in J_{sc} and PCE values compared to the control sample, with the co-doped complex surpassing the un-doped complex. In the case of the un-doped complex, the results highlight the down-shifting contribution of the europium complex by converting the high-energy photons into lower-energy photons, thus increasing c-Si cell absorption of the incident light. For the co-doped complex, using DPEPO as a donor provided better results than resorting to the europium complex as an LDS layer. The observed increase in EQE in the UV region corresponds to a rise in the short-circuit current density, which is a result of the role of DPEPO as a donor. Overall, the solar testing experiments showed preliminary but promising results.

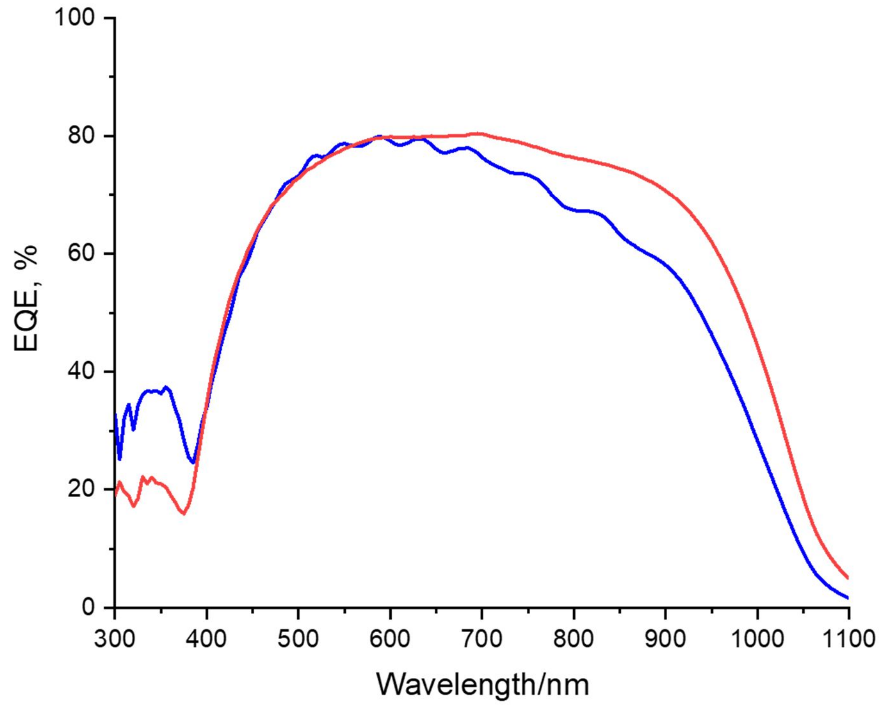

Figure 5.32 External quantum efficiency spectra of the c-Si solar cell encapsulated with $Eu(tta)_3DPEPO$ (red line) and $Eu(tta)_3DPEPO$ co-doped with DPEPO (blue line) in PMMA.

5.4 Conclusions

This chapter addressed the use of Förster resonance energy transfer to enhance ultraviolet excitation of the Eu(III) complexes in PMMA films co-doped with organic molecules. The absorption spectra of the chosen donors (DPEPO, indole, biphenyl and p-terphenyl) complement those of the europium complexes, which makes them useful in harvesting high energy photons in the 250–320 nm region. Examination of the excitation spectra of the europium complexes in the presence and absence of the donors showed that, in each case, an enhancement in UV excitation of the Eu(III) complex was observed, with the exception of Eu(hfac)$_3$DPEPO co-doped with indole.

The energy transfer efficiencies of the different donors were determined. For each complex, DPEPO had the highest energy transfer efficiency: 33% and 38% for Eu(tta)$_3$DPEPO and Eu(hfac)$_3$DPEPO, respectively. p-Terphenyl showed a comparable excellent energy transfer (31%) with Eu(tta)$_3$DPEPO. In the case of DPEPO and biphenyl, where different concentrations of donors were examined with Eu(tta)$_3$DPEPO, it is worth noting that an increase in the concentration does not necessarily result in higher energy transfer efficiency and may only lead to a slight enhancement in the fluorescence excitation energy.

Preliminary experiments of Eu(tta)$_3$DPEPO co-doped with DPEPO were carried out to evaluate their practical performance as spectral convert on c-Si solar cells. Results showed an improvement in the current density, but further studies should be conducted to measure the effectiveness of such a system entirely.

As shown in Eu(tta)$_3$DPEPO and Eu(hfac)$_3$DPEPO co-doped with DPEPO, good energy transfer can occur with low concentrations. This helps in realising the two aims of this chapter: minimising the amount the lanthanide metal used and assisting in harvesting the desired high-energy photons in the ultraviolet region.

5.5 References

1. PostNote – Parliamentary Office of Science and Technology – Houses of Parliament https://www.parliament.uk/globalassets/documents/post/postpn368rare_earth_metals.pdf (accessed 2 April 2021).
2. Vasquez, J. D. a. J. Why Rare Earths May Leave Europe and U.S. Vulnerable. https://www.bloomberg.com/news/articles/2021-02-16/why-rare-earths-are-achilles-heal-for-europe-u-s-quicktake (accessed 2 April 2021).
3. Wang, J.; Guo, M.; Liu, M.; Wei, X., Long-term outlook for global rare earth production. *Resources Policy* **2020,** *65*, 101569.
4. Geological Survey Mineral Resources Program, Rare earth oxide prices in United States. https://www.indexmundi.com/en/commodities/minerals/rare_earths/rare_earths_t3.html (accessed 27 March 2021).
5. Stavridis, J. U.S. Needs a Strong Defense Against China's Rare-Earth Weapon. https://www.bloomberg.com/opinion/articles/2021-03-04/u-s-needs-a-strong-defense-against-china-s-rare-earth-weapon (accessed 2 April 2021).
6. Charalampides, G.; Vatalis, K. I.; Apostoplos, B.; Ploutarch-Nikolas, B., Rare Earth Elements: Industrial Applications and Economic Dependency of Europe. *Procedia Economics and Finance* **2015,** *24*, 126-135.
7. Sigma-Aldrich. https://www.sigmaaldrich.com/catalog/product/aldrich/203254?lang=en&region=GB&gclid=CjwKCAjwgZuDBhBTEiwAXNofRIVWttOhmVpbbLabzd5nAsJooIIesFDXIiPpX1Bi0sHd39sKPIdi1xoCXIgQAvD_BwE (accessed 28 March 2021).
8. Zhang, B.; Zhao, P.; Wilson, L. J.; Subbiah, J.; Yang, H.; Mulvaney, P.; Jones, D. J.; Ghiggino, K. P.; Wong, W. W. H., High-Performance Large-Area Luminescence Solar Concentrator Incorporating a Donor–Emitter Fluorophore System. *ACS Energy Letters* **2019,** *4* (8), 1839-1844.
9. Zhang, B. Donor-emitter fluorophore pairs in luminescent solar concentrators: from material synthesis to device fabrication. 2019.
10. Fernandes, R. V.; Urbano, A.; Duarte, J. L.; Bristow, N.; Kettle, J.; Laureto, E., Tuning the optical properties of luminescent down shifting layers based on organic dyes to increase the efficiency and lifetime of P3HT: PCBM photovoltaic devices. *Journal of Luminescence* **2018,** *203*, 165-171.
11. Danos, L.; Parel, T.; Markvart, T.; Barrioz, V.; Brooks, W. S. M.; Irvine, S. J. C., Increased efficiencies on CdTe solar cells via luminescence down-shifting with excitation energy transfer between dyes. *Solar Energy Materials and Solar Cells* **2012,** *98*, 486-490.

12. Sapsford, K. E.; Berti, L.; Medintz, I. L., Materials for Fluorescence Resonance Energy Transfer Analysis: Beyond Traditional Donor–Acceptor Combinations. *Angewandte Chemie International Edition* **2006,** *45* (28), 4562-4589.
13. Richardson, F. S., Terbium(III) and europium(III) ions as luminescent probes and stains for biomolecular systems. *Chemical Reviews* **1982,** *82* (5), 541-552.
14. Choppin, G.; Bünzli, J., Lanthanide Probes in Life, Chemical and Earth Sciences. *CG Bunzli GR Choppin Elsevier Amsterdam* **1989,** *219*.
15. Geiβler, D.; Hildebrandt, N., Lanthanide complexes in FRET applications. *Current Inorganic Chemistry (Discontinued)* **2011,** *1* (1), 17-35.
16. Selvin, P. R.; Hearst, J. E., Luminescence energy transfer using a terbium chelate: improvements on fluorescence energy transfer. *Proc Natl Acad Sci U S A* **1994,** *91* (21), 10024-10028.
17. Selvin, P. R.; Rana, T. M.; Hearst, J. E., Luminescence Resonance Energy Transfer. *Journal of the American Chemical Society* **1994,** *116* (13), 6029-6030.
18. Főrster, T., 10th Spiers Memorial Lecture. Transfer mechanisms of electronic excitation. *Discussions of the Faraday Society* **1959,** *27* (0), 7-17.
19. https://www.ossila.com/pages/solar-cells-theory#characterisation (accessed 20 MAY 2021).
20. Hu, Y. Exploring Thiophene Oligomers and Ruthenium (II) complexes for their use in dye-sensitised solar cells. University of Edinburgh, 2016.
21. Hierrezuelo-Cardet, P.; Palechor-Ocampo, A. F.; Caram, J.; Ventosinos, F.; Pérez-del-Rey, D.; Bolink, H. J.; Schmidt, J. A., External quantum efficiency measurements used to study the stability of differently deposited perovskite solar cells. *Journal of Applied Physics* **2020,** *127* (23), 235501.
22. Khan, M. S.; Ilmi, R.; Sun, W.; Dutra, J. D. L.; Oliveira, W. F.; Zhou, L.; Wong, W.-Y.; Raithby, P. R., Bright and efficient red emitting electroluminescent devices fabricated from ternary europium complexes. *Journal of Materials Chemistry C* **2020,** *8* (16), 5600-5612.
23. Binnemans, K., Interpretation of europium(III) spectra. *Coordination Chemistry Reviews* **2015,** *295*, 1-45.
24. Reiser, A.; Leyshon, L.; Saunders, D.; Mijovic, M.; Bright, A.; Bogie, J., Fluorescence of aromatic benzoxazole derivatives. *Journal of the American Chemical Society* **1972,** *94* (7), 2414-2421.
25. Berlman, I. B., Identifying the lowest excited singlet state of biphenyl and its analogs. *The Journal of Chemical Physics* **1970,** *52* (11), 5616-5621.
26. Berlman, I. B., 4 - COMPOUNDS. In *Handbook of Fluorescence Spectra of Aromatic Molecules (Second Edition)*, Berlman, I. B., Ed. Academic Press: 1971; pp 67-95.

27. Mei, J.; Leung, N. L. C.; Kwok, R. T. K.; Lam, J. W. Y.; Tang, B. Z., Aggregation-Induced Emission:Together We Shine, United We Soar! *Chemical Reviews* **2015,** *115* (21), 11718-11940.
28. Birks, J. B., Photophysics of aromatic molecules. Wiley Interscience **1970**.

CHAPTER 6: Electronic Energy Transfer from PVK Polymeric Host to Europium Complexes

"The wonder of spectral analysis, analysis at a distance, had literary resonances as well. I had read 'Our Mutual Friend' (written in 1864 just four years after Bunsen and Kirchhoff had launched spectroscopy) and here Dickens imagined a 'moral spectroscopy' whereby the inhabitants of remote galaxies and stars might analyze the light from the Earth to gauge its good and evil, the moral spectrum of its inhabitants."

Oliver Sacks - Uncle Tungsten: Memories of a Chemical Boyhood

Electronic Energy Transfer from PVK Polymeric Host to Europium Complexes

6.1 Introduction

In Chapter 5, energy transfer from organic chromophores to Eu(III) complexes in PMMA was investigated. In these donor-acceptor systems, organic chromophores, such as DPEPO, biphenyl, indole, or p-terphenyl were used as donors with the Eu(III) complex acting as the acceptor. The primary motivation for such investigation was to reduce the quantities of the expensive rare earth metals used and enhance the harvesting of the UV region photons. This chapter aims to present a different approach to implementing energy transfer to Eu(III) complexes. However, the motivations for this approach are the same as the approach described in Chapter 5.

Throughout the previous experiments described in this thesis, the role of the polymer (PMMA) was to serve as a passive host for Eu(III) complexes (Chapter 4) and Eu(III) complexes co-doped with organic chromophores (Chapter 5). This chapter is concerned with the use of an optically active polymer host, poly(N-vinylcarbazole) (PVK) for Eu(III) complexes and Eu(III) complexes co-doped with organic chromophores.

In early works that dealt with luminescent down-shifting layers (LDS) and luminescent solar concentrators (LSCs), most of the attention was directed toward investigating the role of luminophores (e.g., lanthanide ions/complexes, organic dyes, or quantum dots). Therefore most of the studies were concerned with optimising the luminescent species. Consequently, other components of LDS layers and LSCs, such as the host materials of these luminophores, received less attention and were only considered to facilitate the function of luminescent species, ensuring the best possible performance by LSCs and LDS layers.[1-3]

The most widely used host materials in LDS layers and LSCs tend to be polymers. Polymers require less energy to produce, are lighter, versatile, flexible, and more easily processed than other materials such as glass.[4] Polymeric thin sheets can be made by spin-coating or drop-casting (melt-casting) and are not limited to specific shapes (sheets, fibers..etc.).[5] Polymers fit the criteria for a host of luminescent species for the following reasons: they are inexpensive, optically transparent in the visible region, compatible with the optically active materials in terms of dispersion, optimal refractive index, and provide the best medium in facilitating photophysical processes, and exhibit good mechanical properties. [1, 3]For these reasons, PMMA has been the most widely employed polymer for LDS layers and LSCs applications.[1, 3]

However, the traditional host material could be improved to be optically active, to enhance the photostability, which can be affected by prolonged UV illumination, or to increase the matrix's trapping efficiency. Researchers started developing a wide variety of new materials that could be environmentally friendly, endure prolonged UV exposure, be better at trapping photons, or be optically active. For example, Bashir et al. showed that the trapping efficiency of a thin film in LSCs improved upon the introduction of SiO_2 nanoparticles in PMMA doped with organic dye.[6] Griffini et al. reported the synthesis of new crosslinked fluoropolymers that can serve as an alternative to PMMA and demonstrated long lifetimes, offering better long term photostability.[2, 7, 8] Host materials could also be environmentally friendly; Fattori et al. showed the compatibility of the biodegradable polymer in the form of poly(lactic acid), based on fermented plant starch, for LSCs application.[9]

A different but interesting approach is to make the host material optically active, aiding the luminescent species in harvesting light and transferring energy through FRET. The investigation of organic-inorganic hybrid matrices for LSCs, ureasils in particular, as a host material showed the active role of the host matrix in harvesting light and enhancing overall quantum yields. Ureasils are intrinsically photoactive and have been used as host materials for organic dyes[10, 11]and lanthanide ion/complexes.[12, 13] Photoactive di-ureasil hybrids doped with Eu(III) have shown enhancements in the overall quantum yield and long lifetimes, in addition to the occurrence of energy transfer from the host to the europium metal centre.[14-16] Macromolecules such as proteins can be used in LCS application; one of the early studies that exploited photoactive macromolecules as luminescent species was carried out on phycobilisomes; a photosynthetic light-harvesting protein complex in Red Algae, and Cyanobacteria.[17]

However, organic-inorganic hybrid materials or macromolecules, such as proteins, lack the practicality, ease of processing, commercial availability, and cost-effectiveness that can be found in synthetic polymers such as PMMA. A photoactive polymer that can harvest energy and act as an energy donor to the luminescent species, in addition to being a host, can combine the best of both worlds. π-conjugated polymers are considered photoactive and have been used for different light-emitting applications; most notably organic light-emitting diodes (OLEDs),[18, 19 20] but few studies have been carried out for their application as spectral converters (e.g., LSCs) due to their blue emission and low quantum yields in general,[19, 21] although Gutierrez et al. showed that a blend of two π-conjugated polymers could act as an energy sensitiser for perylene bisimide dyes in LSCs.[22]

Poly(N-vinylcarbazole) (PVK) (Figure 6.1) with its electronically dense carbazole moiety has been used in a wide variety of applications, such as an organic polymer cathode for dual-intercalation in Li-ion[23] and Na-ion batteries[24]; and in light-emitting devices; like OLEDs[25], polymer light-emitting diodes (PLEDs)[26], and organic electroluminescence (EL) applications.[27] As a non-conjugated polymer with a charge-transport pendant group, PVK showed good hole-transporting properties due to the presence of the carbazole side group, which led to enhanced performance in OLEDs.[28] In addition to its good compatibility with lanthanide dyes,[29] other advantages of using PVK in OLEDs include its commercial availability, high thermal and photochemical stability.[30]

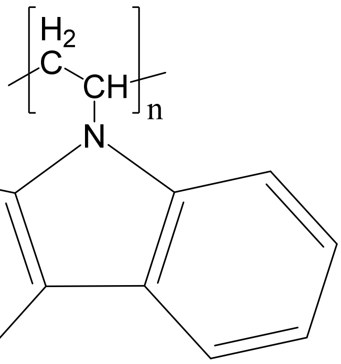

Figure 6.1 Chemical structure poly(N-vinylcarbazole) (PVK)

In the context of LEDs and organic electroluminescence, PVK was not only used as a blue emitter but as a host that can transfer energy to lanthanide β-Diketonate complexes. Liang et al. showed that in PVK films, energy transfer does occur from PVK to complexes such as (Eu(tta)$_4$Py), where Py is monopyridinium.[27] Gui Yu et al. fabricated light-emitting diodes (LEDs) by depositing PVK doped with europium complexes, where the excitation energy of PVK was transferred to the complex NaEu(tta)$_4$.[31] In the studies mentioned above, photophysical properties such as quantum yields and lifetimes of the doped complex and quantitative assessment of the energy transfer efficiencies were not presented. Luo et al. investigated co-doped europium and terbium complexes in PVK films; energy transfer from PVK to the terbium and the europium via FRET was observed, and complexes co-doped in PVK showed longer lifetimes compared to the ones co-doped in PMMA.[29] Diaz-Garcia et al. confirmed by monitoring the europium-centred emission that occurrence of FRET from PVK to europium and samarium complexes, transfer rate calculations based on the lanthanide-centred emission intensity of the films compared to PVK were presented in this study.[32]

6.1.1 Photophysics of Poly(N-vinylcarbazole) (PVK)

The electronic excitation processes and photophysical properties of PVK have been investigated in earlier works by fluorescence spectroscopy.[33-36] Klöpffer et al.[33] was among the early researchers who took note of the fluorescence of pure PVK in solution and film, followed by many researchers examining the nature of PVK fluorescence.[34-37]

The UV absorption spectrum of the PVK film does not differ from that in solution or when compared to the N-isopropyl carbazole monomer unit, which indicates that the carbazole rings in the polymer act independently upon absorption light in solution-phase or film.[33]

On the other hand, the emission spectrum of PVK varies from solution-phase to solid-phase. Vinyl aromatic polymers exhibit two types of fluorescence in the dilute solutions, one can be attributed to the monomer, which would be typical of carbazole moiety in PVK, and the other is a structureless broad emission that is characteristic of an excimer. What is unique in PVK, and unlike other polymers with aromatic groups, the isolated carbazole group (monomer) in PVK shows no emission[33, 35, 38]; the emission observed is due to excimers. It is worth noting that the fluorescence spectra and lifetimes of solid PVK exhibit molecular weight dependency.[36]

Klöpffer et al. and Johnson et al. noted that the ultraviolet excitation of solid PVK yielded broad structureless emission spectra in the violet-blue region; the emission was attributed to the formation of more than one excimer.[33, 35] Pre-requisite for the excimer emission is the stacking interaction of the electronically excited side group with another ground-state side group. In the polymer, this interaction can only occur in suitable conformations of the polymer chain.[33]

Discovered more than sixty years ago, the word excimer was used to describe an excited state that shows an absorption spectrum profile that corresponds to the monomer but nevertheless exhibits structureless broad emission typical of dimers.[39] The identification of excimer fluorescence in aromatic compounds was a result of the work of Förster et al.; it was noted upon photophysical examination that concentrated solutions of pyrene showed a noticeable decrease in the intensity of the monomer band fluorescence and the appearance of an emission spectrum that has no distinct structure and is lower in energy than the emission of the monomer.[40, 41] Birks has defined an excimer as "*a dimer which is associated in an excited electronic state and which is dissociative (e.g., would dissociate in the absence of external restraints) in its ground electronic state*".[42]

Of the many complex photophysical processes in aromatic vinyl polymers such as polystyrene and PVK, the excimer formation processes have attracted the most attention.[33, 35, 43] Unlike polystyrene (PS) or polyvinyl naphthalene, the excimer fluorescence in PVK is not quenched at low temperature because thermal activation is not a pre-requisite for reaching excimer confirmation.[44]

In the light of accumulated evidence of excimer formation, the nature of the excimer fluorescence was further investigated. With respect to pyrene, Klöpffer et al.[45] conducted an experiment with several guest molecules, in which one guest molecule has excitation energy lower than that of the monomer (pyrene) and higher than that of the excimer; as a result, there was no fluorescence emitted by the guest molecule. However, when the guest molecules have excitation energy below that of the pyrene excimer, the guest molecule exhibits an emission, concluding energy transfer is taking place from the monomer to the excimer and from the excimer to the guest molecule.[45, 46]

The fate of singlet excitons in aromatic polymers such as PVK might shed light on how the energy transfer occurs in PVK. Upon illumination, the first excited singlet state is not 'fixed' to the group that has been excited by absorbing light in the first place. Still, it moves or hops around in a random mode until relaxation occurs either by radiative deactivation (emission), non-radiative deactivation, quenching, or trapping.[47]

In the solid PVK, there is no emission from the monomer, but excimer fluorescence is observed; this accounts for energy transfer since absorption of light can occur randomly, whereas emission only takes place from specific centres, in the case of excimers, these are called excimer-forming sites.[47] Furthermore, an excimer with its dissociative ground state cannot be directly excited by electromagnetic radiation. Still, since the excimer emission is prevalent in the solid PVK, the excitation energy transfer to these sites is the only possibility. Nevertheless, the lack of an 'excitable ground state' in excimers makes it implausible that they act as acceptors in a long-range Förster energy transfer. Therefore, it is clear that exciton diffusion is involved in energy transfer.[46]

In a set of experiments carried out by W. Klöpffer.[33] The energy transfer in PVK was investigated using fluorescence quenching molecules: perylene, trinitrofluorenone (TNF), and hexachloro-p-xylene (HCX). Perylene can be an excellent quencher owing to the overlap of molecule's absorption with the emission of PVK. Therefore, energy transfer occurs through FRET from the PVK excimer. Trinitrofluorenone (TNF) can form a donor-acceptor complex with the PVK. However, hexachloro-p-xylene (HCX) cannot act as an acceptor for the excimer donor, because its excited-state energy is too high; therefore, dipole-dipole resonance energy transfer is not probable. It turns out that HCX is as good a quencher as the other guest molecules; therefore, the exciton diffusion process must be involved. Thus, energy transfer in PVK involves competition between the added guest molecules and the excimer-forming sites, acting as traps for the singlet excitons as they migrate along the polymer chain.[33] In the excimer-forming sites, the carbazole side-groups must be packed close to each other. These sites act as efficient traps for excitons.[46] It is worth noting that the range of exciton diffusion in PVK polymer is limited compared to the large ranges found in molecular crystals due to the heavy presence of excimer-forming sites.[48] In PVK, the process of hopping for localised excitons was found to be extremely important in the energy transfer dynamics; the hopping process is more efficient in the film compared to that of the solution.[49]

The emission of the PVK in the solution can be resolved into two peaks; therefore, it can be attributed to the overlap of the spectra of two different excimers, illustrated in Figure 6.2. The lower energy peak (λ_{max} of 410-420 nm) was assigned to "sandwich-like" excimer, where the monomer groups form pairs and the π orbitals of the aromatic rings overlap considerably. The higher energy peak (λ_{max} of 380 nm) was assigned to the partially overlapped configuration where one aromatic ring of a carbazole group eclipses one ring of a neighbour group.[33, 38, 44] Thus, the two excimers play an essential role to trap the singlet excitons by reducing their mobility.[50]

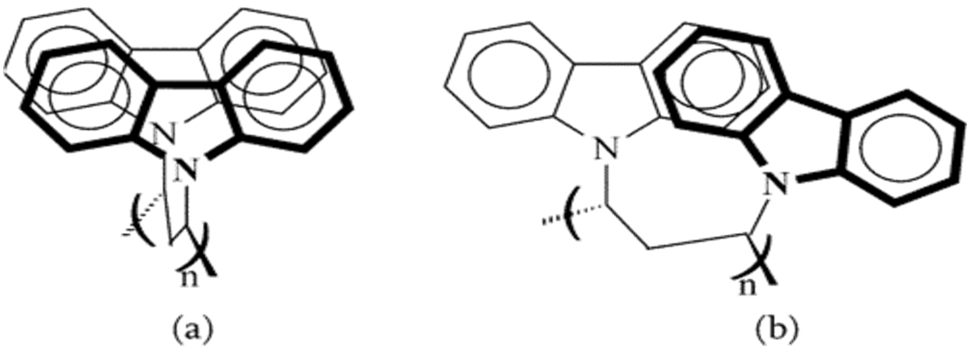

Figure 6.2 Excimer configurations of the carbazole dimer in poly(N-vinylcarbazole) (PVK); (a)"sandwich-like" and (b) partially overlapped (adapted from[43])

In addition to its unique photophysical properties, PVK is also relatively inexpensive as an optically active polymer. At the time of writing this thesis, the cost of PVK was around £61 for five grams[51] compared with £137 for five grams of $EuCl_3.6H_2O$ (according to the Sigma-Aldrich website, March 2021), the starting material for the synthesised complexes presented in this work. Thus, using PVK as an energy donor to Eu(III) complexes might be useful in reducing the cost of the lanthanide metals and promoting the role of polymer in LDS layers and LSCs to an active role. To the extent of the author's knowledge, PVK has not been considered before as an optically active host in LDS layers and LSCs. In addition to that, the investigation of the energy transfer of PVK to $Eu(tta)_3DPEPO$ and $Eu(hfac)_3DPEPO$ along with other donors has not been carried out.

This chapter reports the investigation of energy transfer from the PVK to Eu(hfac)$_3$DPEPO and Eu(tta)$_3$DPEPO. The effect of varying the concentration of the polymer with Eu(tta)$_3$DPEPO was assessed. Co-doping of Eu(tta)$_3$DPEPO with donors molecules, biphenyl, DPEPO, and indole, in PVK was also investigated.

6.2 Experimental

6.2.1 Chemicals

Chloroform was HPLC grade obtained from (Fisher Chemicals) and was used without further purifications. Eu(tta)$_3$DPEPO, Eu(hfac)$_3$DPEPO, and DPEPO were synthesised, as described in Chapter 3. Biphenyl (99.5%), and indole (≥99%), were sourced from Sigma-Aldrich. Poly(N-vinylcarbazole) (PVK average MW. 135,600) was sourced from Fisher Scientific UK Ltd.

6.2.2 Polymeric Film Preparations

PVK polymer was dissolved in chloroform (50 mg/ml). The total concentration of the polymer in the solution was kept fixed to ensure the blank polymer and doped polymer have the same thickness unless stated otherwise in the text. Then, 5.4 wt% of Eu(tta)$_3$DPEPO, 2.5 wt%, 10 wt%, and 16 wt% of Eu(hfac)$_3$DPEPO were added to a solution of PVK without affecting the final concentration of polymer; they were heated at 55 °C and stirred for 5 hr. The exact preparation was carried out when donors were used. A suitable volume of the solution (100 μL) was spin-coated using a pipette on quartz slides (25mm x 25mm x 1mm) for each measurement. Dynamic spin coating (the substrate is already spinning) was used for 60s at 500 rotation per minute (r.p.m) to ensure the formation of transparent, thin, homogenous polymer films. After spin-coating, films were left for 24 hr at room temperature to allow for complete evaporation of the solvent, resulting in transparent films.

6.2.3 PVK-Acceptors Energy Transfer Calculations

The analysis of data in this chapter has had to take into consideration that the absorption spectrum of the PVK matrix (the donor) overlaps the absorption spectrum of each complex (acceptors) over the entire UV excitation range from 250 to 400 nm. Thus, to estimate the efficiency of energy transfer from PVK to the complex, the measured, normalised excitation spectrum of the emission of the complex in PVK was fitted by the calculated, normalised sum of the contributions from direct excitation of the complex and indirect excitation via energy transfer from PVK, as expressed by Equation 6-1. (Assuming that the quantum yield of photoluminescence of the complex is the same for direct and indirect excitation.)

$$I_{\text{Ex Calc}}(\lambda) = \frac{\left(\frac{I_{\text{Abs}}(\lambda)}{I_0(\lambda)}\right)_{\text{Complex}} + \beta\left(\frac{I_{\text{Abs}}(\lambda)}{I_0(\lambda)}\right)_{\text{PVK}}}{\left(\frac{I_{\text{Abs}}(\lambda_{\text{Max}})}{I_0(\lambda_{\text{Max}})}\right)_{\text{Complex}} + \beta\left(\frac{I_{\text{Abs}}(\lambda_{\text{Max}})}{I_0(\lambda_{\text{Max}})}\right)_{\text{PVK}}} \qquad \textbf{Equation 6-1}$$

where $I_{\text{Ex Calc}}(\lambda)$ is the predicted, normalised excitation intensity at wavelength λ, $\left(\frac{I_{\text{Abs}}(\lambda)}{I_0(\lambda)}\right)_{\text{Complex}}$ is the fraction of the incident excitation light intensity absorbed by the complex; $\left(\frac{I_{\text{Abs}}(\lambda)}{I_0(\lambda)}\right)_{\text{PVK}}$ is the fraction of the incident light intensity absorbed by PVK; λ_{Max} is the wavelength of maximum intensity; β is the fitted variable that is indicative of the efficiency of energy transfer from PVK to the complex.

The fractional intensity of the light absorbed by each species is calculated from the total fraction of incident intensity absorbed by the sample (complex + PVK), according to Equations (6-2) to (6-4).

$$\left(\frac{I_{\text{Abs}}(\lambda)}{I_0(\lambda)}\right)_{\text{Total}} = 1\text{-}10^{-A(\lambda)_{\text{Total}}} \qquad \textbf{Equation 6-2}$$

where $A(\lambda)_{\text{Total}}$ is the total absorbance of the sample at wavelength, λ , i.e., the sum of the absorbance of the complex and the absorbance of the PVK; $A(\lambda)_{\text{Complex}}$ is the absorbance of the complex; $A(\lambda)_{\text{PVK}}$ is the absorbance of PVK.

$$\left(\frac{I_{\text{Abs}}(\lambda)}{I_0(\lambda)}\right)_{\text{Complex}} = \frac{A(\lambda)_{\text{Complex}}}{A(\lambda)_{\text{Total}}}\left(\frac{I_{\text{Abs}}(\lambda)}{I_0(\lambda)}\right)_{\text{Total}} \qquad \textbf{Equation 6-3}$$

$$\left(\frac{I_{\text{Abs}}(\lambda)}{I_0(\lambda)}\right)_{\text{PVK}} = \frac{A(\lambda)_{\text{PVK}}}{A(\lambda)_{\text{Total}}}\left(\frac{I_{\text{Abs}}(\lambda)}{I_0(\lambda)}\right)_{\text{Total}} \qquad \textbf{Equation 6-4}$$

The absorption spectrum of the complex in PVK, $A(\lambda)_{Total}$ and the absorption spectrum of PVK alone, $A(\lambda)_{PVK}$ are measured experimentally. In principle, the absorption spectrum of the complex, $A(\lambda)_{Complex}$, can be determined by subtracting $A(\lambda)_{PVK}$ from $A(\lambda)_{Total}$.

At wavelengths below 300 nm, it was not possible to extract a reliable absorption profile of the complex in this fashion because of the minimal contribution of the complex absorbance to the total absorbance and inevitable slight differences in absorbance between the sample (complex plus PVK) and the reference (PVK). Therefore, the absorption spectrum of the complex was constructed by determining the absorbance (by subtraction) at a wavelength where the contribution of the complex was substantial (350 nm for $Eu(tta)_3DPEPO$ complex and 310 nm for $Eu(hfac)_3DPEPO$) and using this value to scale the spectrum measured for the complex in PMMA. (Assuming that the intrinsic absorption spectrum of the complex is the same in PVK and PMMA).

The calculated excitation spectrum (Equation 6-1) was fitted to the experimental data using the non-linear least-squares algorithm in the Solver application in Excel to yield the value of β.

To assess quantitatively the effect of energy transfer from PVK on the excitation spectrum of the complex, the excitation spectrum corresponding to direct excitation, in the absence of PVK, was simulated by scaling the excitation spectrum measured in PMMA. In the case of the $Eu(tta)_3DPEPO$ complex, the excitation spectrum in PMMA was scaled to give the same intensity at 380 nm as the excitation spectrum measured in PVK; at this wavelength, there is absorption only by the complex, not by the PVK matrix. On the other hand, there is no wavelength for $Eu(hfac)_3DPEPO$ at which the complex absorption is exclusive of the PVK. In this case, the scaling factor was calculated by determining the fraction of the incident intensity that would be absorbed at 318 nm (λ_{max} of the excitation spectrum in PVK) by the complex in the absence of PVK given by Equation (6-5).

$$\left(\frac{I_{Abs}(318)}{I_0(318)}\right)_{No\ PVK} = 1\text{-}10^{-A(318)_{Complex}} \qquad \textbf{Equation 6-5}$$

where $A(318)_{Complex}$ is the measured absorbance of the complex (in PVK) at 318 nm.

The ratio of the excitation intensities in the absence and presence of PVK is then given by Equation (6-5) to the value of Equation (6-3) at 318 nm.

6.3 Results and Discussion

6.3.1 Eu(hfac)$_3$DPEPO in PVK Matrix

The UV absorption spectra of PVK film and Eu(hfac)$_3$DPEPO in PVK are shown in Figure 6.3. The absorption spectrum of PVK shows an absorption onset at 27,027 cm^{-1} (370 nm), λ_{max} at 29,411 cm^{-1} (340 nm) ,34,129 cm^{-1} (293 nm), and 38,150 cm^{-1} (262 nm) that can be attributed to the (π-π^* transitions); thus making PVK a good light harvester in the UV region. When Eu(hfac)$_3$DPEPO is encapsulated in PVK film, the complex absorption (shown in Figure 6.3) becomes evident between 300 and 345 nm. In contrast, the absorption at shorter and longer wavelengths is dominated by the PVK matrix.

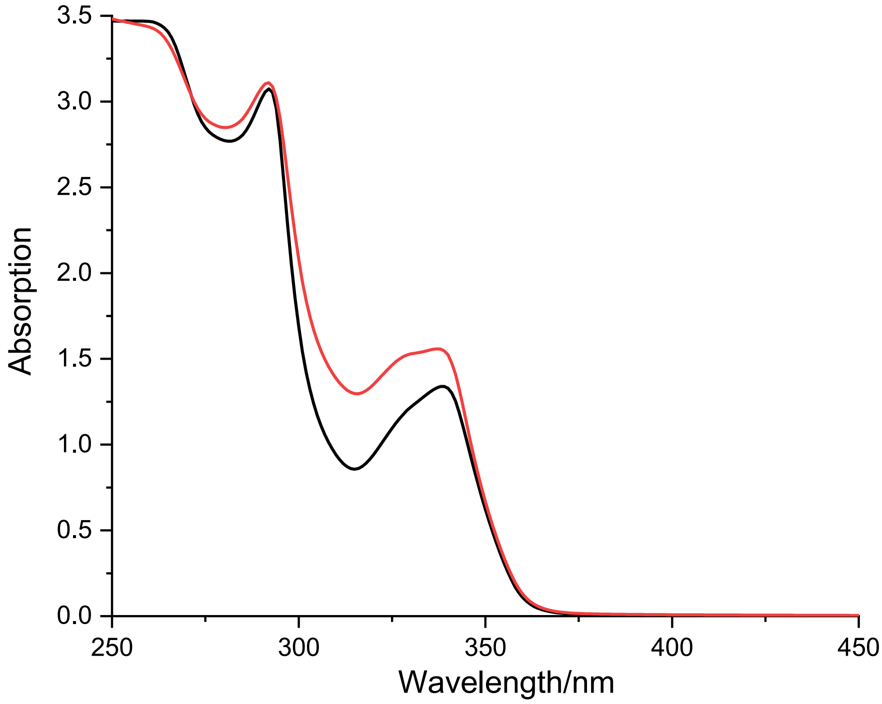

Figure 6.3 UV absorption spectra of PVK (black line) and Eu(hfac)$_3$DPEPO, wt.%10, in PVK (red line).

Subtracting the absorption spectrum of PVK only from that of the complex in PVK reveals the absorbance of the complex at wavelengths above 300 nm (Figure 6.4). Subtraction at wavelengths below 300 nm is unreliable because the contribution of the complex is too small. It should be noted that the relative absorbances of the 10% and 16% samples are consistent with the relative weight fractions. Nevertheless, the 2.5% sample's absorbance is higher than expected for this weight fraction and indicates that the concentration is around half that of the 10% sample.

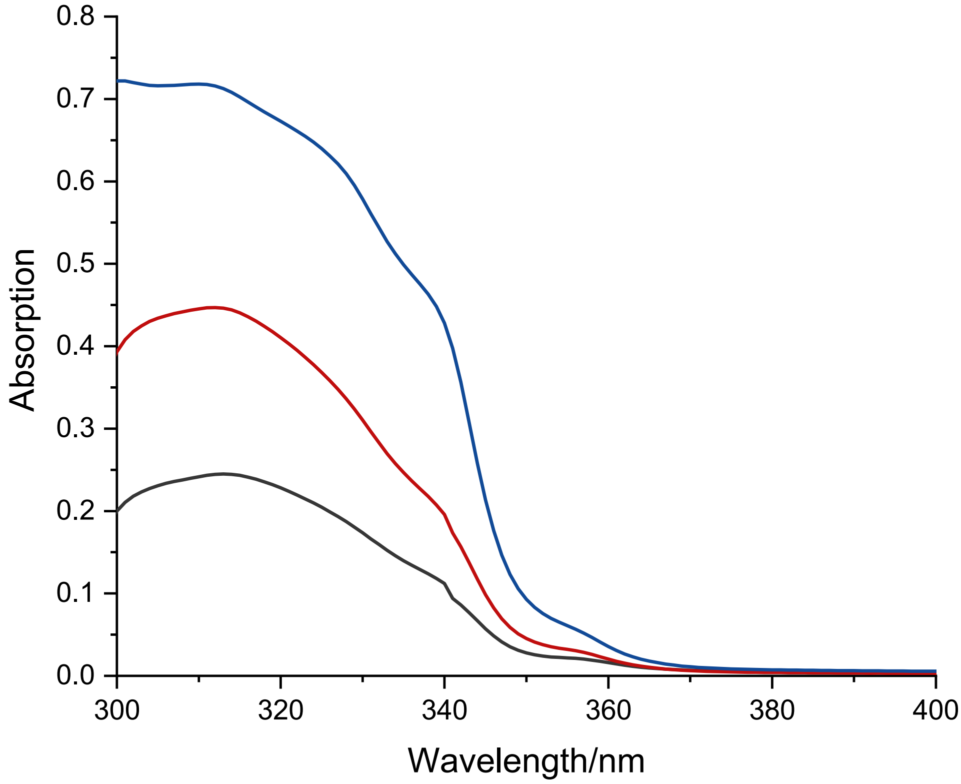

Figure 6.4 Absorbance due to Eu(hfac)$_3$DPEPO at wavelengths greater than 300 nm, for wt.% 2.5(black line),10 (red line), and 16 (blue line).

Figure 6.5 shows the absorption spectrum of Eu(hfac)$_3$DPEPO in PMMA and the fluorescence emission of the PVK. It shows that there is no spectral overlap between the absorption of the complex and the emission of the polymer. The broad structureless spectrum with λ_{max} at 24,271 cm^{-1} (412 nm) is a characteristic of excimer emission (originating from the low energy interchain excimer), which dominates in the solid PVK film noted in section 6.1.1.

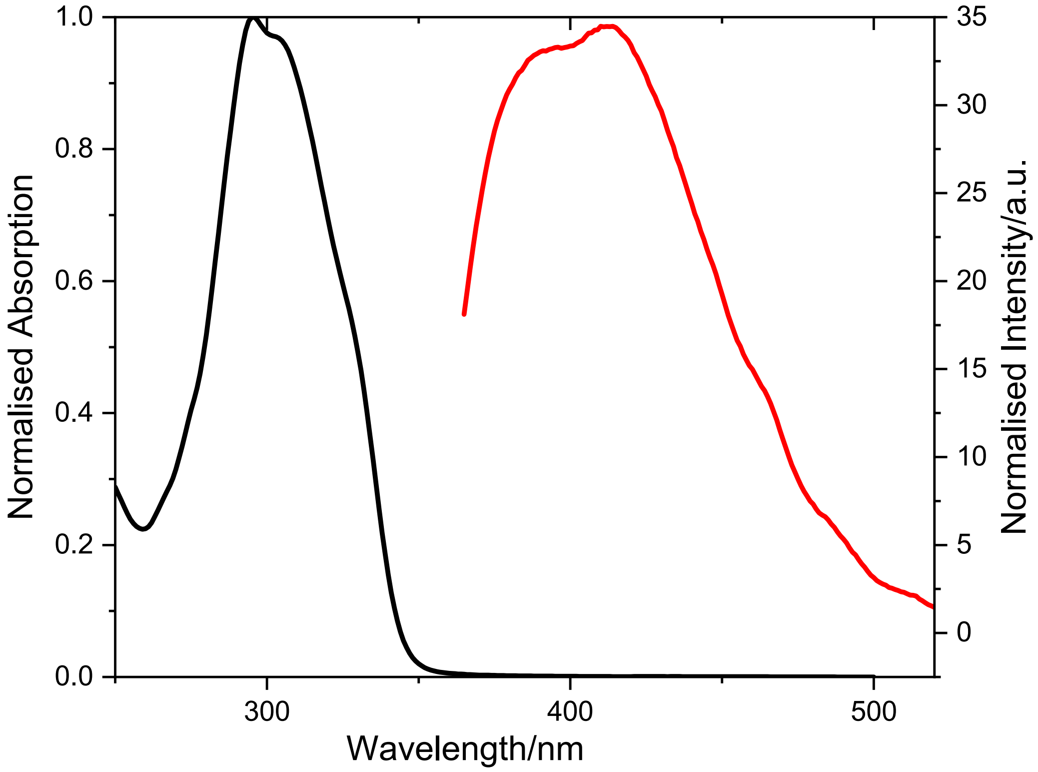

Figure 6.5 Normalised absorption spectrum (black line)of Eu(hfac)$_3$DPEPO in PMMA and the normalised emission spectrum (red line) of PVK film (excited at 340 nm).

Comparing the excitation spectrum of the complex in PVK to that of the complex in PMMA can demonstrate the effect of absorption by the PVK. It may prove energy transfer from the PVK matrix to the complex since PMMA is a passive host and does not act as an energy donor (as shown in Chapter 4). Figure 6.6 shows the excitation spectrum of Eu(hfac)$_3$DPEPO in PMMA and that of the complex in PVK. It is clear that the excitation spectrum of the complex in PVK is significantly different from its intrinsic excitation spectrum(in PMMA), suggesting that the energy transfer from the PVK matrix to the complex is occurring. However, the excitation spectrum of the complex in PVK does not closely resemble the absorption spectrum (Figure 6.3), suggesting that the efficiency of energy transfer is low.

The excitation spectrum peaks in the wavelength range where absorption by the complex, relative to PVK, is most significant. Energy transfer from PVK enhances excitation intensity at wavelengths above 300 nm and shifts excitation maximum to longer wavelength. At shorter wavelengths, absorption by PVK competes with direct excitation and depletes excitation intensity compared with direct excitation of the complex in PMMA.

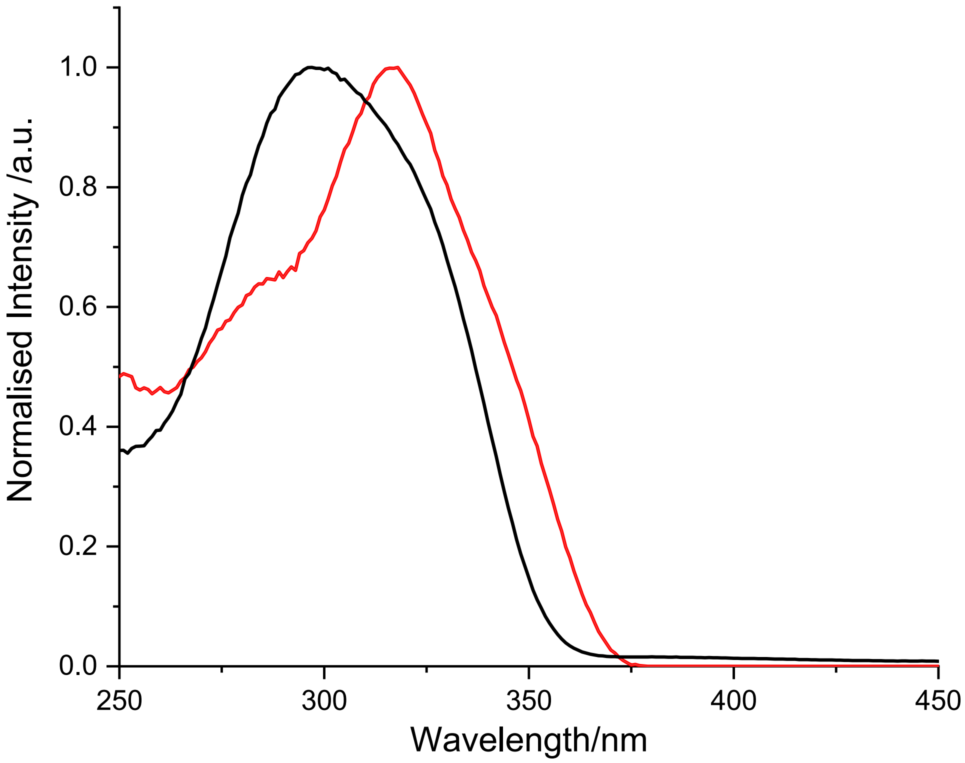

Figure 6.6 Normalised excitation spectra (detected at 611 nm) of Eu(hfac)$_3$DPEPO in PVK (red line) and that of Eu(hfac)$_3$DPEPO in PMMA (black line).

The excitation spectrum of Eu(hfac)$_3$DPEPO in PVK was fitted by the sum of contributions from direct excitation of complex and indirect excitation via absorption by PVK matrix, Equation (6-1), as described in section 6.2.3. The yielded parameter β represents the efficiency of energy transfer from the PVK matrix. Figure 6.7 shows the results of fitting the excitation spectrum of the 10% Eu(hfac)$_3$DPEPO in PVK. The fitted spectrum is compared with the experimental spectrum, and the contribution to the excitation spectrum due to absorption by the PVK matrix is shown.

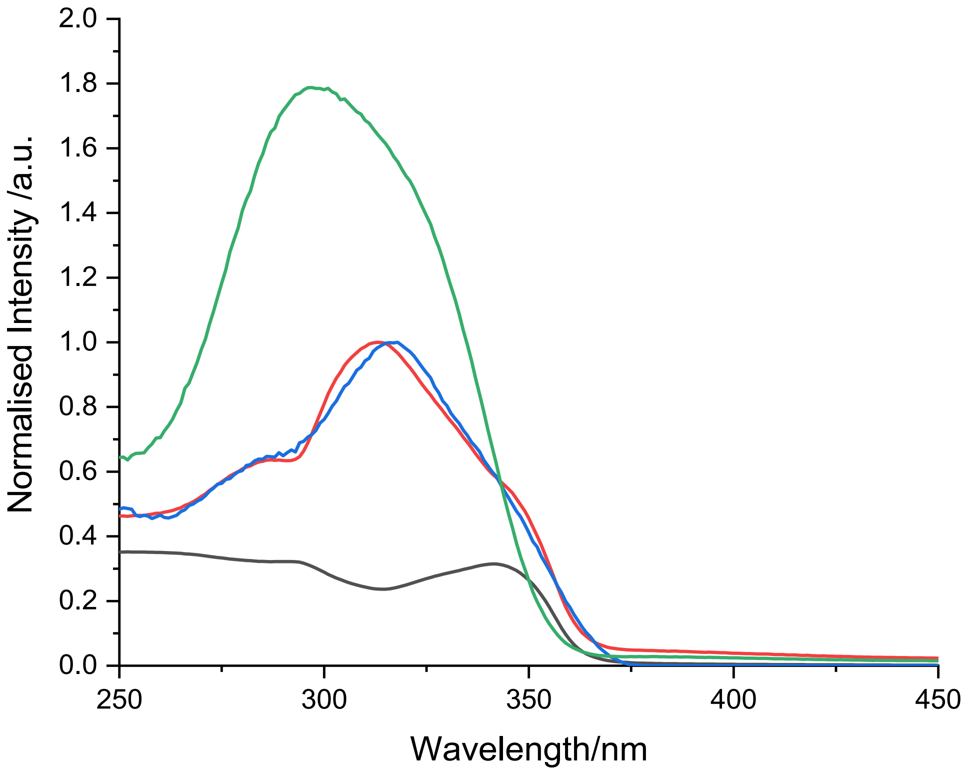

Figure 6.7 Normalised experimental (blue line) and fitted (red line) excitation spectra for wt.%10 Eu(hfac)$_3$DPEPO. The contributions of the PVK matrix to the excitation spectrum (black line) and the predicted excitation spectrum that would be expected under equivalent conditions in the absence of PVK (green line).

The fitted spectrum is in good agreement with the measured spectrum and gives a β value of 0.15 (Table 1), i.e. 15% of the light absorbed by PVK results in excitation of the complex. At wavelengths shorter than ~280 nm and longer than ~345 nm, the majority of the excitation intensity is due to an energy transfer from PVK. The contribution of PVK is lowest at around 315 nm, where it is ~25% of the total excitation intensity. Overall, energy transfer from PVK accounts for 45% of the entire integrated excitation intensity. Figure 6.7 also shows the excitation spectrum expected for direct excitation of the complex in the absence of the PVK matrix (e.g., in PMMA), under equivalent concentration and incident light intensity conditions. Under these conditions, all of the incident light would directly excite the complex. It can be seen that the presence of PVK significantly enhances the excitation intensity at wavelengths longer than ~345 nm, but has a detrimental effect over the majority of the excitation wavelength range. This is the consequence of the high absorbance of the PVK combined with a low energy transfer efficiency.

The PVK matrix essentially acts as a filter, absorbing the majority of the incident light and transferring only a small fraction of its excitation energy to the complex.

Figure 6.8 shows a simulated excitation spectrum for this sample with a hypothetical β value of 0.5. It can be seen that if the energy transfer efficiency from PVK could be increased to this level, there would be a substantial enhancement of the excitation intensity over the majority of the wavelength range.

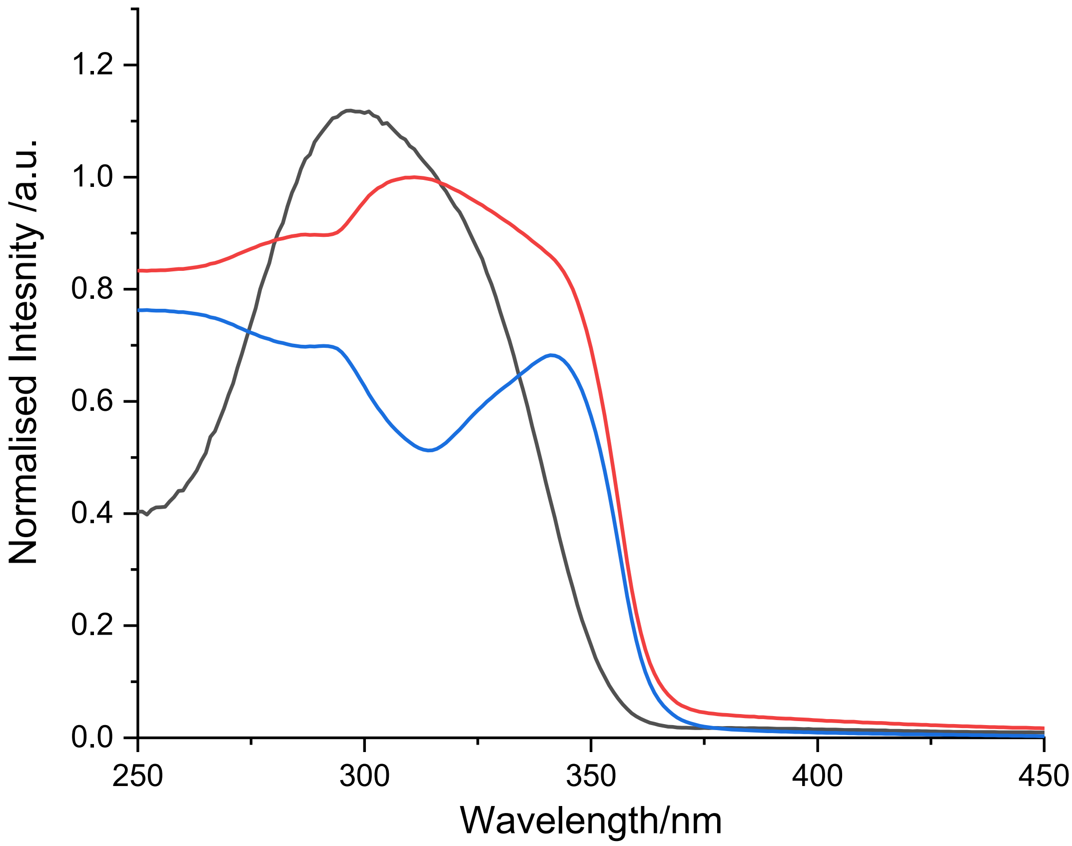

Figure 6.8 Simulated excitation spectrum (red line), for wt.%10 Eu(hfac)$_3$DPEPO in PVK, with β=0.5, predicted excitation spectrum in the absence of PVK (black line), and the contribution of PVK to the excitation spectrum (blue line).

Table 6.1 The value of β and the fraction of the integrated excitation intensity due to energy transfer from PVK for $Eu(hfac)_3DPEPO$ at different concentrations in PVK.

Weight % of $Eu(hfac)_3DPEPO$	β	Fraction of the excitation intensity
2.5	0.17	0.62
10	0.15	0.45
16	0.13	0.32

The β values for the three samples are given in Table 6.1, together with the fraction of the integrated excitation intensity due to PVK. The energy transfer efficiency does not change significantly with the concentration of the $Eu(hfac)_3DPEPO$, remaining at about 0.15 for all three samples. The fraction of excitation intensity arising from energy transfer decreases with increasing complex concentration, from 0.62 for the 2.5% sample to 0.32 for the 16% sample. As the concentration of the complex increases, the fraction of light absorbed by the complex, and hence the contribution from direct excitation, increases. The fitted spectra for these two samples are shown in Figures 6.9 and 6.10. For the 2.5% sample, the PVK-associated enhancement of the excitation intensity at wavelengths above ~345 nm is greater relative to the detrimental effect at shorter wavelengths, compared with the higher concentration samples. The highest concentration sample, 16%, shows the lowest PVK-induced long-wavelength enhancement relative to the undesirable decrease in intensity at shorter wavelengths.

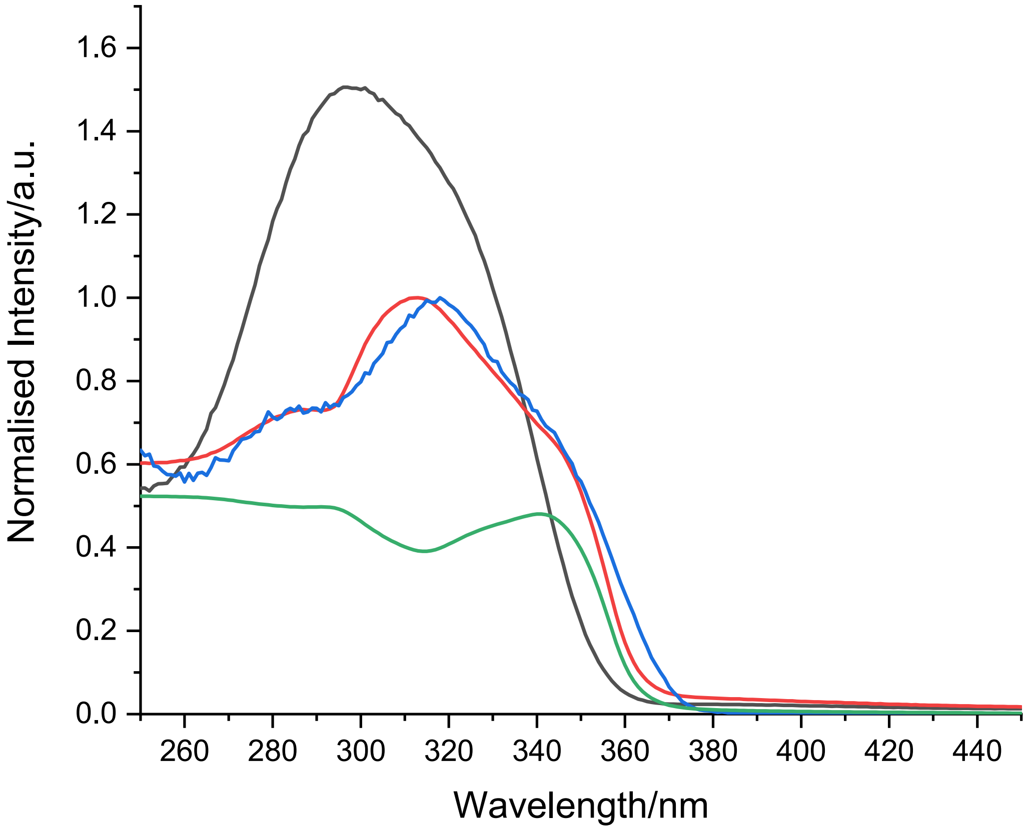

Figure 6.9 Normalised experimental (blue line) and fitted (red line) excitation spectra for wt.% 2.5 Eu(hfac)$_3$DPEPO. The contributions of the PVK matrix to the excitation spectrum are also shown (green line) and the predicted excitation spectrum that would be expected under equivalent conditions in the absence of PVK (black line).

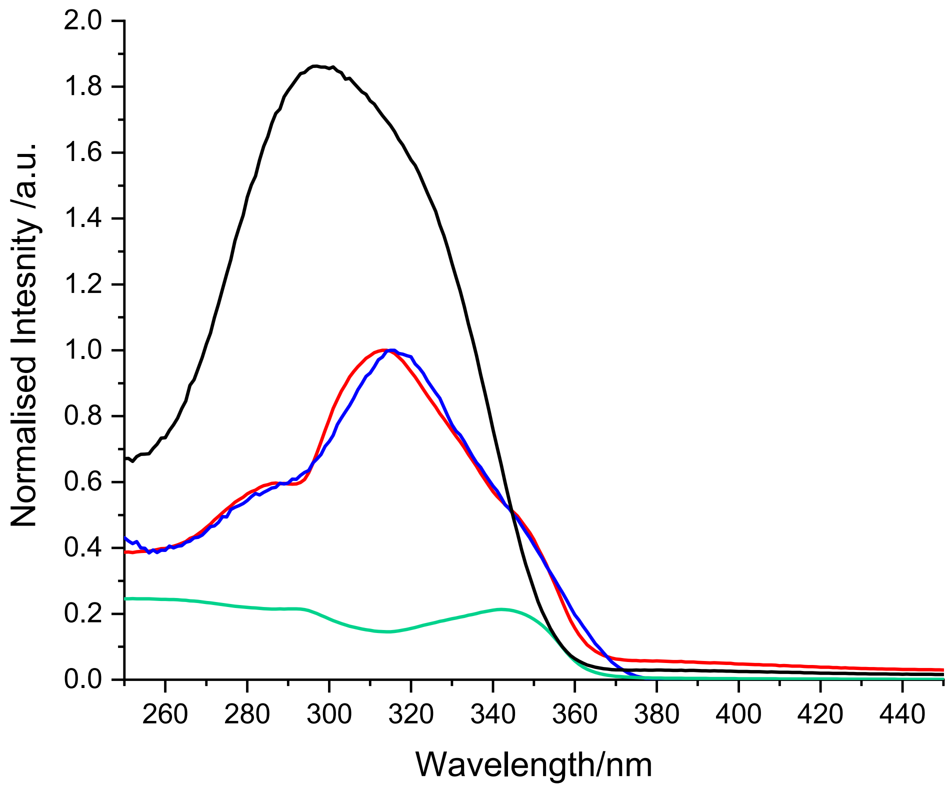

Figure 6.10 Normalised experimental (blue line) and fitted (red line) excitation spectra for wt.%16 Eu(hfac)$_3$DPEPO. The contributions of the PVK matrix to the excitation spectrum (green line) are also shown, and the predicted excitation spectrum that would be expected under equivalent conditions in the absence of PVK (black line).

6.3.2 Eu(tta)$_3$DPEPO in PVK Matrix

The UV absorption spectra of PVK film and 5.4% Eu(tta)$_3$DPEPO in PVK are shown in Figure 6.11. The absorption spectrum of PVK, shows an absorption onset at 27,027 cm^{-1} (370 nm), λ_{max} at 29,411 cm^{-1} (340 nm) ,34,129 cm^{-1} (293 nm), and 38,150 cm^{-1} (262 nm). When Eu(tta)$_3$DPEPO is encapsulated in PVK film, the complex absorption (shown in Figure 6.12) becomes evident between 300 and 400 nm. The absorption at shorter wavelengths is due entirely to the PVK matrix.

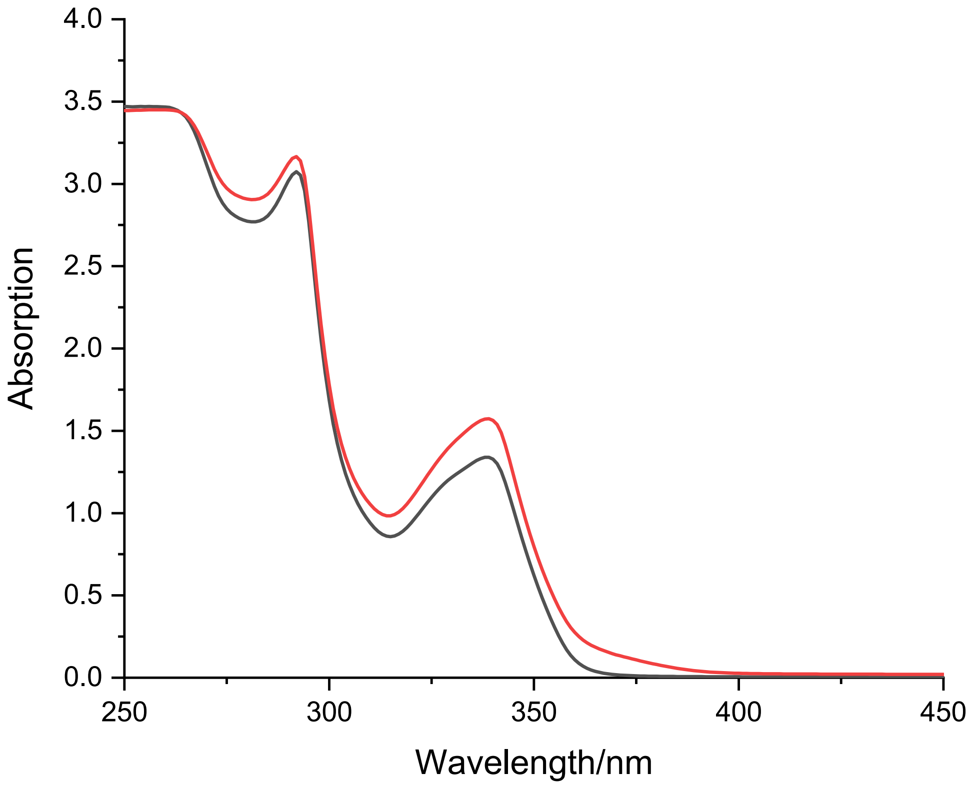

Figure 6.11 UV absorption spectra of PVK (black line) and wt.%5.4 Eu(tta)$_3$DPEPO in PVK (red line).

Figure 6.12 shows the absorption spectrum of Eu(tta)$_3$DPEPO in PMMA and the fluorescence emission of the PVK. It shows that there is minimal spectral overlap between the absorption of the complex and the emission of the polymer.

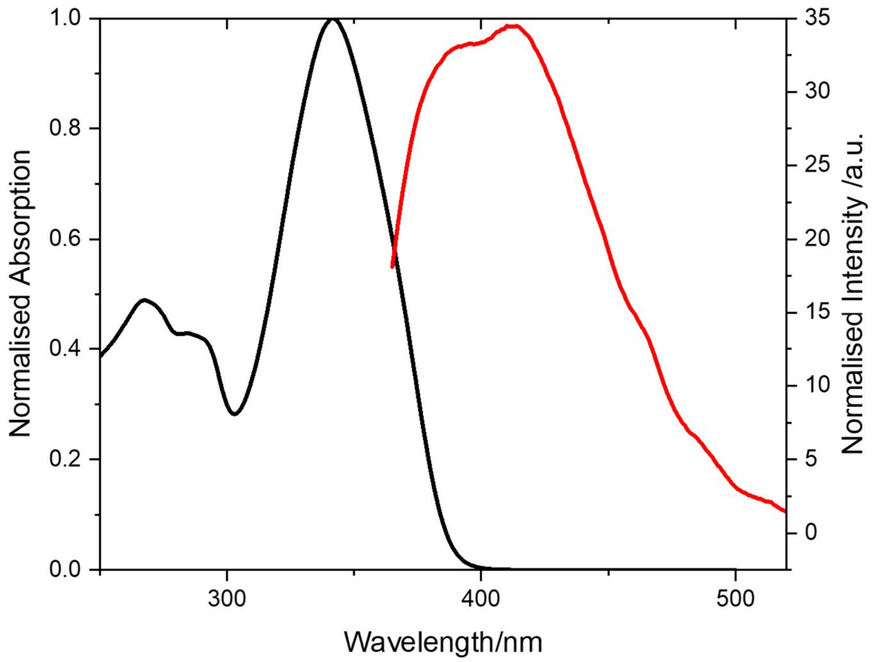

Figure 6.12 Normalised absorption spectrum (black line)of Eu(tta)$_3$DPEPO in PMMA and the normalised emission spectrum (red line) of PVK film (excited at 340 nm)

As for Eu(hfac)$_3$DPEPO, the excitation spectrum of the Eu(tta)$_3$DPEPO in PVK (Figure 6.13) is significantly different from its absorption spectrum (Figure 6.11), suggesting that the energy transfer efficiency from the PVK matrix to the complex is low. Comparison of excitation profiles of complex in PVK and PMMA (Figure 6.13) demonstrates that energy transfer from PVK enhances excitation intensity at wavelengths below 325 nm and above 355 nm. Absorption by PVK depletes the excitation intensity between 325 and 355 nm.

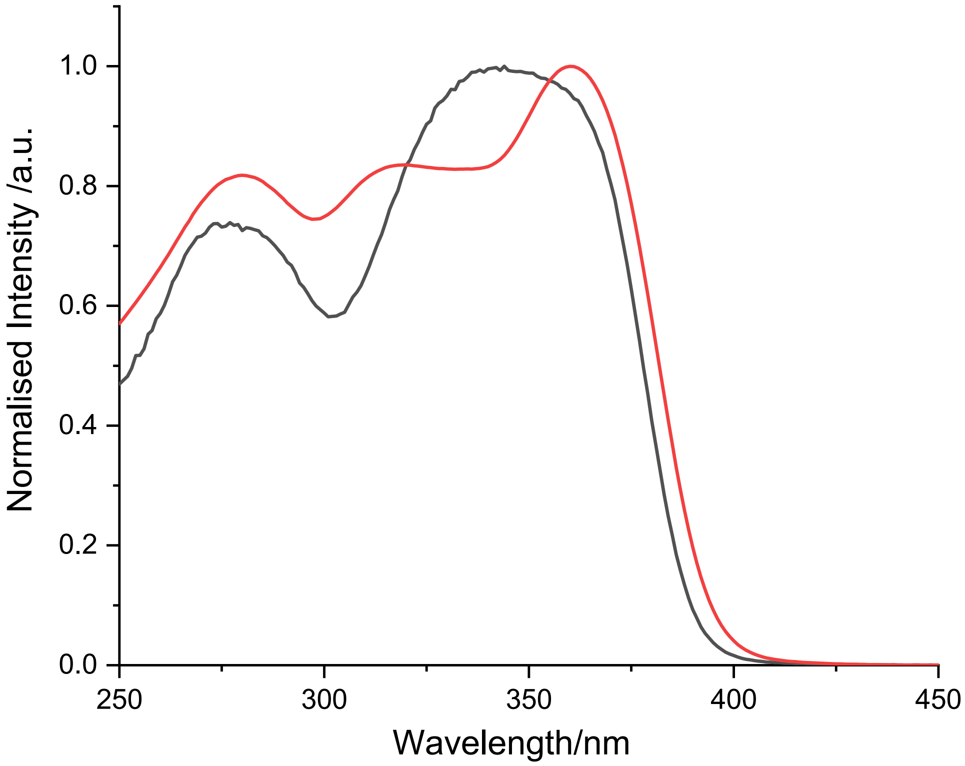

Figure 6.13 Normalised excitation spectra (detected at 611 nm) of wt.%5.4 $Eu(tta)_3DPEPO$ in PVK (red line) and that of $Eu(tta)_3DPEPO$ in PMMA (black line).

Figure 6.14 shows the results of fitting the excitation spectrum. The fitted spectrum is compared with the experimental spectrum. The contribution to the excitation spectrum due to absorption by the PVK matrix and that due to direct excitation is shown.

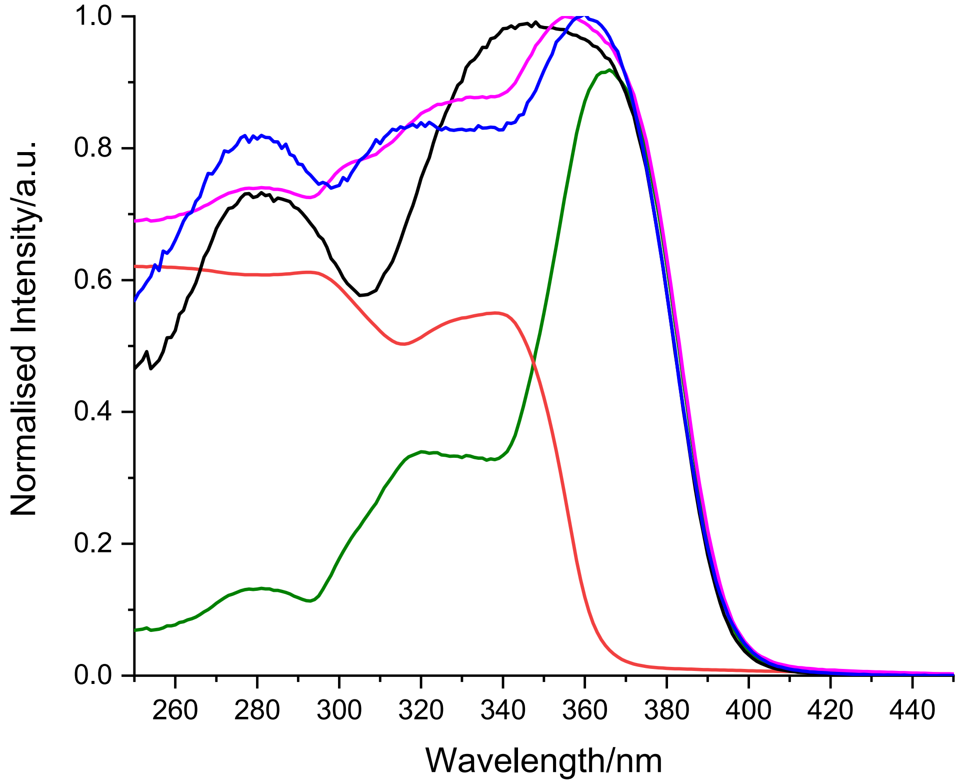

Figure 6.14 Normalised experimental (blue line) and fitted (pink line) excitation spectra for Eu(tta)$_3$DPEPO. The contributions of the PVK matrix to the excitation spectrum (red line) and that due to direct excitation (green line) are also shown, and the predicted excitation spectrum that would be expected under equivalent conditions in the absence of PVK (black line).

The fitted spectrum is in reasonably good agreement with the measured spectrum and gives a β value of 0.19. The discrepancy between the fitted spectrum and the measured spectrum is likely due to small differences between the profiles of the intrinsic excitation spectrum of the complex when incorporated in the PVK matrix and that measured for the complex in PMMA. The energy transfer efficiency from PVK to the 5.4% Eu(tta)$_3$DPEPO is thus estimated to be approximately 0.2, similar to that found for energy transfer to Eu(hfac)$_3$DPEPO.

Below ~345 nm, the majority of the excitation intensity is due to an energy transfer from PVK. At wavelengths above 345 nm, direct excitation of the complex predominates. Overall, energy transfer from PVK accounts for 55% of the total integrated excitation intensity. Figure 6.14 also shows the excitation spectrum that would be expected for direct excitation of the complex in the absence of the PVK matrix, under equivalent conditions of concentration and incident light intensity. Under these conditions, all of the incident light would directly excite the complex. This spectrum is obtained by scaling the excitation spectrum measured in PMMA to give the same intensity at 380 nm as that of the excitation spectrum in PVK at this wavelength; at 380 nm, the excitation intensity in PVK is due entirely to direct excitation of the complex. It can be seen that the presence of PVK significantly enhances the excitation intensity at wavelengths below 325 nm but has a detrimental, intensity-depleting effect between 325 and 355 nm. However, unlike Eu(hfac)$_3$DPEPO, there is a net gain in excitation intensity in the presence of PVK; the increase in intensity exceeds the loss by a factor of about three.

6.3.3 Effect of Varying the Concentration of PVK Matrix on Eu(tta)$_3$DPEPO

The absorption spectra of samples with various concentrations, different thicknesses, of the PVK matrix (concentration of the Eu(tta)$_3$DPEPO was kept fixed) are shown in Figure 6.15. The contribution of the complex to the absorption spectrum is evident in the long-wavelength tail(> 360 nm), shown in Figure 6.16. It can be seen that there is negligible change in absorbance between the 10 (mg/ml) and 20 (mg/ml) PVK samples, indicating that, at these low concentrations, the absorbance in this wavelength range is due entirely to the complex.

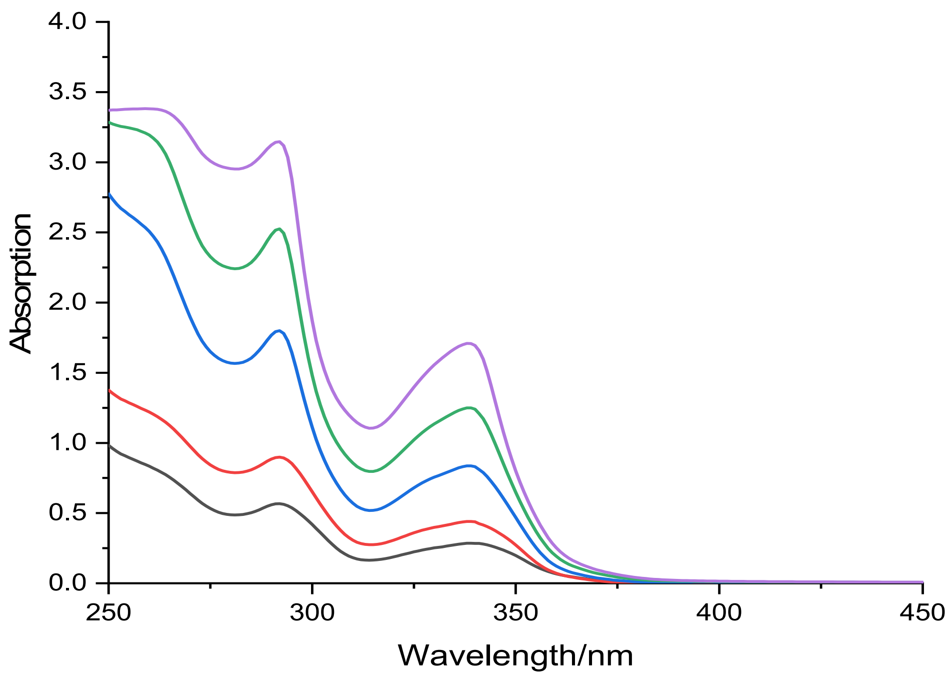

Figure 6.15 UV absorption spectra of wt.%5.4 Eu(tta)$_3$DPEPO in PVK matrix at different concentration (mg/ml), 10 (black line), 20 (red line), 30 (blue line), 40 (green line), and 50 (purple line).

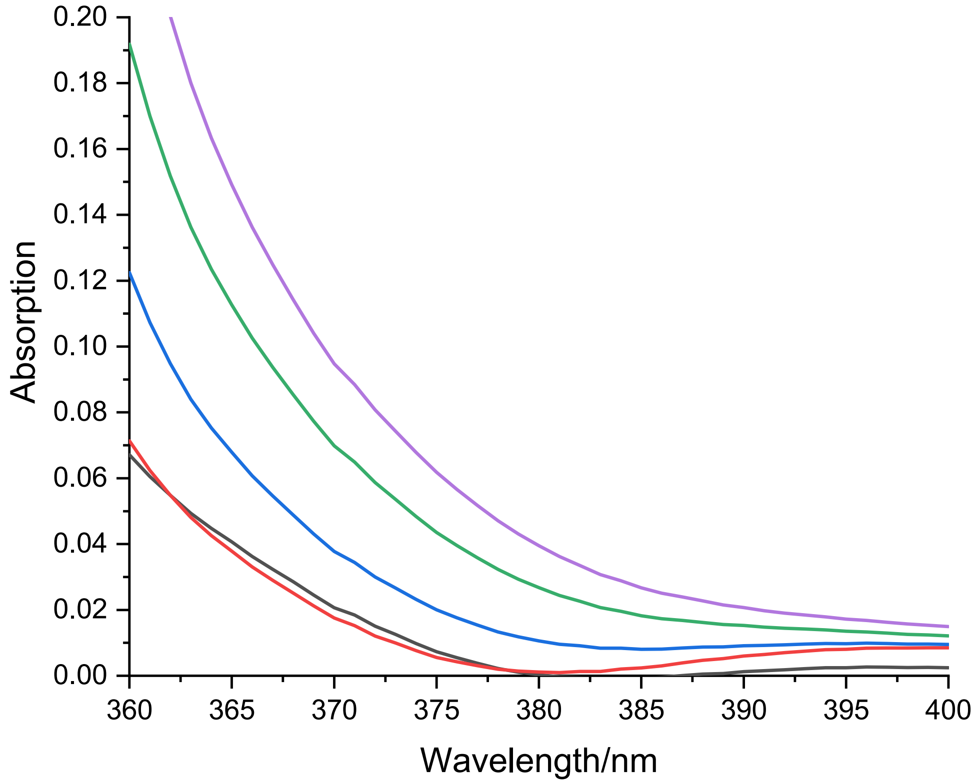

Figure 6.16 The long-wavelength tail of the UV absorption spectra of wt.%5.4 Eu(tta)$_3$DPEPO in PVK matrix at different concentration (mg/ml), 10 (black line), 20 (red line), 30 (blue line), 40 (green line), and 50 (purple line).

Figure 6.17 shows the dependence of absorbance on PVK concentration at 300 nm (where the contribution from the complex is negligibly small). There is a good linear relationship, confirming the relative PVK concentrations of the five films.

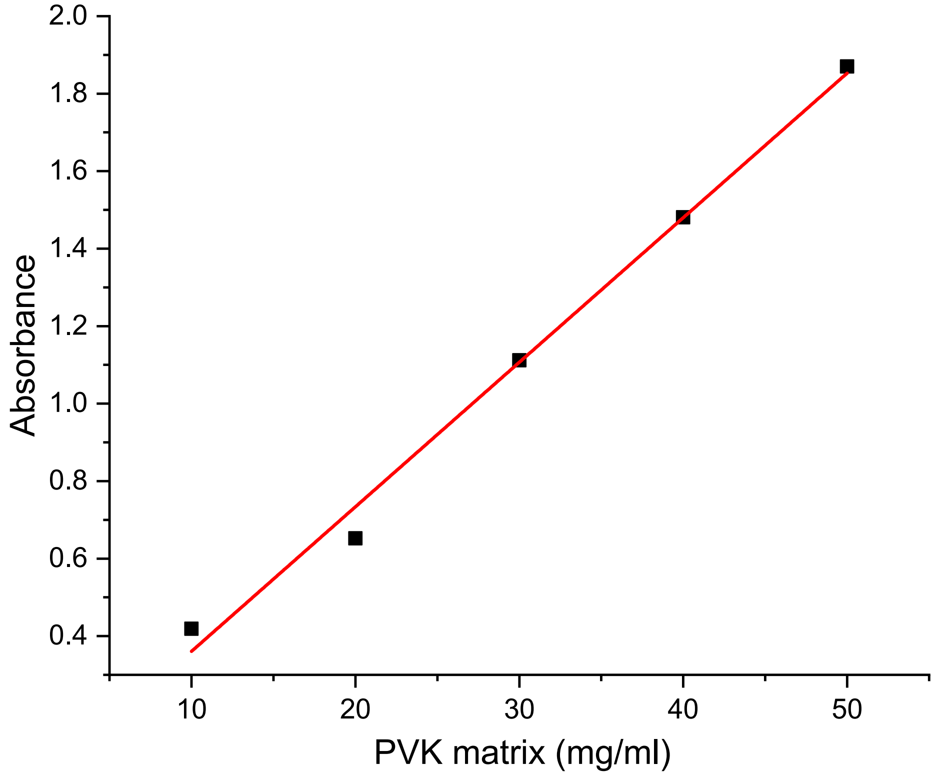

Figure 6.17 Absorbance of 5.4% Eu(tta)$_3$DPEPO at 300 nm versus different concentrations of PVK.

In Figure 6.18, the excitation spectrum of the complex at each concentration of PVK is compared with the excitation spectrum that would be expected in the absence of PVK. It can be seen that the magnitude of the enhancement of the excitation intensity of the complex by energy transfer from the PVK is influenced by the concentration (thickness) of the PVK. This is illustrated in Figure 6.19, which shows the enhancement factor (the ratio of the integrated intensities in the presence and absence of PVK) plotted as a function of the PVK concentration. The maximum enhancement (a factor of almost 1.8) is seen for 20 (mg/ml) PVK and the minimum for the highest PVK concentration 50 (mg/ml). At PVK concentrations greater than 20 (mg/ml), the enhancement factor decreases with increasing PVK concentration. This is a consequence of the increasing, detrimental inner filter effect, which reduces the intensity of light available for direct excitation of the complex.

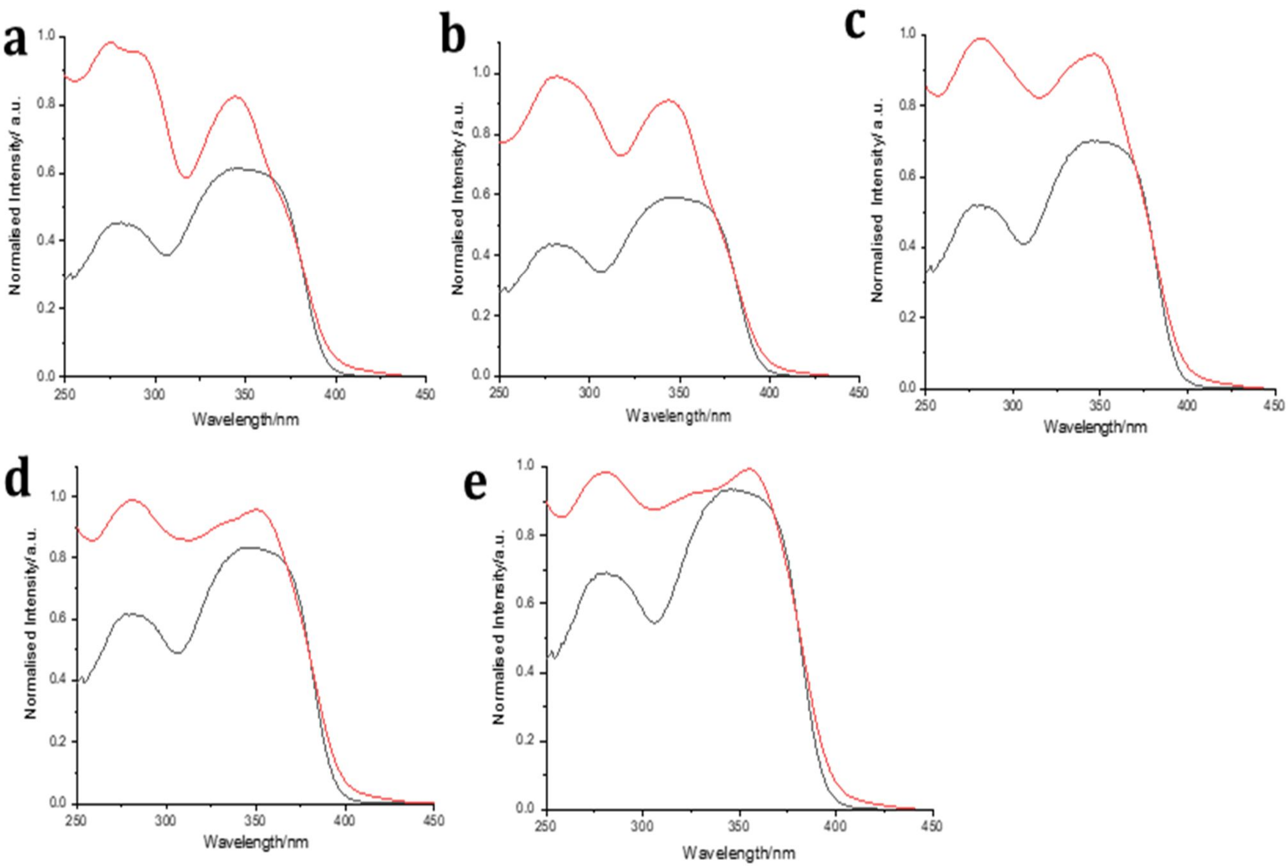

Figure 6.18 Excitation spectrum of wt.%5.4 Eu(tta)$_3$DPEPO in PVK matrix at different matrix concentrations (red line) , in comparison with the predicted excitation spectrum in the absence of PVK (black line). PVK concentration: (a) 10 mg/ml, (b) 20 mg/ml, (c) 30 mg/ml, (d) 40 mg/ml, and (e) 50 mg/ml.

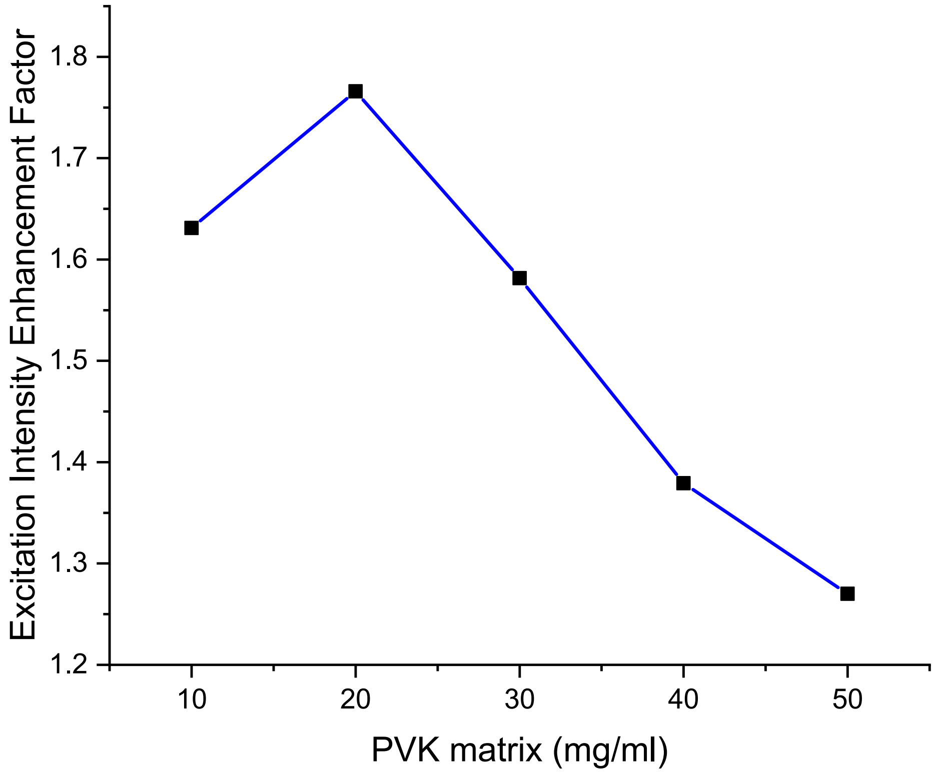

Figure 6.19 Excitation intensity enhancement factor plotted versus PVK concentration.

The emission spectrum of PVK extends from ~380 to 520 nm, peaking at ~412 nm. This emission can be assigned to excimers formed by the interaction of pairs of the carbazole side-groups, as discussed in section 6.1.1. The overlap of this emission spectrum with the absorption spectrum of the $Eu(tta)_3DPEPO$ complex is minimal (Figure 6.12), and there is no overlap with the absorption spectrum of $Eu(hfac)_3DPEPO$ (Figure 6.5)**.** Therefore, it can be deduced that energy transfer to the complexes occurs from the carbazole monomer excited state, not from the excimer species. In undoped PVK, excitation of the monomer is followed by efficient energy transfer (exciton transport) between the carbazole groups until the excitation energy is trapped by an excimer-forming site, resulting in excimer emission. In PVK doped with the europium complexes, each complex acts as a trap for the migrating monomer excitons, competing with the excitation of the excimer-forming sites.

6.3.4 Effect of Co-doping with Donors on $Eu(tta)_3DPEPO$ in PVK Matrix

The effect of co-doping with donors DPEPO (21 mM), biphenyl (42 mM) or indole (70 mM) on 5.4 % $Eu(tta)_3DPEPO$ in PVK (20 mg/ml) was investigated. The effect of energy transfer from the co-doped donor can be seen by comparing the excitation spectra in PVK in the presence and absence of the donor, as shown in Figures 6.20 to 6.22. The combined effects of energy transfer from both the co-doped donor and the PVK can be seen by comparing the excitation spectrum of the co-doped complex in PVK with the excitation spectrum that would be expected in the absence of both donor and PVK, as also shown in Figures 6.20 to 6.22. In the case of DPEPO and biphenyl co-dopants (Figures 6.20 and 6.21, respectively), the excitation intensity is enhanced between 250 and ~320 nm, compared with the effect of energy transfer from the PVK matrix alone. For the DPEPO donor, the magnitude of this additional enhancement is significant compared with the effect of the PVK matrix only, but for biphenyl, the additional enhancement is relatively small. For the indole co-dopant (Figure 6.22), there is no significant enhancement compared with the effect of PVK only, but there appears to be a small effect on the excitation profile.

The absorption spectra of the co-dopant, DPEPO, biphenyl, and indole (as shown in chapter 5) have no absorption overlap with the PVK emission; therefore, FRET from the PVK to the co-dopant is not probable. As shown for the energy transfer from PVK to the europium complexes, DPEPO and biphenyl might act as traps for the migrating monomer excitons, competing with the excimer-forming sites and then transferring the energy to the europium complex through FRET. Another proposed explanation for the excitation enhancement is a combination of two different energy transfer mechanisms: the PVK matrix to the europium complex through exciton diffusion and FRET from the co-dopant to the complex. Therefore a multistep energy transfer process can be proposed to explain the enhancement in the excitation intensity in the case of DPEPO and biphenyl. It is worth noting that a multistep energy transfer mechanism that described the energy transfer in PVK nanoparticles with organic molecules was reported in other work.[52]

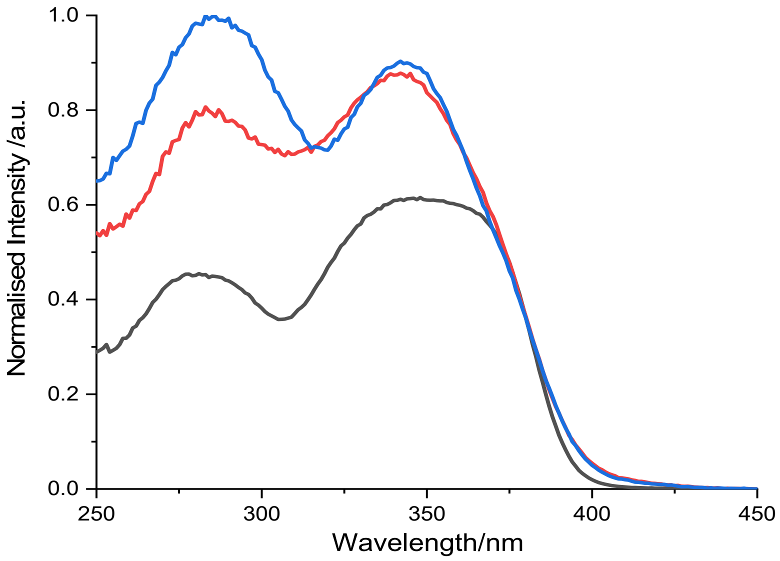

Figure 6.20 Normalised excitation spectra (detected at 611 nm) for the complex co-doped with DPEPO in PVK (blue line) compared with the excitation spectrum in PVK in the absence of donors (red line) and the excitation spectrum predicted under equivalent conditions in the absence of both donor and PVK (black line)

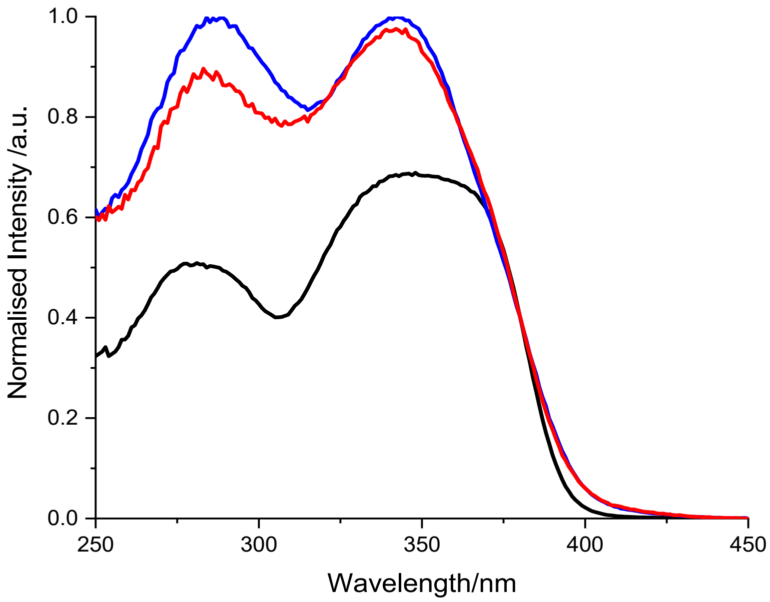

Figure 6.21 Normalised excitation spectra (detected at 611 nm) for the complex co-doped with Biphenyl in PVK (blue line) compared with the excitation spectrum in PVK in the absence of donors (red line) and the excitation spectrum predicted under equivalent conditions in the absence of both donor and PVK (black line)

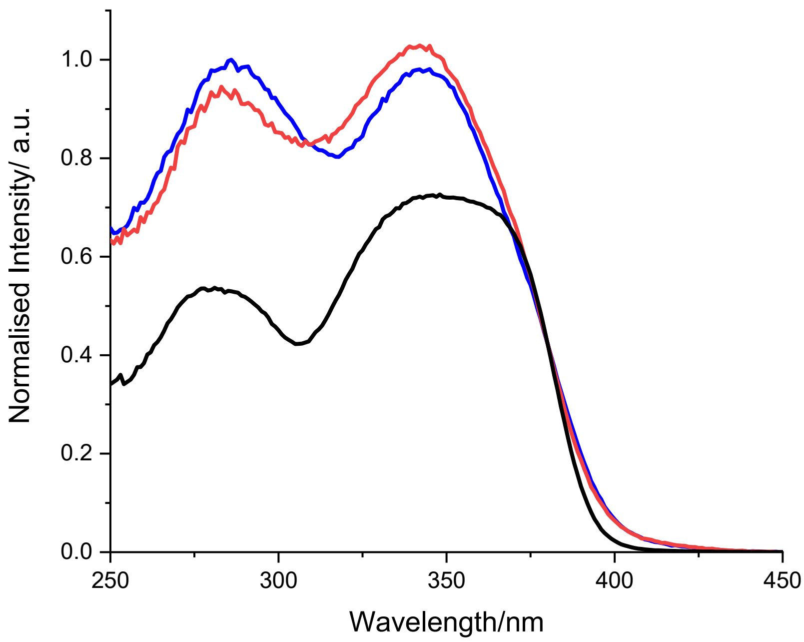

Figure 6.22 Normalised excitation spectra (detected at 611 nm) for the complex co-doped with Indole in PVK (blue line) compared with the excitation spectrum in PVK in the absence of donors (red line) and the excitation spectrum predicted under equivalent conditions in the absence of both donor and PVK (black line)

6.4 Conclusions

We discussed in this chapter the photoactive nature of Poly(N-vinylcarbazole) (PVK) and its unique photophysical properties, such as strong absorption in the UV region, fluorescence emission, and the nature of energy transfer in the polymer matrix. The transparent films obtained of the PVK polymer, in addition to their good absorption in the UV region and their photophysical properties, would make them an excellent candidate as a host material for LSCs and LDS layers application. The use of (PVK) as an active host for Eu(hfac)$_3$DPEPO was investigated. Energy transfer from PVK to the complex was found to occur with an efficiency of ~0.15, and appeared to be independent of complex concentration over the range 2.5 to 16 weight %. Energy transfer from PVK enhances excitation intensity at wavelengths above 300 nm, but has a detrimental effect over the majority of the excitation wavelength range (as shown in Figure 6.7). This is the consequence of the high absorbance of the PVK combined with a low energy transfer efficiency. Therefore, the use of PVK as a matrix for Eu(hfac)$_3$DPEPO, under the conditions used in these experiments, is not advantageous. However, it was predicted that if the energy transfer efficiency could be increased to 0.5, there would be a substantial enhancement of the excitation intensity over the majority of the wavelength range.

In contrast, for Eu(tta)$_3$DPEPO, the use of PVK as a matrix was found to give a beneficial enhancement in excitation intensity (Figure 6.14). The energy transfer efficiency from PVK to the complex was found to be. 0.20, similar to that found for energy transfer in Eu(hfac)$_3$DPEPO. The presence of PVK significantly enhances the excitation intensity at wavelengths below 325 nm and above 355 nm, although there is a detrimental, intensity-depleting effect between 325 and 355 nm. However, unlike Eu(hfac)$_3$DPEPO, there is a net gain in excitation intensity in the presence of PVK; the increase in intensity exceeds the loss by a factor of about 3.

The effect of varying the PVK matrix concertation on the Eu(tta)$_3$DPEPO was investigated. It was observed that the magnitude of the enhancement of the excitation intensity of the complex by energy transfer from the PVK is influenced by the concentration of PVK. A maximum enhancement was observed for 20(mg/ml) PVK. At PVK concentrations greater than 20 (mg/ml), the enhancement factor decreases with increasing PVK concentration.

Energy transfer from PVK to complexes has occurred, despite the lack of spectral overlap in the absorption spectrum of Eu(hfac)$_3$DPEPO and the minimal spectral overlap in the absorption spectrum of Eu(tta)$_3$DPEPO and PVK emission.

Therefore, it can be deduced that energy transfer to the complexes occurs from the carbazole monomer excited state, not from the emitting excimer species. Thus, in PVK doped with the europium complexes, each complex acts as a trap for the migrating monomer excitons, competing with the excitation of the excimer-forming sites.

The effect of adding co-dopant to $Eu(tta)_3DPEPO$ in the PVK matrix was investigated. In the case of DPEPO and biphenyl co-dopants, the excitation intensity is enhanced compared with the effect of energy transfer from the PVK matrix alone. For the indole co-dopant, there is no significant enhancement compared with the effect of PVK only, but there appears to be a small effect on the excitation profile. Thus, a multistep energy transfer process can be proposed to explain the enhancement in the excitation intensity by DPEPO and biphenyl.

Overall, there is potential for the role of PVK as a photoactive polymer in the LSCs and LDS layers, taking advantage of its photophysical properties. The energy transfer efficiency from PVK to the europium complexes studied here is rather low so that competitive absorption by the PVK can have a detrimental rather than a beneficial effect. More work needs to be done to establish the optimum conditions (concentration of complex, concentration of PVK, etc.) for energy transfer from PVK to $Eu(tta)_3DPEPO$. Quantum yield measurements and solar testing should be carried out to understand this work better in the context of LSCs and LDS layer applications. Now that it has been established that excitonic energy transfer occurs from PVK monomer to dopants, it should be possible to select complexes that are likely to be optimum acceptors to maximise harvesting the UV region and decrease the quantities of the lanthanide metals used.

6.5 References

1. Debije, M. G.; Verbunt, P. P. C., Thirty Years of Luminescent Solar Concentrator Research: Solar Energy for the Built Environment. *Advanced Energy Materials* **2012,** *2* (1), 12-35.
2. Roncali, J., Luminescent Solar Collectors: Quo Vadis? *Advanced Energy Materials* **2020,** *10* (36), 2001907.
3. Klampaftis, E.; Ross, D.; McIntosh, K. R.; Richards, B. S., Enhancing the performance of solar cells via luminescent down-shifting of the incident spectrum: A review. *Solar Energy Materials and Solar Cells* **2009,** *93* (8), 1182-1194.
4. Tatsi, E.; Griffini, G., Polymeric materials for photon management in photovoltaics. *Solar Energy Materials and Solar Cells* **2019,** *196*, 43-56.
5. Binnemans, K., Chapter 225 - Rare-earth beta-diketonates. In *Handbook on the Physics and Chemistry of Rare Earths*, Gschneidner, K. A.; Bünzli, J.-C. G.; Pecharsky, V. K., Eds. Elsevier: 2005; Vol. 35, pp 107-272.
6. El-Bashir, S., Photophysical properties of fluorescent PMMA/SiO2 nanohybrids for solar energy applications. *Journal of luminescence* **2012,** *132* (7), 1786-1791.
7. Griffini, G.; Levi, M.; Turri, S., Novel high-durability luminescent solar concentrators based on fluoropolymer coatings. *Progress in Organic Coatings* **2014,** *77* (2), 528-536.
8. Griffini, G., Host Matrix Materials for Luminescent Solar Concentrators: Recent Achievements and Forthcoming Challenges. *Frontiers in Materials* **2019,** *6* (29).
9. Fattori, V.; Melucci, M.; Ferrante, L.; Zambianchi, M.; Manet, I.; Oberhauser, W.; Giambastiani, G.; Frediani, M.; Giachi, G.; Camaioni, N., Poly (lactic acid) as a transparent matrix for luminescent solar concentrators: a renewable material for a renewable energy technology. *Energy & Environmental Science* **2011,** *4* (8), 2849-2853.
10. Kaniyoor, A.; McKenna, B.; Comby, S.; Evans, R. C., Design and Response of High-Efficiency, Planar, Doped Luminescent Solar Concentrators Using Organic–Inorganic Di-Ureasil Waveguides. *Advanced Optical Materials* **2016,** *4* (3), 444-456.
11. Meazzini, I.; Willis-Fox, N.; Blayo, C.; Arlt, J.; Clément, S.; Evans, R. C., Targeted design leads to tunable photoluminescence from perylene dicarboxdiimide–poly(oxyalkylene)/siloxane hybrids for luminescent solar concentrators. *Journal of Materials Chemistry C* **2016,** *4* (18), 4049-4059.
12. Nolasco, M. M.; Vaz, P. M.; Freitas, V. T.; Lima, P. P.; André, P. S.; Ferreira, R. A. S.; Vaz, P. D.; Ribeiro-Claro, P.; Carlos, L. D., Engineering highly efficient Eu(iii)-based tri-ureasil hybrids

toward luminescent solar concentrators. *Journal of Materials Chemistry A* **2013,** *1* (25), 7339-7350.

13. Gonçalves, M. C.; de Zea Bermudez, V.; Sá Ferreira, R. A.; Carlos, L. D.; Ostrovskii, D.; Rocha, J., Optically Functional Di-Urethanesil Nanohybrids Containing Eu3+ Ions. *Chemistry of Materials* **2004,** *16* (13), 2530-2543.
14. Lima, P. P.; Nobre, S. S.; Freire, R. O.; Júnior, S. A.; Sá Ferreira, R. A.; Pischel, U.; Malta, O. L.; Carlos, L. D., Energy Transfer Mechanisms in Organic−Inorganic Hybrids Incorporating Europium(III): A Quantitative Assessment by Light Emission Spectroscopy. *The Journal of Physical Chemistry C* **2007,** *111* (47), 17627-17634.
15. Lima, P. P.; Sá Ferreira, R. A.; Freire, R. O.; Almeida Paz, F. A.; Fu, L.; Alves Jr., S.; Carlos, L. D.; Malta, O. L., Spectroscopic Study of a UV-Photostable Organic–Inorganic Hybrids Incorporating an Eu3+ β-Diketonate Complex. *ChemPhysChem* **2006,** *7* (3), 735-746.
16. Mesquita, M. E.; Nobre, S. S.; Fernandes, M.; Ferreira, R. A. S.; Santos, S. C. G.; Rodrigues, M. O.; Carlos, L. D.; de Zea Bermudez, V., Highly luminescent di-ureasil hybrid doped with a Eu(III) complex including dipicolinate ligands. *Journal of Photochemistry and Photobiology A: Chemistry* **2009,** *205* (2), 156-160.
17. Mulder, C. L.; Theogarajan, L.; Currie, M.; Mapel, J. K.; Baldo, M. A.; Vaughn, M.; Willard, P.; Bruce, B. D.; Moss, M. W.; McLain, C. E., Luminescent solar concentrators employing phycobilisomes. *Advanced Materials* **2009,** *21* (31), 3181-3185.
18. Geffroy, B.; le Roy, P.; Prat, C., Organic light-emitting diode (OLED) technology: materials, devices and display technologies. *Polymer International* **2006,** *55* (6), 572-582.
19. Li, Y.; Zhang, X.; Zhang, Y.; Dong, R.; Luscombe, C. K., Review on the Role of Polymers in Luminescent Solar Concentrators. *Journal of Polymer Science Part A: Polymer Chemistry* **2019,** *57* (3), 201-215.
20. McGehee, M. D.; Bergstedt, T.; Zhang, C.; Saab, A. P.; O'Regan, M. B.; Bazan, G. C.; Srdanov, V. I.; Heeger, A. J., Narrow Bandwidth Luminescence from Blends with Energy Transfer from Semiconducting Conjugated Polymers to Europium Complexes. *Advanced Materials* **1999,** *11* (16), 1349-1354.
21. Sholin, V.; Olson, J.; Carter, S., Semiconducting polymers and quantum dots in luminescent solar concentrators for solar energy harvesting. *Journal of applied physics* **2007,** *101* (12), 123114.
22. Gutierrez, G. D.; Coropceanu, I.; Bawendi, M. G.; Swager, T. M., A Low Reabsorbing Luminescent Solar Concentrator Employing π-Conjugated Polymers. *Advanced Materials* **2016,** *28* (3), 497-501.
23. Yao, M.; Senoh, H.; Sakai, T.; Kiyobayashi, T., Redox active poly (N-vinylcarbazole) for use in rechargeable lithium batteries. *Journal of Power Sources* **2012,** *202*, 364-368.

24. Tang, W.; He, H.; Shi, J.; Cao, B.; Yang, C.; Fan, C., Poly(N-vinylcarbazole) (PVK) as a high-potential organic polymer cathode for dual-intercalation Na-ion batteries. *Organic Electronics* **2019,** *75*, 105386.
25. Zanoni, K. P. S.; Murakami Iha, N. Y., Sky-blue OLED through PVK:[Ir(Fppy)2(Mepic)] active layer. *Synthetic Metals* **2016,** *222*, 393-396.
26. Das, D.; Gopikrishna, P.; Narasimhan, R.; Singh, A.; Dey, A.; Iyer, P. K., White polymer light emitting diodes based on PVK: the effect of the electron injection barrier on transport properties, electroluminescence and controlling the electroplex formation. *Physical Chemistry Chemical Physics* **2016,** *18* (48), 33077-33084.
27. Liang, C.; Li, W.; Hong, Z.; Liu, X.; Peng, J.; Liu, L.; Lu, Z.; Xie, M.; Liu, Z.; Yu, J.; Zhao, D., Energy transfer process from polymer to rare earth complexes. *Synthetic Metals* **1997,** *91* (1), 151-154.
28. Wang, H.; Ryu, J.-T.; Shin, Y. H.; Kwon, Y., Synthesis and Properties of Polymers Containing Charge Transport Pendant Group. *Molecular Crystals and Liquid Crystals* **2009,** *514* (1), 158/[488]-170/[500].
29. Luo, Y.; Yu, X.; Su, W.; Zhang, Z.; Wu, W.; Yan, Q.; Zhang, Q., Energy transfer in a ternary system composed of Tb(DBM)3Phen, Eu(DBM)3Phen, and poly(N-vinylcarbazole). *Journal of Materials Research* **2009,** *24* (10), 3023-3031.
30. Grazulevicius, J. V.; Strohriegl, P.; Pielichowski, J.; Pielichowski, K., Carbazole-containing polymers: synthesis, properties and applications. *Progress in Polymer Science* **2003,** *28* (9), 1297-1353.
31. Yu, G.; Liu, Y.; Wu, X.; Zhu, D.; Li, H.; Jin, L.; Wang, M., Soluble Europium Complexes for Light-Emitting Diodes. *Chemistry of Materials* **2000,** *12* (9), 2537-2541.
32. Díaz-García, M. a. A.; Ávila, S. F. D.; Kuzyk, M. G., Energy transfer from organics to rare-earth complexes. *Applied Physics Letters* **2002,** *81* (21), 3924-3926.
33. Klöpffer, W., Transfer of Electronic Excitation Energy in Polyvinyl Carbazole. *The Journal of Chemical Physics* **1969,** *50* (6), 2337-2343.
34. Hoyle, C. E.; Nemzek, T. L.; Mar, A.; Guillet, J. E., Time Resolved Fluorescence Studies of Poly(N-vinylcarbazole), Poly(1-vinylnaphthalene), and 1, 3-Bis(N-carbazolyl)propane. *Macromolecules* **1978,** *11* (2), 429-431.
35. Johnson, G. E., Emission properties of vinylcarbazole polymers. *The Journal of Chemical Physics* **1975,** *62* (12), 4697-4709.
36. Johnson, G. E.; Good, T. A., Molecular weight dependent emission properties of poly (N-vinylcarbazole) in polymer blends. *Macromolecules* **1982,** *15* (2), 409-417.
37. Johnson, G., Spectroscopic study of carbazole by photoselection. *The Journal of physical chemistry* **1974,** *78* (15), 1512-1521.

38. Evers, F.; Kobs, K.; Memming, R.; Terrell, D. R., Intramolecular excimer emission of poly(N-vinylcarbazole) and rac- and meso-2,4-di-N-carbazolylpentane. Model substances for its syndiotactic and isotactic dyads. *Journal of the American Chemical Society* **1983,** *105* (19), 5988-5995.
39. Stevens, B.; Hutton, E., Radiative Life-time of the Pyrene Dimer and the Possible Role of Excited Dimers in Energy Transfer Processes. *Nature* **1960,** *186* (4730), 1045-1046.
40. K.Kasper., T. F. u., Ein Konzentrationsumschlag der Fluoreszenz. *Zeitschrift für Physikalische Chemie* **1954,** *1* (5_6), 275-277.
41. Förster, T., Excimers. *Angewandte Chemie International Edition in English* **1969,** *8* (5), 333-343.
42. Birks, J. B., Excimers. *Reports on Progress in Physics* **1975,** *38* (8), 903-974.
43. de Sainte Claire, P., Molecular Simulation of Excimer Fluorescence in Polystyrene and Poly(vinylcarbazole). *The Journal of Physical Chemistry B* **2006,** *110* (14), 7334-7343.
44. Johnson, P. C.; Offen, H. W., Excimer Fluorescence of Poly(N-vinylcarbazole). *The Journal of Chemical Physics* **1971,** *55* (6), 2945-2949.
45. Klöpffer, W.; Bauser, H.; Dolezalek, F.; Naundorf, G., Exciton Diffusion in Pyrene-A Thermally Activated Hopping Process. *Molecular Crystals and Liquid Crystals* **1972,** *16* (3), 229-245.
46. Pope, M.; Swenberg, C. E., *Electronic processes in organic crystals and polymers*. Oxford University Press on Demand: 1999; Vol. 39.
47. Klöpffer, W., *Introduction to polymer spectroscopy*. Springer Science & Business Media: 2012; Vol. 7.
48. Klöpffer, W.; Fischer, D., Triplet energy transfer in solid solutions and films of poly(vinyl carbazole). *Journal of Polymer Science: Polymer Symposia* **1973,** *40* (1), 43-56.
49. Nozue, Y.; Hisamune, T.; Goto, T.; Tsuruta, H., Exciton Migration and Trapping at the Excimer-Forming Site in Poly (N-Vinylcarbazole). *Journal of the Physical Society of Japan* **1986,** *55* (11), 4053-4067.
50. Khetubol, A.; Van Snick, S.; Stanislovaityte, E.; Hassinen, A.; Coutiño-González, E.; Vanderlinden, W.; Firdaus, Y.; Fron, E.; Vlasselaer, M.; Simokaitiene, J.; De Feyter, S.; Hens, Z.; Grazulevicius, J. V.; Dehaen, W.; Van der Auweraer, M., Triplet harvesting in poly(9-vinylcarbazole) and poly(9-(2,3-epoxypropyl)carbazole) doped with CdSe/ZnS quantum dots encapsulated with 16-(N-carbazolyl) hexadecanoic acid ligands. *Journal of Polymer Science Part B: Polymer Physics* **2014,** *52* (7), 539-551.
51. https://www.fishersci.com/shop/products/poly-n-vinylcarbazole-approx-m-w-90-000-acros-organics-4/AC329690050 (accessed 22th of May 2021).

52. Martin, C.; Bhattacharyya, S.; Patra, A.; Douhal, A., Single and multistep energy transfer processes within doped polymer nanoparticles. *Photochemical & Photobiological Sciences* **2014,** *13* (9), 1241-1252.

CHAPTER 7: Conclusions and Outlook

"When nature does something unexpected, we learn something about how nature works. It used to be said, before the recent era of revolutionary discoveries, that science was organised common sense. In the modern era it would be more accurate to define science as organised unpredictability."

Freeman Dyson- 'The Importance of Being Unpredictable' (1990)

Conclusions and Outlook

The primary goal of this thesis has been to investigate europium β-diketonate complexes for application in spectral converters, luminescent down-shifting (LDS) layers and luminescent solar concentrators (LSCs), to enhance the efficiency of solar cells by converting UV photons into longer wavelengths in the visible region. The critical role of energy transfer processes was emphasised with respect to the constituting ligands of the europium complexes, europium complexes co-doped with organic molecules, or from an optically active polymeric host to the europium complexes.

This chapter summarises the most important findings from the photophysical point of view and in the context of the LDS layers and LSCs and points out the next step for future work based upon the results presented throughout this thesis.

The photophysical properties of $Eu(hfac)_3DPEPO$ and $Eu(tta)_3DPEPO$ were investigated. The roles that the ligands play in energy transfer were elucidated; tta and hfac ligands have lower triplet states than DPEPO; thus, energy transfer from DPEPO to the metal ion occurs via these ligands. The DPEPO ligand plays a significant role in enhancing the luminescence properties by replacing the solvent molecules, reducing non-radiative deactivation pathways, and, hence, efficient energy transfer and enhancement in the total quantum yields of both complexes.

A special sample mould was designed and 3D-printed to facilitate quantitative measurements of the photophysical properties of europium complexes in films. Encapsulation in PMMA enhances the total quantum yields of both complexes due to an increase in the intrinsic quantum yield of europium emission. This effect is more significant for $Eu(tta)_3DPEPO$, where there is a substantial decrease in the non-radiative decay rate in PMMA compared with DCM. The photophysical properties, such as energy transfer efficiency from the ligand to the europium, radiative lifetime and intrinsic quantum yield in DCM and PMMA, were reported for the complex $Eu(tta)_3DPEPO$ for the first time in a single study. The absorption windows of the two complexes are complementary in covering different parts of the UV/Vis region to harvest the desired high-energy photons from 250–390 nm. The total quantum yield values in PMMA of 0.85 and 0.75 for $Eu(hfac)_3DPEPO$ and $Eu(tta)_3DPEPO$, respectively, make these europium complexes efficient light harvesters in the UV/blue regions and therefore excellent candidates for LSD and LSC applications.

Renewable energy technologies need to be commercially viable; the high cost of rare earth metals might pose a challenge with respect to their practical application in LSCs and LDS. Co-doping europium complexes with organic chromophores offer a way to cut costs and harvest the high energy photons in the UV region. Thus, we addressed the use of Förster resonance energy transfer to enhance ultraviolet excitation of the Eu(III) complexes in PMMA films co-doped with organic molecules. The absorption spectra of the chosen donors, DPEPO, indole, biphenyl, and p-terphenyl, complement those of the complexes, making them useful in harvesting high energy photons in the 250–320 nm region. Examination of the excitation spectra of the europium complexes in the presence and absence of the donors showed that, in each case, an enhancement in UV excitation of the Eu(III) complex was observed, except for $Eu(hfac)_3DPEPO$ co-doped with indole.

The energy transfer efficiencies of the different donors were determined. DPEPO had the highest energy transfer efficiency for each complex, 33% and 38% for $Eu(tta)_3DPEPO$ and $Eu(hfac)_3DPEPO$, respectively. p-Terphenyl showed a comparable energy transfer efficiency (31%) with $Eu(tta)_3DPEPO$. In the case of DPEPO and biphenyl, where different concentrations of donors were examined with $Eu(tta)_3DPEPO$, it is worth noting that an increase in the concentration does not necessarily result in higher energy transfer efficiency may only lead to a slight enhancement in the fluorescence excitation intensity.

Preliminary experiments on $Eu(tta)_3DPEPO$ and $Eu(tta)_3DPEPO$ co-doped with DPEPO were carried out to evaluate their practical performance as spectral converters on crystalline silicon (c-Si) solar cells. Results showed an improvement in the current density and external quantum yield, but further studies should be conducted to measure such a system's effectiveness fully.

As shown for $Eu(tta)_3DPEPO$ and $Eu(hfac)_3DPEPO$, co-doped with DPEPO, good energy transfer can occur at low concentrations of the complex. This helps in realising the two aims of Chapter 5: minimising the amount the lanthanide metal used and assisting in harvesting the desired high-energy photons in the ultraviolet region.

The use of a photoactive polymer matrix, namely Poly(N-vinylcarbazole) (PVK), was explored. The photoactive nature of PVK and its unique photophysical properties were considered, such as strong absorption in the UV region, fluorescence emission, and the nature of energy transfer in the polymer matrix. The transparent films obtained for the PVK polymer, in addition to their good absorption in the UV region and their photophysical properties, would make them an excellent candidate as a host material for LSCs and LDS layers applications. The use of PVK as an active host for $Eu(hfac)_3DPEPO$ was investigated.

Energy transfer from PVK to the complex was found to occur with an efficiency of ~15% and appeared to be independent of complex concentration over the range of 2.5 to 16 wt%. Energy transfer from PVK enhances excitation intensity at wavelengths above 300 nm but has a detrimental effect over most of the excitation wavelength range. This is the consequence of the high absorbance of the PVK combined with a low energy transfer efficiency. Therefore, the use of PVK as a matrix for Eu(hfac)$_3$DPEPO, under the conditions used in these experiments, is not advantageous. However, it was predicted that if the energy transfer efficiency could be increased to 50%, there would be a substantial enhancement of the excitation intensity over the majority of the wavelength range.

In contrast, for Eu(tta)$_3$DPEPO, the use of PVK as a matrix was found to give a beneficial enhancement in excitation intensity. The energy transfer efficiency from PVK to the complex was found to be 20%, similar to that found for energy transfer in Eu(hfac)$_3$DPEPO. The presence of PVK significantly enhances the excitation intensity at wavelengths below 325 nm and above 355 nm, although there is a detrimental, intensity-depleting effect between 325 and 355 nm. However, unlike Eu(hfac)$_3$DPEPO, there is a net gain in excitation intensity in the presence of PVK; the increase in intensity exceeds the loss by a factor of about three.

The effect of varying the PVK matrix concentration on energy transfer to the Eu(tta)$_3$DPEPO was investigated. It was observed that the magnitude of the enhancement of the excitation intensity of the complex by energy transfer from the PVK is influenced by the concentration of PVK. A maximum enhancement was observed for 20 (mg/ml) PVK. At PVK concentrations greater than 20 (mg/ml), the enhancement factor decreases with increasing PVK concentration.

Energy transfer from PVK to the complexes has been observed, despite the lack of spectral overlap between the emission spectrum of PVK and the absorption spectrum of Eu(hfac)$_3$DPEPO, and the minimal spectral overlap with the absorption spectrum of Eu(tta)$_3$DPEPO. Therefore, it can be deduced that energy transfer to the complexes occurs from the carbazole monomer excited state, not from the emitting excimer species. Thus, in PVK doped with the europium complexes, each complex acts as a trap for the migrating monomer excitons, competing with the excitation of the excimer-forming sites.

The effect of adding co-dopant to Eu(tta)$_3$DPEPO in the PVK matrix was investigated. In the case of DPEPO and biphenyl co-dopants, the excitation intensity is enhanced compared with the effect of energy transfer from the PVK matrix alone. For the indole co-dopant, there is no significant enhancement compared with the effect of PVK only, but there appears to be a small effect on the excitation profile. Thus, a multistep energy transfer process can be proposed to explain the enhancement in the excitation intensity by DPEPO and biphenyl.

Overall, there is potential for the role of PVK as a photoactive polymer in the LSCs and LDS layers, taking advantage of its photophysical properties. However, the energy transfer efficiency from PVK to the europium complexes studied here is rather low, so that competitive absorption by the PVK can have a detrimental rather than a beneficial effect. Therefore, more work needs to be done to establish the optimum conditions (e.g., the concentration of complex, the concentration of PVK, etc.) for energy transfer from PVK to $Eu(tta)_3DPEPO$.

Following on from the work presented in this thesis, several points should be pursued further in terms of the photophysical characterisation and better understanding of the results in the context of LSCs and LDS layer applications.

When it comes to optimising the photophysical properties of the lanthanide complexes, careful consideration should go to the ligand design and the position of the triplet state. Providing complete assessments of all relevant photophysical parameters is key to enhancing the general performance of lanthanide complexes. Measuring the quantum yields of all samples by the absolute method would be desirable, especially when dealing with europium complexes co-doped with organic molecules (Chapter 5) or in the presence of an optically active polymer (Chapter 6). obtaining quantum yield results by the comparative method can be challenging.

The results of co-doping europium complexes with organic molecules can be extended by measuring donors at a series of concentrations or changing the solvent. Monitoring the energy transfer process by measuring the lifetime of the donor could provide confirmation of the energy transfer efficiencies. Solar testing should be performed on $Eu(tta)_3DPEPO$ co-doped with DPEPO several times and with a series of concentrations. In addition, the efficiency of $Eu(tta)_3DPEPO$ co-doped with DPEPO should be explored on different solar cells that are insensitive to the short wavelength portion of the solar spectrum, such as cadmium telluride (CdTe).

The use of PVK as a host material should be further investigated. Now that it has been established that excitonic energy transfer occurs from PVK monomer to dopants, it should be possible to select complexes that are likely to be optimum acceptors to maximise harvesting the UV region and decrease the quantities of the lanthanide metals used. Absolute quantum yield measurements on the films should be carried out on the complexes when encapsulated in PVK. In the presence of dopants, a multistep energy transfer can occur; examination of the lifetimes of PVK and dopants might be critical in understanding the energy transfer mechanisms. Solar testing experiments should be carried out to understand this work better in the context of LSCs and LDS layer applications.

Appendix

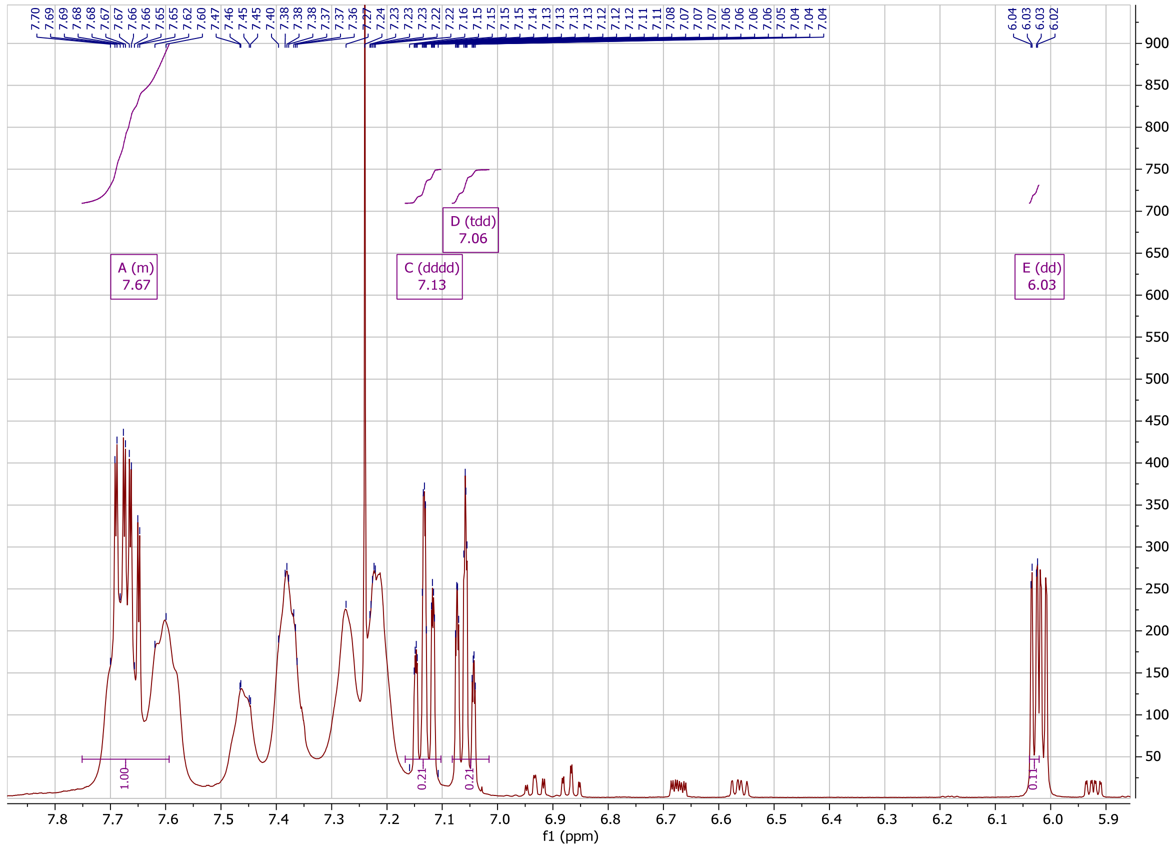

Figure A.1 .^{1}H NMR spectrum (500 MHz) for DPEPO in $CDCl_3$.

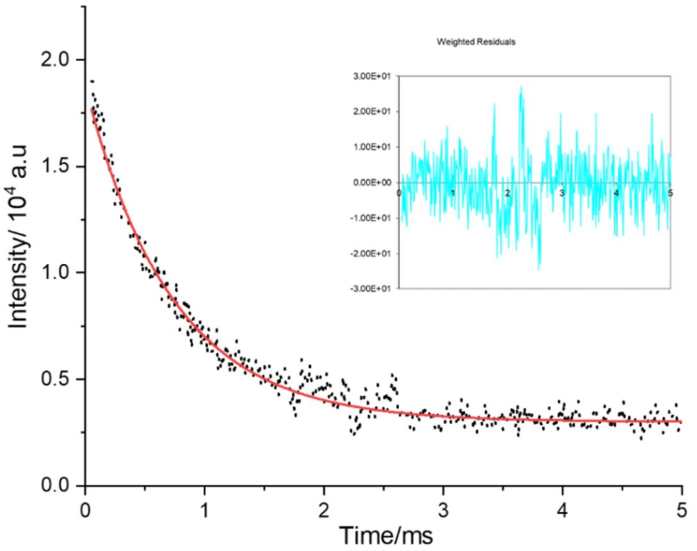

Figure A.2 Decay data (dotted black), fitted single exponential function (red line) and weighted residuals of Eu(tta)$_3$DPEPO co-doped with biphenyl excited at 340 nm and monitored at 610 nm in PMMA.

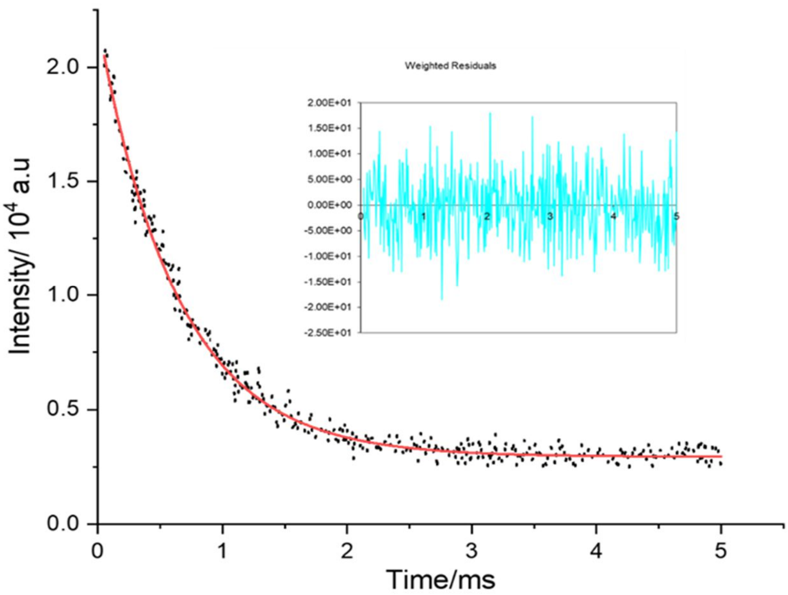

Figure A.3 Decay data (dotted black), fitted single exponential function (red line) and weighted residuals of Eu(tta)$_3$DPEPO co-doped with DPEPO excited at 340 nm and monitored at 610 nm in PMMA.

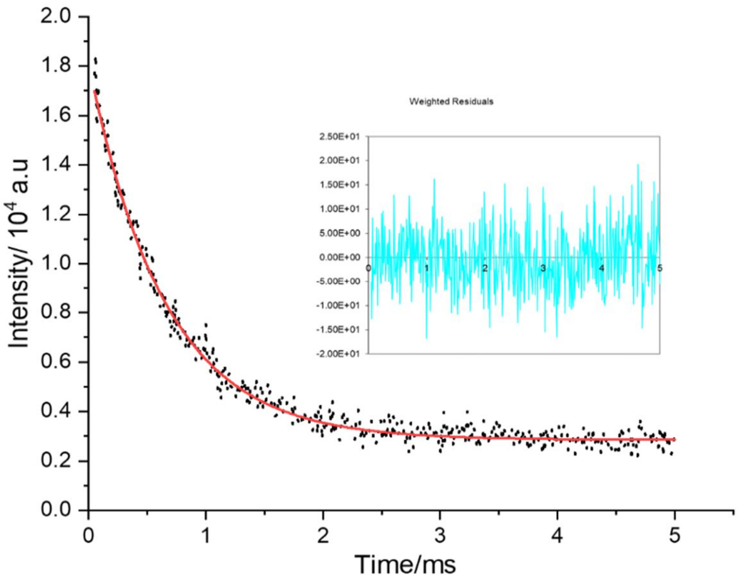

Figure A.4 Decay data (dotted black), fitted single exponential function (red line) and weighted residuals of Eu(tta)$_3$DPEPO co-doped with indole excited at 340 nm and monitored at 610 nm in PMMA.

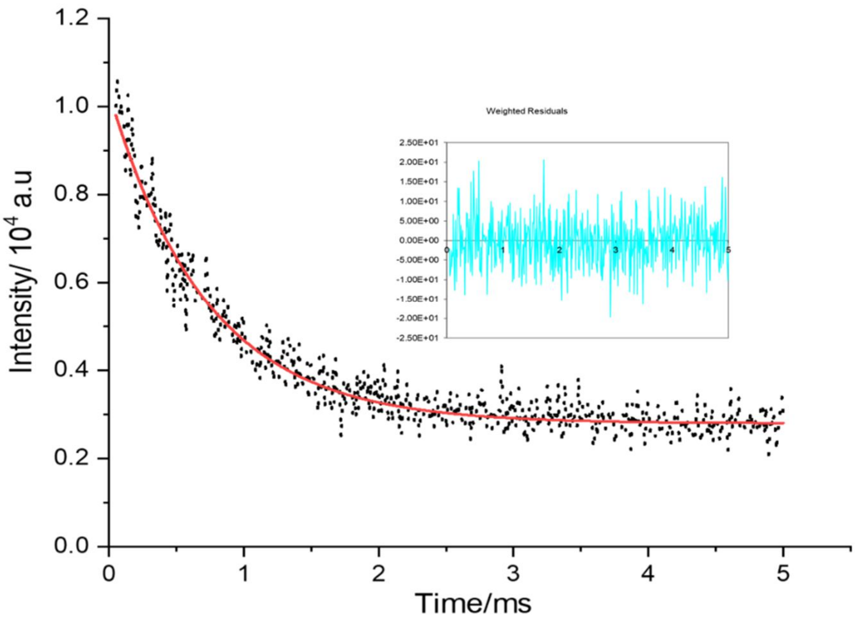

Figure A.5 Decay data (dotted black), fitted single exponential function (red line) and weighted residuals of Eu(hfac)$_3$DPEPO co-doped with Biphenyl excited at 298 nm and monitored at 610 nm in PMMA.

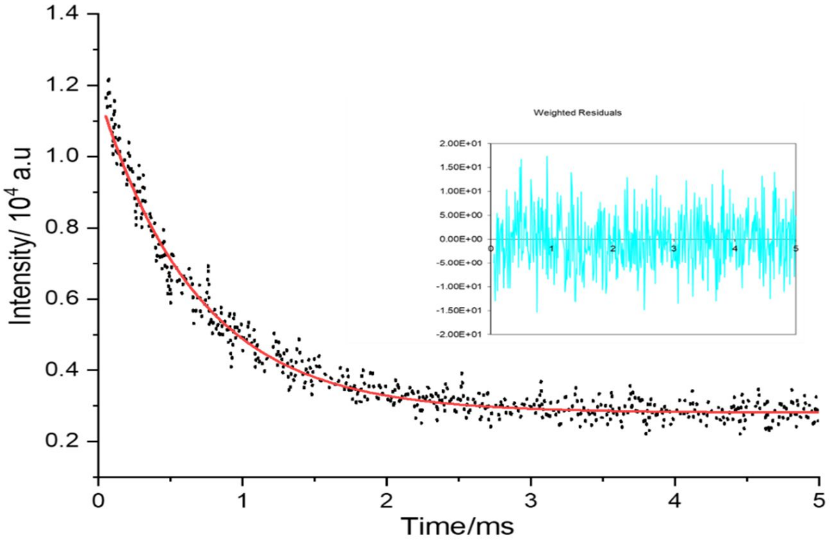

Figure A.6 Decay data (dotted black), fitted single exponential function (red line) and weighted residuals of Eu(hfac)$_3$DPEPO co-doped with DPEPO excited at 298 nm and monitored at 610 nm in PMMA.

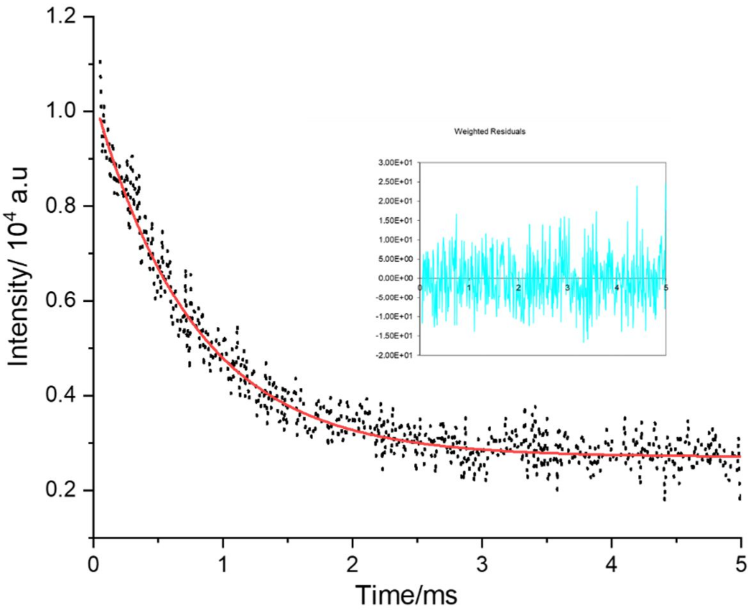

Figure A.7 Decay data (dotted black), fitted single exponential function (red line) and weighted residuals of Eu(hfac)$_3$DPEPO co-doped with indole excited at 298 nm and monitored at 610 nm in PMMA.